Micro-mechanical modeling of human vocal folds : from quasi-static to vibratory loading

Alberto Terzolo

Université Grenoble Alpes

THÈSE

Pour obtenir le grade de

DOCTEUR DE L'UNIVERSITÉ GRENOBLE ALPES

Spécialité : 2MGE - Matériaux, Mécanique, Génie civil, Electrochimie

Arrêté ministériel : 25 mai 2016

Présentée par

Alberto TERZOLO

Thèse dirigée par **Lucie BAILLY**, Chargée de Recherche, CNRS
et codirigée par **Laurent ORGÉAS**, Directeur de Recherche, CNRS

préparée au sein du **Laboratoire 3SR - Sols, Solides, Structures et Risques** dans **l'École Doctorale I-MEP2 - Ingénierie - Matériaux, Mécanique, Environnement, Energétique, Procédés, Production**

Micro-mechanical modeling of human vocal folds: from quasi-static to vibratory loadings.

Modélisation micro-mécanique des plis vocaux humains : des chargements quasi-statiques aux régimes vibratoires.

Thèse soutenue publiquement le **27 janvier 2022**,
devant le jury composé de :

Madame Aline BEL-BRUNON
Maître de Conférence, INSA Lyon, Examinatrice
Madame Pascale ROYER
Directrice de Recherche, CNRS, Examinatrice
Monsieur Grégory CHAGNON
Professeur, Université Grenoble Alpes, Président
Monsieur Stéphane LEJEUNES
Ingénieur de Recherche, CNRS, Rapporteur
Monsieur Yannick TILLIER
Professeur, MINES Paris, Rapporteur
Madame Lucie BAILLY
Chargée de Recherche, CNRS, Directrice de thèse
Monsieur Laurent ORGÉAS
Directeur de Recherche, CNRS, Co-directeur de thèse

"Per aspera ad astra."

In loving memory of
Claudio Terzolo
1961 – 2020

Considerate la vostra semenza:
fatti non foste a viver come bruti,
ma per seguir virtute e canoscenza.

— vv. 118-120 Canto XXVI,
The Divine Comedy,
Vol.1 (Inferno)
[Dante Alighieri]

Acknowledgments

This endeavor becomes a reality with the precious support and help of many individuals and institutions.

First and foremost, I would like to express my deep gratitude to my advisors, Dr. Lucie Bailly and Dr. Laurent Orgéas. Thank you for the continuous support, encouragement and patience throughout this work, your motivation, enthusiasm and immense knowledge have deeply inspired me. It was a great pleasure and honor to carry out this research project under your invaluable guidance.

Besides my advisors, I would like to extend my sincere thanks to all the other distinguished members of the examination panel, headed by Prof. Grégory Chagnon together with Prof. Aline Bel-Brunon, Dr. Pascale Royer, Dr. Stéphane Lejeunes and Prof. Yannick Tillier. Thank you for reading, reviewing and approving my work, as well as for your insightful comments and questions.

I am highly indebted to Thibaud Cochereau and Tomáš Chalupa, the completion of this work would have not been possible without your meaningful scientific expertise and contribution.

I thank profusely all the staffs of Laboratoire 3SR for their kind help and co-operation throughout my stay there. I am particularly thankful to Cécile Bordier for her great empathy and keen interest in my research.

I owe a deep sense of gratitude and appreciation to all my office mates and fellow colleagues who helped me out, directly or indirectly, to successfully conduct this research project. Thank you for the encouragement, stimulating discussions, and good memories.

My heartfelt thanks to my dear friend Franck Ott for his genuine acceptance and thoughtfulness, I will always remember your kindness and constant support. I am equally thankful to my old but gold friend Andrea Cosentino for keeping our long lasting friendship healthy and intact despite my silence and the distance that often separates us.

Words cannot express my deepest gratitude to my family for their unconditional love, encouragement and support to accomplish this work. It was a great comfort and relief to know that you were taking care of everything else when I undertook my research project.

Finally, I would like to express my sincere gratitude to LabEx Tec21, ANR, UGA, Laboratoire 3SR and Gipsa-Lab, under whose auspices and finance this project was made possible.

Contents

List of Figures

List of Tables

Preface and thesis outline

The Oxford University Dictionary defines the term "instrument" as "a contrivance for producing musical sounds." In this regard, the human voice can be considered the oldest musical instrument, dating back to the primitive vocalizations several million years ago. The most primitive use of voice is for survival, to warn, intimidate or to locate and be located. Vocal expression is a full sensory experience (heard but also felt) : it allows to carry not only a very wide range of sounds (with adjustable frequency, intensity and timbre) or meaning words to an audience, but also conveys emotions and character, which makes it essential to our social interactions. From birth, the human voice continues to evolve throughout life, reflecting our age, culture, habits, health and personality. The voice can also represent an essential tool for professionals with a high vocal load, such as artists and teachers.

Voice disorders concern everyone, and can develop at any time, even in people with no physio-pathological predisposition. Disorders can be due to dysfunctional pathologies ascribable to the formation of lesions on the vocal folds, *i.e.*, two vibrating soft tissues in the larynx essential to human phonation, to surgery *sequelae* for laryngeal cancer (3500 cases/year in France, 15% of total cancers), or a laryngeal paralysis. These pathologies generate aero-dynamical and vibration perturbations. However, voice disorders can have a far greater impact than the mere acoustic complication itself would suggest (*e.g.*, impoverishment of the timbre, instability of the fundamental frequency, decrease in loudness): beyond the alteration of speech evaluated according to purely aesthetic criteria, even mild troubles can significantly degrade the intelligibility of its content, and thus hinder communication with others. Pathologies are *de facto* very common for voice artists and teachers (prevalence of 50% in France), and require recurrent work stoppages or even change of career orientation (Inserm report, 2006). In the extreme case of laryngectomy (8000 cases in France), many traumatic complications appear, among which loss of voice and a very high psychological stress. Voice troubles have therefore a high impact on the professional and social life of a person, on his emotions, mental and physical conditions, and communication skills.
Regardless of the disorder, speech therapists and ENT practitioners (ear, nose and throat surgeons) do need fundamental advances from the research community working on voice biomechanics to gain an in-depth scientific knowledge of the mechanics of vibrating tissues, and keep improving their therapeutic plans.

From a scientific point of view, human vocal production is highly complex topic of study because of the many coupled physical phenomena involved, including acoustics, aerodynamics and soft tissue biomechanics. Compared to the acquired knowledge of the acoustic and aerodynamic characterization of the human voice since the 1970s, vocal folds histological and biomechanical peculiarities are still little studied, and their impact on the remarkable vibratory properties of the vocal fold remains elusive.
This gap of knowledge is ascribable to several aspects associated with the biomechanical study of the vocal folds. Protected by laryngeal cartilages, vocal folds are hardly observable using current medical imaging techniques, in particular ultrasound investigation techniques commonly used *in vivo*. Furthermore, vocal fold reduced characteristic size (5-15 mm) does not facilitate the design and implementation of *ex vivo* mechanical tests. *In vitro*

phonatory system simulators exist and are made of vocal folds artificial replicas. Nonetheless, the materials employed in these simulators often derive from homogeneous elastomers characterized by microstructural and macroscale mechanical properties still far from those exhibited by the native tissues. Due to these experimental limitations, the mechanical modeling of laryngeal tissues often remains far from the physiological evidence. Very few theoretical formulations have been proposed at the scale of the tissue fibrous constituents (elastic, collagen and muscle fibers) so far. Yet, multiscale approaches are essential to gain further insights into vocal folds vibro-mechanical performances, and required before any transposition to the medical plan.

Therefore, **the global objective of this thesis is to develop a micro-mechanical model of the human vocal fold in close connection with available histological and mechanical data acquired on vocal tissues from quasi-static to vibratory loadings.** This theoretical study intends to contribute to the development of fiber scale-based approaches so as to better understand the link between vibrating tissues micromechanics and their macroscale performances. The manuscript is structured as it follows:

- Chapter 1 contextualizes the work describing the physiological and physical mechanisms underlying human voice production and vocal-fold vibrations in the larynx. Voice pathologies, clinical observations, treatments and current limitations are detailed. The currently acquired knowledge of the vocal-fold tissue histology and mechanics based on experimental evidence is then reviewed. Finally, an overview of the theoretical and numerical approaches commonly adopted to model vocal folds biomechanics is presented.

- Chapter 2 proposes a micro-mechanical hyperelastic model able to describe the 3D fibrous architecture and the surrounding matrices of the vocal-fold sublayers, and to predict their mechanical behavior for key physiological loading paths, *i.e.*, tension, compression and shear. Regardless of the applied load, it is shown how macroscale nonlinear, anisotropic tissue responses are inherited from original scenarios of fiber scale micro-mechanisms. This chapter is based on an article submitted to the *Journal of the Mechanical Behavior of Biomedical Materials* in 2021.

- Chapter 3 extends the micro-mechanical formulation developed in Chapter 2 to a viscoelastic frame. Chapter 3 assesses the model ability to reproduce vocal-fold tissue time-dependent response under a large variety of loading conditions at various rates : not only low-frequency cyclic and multiaxial loadings upon finite strains, but also high-frequency oscillatory shear small (SAOS) and large (LAOS) deformation loadings. This chapter is based on an article in preparation for the *Journal of the Mechanical Behavior of Biomedical Materials*, in the continuity of the aforementioned submitted article.

- Finally, preliminary numerical developments are presented in Chapter 4. This chapter addresses the implementation of the hyperelastic formulation detailed in Chapter 2 in a finite element (FE) code, toward 3D simulations of vocal fold transient dynamics with relevant histo-mechanical properties.

1

General context: human voice biomechanics

Contents

1.1 Human vocal apparatus

Human voice is the final outcome of a complex physiological process occurring in the vocal apparatus, sketched in Figure 1.1, and involving various portions of the human body (*i.e.* chest, neck and head). Three main components can be identified: (i) the first component is the **lungs**, providing an airstream moving up to the larynx through the trachea. The lungs serve as both a reservoir of air and an energy source, representing the "generator" of the vocal apparatus. (ii) The second component is the **vocal folds** (or "vocal cords"), a pair of soft pliable tissues located in the larynx, and representing the "vibrator" of the vocal apparatus: influenced by the interaction with the pulmonary air being exhaled, vocal folds can deform and vibrate, thereby leading to phonation, *i.e.*, the production of audible air pulse trains. (iii) Finally, the acoustic wave so generated is filtered by vocal tract resonance, whose geometry is shaped by speech articulators (*e.g.*, soft palate, jaw, tongue, teeth, lips) to generate distinguishable voiced sounds, such as vowels and sonorous consonants. The different **cavities of the vocal tract**, also called "resonators" or "modulators", are the third component of the vocal apparatus.

During the production of voiced sounds, the main acoustical source is represented by the vocal-fold vibrations, taking place in the laryngeal area. Thus, in order to better understand the major features of human voice biomechanics, this section provides an anatomical description of the larynx, and summarizes the current knowledge of the phonation process.

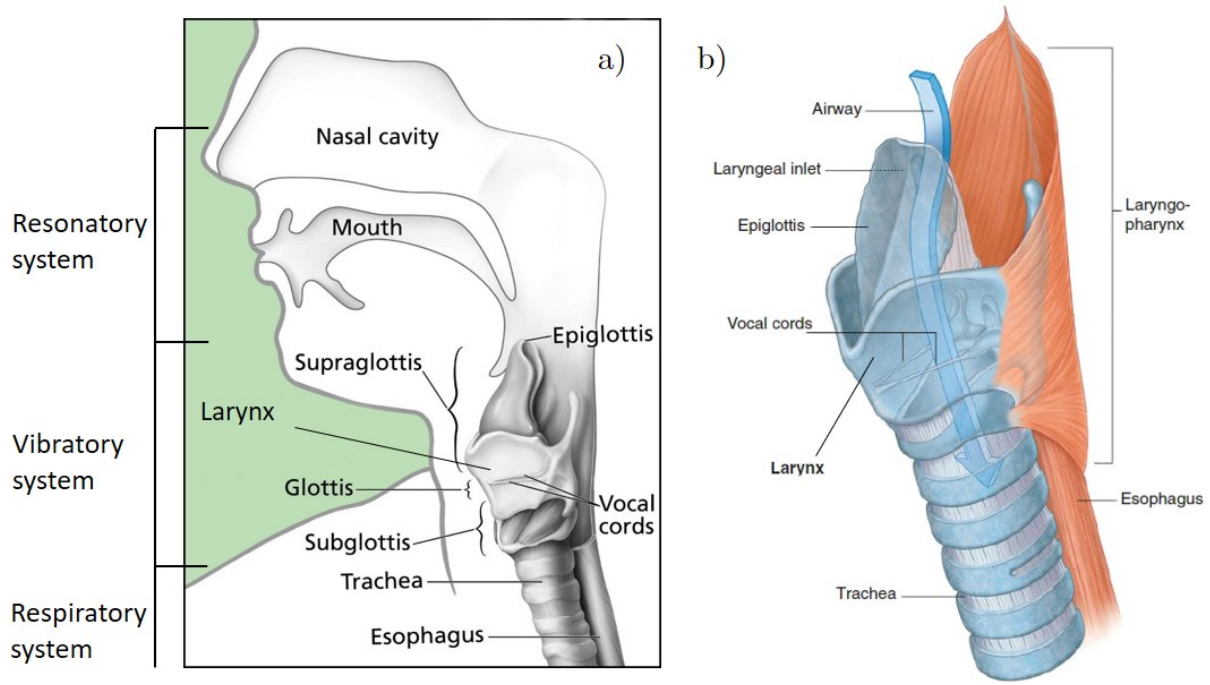

Figure 1.1: Vocal fold apparatus. a) sketch of the main components of the human vocal fold apparatus; b) focus on the laryngeal complex and nearby structures. Adapted from [70, 158].

1.1.1 Anatomy of the larynx

The larynx is a mobile structure that caps the lower respiratory tract. The cavity of the larynx is continuous below with the trachea, and above opens into the pharynx, as illustrated in Figure 1.1 b. Typical dimensions of a human larynx range from 4 to 6 cm in length, and from 3 to 6 cm in width. It is composed of a skeletal framework formed by a series of cartilages interconnected through intrinsic ligaments and fibroelastic membranes, moved by a number of muscles, and joined to surrounding structures through extrinsic ligaments and membranes (see Figure 1.2, Figure 1.3 and Figure 1.4). The hyoid bone is also attached to the larynx (see Figure 1.3 a) though it is usually regarded as a separate structure with a distinctive functional role. Each component is better detailed in the following sections.

Cartilages

Cartilage is a tough, durable form of supporting connective tissue. The firm consistency allows to bear mechanical stresses without permanent distortion. Within the laryngeal tract, cartilages form the supporting framework for softer tissues [189]. Three large unpaired cartilages (cricoid, thyroid and epiglottis) and three pairs of smaller cartilages (arytenoid, corniculated and cuneiform) can be distinguished.

- *Cricoid* – The cricoid cartilage is the most inferior of the laryngeal cartilages, located just above the first tracheal ring, thereby encircling the laryngeal airway, as shown in Figure 1.2 a. It is shaped like a ring, made of a broad *lamina* posterior to the airway and a narrower arch circling anteriorly [80]. The posterior surface of the *lamina* is characterized by two shallow depressions separated by a vertical ridge (see Figure 1.2 b), where is attached the esophagus. The cricoid cartilage has also two articular facets for articulation with the arytenoid and thyroid cartilages, as displayed in Figure 1.2.

- *Thyroid* – The thyroid cartilage is the largest of the laryngeal cartilages. It is bigger, albeit thinner and weaker than the cricoid cartilage. It is formed by a right and a left *lamina*, widely separated posteriorly, but converging and joining anteriorly, as shown in Figure 1.2 c and d. The most superior point of the conjunction between the two broad and flat *laminae* stands for the laryngeal prominence, more commonly known as the "Adam's apple". The *laminae* posterior borders are prolonged to form a superior horn and an inferior horn. The medial surface of the inferior horn has a facet for articulation with the cricoid cartilage.

- *Epiglottis* – The epiglottis is a leaf-shaped cartilage located in the upper part of the larynx (see Figure 1.1 b and Figure 1.3 a). It is attached by its stem to the posterior aspect of the *thyroid* cartilage, and projects postero-superiorly from its attachment to the thyroid cartilage. The epiglottis constitutes the front cover of the laryngeal cavity: the primary function of the epiglottis is to close the larynx entrance when swallowing, preventing food from passing into the respiratory tract.

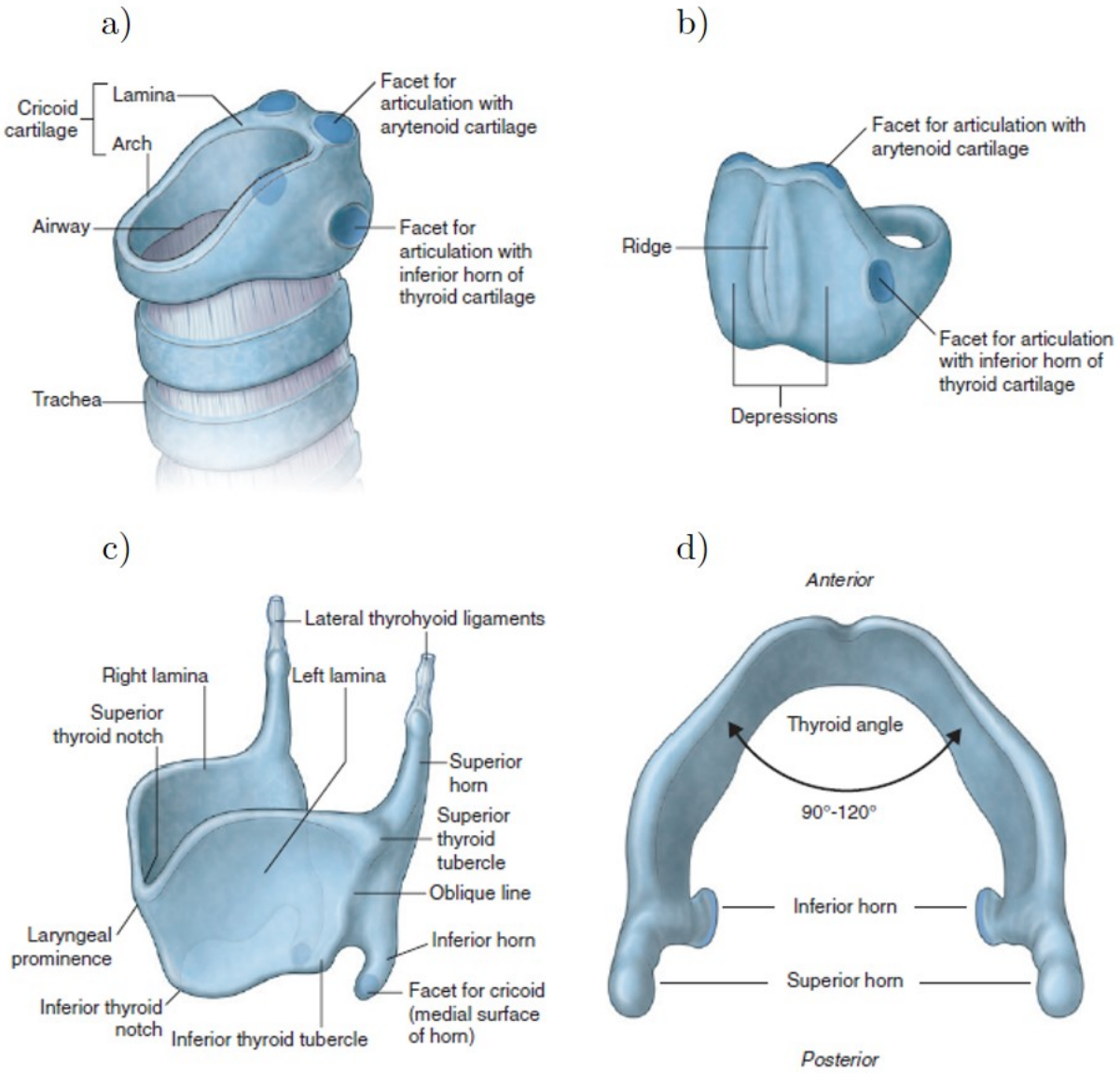

Figure 1.2: Illustration of the cricoid and thyroid cartilage from a anterolateral, a) and c), b) posterior and d) superior view, respectively. Adapted from [70].

- *Arytenoids* – The paired arytenoid cartilages are pyramid-shaped cartilages with three surfaces, a base and an apex, as depicted in Figure 1.3 b and c. They are located posterior to the laryngeal cavity on the cricoid ring: the base is concave and with a smooth surface for articulation with the upper border of the cricoid *lamina*. The anterior angle of the base is elongated into a so-called "vocal process", to which the vocal ligament is attached (see Figure 1.3 d and details below). Accordingly, the mobility of the arytenoids cartilages, along with that of the cricoid cartilage by means of appropriate laryngeal joints (crico-arytenoid and cricothyroid joints) [264], plays a primary role in regulating vocal folds movements and, thereby, controlling voice production (see Figure 1.5).

- *Corniculate and cuneiform* – The corniculate cartilages are two small conical cartilages that articulate with the apices of the arythenoid cartilages, prolonging them postero-

medially (see Figure 1.3 b). Cuneiform cartilages are two small club-shaped nodules of elastic cartilage lying anteriorly to the corniculate cartilages. These cartilages do not actively participate to phonation, and are therefore of minor importance.

Ligaments

The cartilaginous skeleton of the larynx is joined to the surrounding structures by means of extrinsic ligaments. It is also interconnected through intrinsic ligaments and fibroelastic membranes, of which the thyrohyoid and quadrangular membranes, together with the *conus elasticus*, are the most significant (see Figure 1.3 a, b and d). The thyrohyoid membrane is external to the larynx, whereas the paired quadrangular membranes and *conus elasticus* are internal (see Figure 1.3 c). The named ligaments are the median cricothyroid ligament, the hyo-epiglottic and the cricotracheal ligament (see Figure 1.3 a and Figure 1.3 c).

Muscles

The combination of the larynx skeletal framework and corresponding membranes and ligaments is moved by the laryngeal muscles. The latter can be differentiated into extrinsic and intrinsic muscles.

- *Extrinsic muscles* – Extrinsic muscles are external to the laryngeal complex, connecting the larynx to neighboring structures (*i.e.*, sternum, hyoid bone, pharynx). Accordingly, these muscles are not actively involved in the voice production process. Nevertheless, they are of major importance in regulating the larynx overall mobility during phonation and swallowing, particularly along the inferosuperior and anteroposterior directions, and can, thereby, affect the pitch and the quality of the voice. This category includes the paired sternohyoid, thyrohyoid, omohyoid muscles as well as the sternothyroid, stylohyoid and mylohyoid muscles (as secondary muscles in the phonation process, their actions will not be detailed here).

- *Intrinsic muscles* – Conversely, intrinsic laryngeal muscles are responsible for internal configuration changes of the larynx, and represent the main actuators of vocal folds mobility (*e.g.*, they adjust tension in the vocal ligaments, control the inner dimensions of the vestibule and facilitate the closing of the laryngeal inlet). Intrinsic laryngeal muscles are illustrated in Figure 1.4. Among them, the most important with regards to voice biomechanics are :
  - *Cricothyroid* – Cricothyroid muscles are attached to the anterolateral aspect of the cricoid cartilage arch, and extend, superiorly and posteriorly, to connect to the thyroid cartilage (see Figure 1.4 a). They are responsible for forward and downward rotations of the thyroid cartilage at the cricothyroid joints (see Figure 1.5). These actions lengthen the vocal folds, affecting, therefore, the pitch control of phonation.

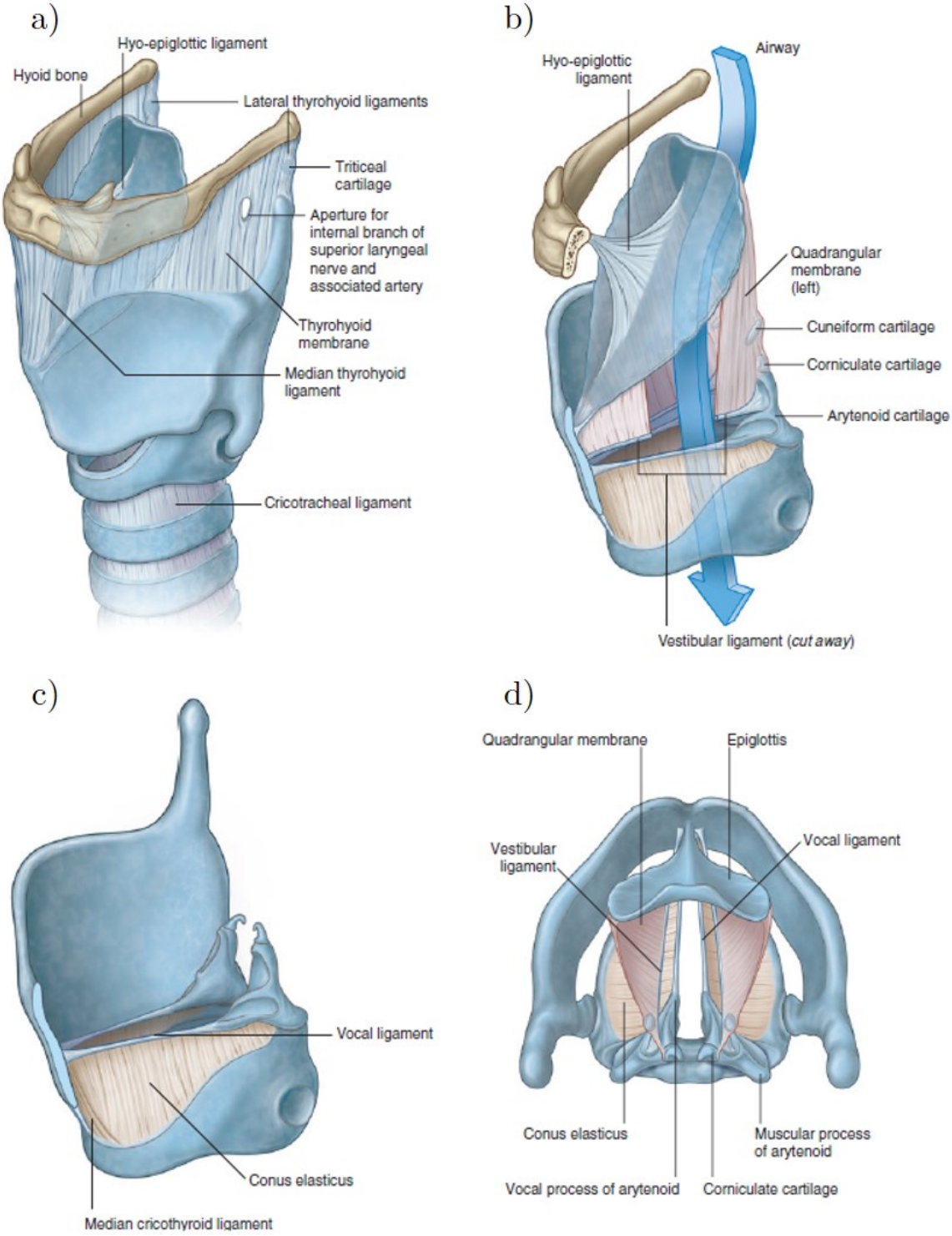

Figure 1.3: Illustration of the extrinsic and intrinsic ligaments and membranes: a) extrinsic ligaments of the larynx; b) the cricothyroid ligaments; c) the quadrangular membrane; d) a superior view of the fibroelastic membrane of the larynx. Adapted from [70].

- *Posterior and lateral crico-arytenoid* – Posterior crico-arytenoid muscles arise from the posterior surface of the cricoid cartilage *laminae*, and converge on the muscular processes of the arytenoid cartilages, as shown in Figure 1.4 b. These muscles abduct and externally rotate the arytenoid cartilages, being thereby the

primary abductors (separators) of the vocal folds.
The lateral crio-arytenoid muscles originate from the upper border of the cricoid cartilages archs, and insert on the muscular processes of the arytenoid cartilages. As opposed to the posterior crico-arytenoid muscles, lateral crico-arytenoid muscles internally rotate the arytenoid cartilages. These actions shorten and adduct (close) vocal folds.

- *Transverse and oblique arytenoid* – The transverse arytenoid (or interarytenoid) muscle is a single unpaired muscle bridging the distance at the back of the larynx between the two arytenoid cartilages (see Figure 1.4 b), helping to fully close the glottis during the vocal-fold adduction process (see Figure 1.5).
  The oblique arytenoid muscles extend from the superior facet of the arytenoid cartilages muscular processes to the apex of the arytenoid cartilages on the other side. Oblique arytenoid muscles can restrict the laryngeal inlet by narrowing the distance running between the arytenoid cartilages and the epiglottis.

- *Thyro-arytenoid and vocalis* – The thyro-artenoids are broad flat muscles lying lateral to the larynx fibroelastic membrane and the laryngeal saccules. They are attached to the lower half of the thyroid cartilage, anteriorly, and posteriorly to the cricothyroid ligament (see Figure 1.4 b and c). On account of their broadness, they act as a sphincter of the vestibule. Moreover, these muscles contract the laryngeal inlet by pulling the arytenoid cartilages and simultaneously pulling the epiglottis toward them. The lower and deeper portion of the thyro-arytenoid muscle is better known as the *vocalis* muscle. This latter bundle is simply considered by some authors as a deeper portion of the thyro-arytenoid, and by others as a distinct and separate muscle. The *vocalis* is parallel with, and just lateral to, the vocal ligament. Its contractions have the effect of shortening the vocal folds, increasing their thickness, along with their stiffness, having a role in the pitch control of the voice [248, 250, 253].

In conclusion, laryngeal intrinsic muscles can be grouped into three categories, based on their functions. The posterior and lateral cricoarytenoids and oblique and transverse arytenoids drive the degree of abduction and adduction of the vocal folds. The cricothyroids, posterior cricoarytenoids (the obliquity of their surfaces leads to an overlap in functions), thyroarytenoids and *vocalis* regulate the length and tension of the vocal folds. The last group of muscles includes the oblique arytenoids and thyro-arytenoids as modifiers of the laryngeal inlet.

1.1.2 Vocal folds and phonation

Vocal folds are two soft pliable structures placed in the laryngeal cavity, *i.e.*, a hollow tubular complex lined by *mucosa* extending from the laryngeal inlet down to the lower border of the cricoid cartilage (see Figure 1.6 a). By the term vocal fold, it is made reference

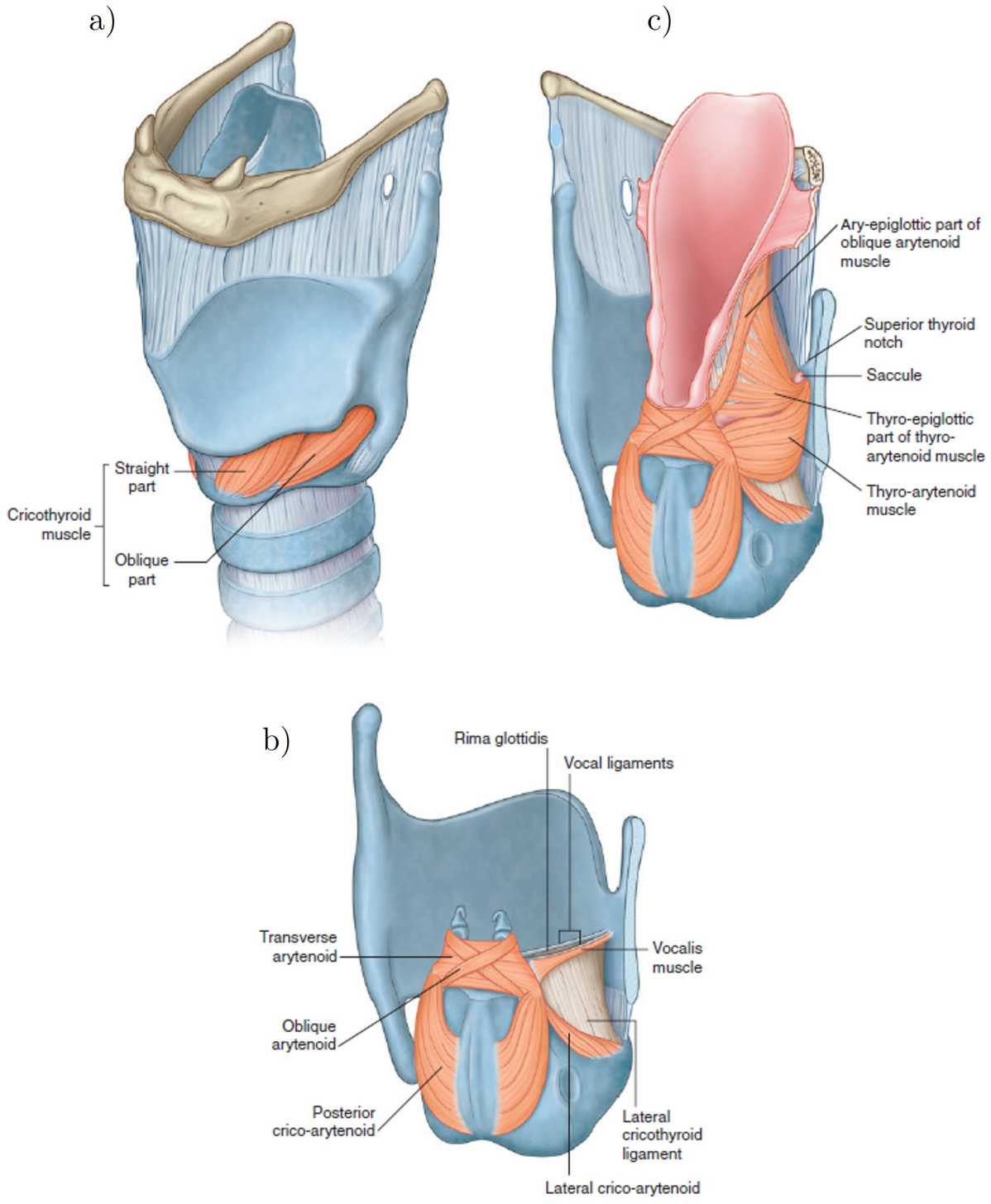

Figure 1.4: Laryngeal muscles: a) cricothyroid muscle; b) crico-arytenoid, oblique and transverse arytenoid, and *vocalis* muscles; c) thyro-arytenoid muscle. Adapted from [70].

to the set of the vocal ligament, the thin laryngeal *mucosa* firmly overlying the former, and the muscular outermost portion of thyroartenoid and *vocalis* muscles (the detailed histological properties of the vocal folds are described in section Section 1.3.1). The *glottis* refers to the space area between vocal folds. The amplitude of the glottal space is around 3 mm. The characteristic size of human vocal folds ranges (in length) approximately between

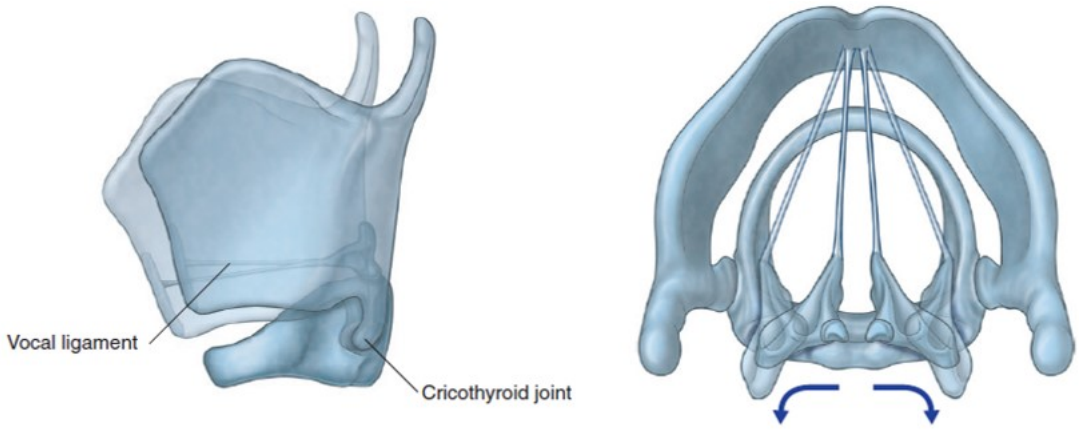

Figure 1.5: Illustration of the cricothyroid joints movements. Adapted from [70].

1.25 cm and 1.75 cm for females, and between 1.75 cm and 2.5 cm for males. Children's vocal folds are much shorter than those of adults. Vocal folds can be stretched up to 3-5 mm along the antero-posterior direction.

Depending on the physiological context (respiration, effort closure, swallowing or phonation), vocal folds geometrical configuration and dimensions are adjusted as illustrated in Figure 1.7:

(i) At rest, during quiet respiration, the laryngeal inlet, vestibule and vocal folds are wide open. The glottis is triangular Λ-shaped: the arytenoid cartilages are abducted, positioned well apart from each other to permit breathing. During forced inspiration, the arytenoids rotate laterally consequently to the action of posterior crico-arytenoid muscles. As a result, the vocal folds are abducted and the glottis widens into a rhomboid shape, significantly increasing the opening of the laryngeal airway.

(ii) Effort closure of the larynx occurs when air is retained in the thoracic cavity to stabilize the trunk (*e.g.*, during heavy lifting). Throughout effort closure, the glottis remains completely closed. The result is to totally and firmly shut the airway.

(iii) When swallowing, the glottis is severely closed and the laryngeal inlet is considerably narrowed. Additionally, the larynx moves up and forward. This action causes the epiglottis to swing toward the arytenoid cartilages to effectively close (or narrow) the laryngeal inlet. The latter up and down movement of the larynx also opens the esophagus. The combination of all these actions prevents solids and liquids from entering the airways.

(iv) To finally produce a voiced sound, the arytenoid cartilages and the vocal folds come together to close the glottis in a "pre-phonatory" position. Consequently, the air flowing from the lungs encounters an obstruction along its path, and tries to make its way by deforming the tissues and pushing against the closed glottis to pass it through. Tension inside the vocal folds (adjusted by the *vocalis* and cricothyroid muscles),

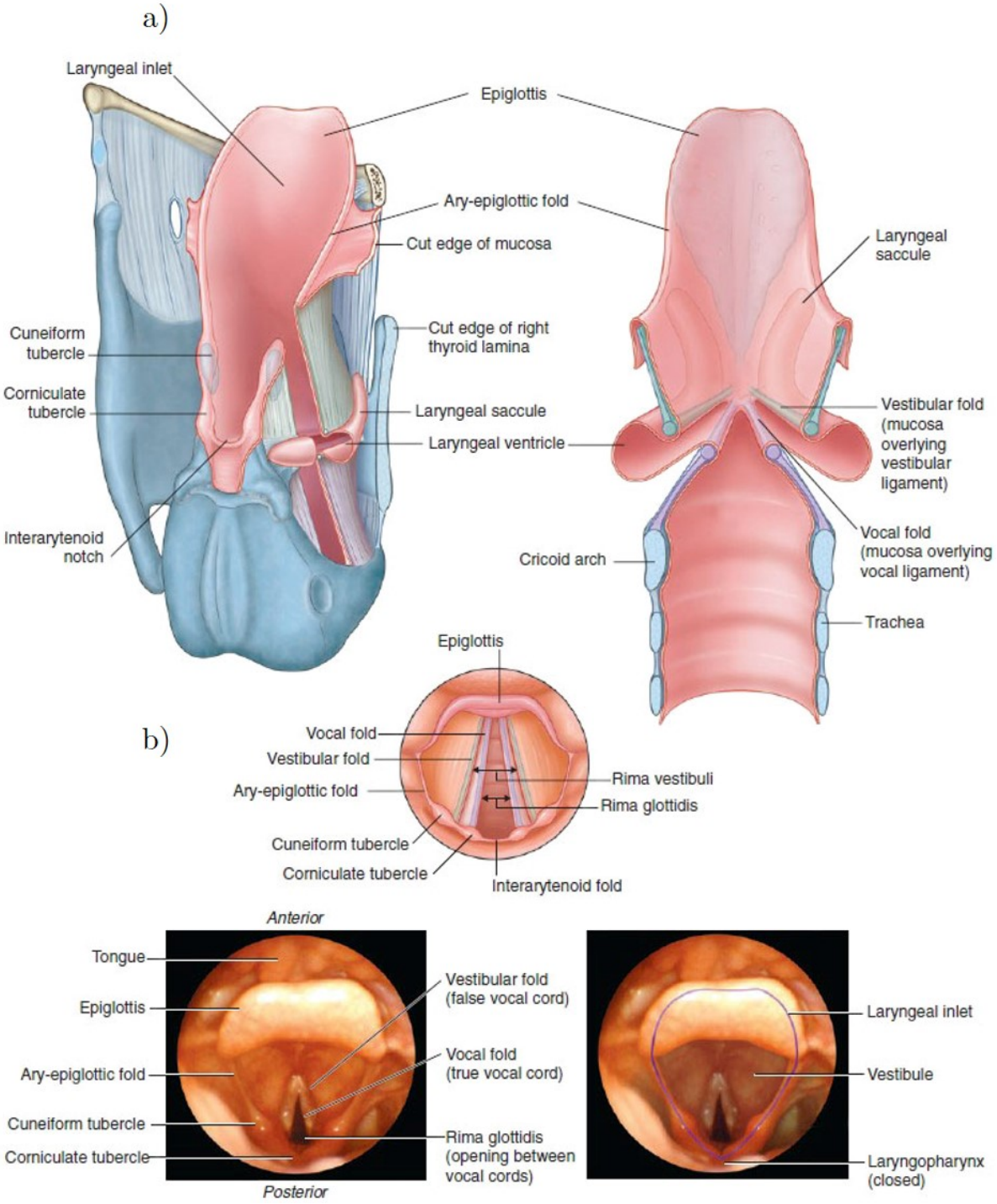

Figure 1.6: Laryngeal cavity: a) posterolateral view (left) and cut away (right) of the laryngeal cavity; b) illustration and labeled photographs of the laryngeal inlet from a superior view. Adapted from [70].

as well as their elasticity, opposes to the glottal opening. This action generates an increase in the subglottal pressure (air pressure in the infraglottic area) until it reaches a threshold value, named the phonation treshold pressure (PTP) or the oscillatory "onset" pressure. This threshold is required to balance the closure of the glottis and let the pulmonary airflow pass through [257]. The resulting re-opening of the glottis induces a new release of the subglottal pressure, yielding to the combination of three

competitive mechanisms: the airflow from the trachea tends to keep the glottis open, whereas the Bernoulli effect, produced by the gradient of pressure between the folds [258], as well as their elastic recoil, recalls them back so as to close the glottis until the onset pressure is attained once again. Under appropriate geometrical, aerodynamic and mechanical conditions, these mechanisms are periodically repeated, resulting in self-sustained vocal-fold vibrations.

Therefore, contrary to the case of the heart, such oscillations do not result from any periodic muscle activity: laryngeal muscles drive the vocal-fold stretching, adduction and abduction, but their periodic self-sustained oscillations emerge from "passive" fluid/structure interactions between the airflow and the vocal-fold tissue. The vocal folds can be seen as a system of nonlinear and coupled oscillators, able to bifurcate toward complex regimes of vibration, responding to gradual variation of geometrical (*e.g.*, their distance or mean glottal width), mechanical (*e.g.*, their stiffness) and aerodynamical (*e.g.*, air pressure) parameters. *In vivo*, vocal folds are subjected to numerous complex and coupled 3D mechanical loadings, experienced upon finite strains at various strain rates: longitudinal tension and compression mainly due to laryngeal muscular contraction, transverse compression as a result of aerodynamic forces and vocal-fold collisions, as well as longitudinal and transverse shear arising from oscillatory motion and frictional contact mechanisms [54, 191].

To provide an order of magnitude, the fundamental frequency of vocal-fold vibrations, f_0, can vary from 50 to 1500 Hz and relates to the tonal pitch: usual speech frequencies can range between 140 and 240 Hz for females and from 100 to 150 Hz for males [98, 160]. Indeed, differences in vocal fold length and thickness result in different vocal pitches: adult male voices are usually lower-pitched than female voices due to longer and thicker folds. Additionally, genetic factors cause variations between members of the same sex, categorizing the different voices into voice types. The intensity of the produced sound corresponds to the amplitude of the wave, and is rather related to the subglottal pressure, which can vary between 300 and 3600 Pa on average [131]. Finally, vocal folds can exhibit numerous patters of vibration as well as degrees of collision, which is rather associated to perceptual differences in voice quality.

Despite the small size, human vocal folds own remarkable vibro-mechanical performances allowing them to generate an outstanding range of sounds compared to that of a musical instrument. These performances, unique in the human body, are possible due to three major properties of the vocal-fold tissue at the macroscale: (i) the ability to endure large reversible deformations during phonation, typically varying between 10–50% stretch during a glide or intonational variations. The elastic recoil takes place in spite of the periodic collisions and 3D multiaxial mechanical stresses the vocal folds are subjected to; (ii) the ability to vibrate with a fundamental frequency of less than 50 Hz to more than 1500 Hz (mean values of 125, 210 and 300 Hz in men, women and child speech, respectively). This frequency range is significantly higher than that of other biological oscillators (*e.g.*, heart and respiratory frequency, at and below 1 Hz, respectively); (iii) the ability to adapt its vibro-mechanical response to external loading

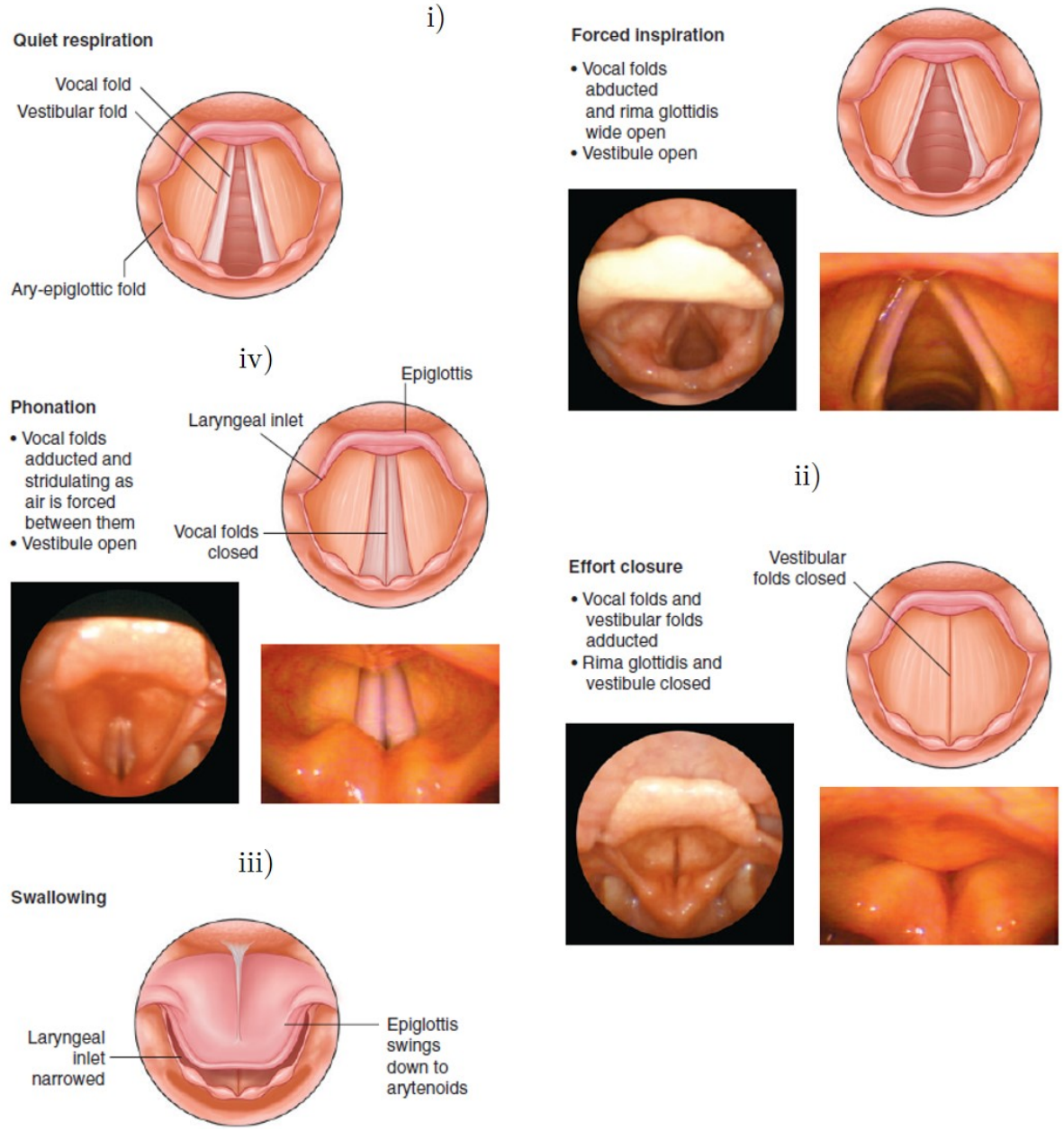

Figure 1.7: Vocal fold configurations and role during (i) quiet and forced respiration; (ii) effort closure; (iii) swallowing; (iv) phonation. Adapted from [70].

conditions, generated by the vocal-tract resonators, and environmental changes (*i.e.*, temperature, humidity). Typically, vocal-fold vibrations occur at 37°C and 100% of relative humidity, and gradually stop as the tissue's upper *mucosa* dries out at ambient conditions.

1.2 Clinical motivations

Like other tissues in the human body, vocal folds can be subjected to many infections, tumors and trauma, resulting in possible tissue damages. The main vocal-fold lesions

are presented below, together with the current therapeutic options and limitations. This clinical background points out the need for further in-depth research on the fundamental processes driving human phonation.

1.2.1 Vocal-fold lesions

Due to their multiple physiological functions (*e.g.*, voicing, breathing, swallowing) and their specific anatomical location in the aero-digestive tract, vocal folds are repeatedly exposed to a number of injurious stimuli. In fact, they commonly withstand phonotrauma (*e.g.*, periodic collisions, vocal abuse, for instance excessive throat clearing, coughing, screaming or yelling, or vocal misuse, *i.e.*, improper use such as speaking very loudly or at an abnormally high or low pitch), chemical trauma (*e.g.*, smoke and pollutants inhalations, alcohol, gastroesophageal reflux) and non-phonatory mechanical trauma (*e.g.*, intubation, microsurgery). Congenital predisposition to malformations of the laryngeal complex is an other possible cause for vocal-fold lesions.

Despite marked self-healing properties [31], the vocal-fold tissue can be damaged past a critical threshold of injury, leading to mild or severe lesions. Most frequent vocal-fold lesions are classified as benign lesions (often due to phonotrauma) or cancerous lesions, also called *carcinomas* (often due to chemical trauma) [231]. These tissue lesions come along with multiple voice disorders, ranging from *dysphonia* (loss of normal vocal function, *i.e.*, hoarseness, breathiness, voice with multiple tones, loss of vocal range) or *aphonia* (*i.e.*, inability to produce voiced sounds) in case of benign lesions, up to severe complications and the negative impact they have on the quality of life (*dyspnea*, *i.e.*, shortness of breath, or *dyshagia*, *i.e.*, difficulty in swallowing) for cancerous lesions. *Dysphonia*, for instance, occurs when injury-induced changes in the tissue composition and biomechanics prejudice vocal fold posturing and mucosal wave initiation/propagation [21, 225]. In addition to vocal dysfunction, patients may also experience frequent coughing, throat clearing or general fatigue. According to conservative estimates, *dysphonia* is considered to affect 28,000,000 people in the US only [260].

- *Benign lesions* – The most frequent benign vocal-fold lesions include nodules, polyps, Reinke's *edema* and cysts, illustrated in Figure 1.8 a-d. In general, benign lesions are characterized by a structural disruption and thickening of the tissue, vascular changes and alterations in the tissue composition [102].
  Vocal-fold nodules, sometimes addressed as singer's nodules or nodes, are small and hard callous-like growths, developing in pairs in the midpoint of the vocal folds (one nodule on each vocal fold, see Figure 1.8 a). They are occasionally associated with abnormal blood vessels. Women between the ages of 20 and 50 years old are more prone to vocal-fold nodules, but both men and women can be affected by them.
  Vocal-fold polyps are different from nodules because they can occur on either one or both vocal folds. They tend to be more vascularized than nodules, thus appearing reddish in color (see Figure 1.8 b). Polyps can vary in size and shape but are usually soft growths, larger than nodules, and resemble blisters.

A different type of vocal fold polyp, termed *polypoid corditis* or Reinke's *edema*, is associated almost exclusively with smoking [111]. It is a polypoid degeneration of one or both vocal folds within Reinke's space (superficial layer of the fold, beneath the epithelium), denoted by a swelling of the subepithelial space.
Finally, vocal-fold cysts are growths characterized by a sac around a fluid-filler or semisolid center (see Figure 1.8 c).

- *Cancerous lesions* – An estimated 10,000 cases of vocal-fold cancer are diagnosed each year in the US. Most cancer experts agree that vocal-fold cancer likely starts as small areas of abnormal cells (*dysplasia*) undergoing sequential changes, that ultimately lead to the development of a cancer. Pre-cancerous lesions may appear as a white or red plaque on the vocal fold, whereas cancers themselves are often larger and thicker than the precancerous lesions. A case of *carcinoma* is illustrated in Figure 1.8 e. Research suggests that removing pre-cancerous lesions may reduce the risk of developing cancer. Cancerous tumors are life threatening if not caught and treated in their early stage. Hopefully they are highly curable and detectable by the appearance of hoarseness (general term describing abnormal voice changes), induced by the vocal fold lesion, that often prompts early evaluation. Other symptoms include chronic sore throat, cough that can bring up blood, sensation of something stuck in the throat or more generally difficulties in breathing and swallowing.

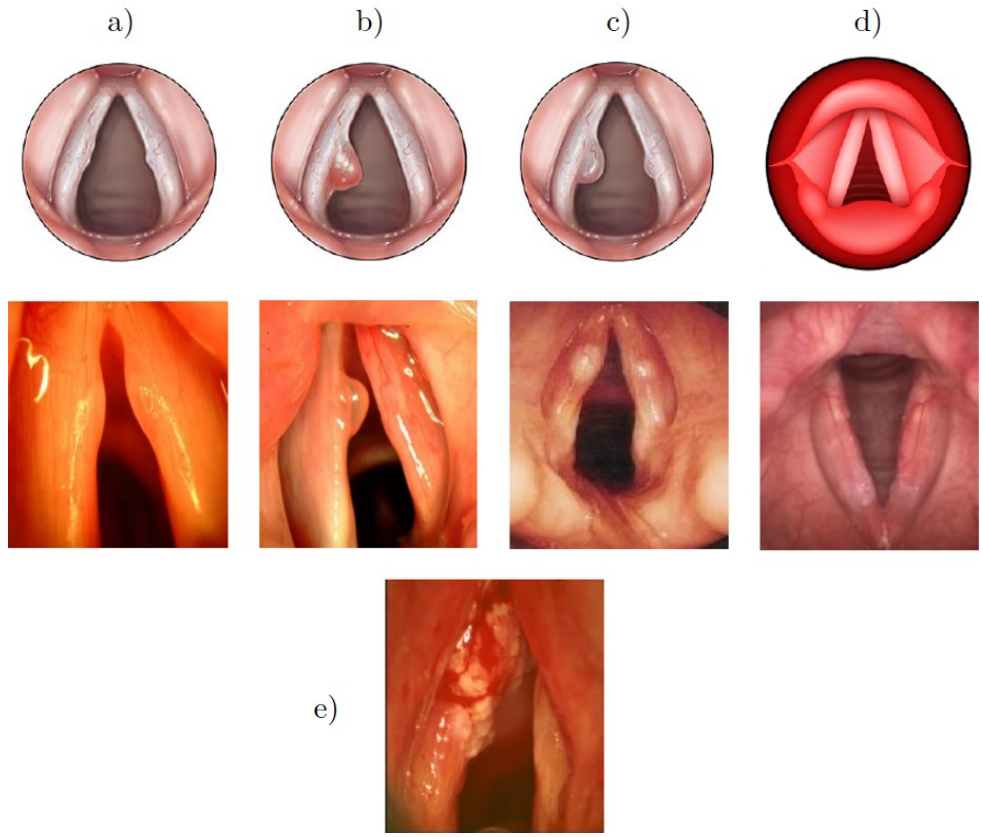

Figure 1.8: Vocal fold lesions. Schematic portrays and/or real case pictures of vocal folds a) nodule; b) polyp; c) cyst; d) laryngitis and e) *carcinoma*. Adapted from [262, 263].

Expected duration of the pathology varies according to the nature of the lesion. Non-cancerous lesions generally do not go away, they must be treated. Vocal-fold nodules can last a lifetime without changing the vocal abuse, they can even come back after therapeutic treatment. With proper voice training instead, they can disappear within 6 to 12 weeks. Vocal fold polyps, with rest, sometimes go away on their own within a few weeks. Most, however, have to be treated. Cancerous tumors must be treated as soon as possible to prevent the cancer from spreading. Current therapeutic options are described hereafter, along with possible complications.

1.2.2 Therapeutic treatments and limitations

Depending on the diagnosis (cause, severity of symptoms, time from the onset of symptoms, location, size etc.), the most indicated and effective therapy may include one or a combination of the following treatments.

- *Voice therapy* – Voice therapy aims at correcting ill-adapted vocal fold gestures through manual laryngeal manipulation, exercises or other activities to strengthen vocal folds, improve breath control during speech, prevent abnormal tension in surrounding muscles and protect the airway during swallowing. This technique relies on a strong know-how of the practitioners, expecting a continuous insight into fundamental phonatory biomechanics to improve their clinical plans.

- *Laryngeal (micro)surgery* – Surgical invasive options consist in bulk injections (with a substance such as body fat, collagen or other approved filler substances), vocal-fold re-positioning, partial or complete cordectomy (*i.e.*, excision of the vocal-fold lesion or resection of the damaged tissue) [215], tracheotomy (*i.e.*, incision in the front of the neck, creating an opening into the trachea bypassing vocal folds), and even partial or total laryngectomy (*i.e.*, partial or total removal of the entire larynx, including the vocal folds) for late-stage cancers. The main objective of vocal-fold cancer treatments is to completely remove or destroy the cancerous growth while preserving as much normal tissue and function as possible. In fact, removing portions or all of a vocal fold can clearly have profound effects on voice quality and swallowing. After total laryngectomy, people need to learn a new speech method, using a special valve inserted surgically between the trachea and the esophagus. This allows air to be sent up the esophagus, creating enough vibrations for understandable speech.

- *Radiation and chemotherapy* – Radiation is the primary treatment for some early-stage laryngeal cancers: it uses high-energy X-rays or particles to destroy cancer cells and prevent them from spreading, shrinking the tumor. Although radiation treatment technology has significantly improved over the years, doses of radiation needed for definitive treatment of vocal-fold cancer may sometimes lead to long-term voice and swallowing problems. Nonetheless, studies have shown that people who are treated with radiation tend to live longer and exhibit less voice problems. If the cancer is small, it can often be destroyed by radiation and surgery is not needed. This can help

to preserve better voice quality. This therapy is essential for people who are too sick to undergo surgery or chemotherapy. Radiation or cordectomy are usually enough to treat most glottic cancers unless there is evidence that the treatment might not have cured the cancer (*e.g.,* finding cancer cells at the edge of the removed tumor). If more treatments are needed, many times chemotherapy is given at the same time as the additional radiation. This combination, called chemoradiation, often works better than radiation alone but it also has more side effects. Alternatively to cordectomy, laser surgery is a viable solution to excise the tumor. Some voice normally remains after these procedures. In worst cases laryngectomy is still required.

Complications of invasive surgical operations may result in vocal-fold scarring (fibrosis), possibly leading to inconsistent results and, in worst cases, to the loss of phonatory abilities. Scarring is the most common cause of *dysphonia* after vocal-fold surgery [110, 268]. Functional consequences include compromised mucosal wave generation and glottic incompetence, as well as incomplete closure of the vocal folds during adduction [153]. Recent studies have examined histological changes after vocal fold scarring in various animal models observing that scars are related to alterations of the tissue superficial layers fibrous structure [127]. Nonetheless, while invaluable experimental models, it should be noted that all animal species exhibit substantial differences in phonatory ability, tissue structure and composition with respect to humans. Dealing with these post-operative complications, alternative restorative solutions have been deemed and investigated over the last decades and are still subjects of ongoing research:

- *Biomaterials* – Biomaterials implantation consists in the injection of a biomaterial into the injured vocal-fold tissue, especially to correct its geometrical configuration (*e.g.*, increase its bulk, medialize its position and improve glottal closure [224]). Critical factors in the proper selection of injectable materials concern injections site, material stability/degrability and mechanical properties. Early investigations for vocal-fold injection were on Teflon and silicone [7, 151]. The long-term efficacy of these materials, primarily injected into the *vocalis* muscle, is generally limited by foreign body response, implant migrations and inflammations [71, 198]. More recent vocal fold augmentation studies focus on the use of biologically derived materials with intrinsic degradability and mechanical properties closely resembling those of the native tissue [145, 153]. Even though the *vocalis* represents the most frequently adopted injection site, many superficial applications of collagen, fat and *fascia* directly injected in the *mucosa* have been equally investigated [30, 83, 217]. Chan and Titze evaluated a variety of materials used in vocal fold augmentation (*e.g.*, crosslinked collagen, fat, gelatin, Teflon) and demonstrated that solutions of native hyaluronic acid (HA) most closely approximate the shear properties of the human vocal *muscosa* [42, 43]. This is not surprising considering that HA influences a number of tissue properties relevant to phonation (*e.g.*, shock absorption, space filling and viscosity). Despite these promising results and improvements in anatomical structure and vocal function, current limitations include potential resorption necessitating either initial over-injection or repeated injections [224].

- *Regenerative therapies* – Researchers are showing growing interest in approaches to the treatment of vocal fold injuries based on principles of regenerative medicine (tissue engineering) [99, 162]. The aim of these therapies is to support functional recovery of normal vibratory behavior and phonatory capability by inhibiting the progression of the wound healing process to scarring, and to restore the natural tissue *mucosa* composition and biomechanical properties. In continuity with prior studies on injectable biomaterials, major efforts are addressed to the development of scaffolds closely approximating the native tissue biomechanics and that may be introduced by minimally invasive techniques [166, 167]. Several studies have shown that HA plays a critical role in determining the shear properties of the vocal *mucosa*, leading it to be the most widely investigated scaffold material for regenerative applications [78, 79]. Additional regenerative therapies are cell transplantation [17, 184], to replace dysfunctional cells and regenerate the injured tissue, and the delivery of soluble bioactive molecules to enhance the efficiency of the healing process [52]. However, these latter techniques may trigger tumor formation and development, related studies towards human *in vivo* applicability are therefore still in progress and limited to *in vitro* employments.

In conclusion, regardless of the vocal-fold lesion, it is clinically observed that the tissue's *mucosa*, made of collagen and elastin reinforcements embedded in a matrix of hyaluronic acid, represents the major critical site of the vocal-fold damage process. This results in the systematic alteration of the mucosa's fibrous microstructure, which comes along with a dysfunction of the tissue macroscale vibro-mechanical performances. Therefore, an in-depth knowledge of the vocal-fold fibrous microstructure and multiscale mechanics impact on its vibratory performances would, from a clinical perspective, facilitate the prevention, identification and understanding of voice disorders, and provide a tangible guidance for improved treatments.

1.3 Vocal-fold tissue histology and mechanics : acquired knowledge from experimental evidence

This section presents a review of the vocal-fold multiscale structural and mechanical properties acquired knowledge based on experimental evidence. The state-of-the-art is followed by a summary of current limitations to be addressed in order to better understand the relationship between the vocal-fold tissue histo-mechanical characteristics and its vibratory properties, as described in Section 1.1.2.

1.3.1 Histological features

Adult vocal folds are known to possess a specific lamellar mesostructure made of three major layers, as displayed in Figure 1.9: an *epithelium* covered by *mucus*, a *lamina propria*

(made in turn of three sublayers), and a stratified muscle (thyroarytenoid or *vocalis*). A general description of each vocal-fold layer is provided in the following.

- *Epithelium* – By contrast with the laryngeal *epithelium*, being mainly a ciliated, pseudostratified respiratory *epithelium*, the vocal-fold most external layer is a thin (approximately 50-60 μm thick) non-keratinized, stratified squamous *epithelium* (see Figure 1.9 a and b). It is composed of closely aggregated polyhedral cells adhering firmly to each other, and to a thin layer of extracellular matrix (ECM). This represents a significant histological variation, conceived to protect the tissue from the mechanical stresses acting on the vocal folds surface (*e.g.*, dynamic impacts ascribed to vocal-fold collisions, abrasion and desiccation from rapid air movements).

- *Lamina propria* – The *lamina propria* is a 1-3 mm-thick loose connective tissue just underneath the mucosal *epithelium*. At birth, the *lamina propria* consists of a single layer of cells. It becomes a bilaminar structure by 2 months of age. Three sublayers are established by 7 years of age [112] (see Figure 1.9 b). The most superficial sublayer constitutes, together with the *epithelium*, the so-called "*mucosa*". It is a nearly 500 μm-thick connective tissue consisting of loose collagen and elastic fibers barely attached to the underlying layers: this specific arrangement produces a sort of space comparable to soft gelatine and called "Reinke's space". The intermediate and deep sublayers of the *lamina propria* are both about 1-mm thick tissues, primarily made up of elastic and collagen fibers respectively. These two sublayers collectively form the "vocal ligament".
  The three sublayers of the *lamina propria* are characterized by distinct fibers' type, density and waviness. While the concentration of the fibrous components is observed to gradually increase from superficial to deep sublayers [176], the fiber waviness typically decreases [15]. On a first approximation, the 3D fibrous networks in the *lamina propria* commonly exhibit a pronounced orthotropy with a preferential major orientation along the antero-posterior direction, and minor and intermediate orientations along the inferosuperior and mediolateral directions, respectively [15] (see Figure 1.10). The *lamina propria*, as a whole, significantly contributes to the tissue's "passive" biomechanical properties (stiffness, elasticity, viscosity) and to the regulation of its water content.

- *Vocalis* – The deepest layer of the vocal fold is primary made of the inferior thyroarytenoid muscle or *vocalis* muscular fibers. These fibers are mainly aligned along the antero-posterior axis, exhibiting a rather transverse isotropy structure [15]. The *vocalis* represents the most voluminous portion of the vocal fold tissue with a thickness of approximately 7-8 mm [250]. This layer is responsible for the tissue "active" contractile properties. The inertia and stiffness of the *vocalis* vary according to the degree of contraction required to reach a given phonatory posture (*e.g.*, shortening, increasing the vocal-folds thickness).

For the sake of simplicity, the vocal-fold multi-layered arrangement is often considered as a bi-layered "body/cover" structure [117, 236, 252]: (i) the "body" gathers the deepest *lamina*

propria's sublayer, together with the *vocalis*; (ii) the "cover" includes the *lamina propria*'s superficial and intermediate layers, together with the *epithelium*. This concept, generally used to model the vocal-fold vibrations (see Section 1.4.1), suggests that the vocal fold can be regrouped into two tissue layers with different histological and, therefore, mechanical properties (see Section 1.3.2).

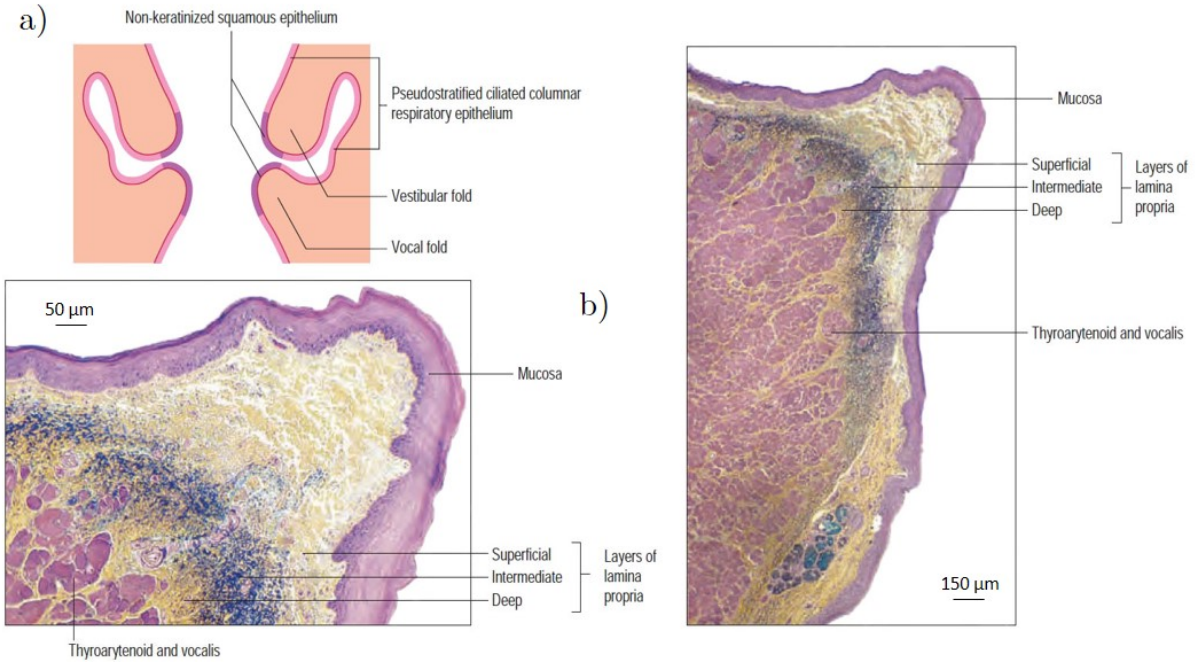

Figure 1.9: Histology of the human vocal-fold tissue: a) coronal view illustration of the laryngeal cavity and its *mucous* membrane distribution; b) vocal folds structure at (left) low and at (right) high power, stained with Movat's pentachrome stain. At higher magnification, the deeper yellow staining of the collagen in the deep layer of the *lamina propria* compared to the superficial layer indicates a higher degree of cross-linking. Adapted from [94].

A further description of the *lamina propria* and *vocalis* microstructure isolated constituents is provided hereafter.

Within the lamina propria – The main components of this connective tissue are cells and the extracellular matrix (ECM). Cells are mainly responsible for the production of the ECM components (*e.g.*, fibroblasts, myofibroblasts) and bring a minor mechanical contribution compared to that of the ECM. The ECM consists instead of different combinations of protein fibers (collagen, reticular and elastic fibers) and amorphous ground substance [172] :

- **Collagen** is the most abundant protein in the human body, representing 30% of its dry weight. A family of 28 collagen types exists in vertebrates, numbered following the identification order [84]]. They are categorized according to their microstructure and, thus, function they cover to ensure different roles. In the vocal folds, six types of collagen are reported to be found : Type I, Type II, Type III, Type IV, Type V and Type VI [96, 105, 244]. While types from IV to VI are associated to the epithelial portion [96, 244], types I, II and III are observed within the *lamina propria* [176]. Yet, **collagen Type I and Type III** are the most abundant categories, and majorly contribute in terms of mechanical properties. Collagen I is considered to have a thicker structure and

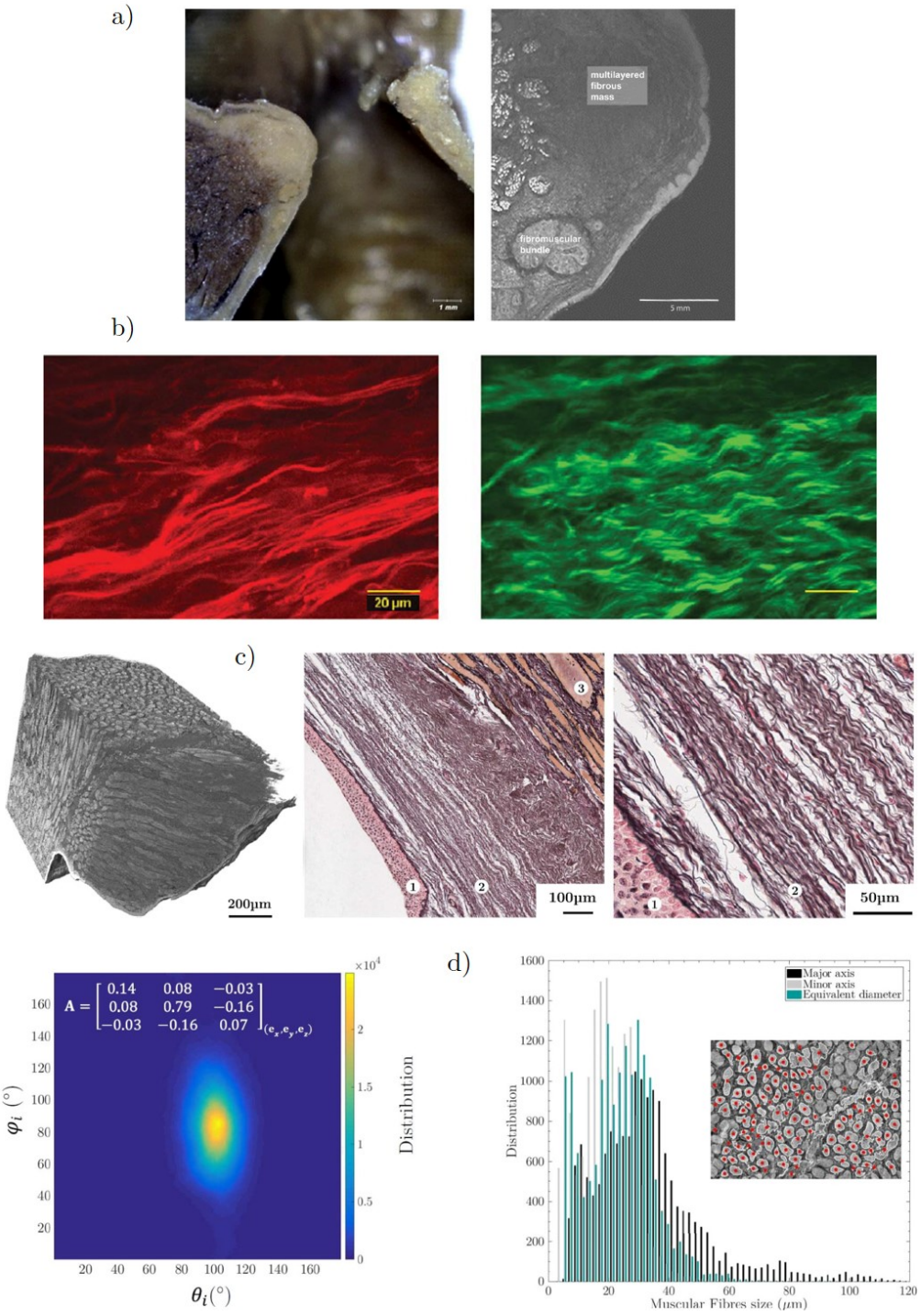

Figure 1.10: Micro-imaging of human vocal fold at rest: a) plastinated vocal folds and MRI imaging carried out by Klepacek *et al.* [147]; b) typical images of elastic and collagen fibrils networks provided by Miri *et al.* (different colors refer to different imaging modalities: two-photon fluorescence, red, and second harmonic generation, green) [192]; c) 3D reconstruction of a *vocalis* sample imaged by synchrotron high-resolution X-ray micro-tomography (left), 2D histological photomicrographs prepared with Reticulin stain (black-violet: collagen fibers; orange: muscle fibers; pink: *epithelium*) reported by Bailly *et al.* [15] (right); d) geometrical descriptors obtained from previous X-ray synhcrotron imaging: 3D orientation map of the collagen and elastin fibrous network in the *lamina propria* (left), statistical characteristic size of muscular fibers in the *vocalis* [15] (right). Adapted from [15, 147, 192].

a higher resistance to traction compared to Type III [84]. Collagen fibers are often grouped into larger aggregates, bundles, packaged and linked together (mean fiber diameter from 1 to 20 μm). At lower scales, collagen fibers themselves constitute assemblies of collagen nanofibrils gathered and interconnected by proteoglycans [85], as displayed in Figure 1.11 a. Within the *lamina propria*, higher levels of collagen are found in male vocal folds than in female's, for both the cover and the ligament [47]).

- **Reticular fibers** mainly consist of collagen Type III, forming an extensive network (*reticulum*) of thin (diameter 0.5-2 μm) fibers for the support of many different cells and are therefore often assimilated to collagen fibers.

- **Elastic fibers** are thinner than Type I collagen fibers. They form sparse networks interspersed with collagen bundles in many human organs [100], particularly those subjected to regular stretching or bending. As the name suggests, elastic fibers display rubber-like properties allowing biological tissues to be stretched and reversibly return to their original shape [3, 62, 172] and therefore conferring them a high mechanical resilience. Furthermore, elastic fibers are made of fibrillin (350 kDa), forming a network of microfibrils (10 nm in diameter) embedded in a cross-linked elastin larger mass (60 kDa) [195, 214]. Both proteins are secreted from fibroblasts and give rise to elastic fibers in a stepwise manner: fibrillin fibrils are assembled around the amorphous structure of elastin to form the ultimate elastic fiber [126, 261]. The amount of elastin within the vocal folds is considerably high (8.5% of the total proteins) compared to that of other elastic structures (*e.g.*, human skin, 3% of the total proteins) [104, 109]. Although the contribution of elastin to the vocal-fold mechanics still remains elusive, such high content possibly explains their remarkable self-healing properties, fundamental to recover from the large-strains and cyclic loadings endured by the tissue during phonation.

- The **ground substance** of the ECM is a highly hydrated (with much bound water) complex mixture, comprising three major kinds of macromolecules: proteoglycans, glycoproteins, and glycosaminoglycans (GAGs). Water in the ground substance is referred to as interstitial fluid, and has a composition similar to that of blood plasma. Filling the space between cells and fibers in connective tissues, the ground substance allows diffusion of small molecules and, on account of its viscous nature, acts as both a lubricant and a barrier to the penetration of intruders. Physical properties of the ground substance also profoundly influence various cellular activities.
  Proteoglycans and glycoproteins are both hybrid components consisting of core proteins covalently attached to various numbers and combinations of polysaccharide chains [95]. The principal proteoglycans include aggrecan, decorin, fibromodulin and perlecan, whereas the most important glycoproteins are the fibroconnectin and the laminin. These interstitial molecules play different roles within the *lamina propria* but mainly act as biological filters [95]. In defiance of taking part to structural preservation of the tissue, proteoglycans and glycoproteins molecules are deemed to bring a minor mechanical contribution [95].

GAGs are long polymeric chains of repeated disaccharide units. The largest and most ubiquitous GAG is **hyaluronic acid** (also called hyaluronan or hyaluronate). Hyaluronic acid (HA) forms a viscous, pericellular network that binds a considerable amount of water, favoring molecular diffusion through the connective tissue, and lubricating various organs and joints in the body [157, 159, 267]. Conversely to previous interstitial molecules, HA primarily contributes to the preservation of the tissue 3D structure [113, 157]. Within the *lamina propria*, due to its viscous nature, HA also acts as a shock absorber, damping the energy transfer produced by collisions and aerodynamic loadings acting on the glottal surface, thereby protecting the inner portion of the tissue [46]. Finally, HA levels are found approximately three times greater in men than in women [35, 109].

Within the vocalis – In the human body, muscle tissue is the fourth "basic" tissue type with *epithelia*, connective tissues and nervous tissue. It is composed of cells that optimize the property of contractility: actin microfilaments and associated proteins generate the forces necessary for the muscle contraction, driving movements within organ systems of the body as a whole. Three types of muscular tissue (*i.e.*, skeletal muscle, cardiac muscle and smooth muscle) can be distinguished on the basis of their morphological and functional characteristics, the structure of each being adapted to its physiological role.

In particular, skeletal (or striated) muscles, as the *vocalis*, are made up of **muscle fibers** (also called "muscle striated cells" or "*rhabdomyocytes*"), which are long, cylindrical multi-nucleated cells with diameters of 10-100 μm [163, 172] (see Figure 1.11 b and Figure 1.10 c). During embrionic muscle development indeed, myoblasts fuse forming myotubes with many *nuclei*. More particularly, the *vocalis* muscle is prevalently composed of Type II cells (white muscular fibers, also called "fast" muscle cells, as opposed to Type I or "slow" muscle cells) [119, 230]. Individual muscle fibers seldom extend from one end of a muscle to the other. Bundles of muscular fibers, termed fascicles, make up a functional unit in which the fibers work together. The single muscle fiber is in turn highly organized, containing primarily long cylindrical filaments called myofibrils that run parallel to the long axis of the fiber and constitute the basic rod-like unit of a muscle fiber [118, 163, 172] as represented in Figure 1.11 b. Finally, as in all other muscles (and specifically in skeletal ones), **intramuscular connective tissue** (primarily made of collagen) is also found within the *vocalis*. Thin layers of connective tissue called *epimysium*, *perimysium* and *endomysium* surround and organize the muscular contractile fibers and fascicles, as sketched in Figure 1.11 b . Such connective tissue aims at transmitting the mechanical forces generated by the contracting muscle to surrounding cells/fibers.

1.3.2 Tissue mechanical behavior

By contrast with many soft tissues (*e.g.*, arteries, skin), vocal folds are not easily reachable *in vivo* by any medical 3D imaging techniques, due to their surrounding protective cartilages. Gold standard techniques used for their direct visualisation (high-speed cinematography, videostroboscopy) only provide partial 2D views of the vocal-fold superior plane (see

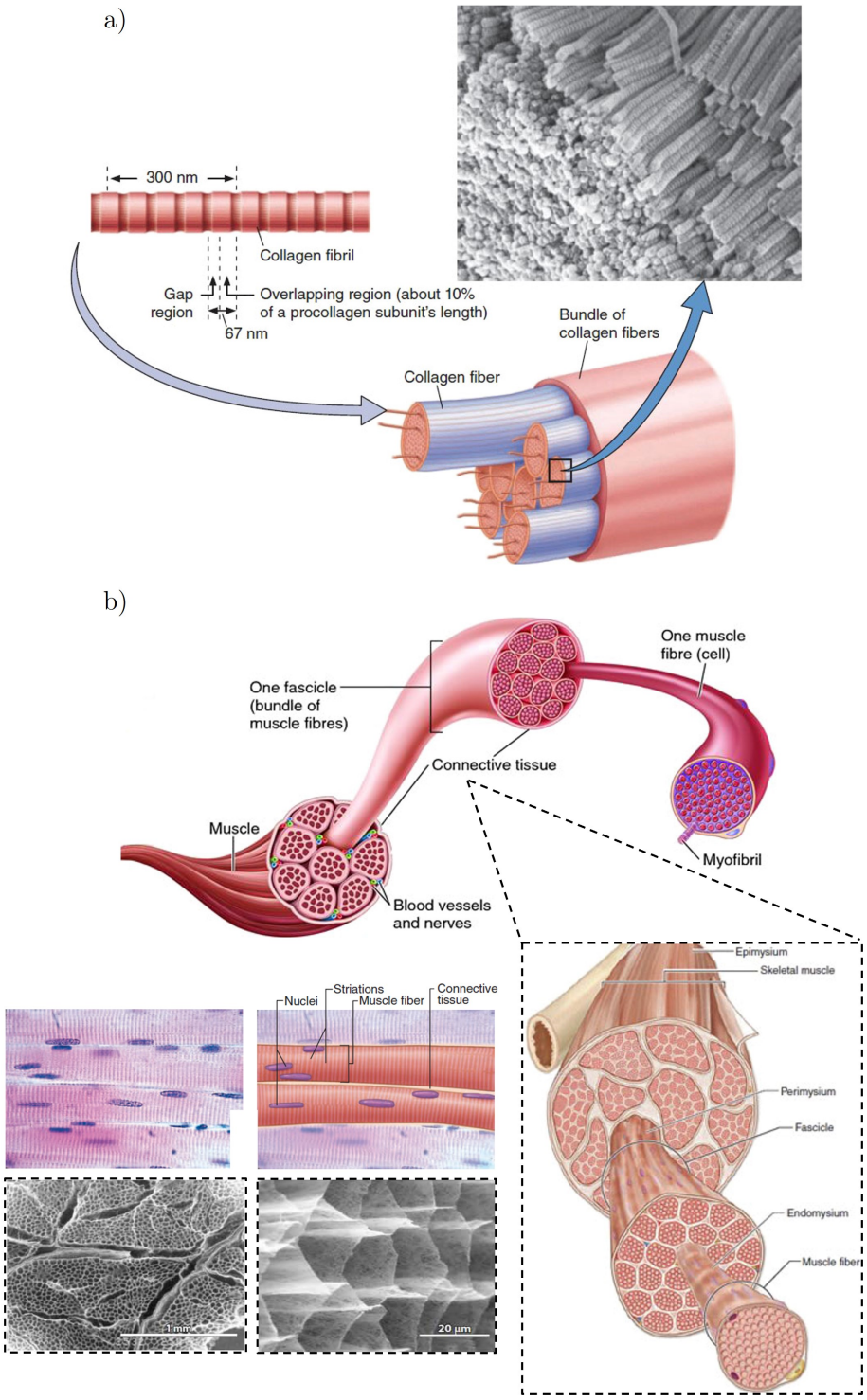

Figure 1.11: Hierarchical multiscale assembly of a) collagen and b) muscle fibrous architectures. Collagen fibrils assemble and are linked together in larger collagen fibers that often form into larger aggregates bundled and linked together by other collagen. *Vocalis* muscle is composed of large, elongated, multi-nucleated fibers with cross-striations. It is enclosed within a thick layer of dense connective tissue (*epimysium*) and contains several fascicles of muscle fibers, each wrapped in a thin but dense connective tissue layer (*perimysium*). Within fascicles, individual muscle fibers are surrounded by a delicate connective tissue layer (*endomysium*) and contain several parallel bundles called myofibrils. Adapted from [26, 189].

Figure 1.8 for instance). Besides, the actual mechanical loadings applied on the tissue are hardly measurable *in vivo*. Thereby, it is very delicate to perform any quantitative biomechanical measurements under physiological *in situ* conditions. Alternatively, the mechanical properties of the vocal tissue have been mainly investigated on excised vocal folds so far. Acquired *ex vivo* data are reported hereafter, first at the scale of the vocal-fold tissue (or that of its constitutive layers), then at the scale of its main micro-constituents.

Tissue and layers scale (macro, meso)

Quasi-static loadings – Previous authors have mostly characterized the vocal-fold tissue's mechanical response under quasi-static loadings, focusing on its "passive" nonlinear and anisotropic stress-strain response [47, 51, 54, 68, 93, 143, 148, 190]. Within this category, two types of experiments were conducted on human or animal dissected vocal folds over the last decades:

- "Structural" mechanical tests performed on 3D excised (hemi)larynges, where vocal folds are still connected to their original anatomical environment (thereby closer to the native tissue physiological conditions). These tests generally yielded to 3D deformation fields of the vocal-fold superficial layer, in response to static tensile local forces [69].
- "Material" mechanical tests, more frequently performed on thin membranes excised from the vocal folds. These tests mainly consist in uniaxial tensile tests or aspiration/indentation tests, leading to in-plane stress-strain responses or maps of local elastic moduli respectively, ranging from a few kPa up to few MPa according to the applied level of strain and loading direction [47, 143, 148, 190, 254, 275]. Typical stress-strain curves and evolution of tangent moduli during loading are illustrated in Figure 1.12 a, in the case of several *vocalis* samples subjected to a cyclic tensile test in the longitudinal direction [53].

These prior studies point out the progressive strain-stiffening response of the tissue stretched along its longitudinal direction (antero-posterior axis), as well as its typical hysteretic behavior during load-unload tensile sequences. Even if vocal folds strain-induced microstructural evolution is still to be characterized experimentally, the tensile J-shaped stress-strain behavior is often attributable to the progressive deployment, and corresponding mechanical contribution, of wavy collagen fiber bundles. The stress hysteretic behavior observed during cycling is instead often postulated to be ascribable to viscoelastic effects related to structural rearrangements of the tissue. Comparing uniaxial tensile responses of the tissue's different sublayers, the vocal ligament was found to be stiffer than the cover for males, but quite the opposite was observed for females [47]. These studies additionally highlight the significant inter- (due to age and gender-related differences notably) and intra-subject variability of the obtained mechanical responses (see Figure 1.12 a), as for other soft living materials [37].

Recently, Cochereau *et al.* [54] extended the aforementioned mechanical database characterizing the cyclic and finite strain behavior of the *lamina propria* and *vocalis* layers of

human vocal folds under multiaxial loadings: the same tissues were successively subjected to tension, compression and shear to minimize the inter- and intra-individual variability. Nonlinear mechanical tendencies were observed for all loading conditions: a J-shape strain stiffening response under longitudinal tension and transverse compression, albeit far less pronounced in shear, stress accommodation and stress hysteresis regardless of the loading mode. Furthermore, recorded stress levels during longitudinal tension (*i.e.*, along the fibers preferential direction) were measured much higher for the *lamina propria* than for the *vocalis*. Nevertheless, *lamina propria* and *vocalis* responses under transverse compression as well as transverse and longitudinal shear were reported to be of the same order of magnitude.

Dynamic loadings – Vocal-fold mechanical properties time-dependency equally plays a major role, accounting for the dynamic stimuli the tissues are subjected to during phonation. In this respect, significant contributions focusing on dynamic loadings were brought by Chan et al. [40, 41, 44, 47] over these last decades. They characterized the viscoelastic properties of human vocal folds under shear loading, so as to better understand the "mucosal wave" propagation on the vocal fold surface during self-sustained oscillations [44, 95, 248]. They used both parallel-plate rotational [44] and simple-shear rheometers [41]. Typical measurements are reported in Figure 1.12 b and c, displaying the evolution of vocal-fold covers major dynamic viscoelastic quantities measured along the longitudinal direction (*i.e.*, dynamic elastic and viscous shear moduli G′, G″, damping ratio $\mu = G''/G'$, and dynamic viscosity $\eta = G''/\omega$, ω being the pulsation), as a function of the oscillation frequency (initially from 0.01 up to 15 Hz [44], later up to 300Hz [41]). For decades, measurements were carried out at, and limited to, small-strain amplitude oscillatory shear (SAOS). They were only recently extended to large-amplitude oscillatory shear (LAOS) testing [40] (see Figure 1.12 c).

These former studies show that dynamic moduli are increasing (resp. decreasing) nonlinear functions of the applied level of frequency (resp. strain), while the dynamic viscosity decreases monotonically with the frequency (*i.e.*, shear thinning behavior). More specifically, modulus G′ was observed to be lower than G″ at lower frequencies, until reaching a "cross over" point at about 50 Hz. In the frequency range before the crossover point, called the terminal region, G′ is lower than G″, with the specimens demonstrating a fluidlike response dominated by their viscous properties. In the frequency range after the crossover point, called the rubbery region or plateau region, G′ is higher than G″, indicating predominantly elastic properties in the specimens, a characteristic of viscoelastic solids. In other terms, the damping ratio ξ was found above 1 at lower frequencies (< 50 Hz), suggesting that the vocal fold cover was, on average, overdamped over this terminal region. Conversely, at higher frequencies, in the rubbery region the damping ratio was regularly below 1, meaning that the vocal fold cover remained underdamped such that oscillations could be readily sustained during phonation. An intersubject variability of an order of magnitude was finally observed, partially reflecting age-related and gender-related differences.

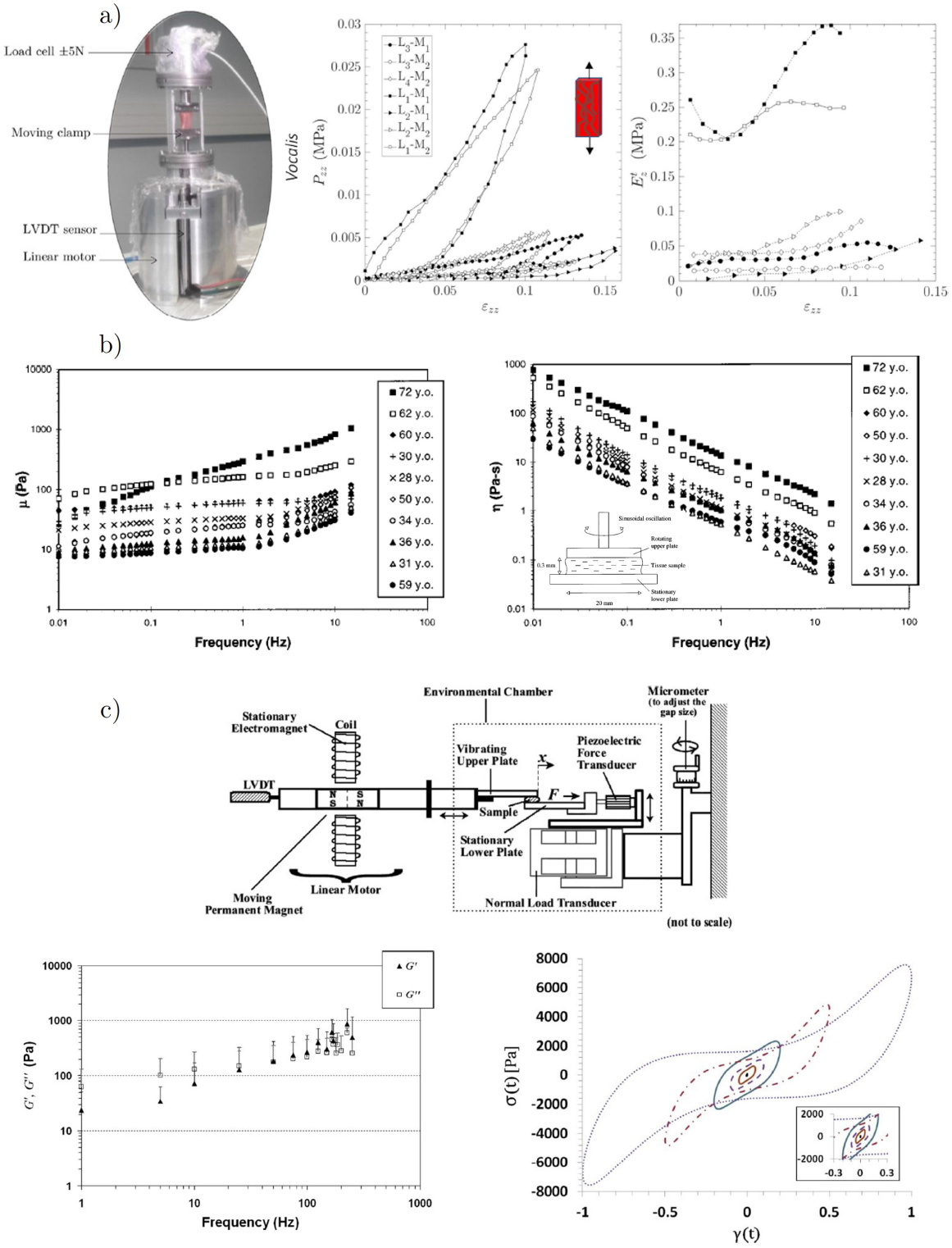

Figure 1.12: Macroscale mechanical characterization of the vocal-fold tissue: a) experimental strain-controlled micro-press device adopted by Cochereau *et al.* [54] (left) to obtain *vocalis* muscle tensile longitudinal stress-strain curves and moduli (right); b) dynamic storage modulus (left) and viscosity (right) measured at low audio frequencies by Chan and Titze [44] by means of a controlled-stress parallel-plate rotational rheometer; c) controlled-strain simple-shear rheometer system (top) used to acquire SAOS dynamic moduli (frequency varied between 1 and 250 Hz at 1% deformation) [41] (bottom left), later extended to obtain LAOS stress-strain curves [40] (bottom right). Adapted from [40, 41, 44, 54].

Micro-constituents scale (micro)

To the author's knowledge, there are hardly any data on vocal folds mechanics at the microscopic scale available in the literature. Although micro-mechanical characterization remains rather delicate, even for *ex vivo* conditions, there are nevertheless a few studies on the elementary constituents of other biological tissues or biomaterials. The acquired knowledge of collagen, elastin, muscle fibrils/fibres and HA (all major vocal folds microscopic components) mechanics is summarized below:

- **Collagen fibrils** – The mechanics of collagen at the fibrillar scale has been extensively characterized using atomistic modeling [90], atomic force microscopy (AFM) [238, 239, 259, 273], micro-electromechanical systems (MEMS) [73, 233, 234], nanoindentation [9] and X-ray diffraction testing [228] (see Figure 1.13). Gautieri *et al.* [90] reported a recapitulation of isolated solvated collagen fibrils different viscoelastic descriptors extrapolated from several authors' experiments (*e.g.*, Young's modulus, viscosity, relaxation modulus and time). These data are reported in Figure 1.13 e.
- **Elastin** – Due to the extensive cross-linking, elastin is nearly insoluble, and thus, structural information about elastin fibers remains limited. Nonetheless, Guthold *et al.* [103] report elastin fibers to have a Young's modulus of about 1 MPa and a large failure strain of 150%.
- **HA** – Bulk HA elastic and loss moduli were measured under quasi-static loading conditions by Heris *et al.* [115], using a controlled stress rheometer at room temperature, and compared to that of a hybrid HA/Ge hydrogel as displayed in Figure 1.14. Results show HA storage moduli ranging from 30 to 50 Pa and lower viscous moduli not exceeding 5 Pa.
- **Muscular fibers** – It was recently shown that human muscle fibers exhibit different passive mechanical properties when compared to those of muscular bundles, which contain a connective tissue matrix layer (*i.e.*, *perimysium*) that individual fibers do not (see Figure 1.15 b). Bundles display a larger nonlinear stress at a given strain, whereas single fibers often demonstrate a highly linear response. By comparing mechanical data obtained from a group of dissected individual fibers to that of a fiber bundle, Ward *et al.* [266] showed that the modulus nonlinear increase is attributable to the mechanical properties of the ECM. It was additionally found that the stress-strain curves nonlinearity and modulus magnitude considerably increase across the fiber, bundle, fascicle, and whole muscle size scales (see Figure 1.15 c).

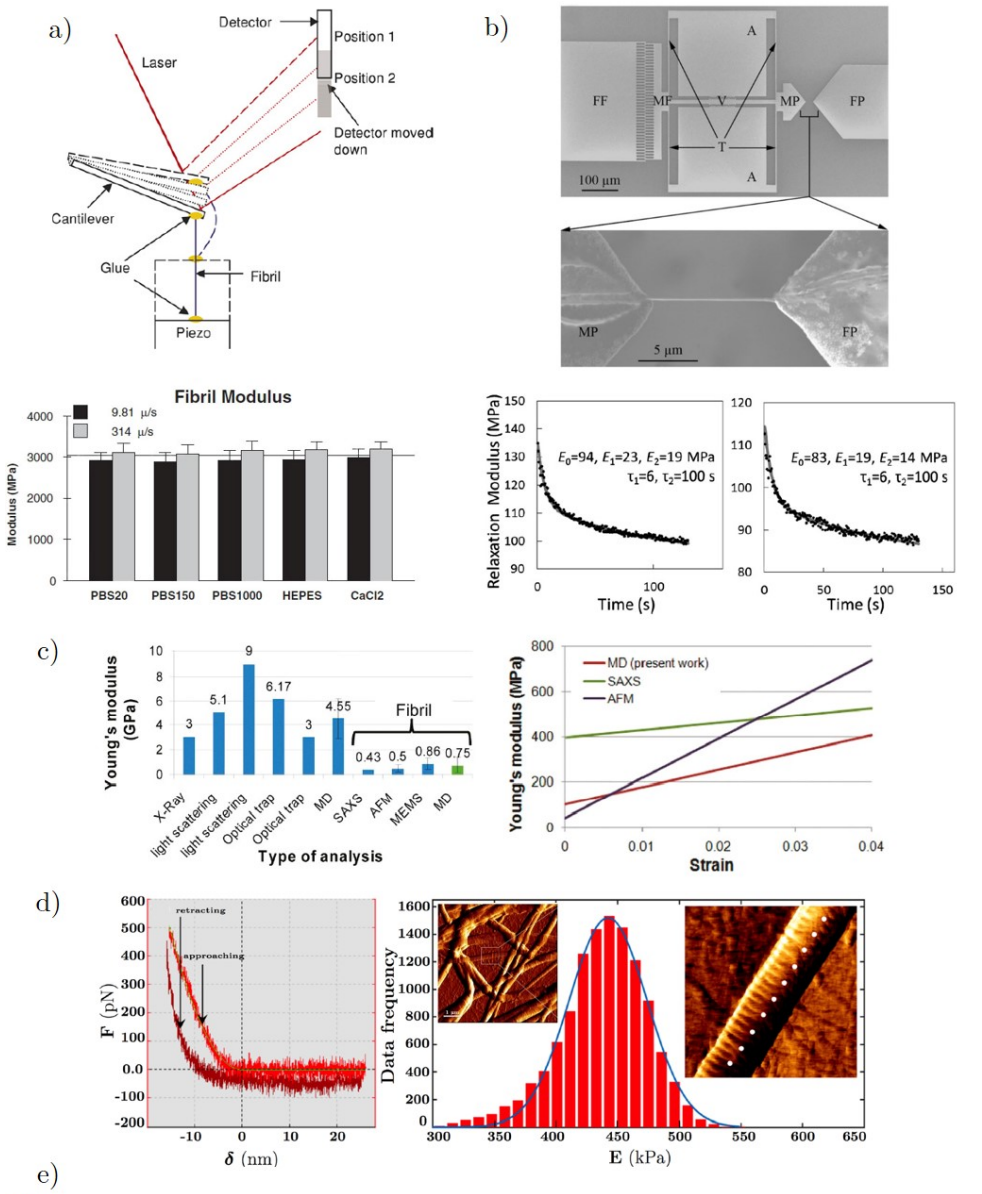

Table
Viscoelastic properties of solvated collagen fibrils and collagen molecules.

Fibril			
	Young's modulus (GPa)	0.43	X-ray diffraction (Sasaki and Odajima, 1996a)
	Average value 0.9 GPa	0.4–0.5	MEMS stretching (Eppell et al., 2006)
		0.2–0.5	AFM testing (Van Der Rijt et al., 2006)
		0.86 ± 0.45	MEMS testing (Shen et al., 2008)
		0.47 ± 0.41	MEMS testing (Shen et al., 2010)
		2.89 ± 0.23	AFM testing (Svensson et al., 2010a)
		1.87–1.94	AFM testing (Svensson et al., 2010b)
		0.3–1.2	Atomistic modeling (Gautieri et al., 2011)
		0.12 ± 0.05	MEMS testing (Shen et al., 2011)
	Viscosity (GPa·s)	0.09–1.63	MEMS testing (Shen et al., 2011)
	Relaxation time (s)	7–102	MEMS testing (Shen et al., 2011)

Figure 1.13: Micro-mechanical characterization of collagen fibrils: a) simplified schematic of the AFM set-up used by Svensson *et al.* [238] (top) to measure single collagen fibrils modulus at two deformation rates [239] (bottom); b) representative schematic of the MEMS mechanical testing device adopted by Shen *et al.* [233] (top) to characterize the viscoelastic relaxation-modulus-time behavior of individual collagen fibrils (bottom); c) direct comparison of the Young's modulus obtained for solvated single collagen microfibrils featuring various experimental results and the authors' atomistic model [90]; d) representative AFM results (detected force F versus tip-sample separation δ and Gaussian distribution of the elastic modulus) provided by Asgari *et al.* [9]; e) summary proposed by Gautieri *et al.* [91] of several experimental and computational studies aimed at characterizing solvated collagen fibrils viscoelastic properties. Adapted from [9, 90, 91, 233, 238, 239].

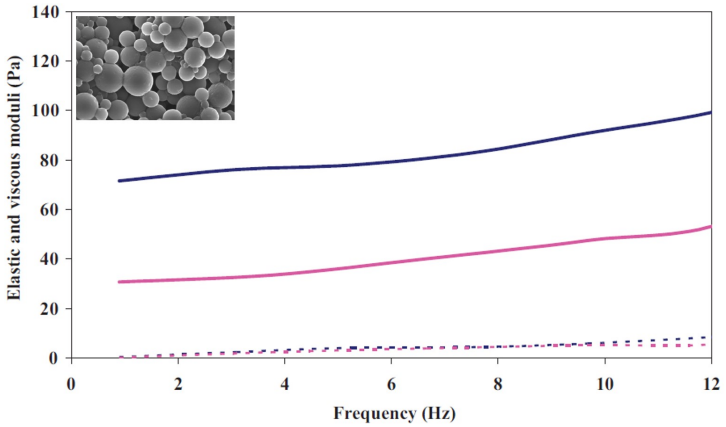

Figure 1.14: Viscoelastic micro-mechanical characterization of bulk HA and HA/Ge composite network. Solid and dashed pink lines: elastic and viscous modulus of the bulk HA; solid and dashed dark blue lines: elastic and the viscous modulus of the composite. Adapted from [115].

To sum up the advances and limitations on vocal-fold histology and biomechanics over the last decades regarding:

- **Vocal-fold histology:** Since the 2010s, a few authors have started to investigate the microscopic collageneous fibrous microstructure of the vocal fold tissue at rest, opening a new insight into voice biomechanics. The standard staining techniques commonly used to investigate vocal-fold histology were extended and completed by new 3D (sub)micro-imaging techniques, such as micro-magnetic resonance imaging (MRI) [49, 116, 147], mutiphoton nonlinear laser scanning microscopy (NLSM) [141, 192], optical coherence tomography (OCT) [88, 149, 185], high resolution synchrotron micro-CT [15], and laboratory nano-CT [141]. These techniques allowed to better characterize the vocal-fold tissue layers hierarchical architectures in the undeformed state, and to determine some microstructural descriptors of their fibrous networks, such as 3D orientation maps, fibers' characteristic size and topological shape.
- **Vocal-fold biomechanics:** The mechanical database acquired by several authors over the last twenty years shows how vocal-fold tissue layers behave as many other soft living tissues subjected to finite strains, *i.e.*, exhibiting nonlinear viscoelastic and anisotropic tendencies, strain hardening and strain rate sensitivity, stress hysteresis and accommodation. These macroscopic features are known to be related both to their inner gel-like ground substances and oriented fibrous architectures which, based on the applied loading mode and direction, are differently reoriented, deformed and more generally rearranged.

However, to date, the acquired knowledge of such macro-, meso- and microscale rearrangement occurring under relevant physiological loadings remains elusive. Several hypotheses are therefore often put forward to explain how macroscopic observed trends are inherited from lower scales constituents and mechanisms: concerning the *lamina propria* ECM, it is often acknowledged that the fibrous collagen proteins provide vocal folds with the structural framework required to bear tensile solicitations experienced

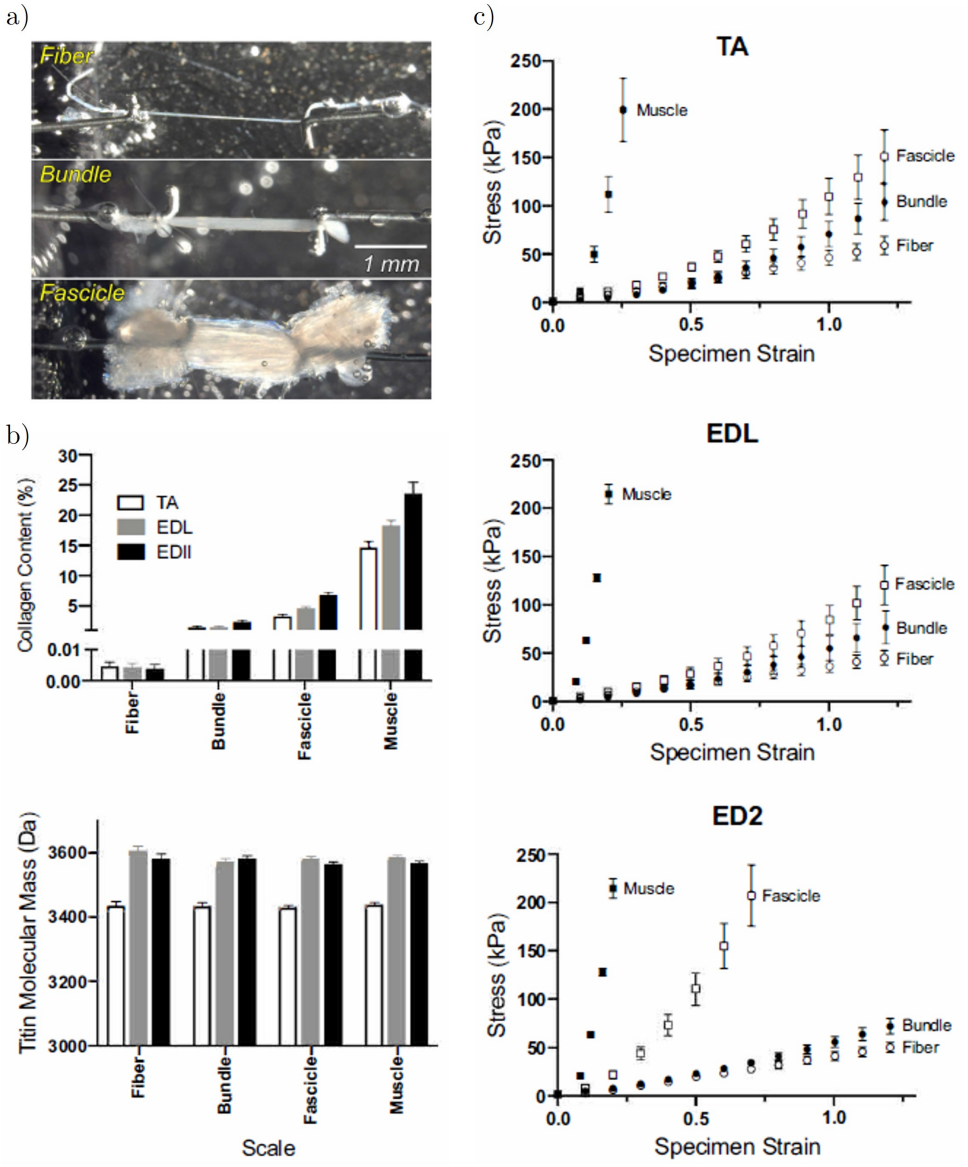

Figure 1.15: Scaling of passive mechanical properties in muscular fibers: a) photomicrograph of samples at the single fiber, fiber bundle and fascicle scale; b) comparison of collagen content (%) and titin molecular weight (Da) measurements using TA, EDL and ED2 at different muscular scales; c) passive stress-strain curves for TA, EDL and ED2 at different muscular scales. Adapted from [266].

during phonation. Elastin proteins are instead considered to confer elasticity and resilience, allowing vocal folds repeated stretching and subsequent passive recoil. Finally, it is often speculated that HA and other interstitial proteins of the ground substance, interacting with the neighboring fibers, contribute to the regulation of the tissue viscosity [95, 96]. Regarding the *vocalis*, the exact role played by collageneous and muscular fibrous network in its overall mechanical behavior is still unclear and therefore often left aside.

In conclusion, based on the available experimental evidence, the currently acquired knowledge is still not sufficient to understand the underlying relationship existing between the vocal tissues histo-mechanical characteristics and their remarkable vibro-

mechanical properties.

1.4 Biomechanical modeling

As detailed in the previous sections, although the continuous progress made in 3D (sub)micro-imaging and a rich biomechanical database collected over the last twenty years, the quantitative characterization of human vocal folds remains a rather challenging task. In particular, the characterization of their 3D fibrous architecture and the strain-induced evolution of their meso/microstructural parameters still represents an active research topic.

Based on these experimental limitations, since the 1970s, various theoretical and numerical models of the vocal-fold mechanics have been developed to understand the fluid-structure-acoustic interactions that occur during glottal vibrations [5]. Among these models, two formulations are usually proposed, depending on the scale they focus on: **macroscopic approaches**, conceiving the vocal-fold tissue as fully homogeneous or as an assembly of homogeneous sublayers, and **multiscale approaches** accounting for the presence of a heterogeneous microstructure.

1.4.1 Macroscopic approaches

Most of the physical models of phonation rely on macroscopic approaches, assuming a vocal tissue made of homogeneous layers with phenomenological mechanical properties (with linear or nonlinear, time-(in)dependent constitutive laws). These models are normally grouped into two main categories: lumped element models of vocal folds and continuous models. Each category is further detailed in the following.

Lumped element models

Since the 1970s [82], lumped element models (or multi-mass models) represent the most classical and popular approach to study the vocal-fold flow-induced vibrations, characterized by relatively low mathematical complexity and computational cost. The fundamental idea is to divide the vocal-fold tissue into small portions of masses, coupling the neighboring masses *via* springs and viscous dampers (dashpots). Depending upon the number of masses (n), the model may represent simple low-dimensional self-sustained oscillations of the vocal folds [82] or more complex vibrations with many oscillatory modes [150]. The movement of these masses can be free (three dimensions of translations, three axes of rotation) but it is more generally limited to either one or two directions in translation, and at most one possibility of rotation. The global approach is based on the coupling between partial differential equations (PDEs) to describe the airflow inside the glottis, the "vocal-fold" structural vibrations, and the acoustic field in the trachea and the vocal tract, under simplified assumptions (*e.g.*, quasi-steady and incompressible glottal flow described

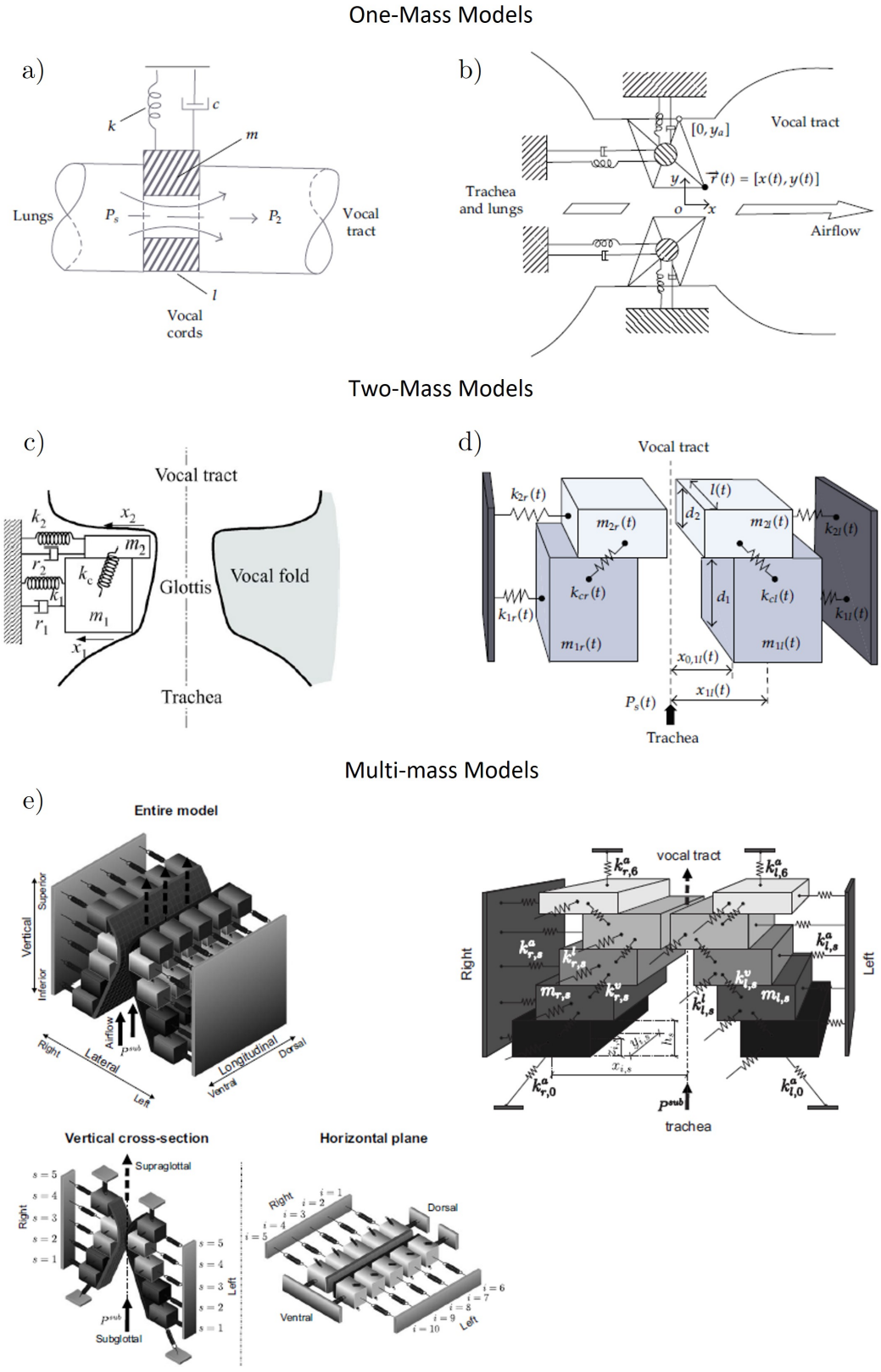

Figure 1.16: Vocal fold lumped element models: a) and b) illustrate schematics of one-mass models with 1 [82] and 2 [2] DF respectively; c) and d) display schematics of 1 DF two-mass stationary [170] and nonstationary [269] models; (e) shows a schematic representation of a full three-dimensional nonstationary multi-mass model of the vocal fold tissue [271]. Adapted from [2, 82, 170, 269, 271].

by Bernoulli's equation). In order of increasing complexity, *i.e.*, with an increasing number of degrees of freedom, the mechanical behavior of the vocal folds during phonation is simulated using one-mass models (n = 1), two-mass models (n = 2) or multi-mass models (n > 2):

- *One-mass models* – One of the simplest models of the vocal fold is a one-mass system with a single degree of freedom (DF), initially introduced by Flanagan and Landgraf [82], adopted and extended by a significant number of other authors [188, 247, 249]. A schematic representation of the model is shown in Figure 1.16 a. The vocal-fold vibrations are modeled using a single mass-spring oscillator with a damping driven by the airstream flowing from the lungs. In this case, self-sustained vibrations are predicted by the model only if the acoustical coupling with the vocal tract is triggered. Conversely, the model does not reproduce the vertical phase difference, required for efficient flow-induced oscillation. Furthermore, the presence of a viscous damping term makes steady-state motion possible. Adachi and Yu [2] modified the aforementioned model to make it vibrate both parallel and perpendicular to the airflow (see Figure 1.16 b). Different elastic properties could also be accounted for along the two directions of oscillation [10, 11].

- *Two-mass models* – In 1972 Ishizaka and Flanagan [133] introduced a two-mass system developed for speech synthesis purposes. This model remains a gold-standard in the literature, able to simulate the core mechanisms driving vocal-fold vibrations such as the phase shift of vocal folds lower and upper edges, enabling the energy transfer from the airstream to the vocal folds [101]. The latter mechanism can be modeled by conceiving each fold with two coupled oscillators (see Figure 1.16 c). In the native model, the two vocal folds were assumed to be identical and to move symmetrically with respect to the glottal midline.
  Since the 1970s, however, various extended versions of this model have been developed and proposed. In particular, the elastic and damping properties of the vocal tissue were changed from linear to nonlinear functions of the displacement and velocity, respectively. Asymmetry, in vocal-fold geometrical and/or mechanical properties, was also progressively introduced [60, 134, 235]: in this case, upper and lower mass differential equations of the motion remain identical, but the left and right vocal folds become asymmetric, yielding to different motions. Geometrical and mechanical parameters (mass, stiffness), kept constant in the early versions of the model, were also modified to account for time-dependency [269], as sketched in Figure 1.16 d.
  Therefrom, although rather simple at first glance, two-mass models allow to explain many observed experimentally phenomena (*e.g.*, the ability to simulate register changes, vibration onset-offset patterns, vocal folds asynchronous motion yielding to nonstationnary oscillations, subharmonic vibrations, biphonation, *i.e.*, two-frequency oscillations, chaotic phenomena in pathological or singing voices, *etc.*) [14, 60, 81, 169, 170, 205, 226, 235, 269]. Despite their simplicity and efficiency, the major shortcoming of two-mass models remains the lack of direct correlation between the model mechanical parameters and the physiological ones (*e.g.*, between the stiffness of the springs and the effects of *vocalis* contraction) [5].

- *Multi-mass models* – Generalizations of the previously mentioned models can be obtained by combining one or two DF one-mass systems with two-mass systems, where each mass has one DF. Yang *et al.* [271] applied this principle to a five-mass system where each mass has three DF (see Figure 1.16 e): not only lateral and longitudinal, as it was already the case in 2D models, but also vertical vibrations. This kind of approach is certainly the most appropriate as it accounts for the tridimensionality of vocal folds vibrations. The collision impact force is additionally included in the model. The influence of the aerodynamic force, generating the 3D mass elements oscillations, is equally investigated. The Bernoulli-type driving force, produced by the glottal flow, not only depends on the subglottal pressure but also on vocal folds geometrical configuration. The resulting model allows therefore the 3D visualization of human vocal folds vibrational regimes for both symmetric and asymmetric configurations. Finally, a nonstationary multi-mass model of the vocal folds with two DF and time-dependent parameters, related and optimized to vocal-fold extracted vibrations, was proposed by Wurzbacher *et al.* [270].

Continuous models

Aside from multi-mass models, continuous models have been developed since the early 2000s to account for structures and geometries closer to vocal-fold morphology (*e.g.*, multilayered structure). This kind of approach is aimed at resolving all the physical details involved in the phonation process in space and time. Therefore, in these models, the PDEs of the flow, structural mechanics, acoustic fields and their relative couplings have to be solved numerically, mostly using the finite element method (FEM). Different possible continuous models approaches are presented hereafter in order of increasing complexity:

- *2D geometries* – A first 2D FEM continuum model was proposed by Alipour *et al.* for the computation of the vocal-fold vibrations [4], as illustrated in Figure 1.17 a. The mechanical field was discretized with finite elements, whereas the fluid forces were modeled using the Bernoulli's approximation. The comparison between a Bernoulli and a 2D Navier-Stokes solver is addressed by de Vries *et al.* [265] for a hemilarynx geometrical configuration. Thomson *et al.* used a hemilarynx continuum mechanical model to study the onset of the self-sustained vocal fold oscillations. They showed that a cyclic variation of the glottis profile from a convergent to a divergent shape is a key factor to establish self-sustained vocal-fold oscillations [245]. The first fluid-structure interaction (FSI) model with fully resolved flow computations was probably developed by Luo *et al.* [171], using a 2D realistic geometry and applying an immersed boundary (IB) method.

- *Modeling of glottal collision* – A critical problem of FEM continuum models is to account for the periodic contact between the vocal folds. Different strategies can be employed with this respect. One of the first structural models encompassing vocal folds contacts was proposed by Alipour *et al.* [4]: each FE node of the vocal-fold

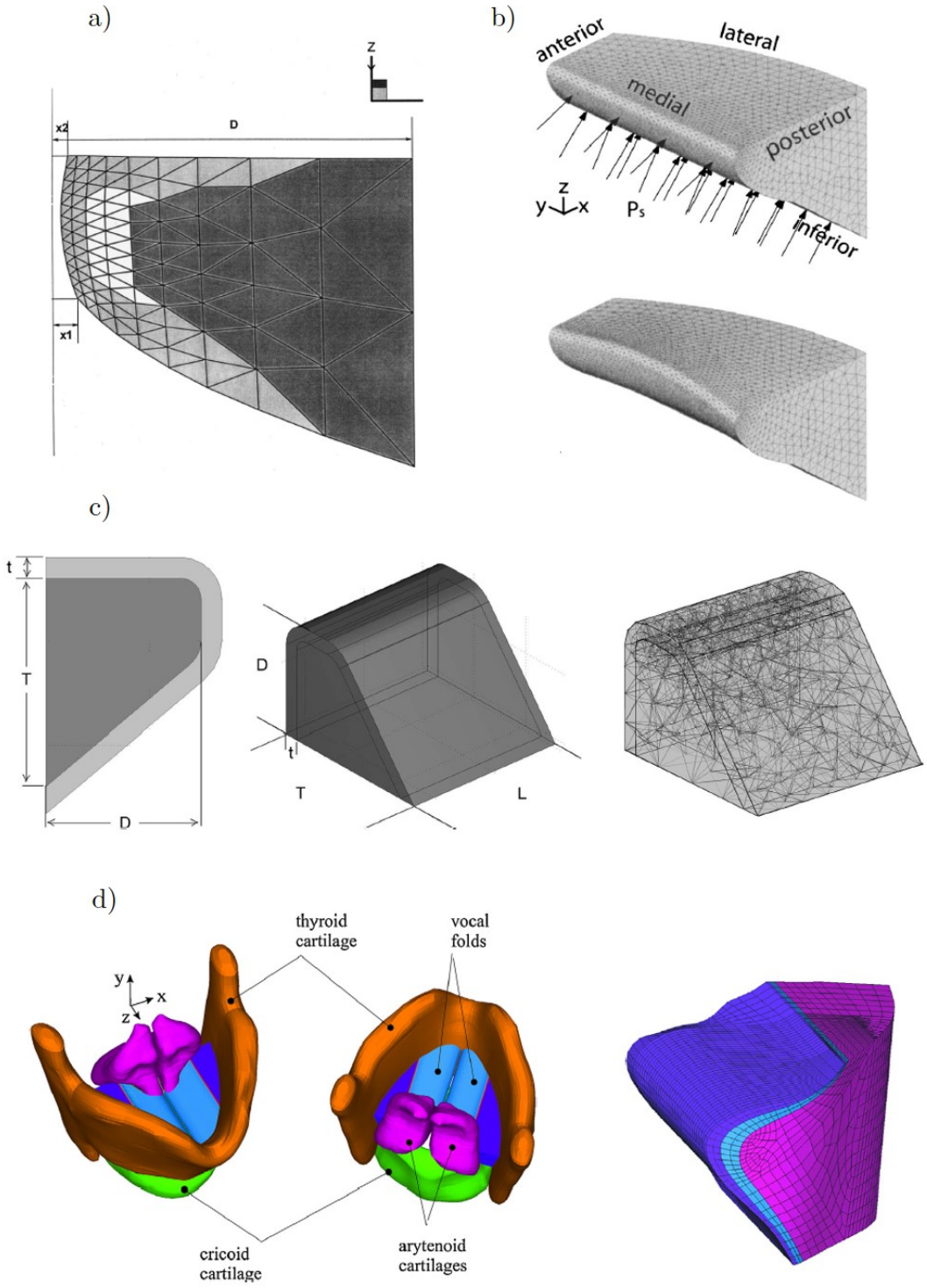

Figure 1.17: FE models of the vocal fold tissue: a) 2D FE vocal-fold mesh (dark, light grey and white respectively represent the vocal-fold body, cover, and ligament) proposed by Alipour *et al.* [4]; b) 3D FE model problem formation in the undeformed configuration used by Gunter [101] to calculate the initial conditions for glottal closure (top, arrows indicate direction and location of the applied subglottal pressure), problem solution in the deformed configuration (bottom); c) geometrical diagrams (coronal cross section and isotropic view) and mesh of the FE vocal-fold model adopted by [57]; d) 3D FE model of the human larynx and vocal-fold tissue developed by Vampola *et al.* [256]. Adapted from [4, 57, 101, 256].

surface reaching the symmetry plane looses one DF. Horáček *et al.* combined a Hertz formulation, to implement glottal contact, with a low DF model for the simulation of vocal-fold oscillations [124, 125]. Tao *et al.* considered a collision model within a strongly coupled fluid-structure algorithm to better simulate the interactions process [243]. The augmented Lagrangian method was used as contact algorithm in their self-oscillating 3D model. Rosa *et al.* [223] proposed a full flow-structural mechanical model adopting a similar approach: when contact is detected, a force is computed to prevent the concerned nodes from interpenetration. The major challenge in modeling FSI computations using volume discretization methods, among which the FEM, is to ensure that there are no zero-volume (3D) or zero-area (2D) elements [5]. This can be achieved by enforcing a minimum gap between vocal folds in contact formulations [63, 171]. Zheng *et al.* coupled a sharp-interface IB method flow solver with a FEM solid dynamics solver for 2D and 3D problems. A penalty coefficient method introduced by Belytschko [20] was conversely implemented to model vocal-fold contact.

- *3D geometries* – Fully 3D coupled FEM simulations analyzing human phonation are still particularly challenging, even disposing of current computing resources. A first 3D FE fluid-solid coupled model was proposed by Rosa *et al.* [223], accounting for a contact-impact algorithm and assuming that the laryngeal tissue is transversely isotropic and divided into three layers (vocal cover, ligament and body). More recently, a 3D FE model of the human larynx was developed by Vampola *et al.* [256], based on computer tomography (CT). It includes the modeling of the laryngeal cartilages (aryenoids, thyroid and cricoid), as displayed in Figure 1.17 d. This latter model is fully parametric: vocal folds geometry can be conveniently modified, enabling tuning or optimization procedures to find proper model geometric and material parameters related to the considered vocal-fold vibratory peculiarities. Furthermore, the model was particularly developed to account for numerical simulations of vocal-fold vibrations with collisions. Nonetheless, the model is not suitable to predict the onset of the periodic oscillations: the self-sustained vibrations are instead simulated employing a prescribed intraglottal pressure given by a periodic function in the time domain. Such intraglottal pressure is generated by a 2D aeroelastic model of the vocal-fold vibrations [124, 125]. Regarding the tissue biomechanics, vocal folds are modeled as a three-layered structure, composed of the vocal cover, ligament and *vocalis* muscle, owning transversely isotropic elastic properties. Results report a computed vibratory motion qualitatively similar to the patterns obtained from experimental studies, with trajectories of the vocal folds closely resembling those measured on excised larynges excited by the airflow rate. Furthermore, vocal-fold tissue predictions during the phonatory regime highlight a triaxial stress state: any stress components (periodically changing in magnitude and direction) can therefore be neglected. This clearly points out the heterogeneous multiaxial solicitations the vocal-fold tissue is subjected to during physiological vocal-fold vibrations. More specifically, maximum stress levels were detected in the ligament close to the vocal folds surface, decreasing with the tissue depth, during both the opening and closing phase of the glottis.

1.4.2 Multiscale formulations

All the physical models of phonation examined so far rely on macroscopic phenomenological approaches, assuming a vocal tissue made up of homogeneous sublayers with quasi-linear elastic and, often, transverse isotropic material properties. Thereby, these approaches leave aside vocal folds fibrous microstructure and histo-mechanical characteristics, though responsible for their complex mechanical behavior (*e.g.*, nonlinearity and multiscale structural rearrangements, distinct degree of anisotropy within different layers, time-dependent behavior) [44, 54, 143, 193]. This is a striking backwardness compared with the amount of studies carried out on the micro-mechanics of other biological tissues [38, 122, 128].

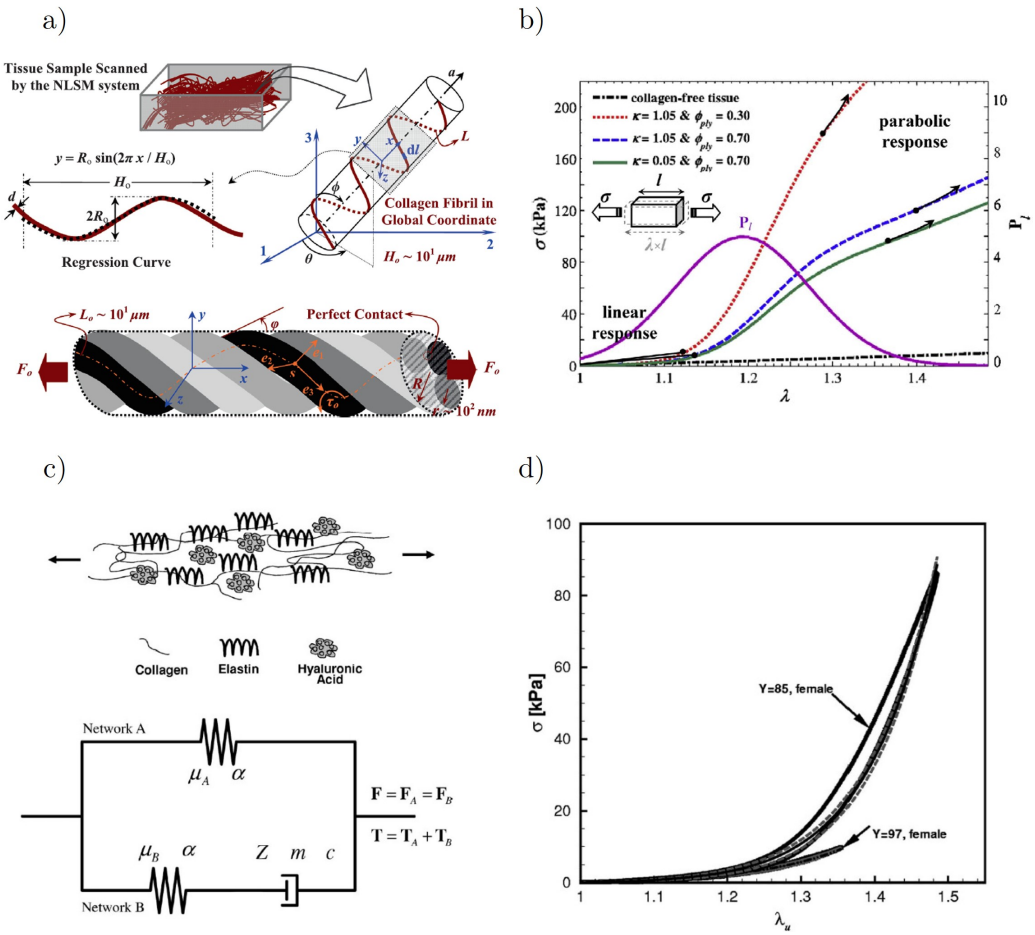

Figure 1.18: Multiscale modeling of the vocal-fold tissue: a) and c) represent schematic representations of the micro-mechanical constitutive models developed and proposed by Miri *et al.* [194] and Zhang *et al.* [275], respectively; b) and d) illustrate corresponding stress-strain predictions. Adapted from [194, 275].

Since the 2010s, however, a few authors have started to model the collageneous fibrous microstructure of the vocal folds, opening a new insight into voice biomechanics [143, 191, 193, 194]. These formulations were supported by recent advances in the experimental characterization of collagen at the fibrillar level, as described in Section 1.3.2. Therefrom, first fiber-scale formulations started focusing on the development of **nonlinear hyperelastic**

and anisotropic constitutive models to simulate the tensile J-shaped response of the vocal-fold tissue. In this regard, two pioneer studies are:

- Kelleher *et al.* [143] proposed a microstructurally-informed model of the vocal-fold ligament, based on the reference formulation developed by Gasser, Ogden and Holzapfel (the so-called "GOH model" [89]) and adjusted on uniaxial tensile data. Interstitial proteins were accounted for using an incompressible, isotropic neo-Hookean formulation, while the fibrous proteins were modeled using an exponential, anisotropic, hyperelastic stress potential. The collagen fibers dispersion was described by a statistical orientation function acquired from 2D microscopic data obtained on the vocal ligament using second-harmonic generation imaging [192]. Beam theory was finally used to predict the fundamental frequency of phonation as a function of the model constitutive and microstructural parameters.
- Miri *et al.* [194] suggested a geometrical idealization of the collagen fibrils multi-strand rope-like ply structure within the *lamina propria* as shown in Figure 1.18 a [29, 200]. Using classical rope mechanics, they computed a hyperelastic function able to describe the deployment of crimped fibrils. The model parameters were fitted based on morphological and mechanical data from porcine vocal folds, owning a structure rather similar to that of human vocal folds [104, 105]. However, it should be noted that human vocal folds display more regularly oriented collagen and elastin networks compared to those of porcine vocal fold, characterized instead by a more randomly distributed structure [192]. In conclusion, this model highlighted the mechanical contribution of the helical structure of collagen to the nonlinear elasticity of the vocal tissue under tensile loading (Figure 1.18 b).

These promising microstructure-inspired studies present, however, some drawbacks: interactions between ECM components were neglected despite the density of the considered fibrous media; the evolution of non-collageneous ECM proteins (*e.g.*, elastin fibers) was excluded from the models formulation; they exclusively focused on quasi-static and uniaxial tension, leaving therefore aside the coupled multiaxial and dynamic solicitations vocal folds are subjected to *in vivo*.

To account for **vocal folds time-dependent behavior**, several histology-inspired formulations were proposed to predict vocal-fold tissue viscoelastic properties (*e.g.*, [45, 275, 277]). In particular, Zhang *et al.* [275, 277] proposed a 1D rheological constitutive model of the vocal cover reflecting the molecular interactions between fibrous and interstitial proteins. As represented in Figure 1.18 c, the model considers various parallel material networks: one hyperelastic time-independent equilibrium network, in parallel with one (or two) time-dependent inelastic network(s). Ogden's hyperelastic formulation [202] was therefore coupled with viscoplastic flow rule(s) [22, 23] and adjusted to simulate the large-strain time-dependent tensile behavior of the human vocal-fold cover. The model parameters were varied to take into account the age- and gender-related effects and to establish a link between the tissue constitutive properties and the histological structure of the *lamina propria*. More specifically, the authors tried to correlate the relative densities of collagen and elastin

fibers with the model constitutive parameters [107, 108]. The model was finally shown able to predict the fundamental frequency of phonation (FFP) expected for different genders and ages (see Figure 1.18 d). However, no specific assumptions were made with regard to the real physical contribution of collagen, elastin or interstitial protein molecules to any of the networks considered in the model. The role played by each microstructural component of the vocal-fold tissue in the FFP regulation could therefore not be interpreted.

In conclusion, since the 1970s, multi-mass models of the vocal folds provide an elegant and qualitative description of the fluid/stucture/acoustic interactions taking place during human phonation. As reduced order models, they are able to encompass the dominant modes of glottal vibrations. However, they are necessarily limited to simple brick-shaped geometries and the identification of their model parameters (geometric, mechanical, aerodynamic) with respect to physiological data often remains a challenging task.

FEM approaches represent instead, since the early 2000s, a suitable approach to account for complex boundaries, driving forces, collision problems and coupled multiphysical phenomena. Nevertheless, a significant obstacle to accurate numerical simulations of human phonation is the scarcity of tissues available biomechanical data due to experimental limitations. To reduce the number of independent parameters to deal with, current finite element models are often based on various assumptions regarding the tissue biomechanics (*i.e.*, linear elasticity, planar displacement, incompressibility).

Since the 2010s, a few authors have started to model the vocal-fold tissue collageneous fibrous microstructure and their nonlinear anisotropic mechanical behavior. These approaches are very promising to gain an in-depth understanding of the underlying correlation between the vocal folds histological features and their unique vibro-mechanical performances. Nonetheless, these theoretical formulations at the fiber scale need to be further developed, validated and extended to dynamical loadings as endured by the vocal tissue during phonation.

1.5 Conclusion

This first chapter introduced the global context of the work, recalling the current knowledge of human phonation, vocal-fold histology and biomechanics.

Succinctly, phonation is the final outcome of a highly complex multi-physical process occurring in the larynx. There, vocal folds are one centimeter-scale soft pliable vibrating structures, subjected *in vivo* to numerous complex and coupled 3D mechanical solicitations (tension, compression and shear), experienced upon finite strains and at various strain rates. Each vocal fold can be thought as a lamellar structure composed of a mucosal *epithelium*, the *lamina propria*, composed of collagen and elastin microfibrils' networks, and the *vocalis* muscular layer. The link between these histological characteristics and vocal-fold tissue vibro-mechanical performances still remains an open question. This is

mainly ascribable to their challenging experimental characterization: vocal folds fibrous architectures are not easily observable *in vivo*; *ex vivo* mechanical tests are scarce and complex to interpret. Consequently, most of the vocal-fold mechanical models developed so far (low-order multi-mass and high-order continuum FEM) rely on phenomenological macroscopic approaches, coarsely assuming a homogeneous vocal tissue with (transverse) isotropic quasi-linear elastic properties. Since 2010, a few authors have started to investigate and model the vocal-tissue collageneous fibrous microstructure, accounting for the tissue anisotropy, heterogeneity and mechanical nonlinearity at different spatial scales, opening a new insight into voice biomechanics. Nonetheless, these models present the following drawbacks and should be therefore further developed: (i) they lack of any direct experimental validation at multiple scales; (ii) they adopt time-independent formulations that are not suitable to capture the complex mechanics of vibrating tissues; (iii) they exclusively focus on quasi-static and uniaxial tension loading conditions, leaving aside the coupled multiaxial and dynamic solicitations endured by vocal folds *in vivo*.

Thereby, the present work proposes an innovative micro-mechanical model of the vocal-fold tissue based on recent histo-mechanical evidence, suitable to account for vocal fold layers fibrous architectures and surrounding matrices, and able to predict their multiscale and time-dependent behavior accordingly. The manuscript is structured as it follows. Chapter 2 presents a first hyperelastic formulation idealizing vocal-fold sublayers (*i.e.*, *lamina propria* and *vocalis*) 3D fibrous architectures and surrounding matrices and capable of predicting their mechanical behavior for key physiological quasi-static and multiaxial loadings (*i.e.*, uniaxial tension, compression and shear) upon finite strains. Chapter 3 extends this micro-mechanical formulation to a viscoelastic frame and assesses the model ability to reproduce sublayers time-dependent response, not only at low-frequency cyclic and multiaxial loadings upon finite strains, but also over a wide spectrum of frequencies. Chapter 4 finally addresses the implementation of this model in a finite element code, toward 3D simulations of vocal fold transient dynamics with relevant histo-mechanical properties. Concluding remarks on obtained results and model limitations, as well as recommendations and future perspectives, end the manuscript.

2

A micro-mechanical model for the soft fibrous tissues of vocal folds

This chapter is based on an article submitted to the *Journal of the Mechanical Behavior of Biomedical Materials* in October 2021: A. Terzolo, L. Bailly, L. Orgéas, T. Cochereau, N. Henrich Bernardoni, "A micro-mechanical model for the fibrous tissues of vocal folds".

Contents

2.1 Introduction

As detailed in Chapter 1, human vocal folds possess a complex lamellar structure with two principal layers: the *lamina propria*, *i.e.*, a loose connective tissue and the *vocalis*, or inferior thyroarytenoid muscle. Each layer is a soft material with architectured networks of collagen, elastin and/or skeletal muscle fibers (see Figure 2.1; [15, 34, 117]). Clinical observations clearly support the major role played by such fibrous microstructure in the vocal-fold vibrations: in cases of benign or cancerous lesions, alterations of fiber-scale arrangement of the *lamina propria* systematically induce a vibratory dysfunction [77, 79, 111]; with aging, a loss of elastin fibers, fibrosis or muscle atrophy, together with vocal and perceptual changes such as hoarseness, low pitch and breathiness have also been observed [218, 229, 230]. However, to date, the acquired knowledge is still not sufficient to understand the relationship between the microstructural characteristics of vocal folds and their macroscale performances.

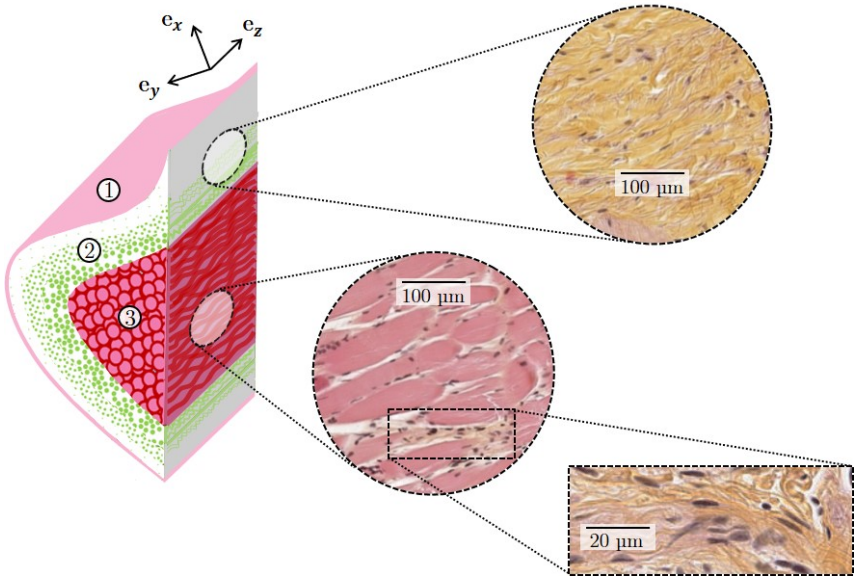

Figure 2.1: Human vocal-fold histology. One fold idealized scheme with focus on the fold sublayers and fibrous microstructure: ① *Epithelium*, ② *Lamina propria*, ③ *Vocalis* muscle (left). Corresponding 2D histological photomicrographs prepared with HES staining: collagen fibers (yellow-orange); cytoplasms, striated muscular and elastin fibers (pink); *nuclei* (black-purple) (right). Adapted from [15].

This is mainly ascribed to their challenging experimental multiscale characterization. Despite the increasing progress made in 3D micro-imaging [15, 49, 88, 116, 141, 147, 149, 193], vocal folds, together with their fibrous architectures, are still hardly observable *in vivo* [59, 185]. Though a large biomechanical database has been collected on excised vocal folds over the last twenty years [40, 46, 54, 143, 191, 220], the 3D microscale rearrangement of loaded tissues is still to be explored. At the same time, the development of macroscopic (tissue scale) or micro-mechanical (fiber scale) models of phonation is a promising alternative to gain an in-depth understanding of vocal-fold biomechanics:

- In macroscopic approaches, phenomenological exponential and power-law functions are commonly proposed to describe the stress-strain responses typically observed when deforming soft biological tissues [18, 120, 123, 164, 165, 186]. However, doing so, the model parameters can hardly be related to the material intrinsic structure and mechanics, and need to be adjusted based on the applied loading path. This first approach is robust and adequate in the absence of tissue histo-mechanical data.

- Microstructure-based formulations are instead inspired from histological evidence, and conceived to correlate the model parameters to the physical and structural properties of the tissue (*e.g.*, cells, fibers and surrounding matrices). To name a few, the shape, the amount, the orientation and the tortuosity of fibers are all relevant structural parameters that are usually considered. Therefrom, to determine the macroscale mechanical behavior of the tissue, homogenization techniques [12, 173–175, 178, 180, 181, 201], energetic approaches [194, 199, 203, 207, 208], statistical descriptions [49, 89, 140, 156] or variational considerations [56, 86, 154, 179, 182] are used. Nonetheless, the identification and validation of these frameworks with multiscale experimental data remains a challenging task.

By contrast with many other soft tissues (*e.g.*, arteries, heart, skin), most of the theoretical approaches adopted to model the vocal-fold mechanical properties still rely on macroscopic formulations. Since the 2010s, a few authors have been proposing micro-mechanical models for the vocal-fold tissues, opening a new insight into voice biomechanics [143, 194]. These approaches allowed to predict the tensile behavior of the *lamina propria* but their relevance was not assessed for significant biomechanical loadings such as transverse compression and longitudinal shear [101, 242, 256]. Furthermore, theoretical formulations still need: (i) to be fed up with 3D microstructural descriptors of human vocal-fold sublayers and to account for fiber-to-fiber mechanical interactions likely to occur within such dense media [72]; (ii) to be extended to the specific micro-arrangement of the *vocalis* muscle.

Within this context, this study proposes a micro-mechanical model able to reproduce the nonlinear anisotropic mechanical properties of vocal-fold layers (*lamina propria*, *vocalis*) subjected to multiaxial finite strains, from the knowledge of their 3D fibrous architecture. It combines the use of *ex vivo* database acquired on human vocal-fold microstructures over the last ten years, with a recent study on their finite strain macroscale mechanics in longitudinal tension, transverse compression and longitudinal shear [54]. The chapter is structured as it follows. Section 2.2 introduces an improvement of the theoretical formulation firstly proposed and validated in the context of vascular biomechanics [12, 13]. The model identification procedure is described in Section 2.3. Section 2.4 presents the vocal-fold multiscale predictions as well as a micro-parametrical study, to investigate how changes in the tissue's 3D fibrous configuration may impact its vibro-mechanical response.

2.2 Micro-mechanical model

2.2.1 Experimental observations and assumptions

In line with histological evidence [15, 109, 144, 176, 194] (see Figure 2.1), both *lamina propria* and *vocalis* can be thought as 3D incompressible composite structures made of a gel-like matrix reinforced by a network of fibers. Furthermore, each fiber can be seen as a bundle of quasi-aligned (myo)fibrils with wavy shapes and preferred orientations at rest:

- The *lamina propria* is made of cells and an extracellular matrix (ECM) embracing amorphous ground substances (*e.g.* hyaluronic acid), entangled fibrous networks of collagen (mainly Type I and III) and elastin [193]. Collagen plays a key role in the mechanics of soft tissues and is, by weight, the most abundant fibrous protein in the human *lamina propria*, representing at least 50% of the total proteins (less than 10% for elastin) [104, 105, 244]. The *lamina propria* is finally known to be arranged in three sublayers with distinct fibers' type, density and arrangement, albeit very challenging to model due to a lack of quantitative topological descriptors. For this reason, in the following, the tissue multilayered arrangement is simplified in a mono-layered structure. The fibrous network of its ECM is assumed to contain a single population of collagen fibers, *i.e.*, fiber bundle of collagen fibrils, embedded in a surrounding matrix including all the remaining tissue components (cells, elastin, ground substances).

- The *vocalis* is primarily made of muscle fibers grouped into fiber bundles (or *fasciculi*) and wrapped together by connective tissue sheaths [15] (see Figure 2.1). Its ECM is dominated by collagen in terms of mass, and organized into three interconnected levels: *epimysium* surrounding the whole muscle, *perimysium* surrounding fascicles, and *endomysium* surrounding individual muscle fibers [27, 266]. Collagen was recently shown to be a crucial load-bearing component in the finite strain passive response of skeletal muscles [266]. Therefore, in the following, each muscle fiber is approximated by a bundle of myofibrils wrapped by a sheath of collagen fibers (*i.e.*, bundles of collagen fibrils). The remaining constituents of the muscle ECM (elastin, proteoglycans, glycoproteins) constitute the matrix of the micro-mechanical model [213].

2.2.2 Idealization of the vocal-fold layers' fibrous architectures

Regardless of the considered vocal-fold layer (*i.e.*, *lamina propria* or *vocalis*), its microstructure is idealized by the periodic repetition of a Representative Elementary Volume (REV) inspired from that already proposed for rubber-like materials [8, 19, 28] or self-entangled superelastic wires [219], as sketched in Figure 2.2 a. In the undeformed configuration $\mathscr{C}_0$ (resp. deformed configuration $\mathscr{C}$), the REVs can be seen as prisms with a truss of $N = 4$ bars, of identical initial length ℓ_0 (resp. actual lengths ℓ_i), embedded in a matrix and connected at their extremities to a central node C_0 (resp. c_0) and to the nodes C_i (resp. c_i), $i \in [1, \dots, N]$ of corresponding neighboring REVs. The initial (resp. actual)

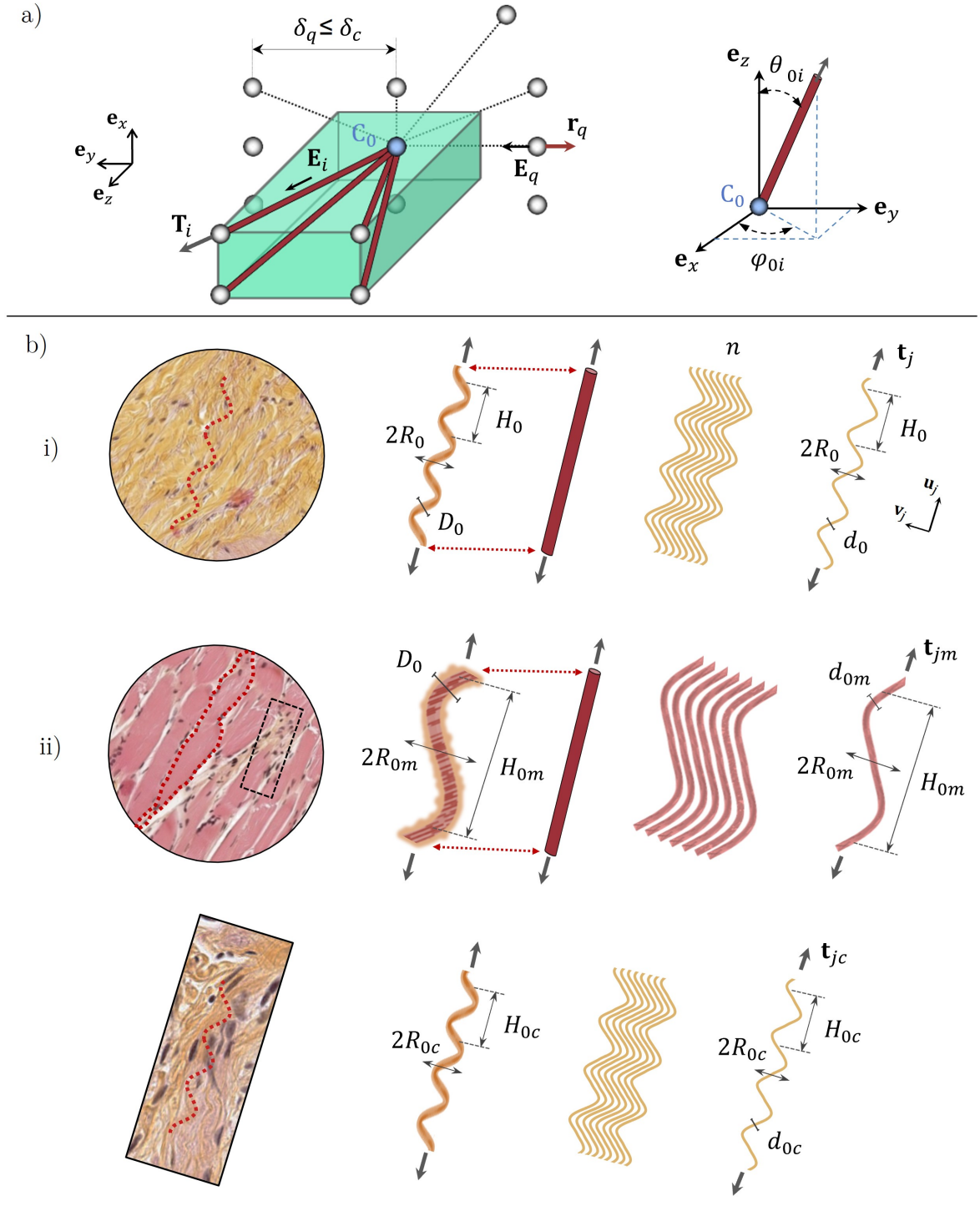

Figure 2.2: Idealized geometry of the vocal-fold sublayers: a) REV in the undeformed configuration $\mathscr{C}_0$ – a node of periodicity C_0 (blue) and a 4-bar truss (brown) embedded in a soft isotropic matrix (green). Dotted lines illustrate the possible steric interactions of C_0 with the neighboring nodes; b) correspondence fiber-bar for i) *lamina propria* and ii) *vocalis*, conceived as fiber bundles of collagen (orange) and/or muscular fibrils (pink).

orientation of each bar i is denoted by the direction of its unit vector $\mathbf{E}_i = \mathbf{C}_0\mathbf{C}_i/\|\mathbf{C}_0\mathbf{C}_i\| = \sin\theta_{0i}\cos\varphi_{0i}\,\mathbf{e}_x + \sin\theta_{0i}\sin\varphi_{0i}\,\mathbf{e}_y + \cos\theta_{0i}\,\mathbf{e}_z$ (resp. $\mathbf{e}_i = \mathbf{c}_0\mathbf{c}_i/\|\mathbf{c}_0\mathbf{c}_i\| = \sin\theta_i\cos\varphi_i\,\mathbf{e}_x + \sin\theta_i\sin\varphi_i\,\mathbf{e}_y + \cos\theta_i\,\mathbf{e}_z$) where $\mathbf{e}_x$, $\mathbf{e}_y$ and $\mathbf{e}_z$ lie along the medio-lateral, infero-superior

and antero-posterior anatomical directions (see Figure 2.1). In the following, for the sake of simplicity, it was assumed that $\forall i$, $\theta_{0i} = \theta_0$ and $\varphi_{0i} = \pm\varphi_0 \mp k\pi$, $k \in [0, 1]$.

Therefrom, as illustrated in Figure 2.2 b, each bar i represents the chord of a wavy (collagen or muscle) fiber bundle i. Additionally, each fiber bundle i is modeled as an assembly of n identical and parallel fibrils of equal waviness and length. Furthermore, each fibril j is defined by its initial diameter d_0, length ℓ_0^f (resp. actual ℓ_j^f), and tortuosity $\xi_0 = \ell_0^f/\ell_0$ (resp. $\xi_j = \ell_j^f/\ell_i$). A monomodal sinusoidal function is used to describe each fibril's initial waveform of amplitude R_0 and spatial periodicity H_0 [56, 155, 194], *i.e.*, with $v(u) = R_0 \sin\frac{2\pi}{H_0}u$ in $(\mathbf{u}_j,\mathbf{v}_j)$, as sketched in Figure 2.2. The bars were assumed to contain 10 typical sinusoidal periods between nodes. This arbitrary choice is not a restriction. Therewith:

- In the *lamina propria* (see Figure 2.2b-i), the volume fraction of fibrils in the REV is $\Phi = V_f/V_{REV}$, where $V_{REV} = 4\ell_0^3 \sin^2\theta_0 \cos\theta_0 \cos\varphi_0 \sin\varphi_0$ is the volume of the REV and where $V_f = \pi N n d_o^2 \ell_0^f/4$ with $\ell_0^f = \int_0^{\ell_0} \sqrt{1 + (\frac{2\pi R_0}{H_0}\cos(\frac{2\pi}{H_0}u))^2}\, du$.

- In the *vocalis* (see Figure 2.2b-ii), even if collagen and muscle families refer to a same bar, hence with the same mean orientation $(\theta_i\ ,\varphi_i)$, each family is characterized by distinct geometrical parameters, labeled with the subscript c (resp. m) for collagen (resp. muscular) fibrils. Thus, the volume fraction of fibrils can be decomposed as it follows: $\Phi = \Phi_c + \Phi_m$, where Φ_c and Φ_m are the volume fractions of collagen and myofibrils, respectively, with waveform parameters H_{0k}, R_{0k} and diameters d_{0k}, $k \in \{c, m\}$.

2.2.3 Micro-mechanical behavior of the constitutive materials

Matrix – Independently of the considered vocal-fold sublayer, the gel-like matrix is in first approximation reasonably modeled as a soft isotropic, hyperelastic and incompressible material. Its mechanical behavior is therefore described by a simple neo-Hookean formulation [255], characterized by a volumetric strain-energy function $W = 0.5\,\mu(1-\Phi)(I_1 - 3)$, where μ is the shear modulus of the matrix, and $I_1 = \mathrm{tr}(\mathbf{B})$ where $\mathbf{B} = \mathbf{F}\cdot\mathbf{F}^T$ ($\mathbf{F}$ being the macroscopic transformation gradient).

Fibrils

Tension – As sketched in Figure 2.3 a, when stretched with a strain $\varepsilon_j = \ln\frac{\ell_j}{\ell_0}$, the mechanics of wavy fibrils is firstly dominated by their progressive unfolding, regimes (i) and (ii), up to a critical strain $\varepsilon_c = \ln\xi_0$. Once fully unfolded, they behave as straight elastic rods showing a quasi-linear tensile response with a Young's modulus E_f, regime (iii) [55, 91]. The overall mechanical response is well described by the following constitutive relation [204]:

$$\mathbf{t}_j = \frac{\pi d_0^2}{4}\left[E_{eq0}\varepsilon_j + \frac{E_f - E_{eq0}}{2}\left(\varepsilon_j + \sqrt{\left(\varepsilon_j - \ln\xi_0\right)^2 + \alpha^2} - \sqrt{\ln^2\xi_0 + \alpha^2}\right)\right]\mathbf{e}_i \qquad (2.1)$$

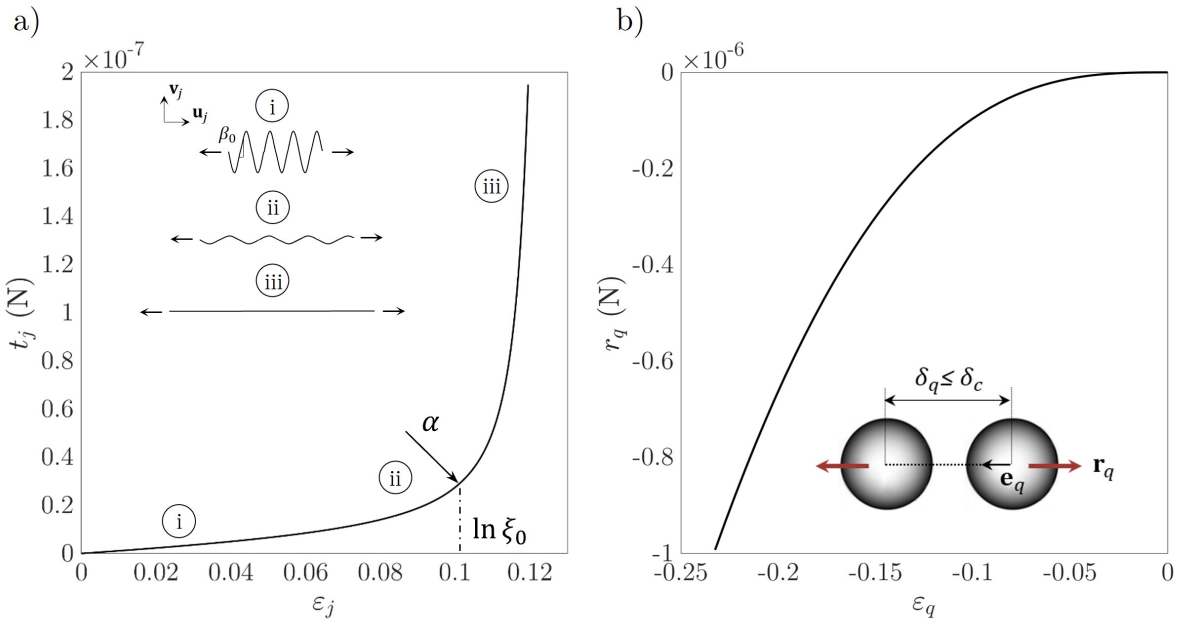

Figure 2.3: Micro-mechanics modeling: a) strain-tension curve at the fibril scale; b) strain-repulsion force curve modeling fiber-to-fiber interactions.

where $\mathbf{t}_j$ is the tension along the fibril j. In the latter equation, α is a parameter that ensures a smooth transition between the different regimes. Additionally, E_{eq0} is the initial tangent modulus measured on $(t_j\ ,\ \varepsilon_j)$ curves. Its expression can be analytically obtained [211]:

$$E_{eq0} = E_f \left\langle \cos\beta_0 \right\rangle / [\ \left\langle \cos^2\beta_0 \right\rangle + 16 \left\langle v^2 \right\rangle / d_0^2\ ] \tag{2.2}$$

where $\langle\cdot\rangle = \frac{1}{\ell_0}\int_0^{\ell_0} \cdot\, du$, $\beta_0 = \arctan\left(2\pi\frac{R_0}{H_0}\cos\frac{2\pi}{H_0}u\right)$ and $\left\langle v^2 \right\rangle = R_0^2/2$. In the particular case of the *vocalis* (see Figure 2.2b-ii), it is worth noticing that the tension force $\mathbf{t}_{jk}$ within each fibrillar network (collagen or muscular) is characterized by distinct fibril Young's modulus E_{fk} and toe-region parameter α_k.

Compression – The stiffening tensile regimes (ii) and (iii) are not prone to occur during fibrils compression. Instead, fibrils are rather expected to increase their crimping. To account for this tension-compression asymmetry, it is here simply assumed that fibrils compression follows the same tendency detailed in tension during regime (i) solely:

$$\mathbf{t}_j = \frac{\pi d_0^2}{4} E_{eq0}\ \varepsilon_j\ \mathbf{e}_j \tag{2.3}$$

Fibers – Between nodes, fiber bundles can be seen as wavy beams of parallel fibrils (see Figure 2.2 b), being transverse shear interactions significantly weaker than their longitudinal tensile response. Therefrom, the tension-compression force $\mathbf{T}_i$ in the fiber i can be simply

expressed (with N = 4) as:

$$\mathbf{T}_i = \sum_{j=1}^{n} \mathbf{t}_j = n\ \mathbf{t}_i = \frac{\Phi V_{REV}}{\pi d_0^2 \ell_0^f} \mathbf{t}_i \tag{2.4}$$

In the case of two fibrils families (*vocalis*), this generic equation comes to:

$$\mathbf{T}_i = \frac{V_{REV}}{\pi} \left(\frac{\Phi_c}{d_{0c}^2 \ell_0 \xi_{0c}} \mathbf{t_{ic}} + \frac{\Phi_m}{d_{0m}^2 \ell_0 \xi_{0m}} \mathbf{t_{im}} \right) \tag{2.5}$$

Fiber-to-fiber interactions: steric hindrance – When fibrous networks are subjected to mechanical loading, the resulting deformation does not uniquely arise from the (un)folding of fiber bundles, which may also rotate and get closer one another. These motions are physically constrained by steric hindrance, generating fiber-to-fiber interactions [72]. These constraints are not taken into account by standard eight-chain models [8], whereas they should alter the REV deformation micro-mechanisms and, thus, its macroscale effective properties. Therefore, in a first approach, repulsive forces were added between neighboring unconnected nodes of the truss to take into account these steric interaction forces. More precisely, in the deformed configuration $\mathscr{C}$, once the relative distance δ_q between the two unconnected nodes C_0 and C_q ($q \neq 0$) exceeds a critical value δ_c, a repulsive force is activated to reproduce the contact interactions between the concerned fibers. By periodicity, this comes to the interactions between C_0 and its 5 neighboring nodes, as illustrated in Figure 2.2 a (see dotted lines). The resulting $M = 5$ fiber-to-fiber interaction forces are noted $\mathbf{r}_q$ and expressed using the following power-law-based function:

$$\mathbf{r}_q = r_q\ \mathbf{e}_q = \beta\ H(\varepsilon_q)\ \varepsilon_q^3\ \mathbf{e}_q \tag{2.6}$$

where $\varepsilon_q = \ln\left(\frac{\delta_q}{\delta_c}\right)$, $\mathbf{e}_q = \mathbf{c}_q\mathbf{c}_0 / \|\mathbf{c}_q\mathbf{c}_0\|$, $H(.)$ is the Heaviside function, and where β is an interaction coefficient. A typical strain-repulsion force curve is shown in Figure 2.3 b.
In the case of the *vocalis*, owning two families of fibrils, only one coefficient of interaction β and one length of interaction δ_c are defined, being steric interactions only modeled at the fiber scale.

2.2.4 Macro-mechanical behavior of the overall composites

Based on the approach previously developed for aortic tissues [12, 13], the macroscale mechanical behavior of the *lamina propria* and the *vocalis* tissues can now be determined. Regardless of the considered layer, its macroscopic Cauchy stress tensor $\boldsymbol{\sigma}$ is expressed as:

$$\boldsymbol{\sigma} = -p\boldsymbol{\delta} + \boldsymbol{\sigma}_m + \boldsymbol{\sigma}_f + \boldsymbol{\sigma}_s \tag{2.7}$$

where p is the incompressibility pressure, $\boldsymbol{\delta}$ the identity tensor, $\boldsymbol{\sigma}_m$ and $\boldsymbol{\sigma}_f$ represent the stress contribution of the matrix and the fibrous network, respectively, and where the stress

term $\boldsymbol{\sigma}_s$ is induced by steric interactions.

Matrix – From the previous assumptions, it follows that:

$$\boldsymbol{\sigma}_m = \mathbf{F} \cdot \left(\frac{\partial W}{\partial \mathbf{F}} \right)^T \tag{2.8}$$

Overall fibrous network – Using the homogenization method for trusses of hyperelastic bars [36], the bar $\boldsymbol{\sigma}_f$ and the steric $\boldsymbol{\sigma}_s$ tensors can be expressed as:

$$\boldsymbol{\sigma}_f = \frac{1}{V_{REV}} \sum_{i=1}^{N} \mathbf{T}_i \otimes \ell_i \mathbf{e}_i = \frac{\Phi}{\pi d_0^2 \xi_0} \sum_{i=1}^{N} t_i \lambda_i \, \mathbf{e}_i \otimes \mathbf{e}_i \tag{2.9}$$

and

$$\boldsymbol{\sigma}_s = \frac{\Phi}{\pi d_0^2 \xi_0} \sum_{q=1}^{M} r_q \delta_q^* \, \mathbf{e}_q \otimes \mathbf{e}_q \tag{2.10}$$

for the *lamina propria*, with $\lambda_i = \frac{\ell_i}{\ell_0}$ and $\delta_q^* = \delta_q / \ell_0$, and:

$$\boldsymbol{\sigma}_f = \frac{\Phi_c}{\pi d_{0c}^2 \xi_{0c}} \sum_{i=1}^{N} t_{ic} \lambda_i \, \mathbf{e}_i \otimes \mathbf{e}_i + \frac{\Phi_m}{\pi d_{0m}^2 \xi_{0m}} \sum_{i=1}^{N} t_{im} \lambda_i \, \mathbf{e}_i \otimes \mathbf{e}_i \tag{2.11}$$

and

$$\boldsymbol{\sigma}_s = \left(\frac{\Phi_c}{\pi d_{0c}^2 \xi_{0c}} + \frac{\Phi_m}{\pi d_{0m}^2 \xi_{0m}} \right) \sum_{q=1}^{M} r_q \delta_q^* \, \mathbf{e}_q \otimes \mathbf{e}_q \tag{2.12}$$

for the *vocalis*. Thus, the overall response of the *lamina propria* (resp. *vocalis*) depends on 11 (resp. 17) input parameters to be determined at rest:

6 (resp. 10) histological parameters: the fibril diameter d_0 (resp. d_{0k}), their waviness amplitude R_0 (resp. R_{0k}), spatial periodicity H_0 (resp. H_{0k}) from which the tortuosity ξ_0 (resp. ξ_{0k}) can be estimated, the fibrils volume fraction Φ (resp. Φ_k) and initial 3D fiber orientation (θ_0 , φ_0).

5 (resp. 7) mechanical parameters: the fibrils Young's modulus E_f (resp. E_{fk}), the matrix shear modulus μ, the transition parameter α (resp. α_k) and the interaction coefficients β and δ_c related to the steric effects.

2.3 Model identification

The identification of the histo-mechanical parameters of the model was performed by adjusting its predictions to biomechanical data recently acquired on human vocal-fold tissues [54]. To do so, a representative set of *lamina propria* and *vocalis* sublayers (hereinafter noted as LP_i and V_i, $i \in [1, 2]$) was selected from the reported database. Each sample

was sequentially subjected to a series of finite strain and cyclic physiological loadings, *i.e.*, longitudinal tension, transverse compression, and longitudinal shear. Only the first load-unload sequences were considered, as displayed in Figure 2.4 for samples (LP_1 , V_1), and in Appendix A. - Figure 1 for samples (LP_2 , V_2).

2.3.1 Simulated mechanical tests

The REVs were subjected to the following loading conditions to reproduce the experimental loading paths:

- *Uniaxial tension* $\mathbf{e}_z$ – To simulate uniaxial tension along the vocal folds longitudinal direction $\mathbf{e}_z$, with $\mathbf{F} = F_{xx}\,\mathbf{e}_x \otimes \mathbf{e}_x + F_{yy}\,\mathbf{e}_y \otimes \mathbf{e}_y + F_{zz}\,\mathbf{e}_z \otimes \mathbf{e}_z$ and $\boldsymbol{\sigma} = \sigma_{zz}\,\mathbf{e}_z \otimes \mathbf{e}_z$, the component F_{zz} was imposed, whereas F_{yy} was computed to ensure the transverse stress-free state condition $\sigma_{xx} = \sigma_{yy} = 0$. The component $F_{xx} = 1/F_{yy}F_{zz}$ was computed by means of the incompressibility assumption. The hybrid conditions finally allowed to determine the pressure p.
- *Uniaxial compression* $\mathbf{e}_x$ – A similar procedure was used to reproduce uniaxial compression along the transverse direction $\mathbf{e}_x$.
- *Simple shear (*$\mathbf{e}_z$, $\mathbf{e}_x$*)* – To simulate simple shear in the longitudinal plane ($\mathbf{e}_z$, $\mathbf{e}_x$), the REVs were subjected to $\mathbf{F} = \boldsymbol{\delta} + \gamma_{zx}\,\mathbf{e}_z \otimes \mathbf{e}_x$ and $p = 0$, where γ_{zx} is the imposed shear strain.

The resulting stress predictions of the model were finally expressed using the first Piola-Kirchoff stress tensor $\mathbf{P} = \boldsymbol{\sigma} \cdot \mathbf{F}^{-T}$.

2.3.2 Optimization protocol

In order to fit macroscale stress-strain responses, the following protocol was adopted to obtain optimized sets of histo-mechanical data:

(i) As far as possible, all input histological parameters were determined from microstructural analyses conducted on unloaded samples, previously observed using 2D standard optical microscopy [54]. Alternatively, remaining histo-mechanical parameters were initialized and bounded within a range of admissible physiological values extrapolated from the literature.

(ii) A least-squared approach was subsequently used to minimize the discrepancies between theoretical and experimental stress tensors. To do so, a nonlinear constraint optimization was carried out, as in [12]. For each tested sample, this procedure accounted for the different loading conditions the sample was subjected to. Considering the complexity of the optimization problem, the uniqueness of the solution could not be established. Nevertheless, it is worth noticing that the set of optimized parameters does not depend on the applied loading mode. Furthermore, as the proposed model is purely hyperelastic, it cannot reproduce the hysteresis experimentally observed [54].

The optimization was accordingly adjusted to experimental "neutral" stress-strain curves, lying in between the loading and unloading paths.

2.4 Results and discussion

2.4.1 Histo-mechanical parameters: choice of initial guesses and optimized values

In order to obtain the optimized histological parameters reported in Table 2.1 and Table 2.2, for the *lamina propria* samples, and in Table 2.3 and Table 2.4 for the *vocalis* specimens, initial guess corridors discussed hereafter were initially considered.

Lamina propria

Sample	θ_0 (°)	φ_0 (°)	H_0 (μm)	R_0 (μm)	d_0 (μm)	Φ	ξ_0
LP_1	16	83	42	5	0.4	0.46	1.129
LP_2	16	83	42.5	5	0.4	0.48	1.126

Table 2.1: Set of histological parameters identified for *lamina propria* samples, LP_i. Gray-colored columns refer to quantities computed as a function of the determined histological parameters.

Sample	E_f (MPa)	μ (Pa)	α	β (N)	δ_c (μm)
LP_1	847	330	$4.4\ 10^{-3}$	$2\ 10^{-4}$	66
LP_2	847	290	$4.3\ 10^{-3}$	$4\ 10^{-4}$	65.7

Table 2.2: Set of mechanical parameters identified for *lamina propria* samples, LP_i.

Collagen volume fraction Φ: Depending on the tissue depth $\mathbf{e}_x$, Φ is reported to vary between 0.15 and 0.55 [34, 105, 194, 244]. Although the upper limit appears to underestimate the volume fraction of collagen in the deepest portion of the sublayers micrographs (see Figure 2.1), it is relevant when averaged over the whole sample thickness. Within this range of admissible values, the optimization led to $\Phi \approx 0.47$ for both LP_i samples.

Collagen fibril's diameter d_0: d_0 is known to range between 10 nm (collagen Type III) and 500 nm (Type I) [9, 84, 91, 92, 273]. By imposing these physiological boundaries, $d_0 = 400$ nm was obtained for each sample.

Fibril's sine waveform parameters (H_0 ; R_0): The spatial period and amplitude of wavy collagen fibrils at rest were bounded within the corridors (10–70 μm ; 1–10 μm), respectively [15, 194]. The optimization conducted to similar values for both samples, close to (42 μm ; 5 μm), implying an initial tortuosity ξ_0 of about 1.13.

Network 3D orientation (θ_0 ; φ_0): The 3D angular distribution of collagen fibrils in the *lamina propria* (θ_0 ; φ_0) = (30° ; 39°) was extrapolated from recent 3D CT images obtained on a single unloaded sample [15], showing a pronounced preferential orientation along $\mathbf{e}_z$ and a slight orthotropy in the perpendicular plane. To account for the inter-sample variability, values were let free to vary within the range (0–50°; 20–90°). The optimization led to (θ_0 ; φ_0) ≈ (16° ; 83°) for both samples, a nearly 2D network in the plane ($\mathbf{e}_z$, $\mathbf{e}_y$). It should be noticed that a quasi-plane network (*i.e.*, θ_0 ≤ 35° and φ_0 ≥ 80°) was required by the model to properly reproduce the *lamina propria* shear response.

Collagen fibril Young's modulus E_f: Though very challenging, the mechanical properties of a single collagen (Type I) fibril have been rather extensively investigated using AFM, MEMS technology and X-ray diffraction [33, 91, 168, 233, 273]. In aqueous media, the tangent modulus measured under longitudinal tension, E_f, was reported to range from 1 MPa at small strains up to an asymptotic value of 1 GPa at finite strains, where a linear stress-strain regime is attained. Imposing these constraints, E_f ≈ 850 MPa was obtained for both LP_i samples.

Matrix shear modulus μ: This parameter was firstly initialized with the shear modulus of hyaluronic acid μ_{HA} ≈ 20-50 Pa [115], *i.e.*, the most abundant component of the ground substance within the *lamina propria* [46, 77–79, 95, 104, 109, 115]. In order to account for other components within the matrix (*e.g.*, cells and elastin), μ was let free to vary up to 1.5 MPa, *i.e.*, the estimated Young's modulus of isolated elastin fibers [272, 273]. The optimization finally conducted to $\mu \approx \mathcal{O}(10^2)$ Pa for both samples.

Transition parameter α: Initially let free, the optimization lead to $\alpha \approx \mathcal{O}(10^{-3})$ for both samples. Optimized values were further confirmed comparing the tension t_j predicted by the micro-mechanical model for a stretched fibril (d_0, H_0, R_0, E_f) to that obtained by the FE simulation of the stretching of a corrugated elastic beam with identical properties.

Interaction coefficients β and δ_c: β and δ_c were freely adjusted during the optimization, respectively leading to ≈ $\mathcal{O}(10^{-4})$ N and ≈ 66 μm for both samples. To the author's knowledge, contact forces endured by entangled collagen fibers in such soft living tissues are not documented. This is probably ascribable to experimental limitations. However, the reaction forces determined on collagen fibrils using transverse nano-indentation [9], with an amplitude of $\mathcal{O}(10^2)$ pN, show a substantial agreement with the fiber-fiber reaction forces r_q predicted by the model during transverse compression (see Figure 2.6). It is also worth noticing that interaction length δ_c remains rather close to the respective fiber's "encumbrance", *i.e.*, $\mathcal{O}(2R_0 + D_0)$, where typical values of the collagen fiber bundle diameter D_0 range between 1 and 20 μm [27, 84].

Vocalis

Sample	θ_0 (°)	φ_0 (°)	H_{0k} (μm)	R_{0k} (μm)	d_{0k} (μm)	Φ_k	ξ_{0k}
V_{1_c}	33	70	28	6.4	0.4	0.10	1.4
V_{1_m}	33	70	1 350	130	1	0.70	1.08
V_{2_c}	28	67	30	5.5	0.4	0.12	1.28
V_{2_m}	28	67	1 620	90	1	0.70	1.03

Table 2.3: Set of histological parameters identified for *vocalis* samples, V_i ($k \in \{c, m\}$ labels collagen or muscular fibrils accordingly) . Gray-colored columns refer to quantities computed as a function of the determined histological parameters.

Sample	E_{fk} (MPa)	μ (Pa)	α_k	β (N)	δ_c (μm)
V_{1_c}	847	900	$4.4\ 10^{-3}$	$2.2\ 10^{-4}$	367
V_{1_m}	0.05	900	$1.1\ 10^{-2}$	$2.2\ 10^{-4}$	367
V_{2_c}	847	980	$4.4\ 10^{-3}$	$7.6\ 10^{-5}$	360
V_{2_m}	0.05	980	$2.7\ 10^{-2}$	$7.6\ 10^{-5}$	360

Table 2.4: Set of mechanical parameters identified for *vocalis* samples V_i ($k \in \{c, m\}$ labels collagen or muscular fibrils accordingly).

Collagen sheaths parameters d_{0c}, E_{fc}, α_c were respectively set equal to the optimized values d_0, E_f, α previously obtained for the *lamina propria* samples (see Table 2.1 and Table 2.2). Furthermore, the equivalent myofibril diameter was set to $d_0 = 1$ μm which is in line with measurements performed on V_i micrographs [54] and with available data in the literature [15, 50, 55, 163, 196, 230].

Volume fractions Φ_k: Myofibrils' (resp. collagen fibrils') volume fraction Φ_m (resp. Φ_c) in the *vocalis* was measured within the range 0.60 – 0.80 (resp. 0.05 – 0.15). If hardly any data are reported regarding Φ_m for skeletal muscles, obtained measurements for Φ_c appear to be consistent with the values collected on rabbit tissues [266], varying from 0.10 to 0.25. Therefrom, within these ranges of admissible values, the optimization led to $\Phi_m \approx 0.70$ (resp. $\Phi_c \approx 0.10$) for both V_i samples.

Muscular and collagen fibril's sine waveform parameters (H_{0k} ; R_{0k}): The spatial period and amplitude of wavy myofibrils (H_{0m} ; R_{0m}) were bounded within narrow corridors (1 300 – 1 700 μm ; 70 – 140 μm) [15]. The optimization conducted to distinct values for V_i samples, corresponding to an initial tortuosity ξ_0 of 1.08 and 1.03 respectively. This stands for rather straight fibrils at rest in both cases, in line with what shown in Figure 2.1. Regarding collagen fibrils' tortuosity, *lamina propria* physiological bounds were preserved, yielding to (H_{0c} ; R_{0c}) $\approx$ (30 μm ; 6 μm). The model identification therefore suggests that collagen fibrils wrapping myofibril bundles in the *vocalis*, at rest, are wavier (from 15 up to 23%) than those laying in the *lamina propria*. This finding is in agreement with previous micrographs of collagen sheaths, showing a double wavelength due to a first muscular undulation entwined with a second-degree collagen crimping.

Network 3D orientation (θ_0 ; φ_0): As for the *lamina propria*, the initial orientation of the muscular network was determined extrapolating 3D descriptors from *vocalis* X-ray images [15], (θ_0 ; φ_0) $\approx$ (33° ; 53°). The model identification eventually led to (θ_0 ; φ_0) $\approx$ (30° ; 68°) for both samples.

Myofibril Young's modulus E_{fm}: The "passive" longitudinal Young's modulus of frog and rabbit myofibrils [177, 266] is reported to range from 1 to 35 kPa below 10% strains, rising up to $\approx$ 60 kPa at finite strains. Within this range of admissible values, the optimization returned $E_{fm} \approx 50$ kPa for both V_i samples.

Matrix shear modulus μ: *Vocalis* ground substance composition was assumed to be close to that of the *lamina propria*. Accordingly, *vocalis* matrix shear modulus μ was calibrated on HA data, as detailed for the *lamina propria*. This conducted to $\mu \approx \mathcal{O}(10^3)$ Pa for both samples.

Parameter α_m: Optimization lead to $\alpha_m \approx \mathcal{O}(10^{-2})$ for both samples.

Interaction coefficients β and δ_c: As for the *lamina propria*, no constraints were applied to β and δ_c, yielding to values of $\beta \approx \mathcal{O}(10^{-4})$ and $\mathcal{O}(10^{-5})$ N for each V_i sample and $\delta_c \approx 360$ μm for both samples.

2.4.2 Macro and microscale predictions

A comparison between the model macroscale predictions and the corresponding experimental data is shown in Figure 2.4, for both sublayers (LP_1 and V_1 , results obtained for LP_2 and V_2 are reported in Appendix A. - Figure 1) and the three considered loading modes, *i.e.*, longitudinal tension, transverse compression, longitudinal shear. For each loading case, the stress-strain response of a homogeneous isotropic neo-hookean material owning the same mechanical properties as the respective matrix was superimposed to better understand the contribution of each phase to the overall composite behavior. The strain-induced evolution of microscale descriptors is displayed in Figure 2.5 and Figure 2.6.

- *Longitudinal tension* – Regarding the *lamina propria*, model predictions satisfyingly reproduce the macroscale non-linear stress-strain response with a typical J-shape strain-hardening (Figure 2.4 a). The stress contribution predicted for the matrix-equivalent medium is negligible compared to that of the composite layer overall response. This emphasizes the major mechanical role played by the collageneous fibrous network in longitudinal tension and is supported by lower-scale mechanisms predictions: as shown in Figure 2.5 a, collagen fibrils are permanently stretched, and gradually unfolded, as the load is applied. Their tensile response is coupled with a noticeable rotation and progressive alignment toward the loading direction $\mathbf{e}_z$: angles θ_i decrease down to 10° at $\varepsilon_{zz} \approx 0.10$. These micro-mechanisms result in finite deformations of the REV, highly stretched along $\mathbf{e}_z$, shrunk along $\mathbf{e}_y$ (*e.g.*, with $\varepsilon_{yy} \approx -0.60$ at $\varepsilon_{zz} = 0.10$ for LP_1), but also expanded along $\mathbf{e}_x$ (*e.g.*, with $\varepsilon_{xx} \approx 0.50$),

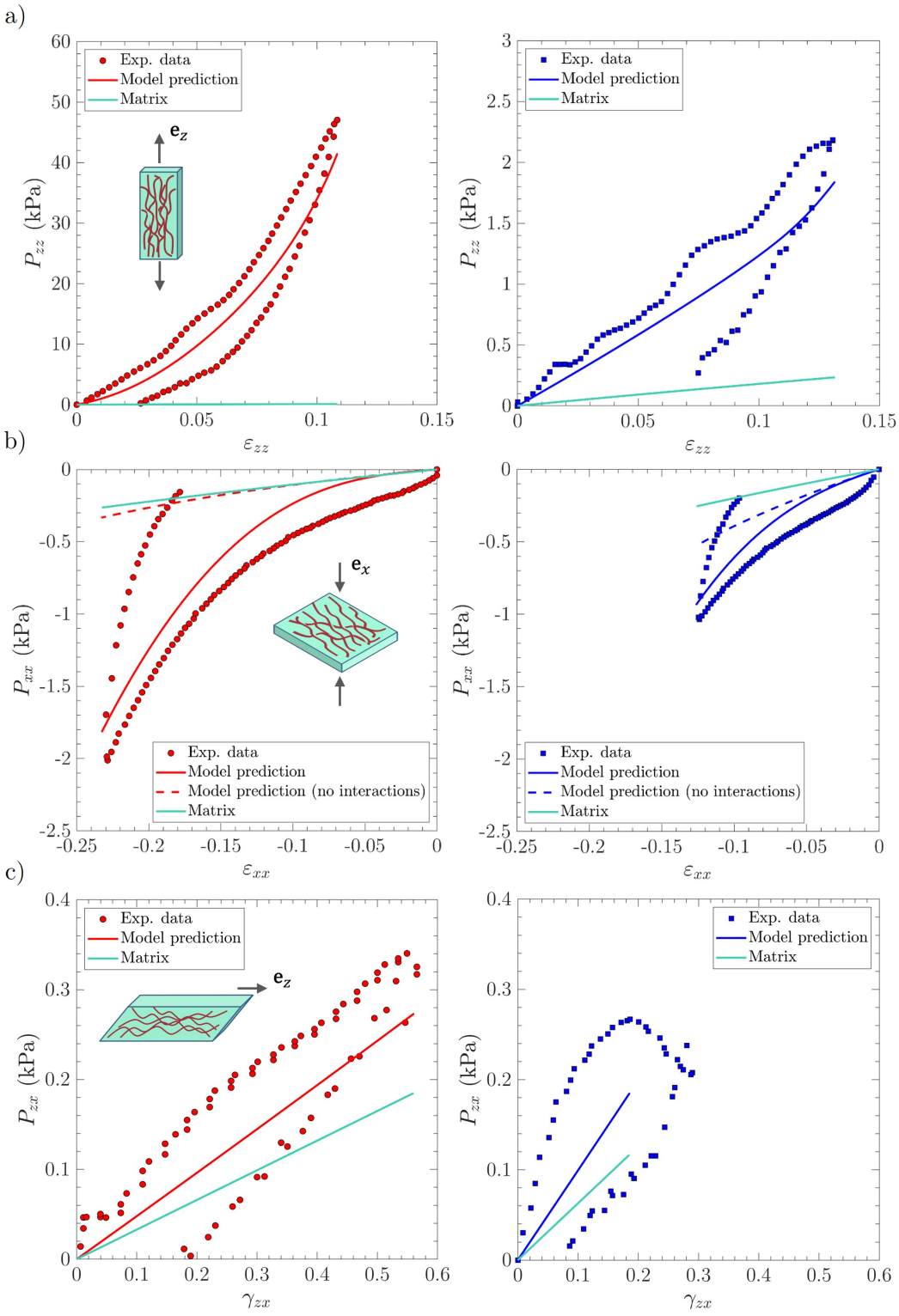

Figure 2.4: Macroscopic stress-strain curves of vocal-fold sublayers under multiaxial loadings. Experimental data *vs.* model predictions obtained for *lamina propria* sample LP_1 (left, in red) and *vocalis* sample V_1 (right, in blue): a) longitudinal tension; b) transverse compression; c) longitudinal shear.

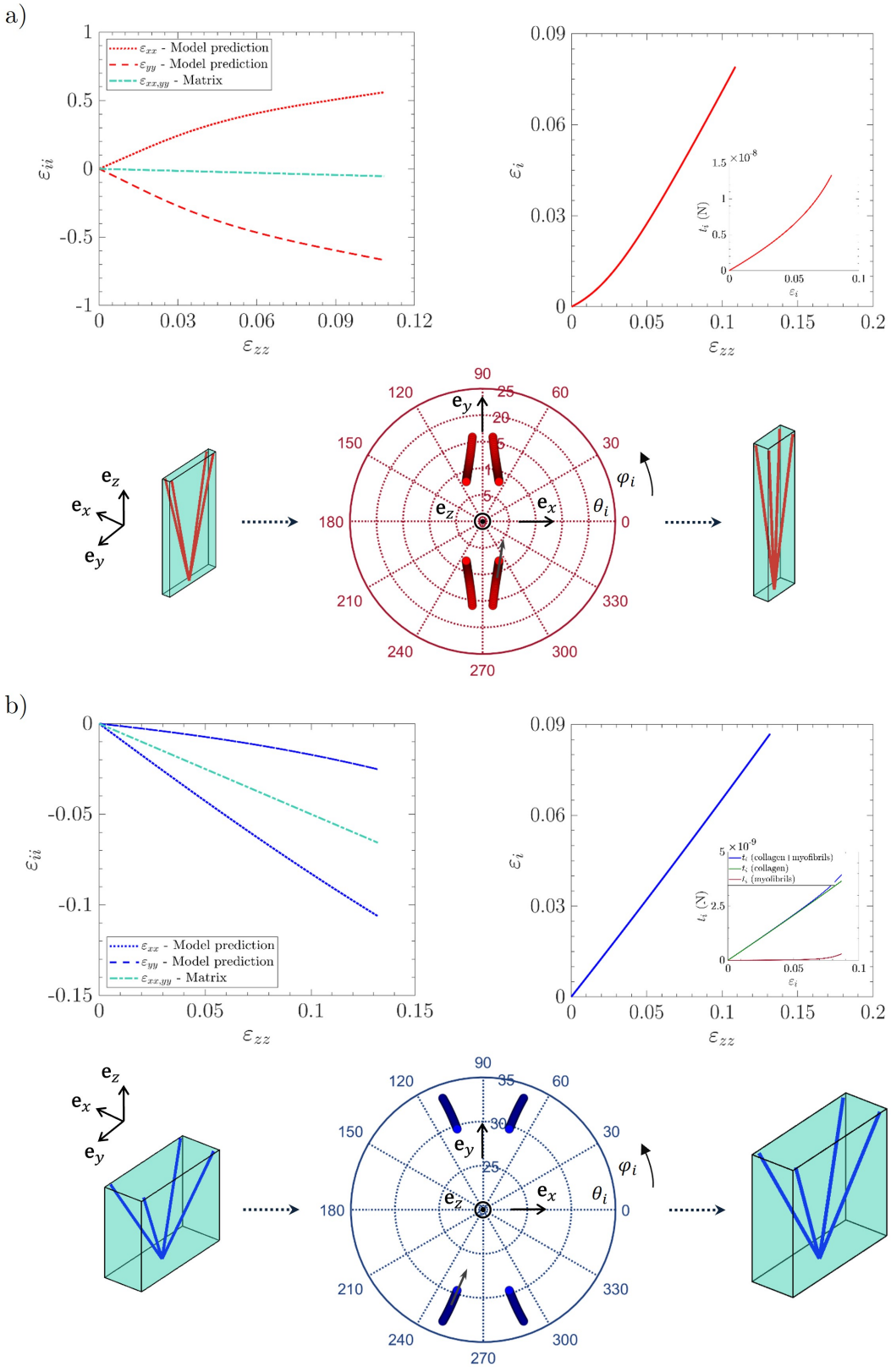

Figure 2.5: Strain-induced evolution of multiscale descriptors predicted for a) *lamina propria* sample LP_1 and b) *vocalis* sample V_1 during tension along $\mathbf{e}_z$: macroscopic loading paths (top left); stereographic projection of orientation vectors $\mathbf{e}_i$ from initial to final state, $i \in [1..4]$ (bottom); strain variation of the fibril chord ε_i and corresponding tension t_i (top right).

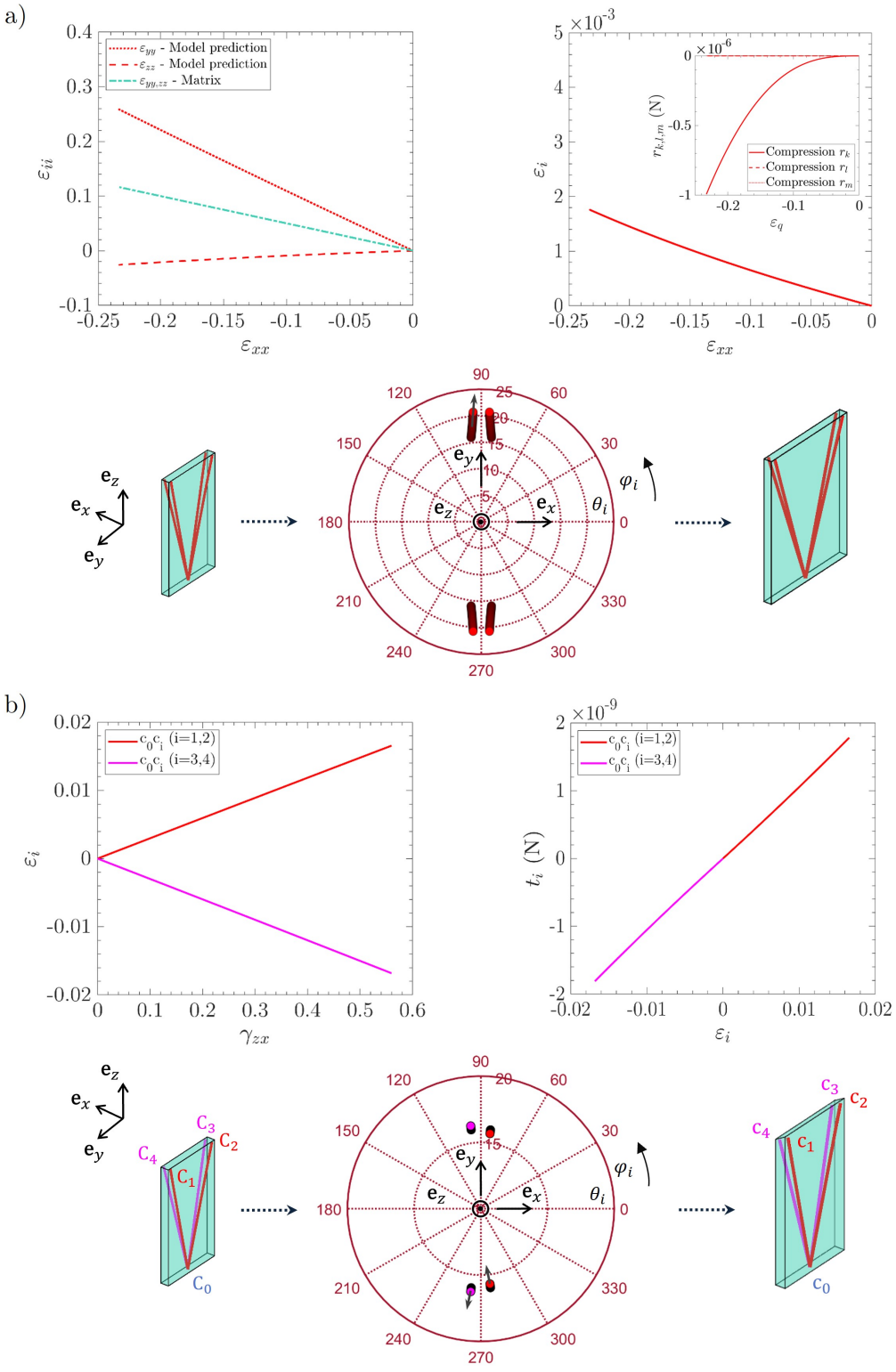

Figure 2.6: Strain-induced evolution of multiscale descriptors for *lamina propria* sample LP_1: a) compression along $\mathbf{e}_x$ – macroscopic loading paths (top left), stereographic projection of orientation vectors $\mathbf{e}_i$ from initial to final state, $i \in [1..4]$ (bottom), strain variation of the fibril chord ε_i and corresponding steric interactions $r_{k,l,m}$ (top right); b) shear in the ($\mathbf{e}_z$, $\mathbf{e}_x$) plane – strain variation of the fibril chord ε_i (top left) and corresponding tension t_i (top right), stereographic projection of orientation vectors $\mathbf{e}_i$ from initial to final state, $i \in [1..4]$ (bottom).

thereby showing a marked auxetic behavior, yet only slightly observed experimentally. Conversely, transverse deformations would be close to $\varepsilon_{yy} = \varepsilon_{xx} \approx -0.05$ without any fibers ($\Phi = 0$), *i.e.*, for an incompressible isotropic material (see Figure 2.5 a, in green). The predicted auxeticity is probably attributable to the *lamina propria* collageneous network structural anisotropy as well as the imposed the incompressibility constraint.

Concerning the *vocalis*, macroscopic tensile responses are similarly rather well predicted by the model (see Figure 2.4 a), whereas the micro-mechanisms slightly differ due to histo-mechanical discrepancies between the considered tissues. The less pronounced nonlinear response of the *vocalis* is attributable both to a lower initial tortuosity ξ_0 and the negligible stiffness of muscular fibers compared to that of collagen. It is worth noticing that Figure 2.5 b reveals the major role played by the collagen sheaths surrounding muscle fibers, as recently reported by Ward *et al.*[266] for passive tensile properties. Still, compared with the *lamina propria*, a minor volume fraction of collagen leads to lower stress levels at the macroscale.

- *Transverse compression* – The nonlinear response and strain hardening of the *lamina propria* is equally predicted for transverse compression along $\mathbf{e}_x$, *i.e.*, applied perpendicularly to the fiber preferential orientation. However, in this case, the macroscale nonlinearity is not inherited from the coupled unfolding/rotation of the collageneous network: indeed, Figure 2.6 a shows that the fibrils' extremities are barely stretched ($\forall\ \varepsilon_{xx},\ \varepsilon_i \approx 0$, $t_i \approx 0$ and $\xi_i \approx \xi_0$). Fibers rotations in the longitudinal plane ($\mathbf{e}_y$, $\mathbf{e}_z$) are also moderate, *e.g.*, angles θ_i (resp. φ_i) of about 5° (resp. 2°) at $\varepsilon_{xx} \approx -0.25$. Auxetic effects along $\mathbf{e}_z$ are still predicted, albeit less marked than in longitudinal tension. The cause of the nonlinearity experienced at the tissue scale should rather be sought in steric interactions: Figure 2.6 a shows non-zero microscopic repulsion forces r_k predicted along the loading direction, while interaction forces in the other $\mathbf{e}_q$-directions (see Figure 2.2), here noted r_l and r_m, are not triggered. More generally, among all the modeling cases considered in the present study, steric interactions were uniquely activated under compressive loadings. Furthermore, Figure 2.4 b displays what macroscale predictions would be like when neglecting steric hindrance effects ($\beta = 0$, see dotted lines), showing a quasi-linear mechanical behavior extremely close to that of the matrix. By contrast with the trends obtained in longitudinal tension, this highlights the major mechanical contribution of the matrix under compression at low strains, and its strong attenuation once steric interactions are triggered (for $\varepsilon_{xx} \approx -0.05$). Similar results are obtained for *vocalis* sample V_1, as reported in Appendix A. - Figure 2 a, though a faster fiber recruitment and unfolding is predicted in that case.

- *Longitudinal shear* – Leaving aside the experimental artifacts, notably observed for the *vocalis* [54], the quasi-constant strain hardening exhibited under longitudinal simple shear is well reproduced for both sublayers (Figure 2.4 c). The predicted mechanical behavior is very close to that of the sole matrix. This is attributable to the mechanisms evidenced at the microscale and illustrated in Figure 2.6 b for LP_1 (see Appendix

A. - Figure 2 b for V_1): fibers rotation is negligible and their unfolding is rather limited. More specifically, fibers $i = \{1, 3\}$ are compressed, while fibers $i = \{2, 4\}$ are slightly stretched ($\forall i, |\varepsilon_i| < 0.02$) so that they remain crimped during the load, the complete unfolding of the fibers being predicted for $\gamma_{zx} \approx 3$.

2.4.3 Effect of fiber orientation on the monotonic and vibratory properties

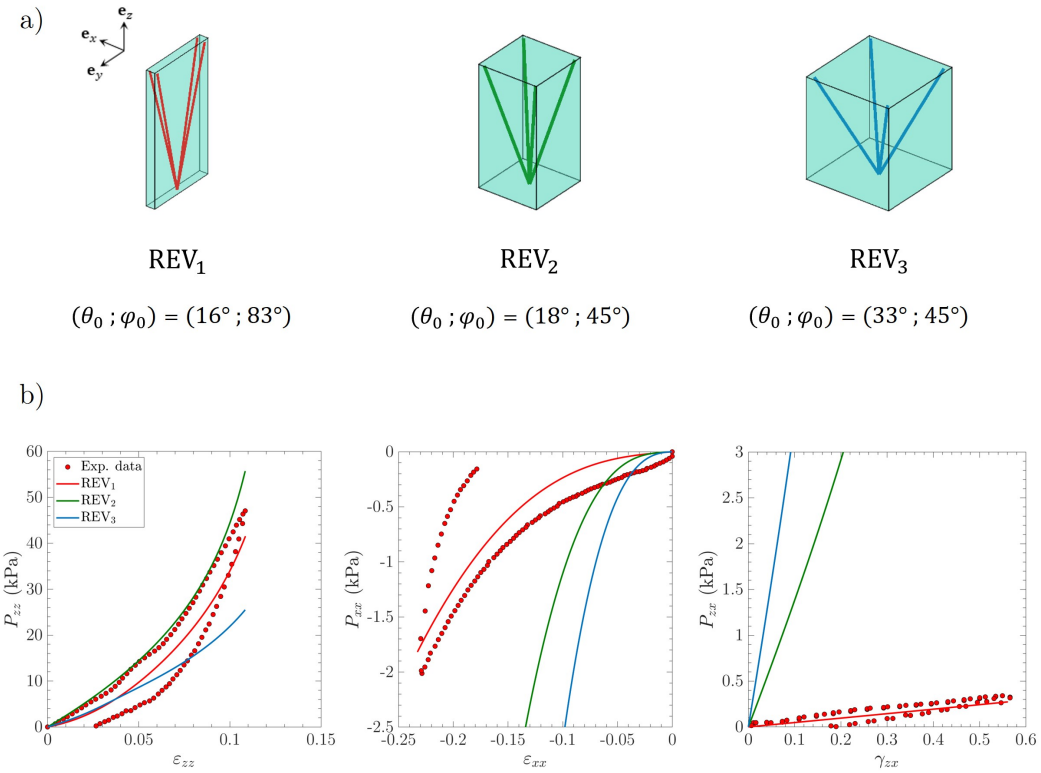

Figure 2.7: *Lamina propria* fibrous microstructure influence on monotonic properties: a) panel of the three REVs in the undeformed configuration $\mathscr{C}_0$ proposed to gauge the effect of 3D fiber orientations on the *lamina propria* monotonic mechanics; b) predicted stress-strain curves obtained for each REV subjected to longitudinal tension, transverse compression and longitudinal shear (from left to right), along with reference experimental data (LP$_1$).

The identified model can also be used to further investigate the effect of alterations in the fibrous configuration on the tissue mechanics, subjected to both quasi-static and vibratory loadings. More specifically, a major focus is here drawn to the role played by fiber orientation, *i.e.*, degree of alignment and symmetry along the antero-posterior direction $\mathbf{e}_z$, of the *lamina propria* sample LP$_1$ by studying the mechanics of REVs owning identical histo-mechanical properties (see Table 2.1 and Table 2.2), albeit different initial orientations $(\theta_0\,;\varphi_0)$. As illustrated in Figure 2.7 a, three distinct 3D configurations were selected: (i) a first quasi-planar orthotropic structure REV$_1$, resulting from the previous model identification (sample LP$_1$); (ii) a transverse isotropic structure with moderately oriented fibers along $\mathbf{e}_z$, noted REV$_2$, being a standard rotational symmetry assumption

often adopted to model the vocal-fold tissue (*e.g.*, [61, 144, 227]); (iii) a transverse isotropic structure with a relatively weak fibers alignment, noted REV_3.

- *Monotonic loading* – The predicted stress-strain curves obtained for the three structures subjected to longitudinal tension, transverse compression and longitudinal shear are presented in Figure 2.7 b. Globally, strongly oriented structures exhibit stiffer responses under longitudinal tension, while less oriented configurations offer higher resistance to longitudinal shear and transverse compression. In particular, a comparison of the responses exhibited by REV_1 and REV_2 allows to highlight the impact of the microstructural symmetry: despite similar θ_0-values, their multiaxial responses differ drastically. In tension, REV_1 shows lower stress levels and tangent moduli, as it requires to open along $\mathbf{e}_x$ before enabling fibers to work in tension along $\mathbf{e}_z$. Instead, a transverse isotropic structure limits fibers' rotation along the loading direction, thus leading to an earlier fiber recruitment, which stiffens the macroscopic response of the tissue. Likewise, REV_1 stress-strain curve looks softer in compression because the REV contraction, and corresponding repulsive forces due to steric hindrance, along $\mathbf{e}_x$ is induced after moderate in-plane fibers rotation and global opening of the structure along $\mathbf{e}_y$. Qualitative trends are similar in shear, even if the fibers rotation is negligible in this case: fibers recruitment is faster for REV_2, inducing higher stress levels at the macroscale. In conclusion, a rather small change in the initial orientation of the fibrous network may activate a series of combined nonlinear micromechanisms of deformation (*e.g.*, fibers' rotation, uncrimping, tension, compression and steric interactions), which in turn strongly impact the multiaxial response of the tissue at the macroscale. Finally, this study points out that a transverse isotropic structure should not be used to model the mechanical behavior of the *lamina propria*. An orthotropic structure represents a more suitable fibrous configuration.

- *Vibratory loading* – To better highlight the impact of these fiber-scale micro-mechanisms on vocal-fold vibrations, a simplified analysis of the *lamina propria* vibratory properties was finally addressed using beam theory. Various beam models can be found in the literature to semi-quantitatively describe the vocal-fold vibration [25, 66, 251, 276, 277], albeit with a poor correlation with the tissue's microstructural features. The approach proposed by Kelleher *et al.* [144] was here adapted to the present micro-mechanical model to compute the natural frequencies of vibration of $\text{LP}_0 1$ for transverse vibrations. Thus, at a first approximation, the *lamina propria* is modeled as a pinned-pinned Timoshenko beam of rectangular cross-section (initial length L_0, width w_{0_y}, thickness w_{0_x}), with incompressible, anisotropic and hyperelastic properties. When subjected to a tensile strain ε_{zz} along the antero-posterior direction $\mathbf{e}_z$, the corresponding frequency of the n^{th} mode of vibration of the beam, noted F_n, can be expressed as it follows [144]:

$$F_n(\varepsilon_{zz}) = \frac{n^2\pi^2}{L^2}\sqrt{\frac{E_t I}{\zeta\rho A}\left(1 + \frac{fL^2}{n^2\pi^2 E_t I} + \frac{f}{k_s G_t A}\right)}, \tag{2.13}$$

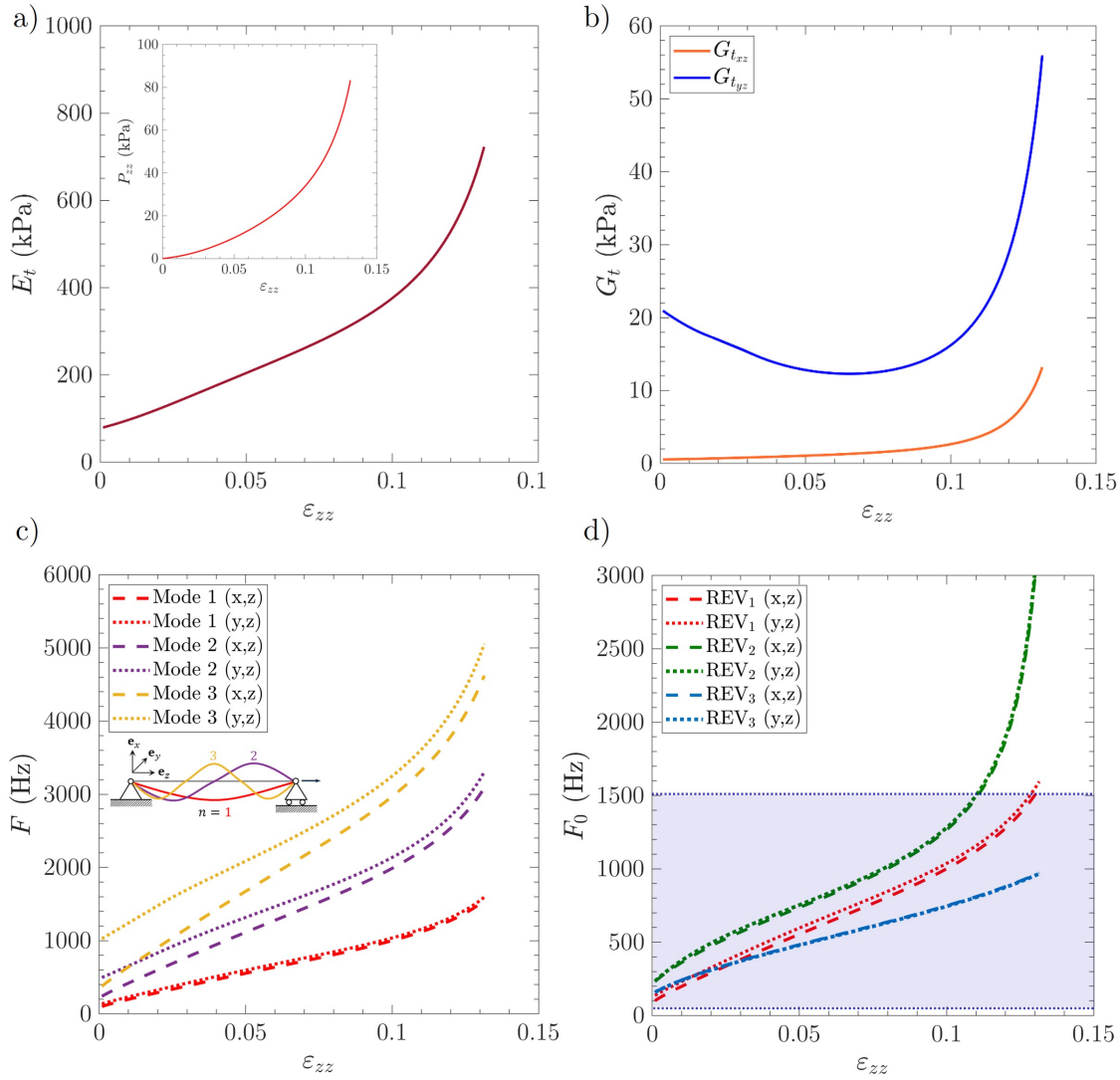

Figure 2.8: *Lamina propria* fibrous microstructure influence on vibratory properties as functions of the applied tensile strain ε_{zz}: a) tangent longitudinal modulus E_t, determined from the predicted nominal stress P_{zz} (REV$_1$, see inset); b) tangent transverse shear moduli $G_{t_{xz}}$ and $G_{t_{yz}}$ (REV$_1$); c) first three modal frequencies in the planes of vibration $(\mathbf{e}_x, \mathbf{e}_z)$- and $(\mathbf{e}_y, \mathbf{e}_z)$ (REV$_1$); d) fundamental frequency F_0 obtained for the three structures REV$_1$, REV$_2$ and REV$_3$ (blue-shaded area: human voice F_0 range).

with

$$\zeta(\varepsilon_{zz}) = 1 + n^2\pi^2 \left(\frac{I}{AL^2} \left(1 + \frac{f}{k_s G_t A} \right) + \frac{E_t I}{k_s G_t A L^2} \right), \tag{2.14}$$

where $L = L_0\, \mathrm{e}^{\varepsilon_{zz}}$ is the beam length, $A = w_x w_y$ its cross-section ($w_x = w_{0x}\, \mathrm{e}^{\varepsilon_{xx}}$, $w_y = w_{0y}\, \mathrm{e}^{\varepsilon_{yy}}$), $f = A\, \sigma_{zz}$ the applied longitudinal tension, ρ the tissue density, k_s the Timoshenko's shear correction coefficient ($k_s = 5/6$ for a beam of rectangular cross-section) and where E_t is the longitudinal tangent modulus predicted by the micro-mechanical model at ε_{zz} (see Figure 2.8 a). Accounting for the orthotropic properties of the *lamina propria*, two planes of vibration $(\mathbf{e}_x, \mathbf{e}_z)$ and $(\mathbf{e}_y, \mathbf{e}_z)$ were considered thereafter. The beam's second moment of inertia $I = w_x\, w_y^3/12$ (resp. $w_y\, w_x^3/12$) and its predicted tangent shear modulus $G_t = G_{t_{xz}}$ (resp. $G_{t_{yz}}$) were varied accordingly (see Figure 2.8 b). Assuming $\rho = 1040$ kg.m^{-3}, $L_0 = 17$ mm and

$w_{0x} = w_{0y} = 1.5$ mm [54, 144], the natural frequencies of the first three modes of vibration ($n = 1..3$) were obtained, the latter modes being expected to account for 99% of the energy at the onset of vocal-fold self-oscillation [144]. Corresponding predictions $F_1 < F_2 < F_3$ are displayed in Figure 2.8 c for both planes of vibration. The increase with the applied pre-strain ε_{zz} is ascribed to the stiffening of E_t (see Figure 2.8 a). Additionally, the marked orthotropy of REV_1 induces a significant difference between F_2 and F_3 depending on the plane of vibration. It is worth noticing that F_1 is also referred to as F_0, being, at a first approximation, the expected acoustical fundamental frequency of vibration during phonation. A comparison of F_0 predictions for REV_1, REV_2 and REV_3 is reported in Figure 2.8 d. Regardless of the considered configuration, a nonlinear evolution of F_0 with the applied strain is observed at all frequencies, in quantitative agreement with typical *in vivo* F_0 data (50 – 1 500 Hz) [32, 152] and with former theoretical works based on the gold-standard Gasser-Ogden-Holzapfel constitutive model [89, 144]. More importantly, the induced effect of the initial fiber orientation on F_0 is clearly highlighted.

2.5 Conclusion and future work

In this chapter, an idealized description of human vocal-fold sublayers, *i.e.*, the *lamina propria* and the *vocalis*, 3D fibrous architecture is initially proposed based on histological evidence. Therefrom, a 3D micro-mechanical model for the vocal-fold tissues is developed and identified on four experimental targets, *i.e.*, two *lamina propria* and two *vocalis* samples. Based on a single set of histo-mechanical parameters per sample, the present model is not only able to reproduce its nonlinear and anisotropic behavior under key physiological loadings (*i.e.*, tension, compression, shear), but also to predict the underlying deformation micromechanisms at the fiber scale, *i.e.*, a complex and path-dependent combination of 3D fibers rotation, matrix/fibers deformation and interactions. These micromechanisms are analyzed to clarify the inherited macroscopic tendencies. More specifically, this study highlights the major role of the 3D fiber orientation in longitudinal tension, steric hindrance in transverse compression and the matrix contribution in longitudinal shear. It is also shown how a slight change in the histo-mechanical configuration can significantly alter both the tissue monotonic and vibratory properties, affecting in turn vocal folds vibrations. Further developments are needed to improve the proposed micro-mechanical model. Although challenging to identify and quantitatively characterize, the introduction of microscale time-dependent phenomena is required to account for viscoelastic effects clearly exhibited experimentally, such as strain-rate sensitivity and hysteresis, typically observed during cyclic loading. This is addressed in Chapter 3. Additionally, the mechanical contribution of "active" myofibrils should be equally taken into account, so as to better understand the relative contribution of the *vocalis* and the *lamina propria* in the regulation of F_0. Finally, damage mechanisms could be investigated by conveniently modifying the constitutive laws at the fiber scale.

3

A fibril scale model for the finite strain viscoelasticity of vocal-fold tissues

This chapter is based on an article in preparation for submission to the *Journal of the Mechanical Behavior of Biomedical Materials*.

Contents

3.1 Introduction

As described in Chapter 2, vocal folds vibratory properties are closely related to the nonlinear and anisotropic mechanical behavior exhibited by their tissues, which is in turn attributable to the micro-mechanisms of deformation occurring at the collageneous fiber scale these tissues are made up of. A main focus was so far brought to the elastic response of the *vocalis* and the *lamina propria*. This allowed to emphasize the role of these micro-mechanisms upon finite strains, for quasi-static loading conditions. In the following, another major component of the vocal-fold oscillations will be addressed, *i.e.*, their damping capacity.

By definition, damping refers to the dissipation of mechanical energy of a vibrating structure to the surrounding environment [6]. Regardless of the structure examined, dissipation usually arises from different components, such as: (i) internal dissipation of its constituents; (ii) viscous damping due to the fluid the structure is surrounded by; (iii) dissipation due to local deformation and friction at the boundaries where external constraints are applied, or at the interfaces between different layers of the structure. During phonation, the damping properties of the vocal folds can be typically evidenced at the end of a vocal emission [65]: as illustrated in Figure 3.1, when the subglottal pressure drops and, thereby, the driving force disappears, the energy dissipation occurring in the system leads to a gradual decrease in the amplitude of the vocal-fold oscillations toward zero. To restore and maintain a steady state of oscillation instead, a positive transfer of energy from the driving source (airflow) to the vocal folds is required, so as to compensate for the energy lost in the damping (note that in the absence of damping, oscillations could be self-sustained with a net zero energy transfer) [64, 246, 252, 280]. The damping ratio, usually noted ζ, is a measure to describe how the mechanical energy is dissipated in a vibrating system after a perturbation. This dimensionless parameter defines the level of damping in the system relative to a critical damping, *i.e.*, the minimum value of damping that prevents the system from oscillating. ζ can also be thought as the decay rate of the damped oscillations with respect to the frequency. Depending on the given geometrical and mechanical configuration, the system can be underdamped ($\zeta < 1$), critically damped ($\zeta = 1$) or overdamped ($\zeta > 1$). A modal damping ratio ζ_i can also be considered for each mode mode i of vibration.

Though of major importance to better understand the flow-induced vibrations of the vocal folds and their transient dynamics, the (modal) damping ratio is rather difficult to identify and to quantify *in vivo*. In the 2000s, Svec *et al.* proposed a procedure to measure the frequency response of human vocal folds placed in a given prephonatory configuration [237], as reported in Figure 3.1. Therefrom, the resonance frequencies of the vocal folds $F_i = \omega_i/2\pi$ and associated quality factors, $Q_i = 1/2\zeta_i$, were extracted for each mode i, leading to an estimate of modal damping ratios of the vocal folds (in the prescribed configuration). Alternatively to this rather delicate *in vivo* approach, several authors have sought to characterize the time-dependent properties (among which the damping ratio) of excised vocal folds. As for other soft biological tissues [114, 121, 139, 209, 210, 274], the time-dependent responses exhibited: (i) a strain rate sensitivity of the stress-strain behavior [54]; (ii) stress-relaxation at fixed strain up to a strain-dependent equilibrium state

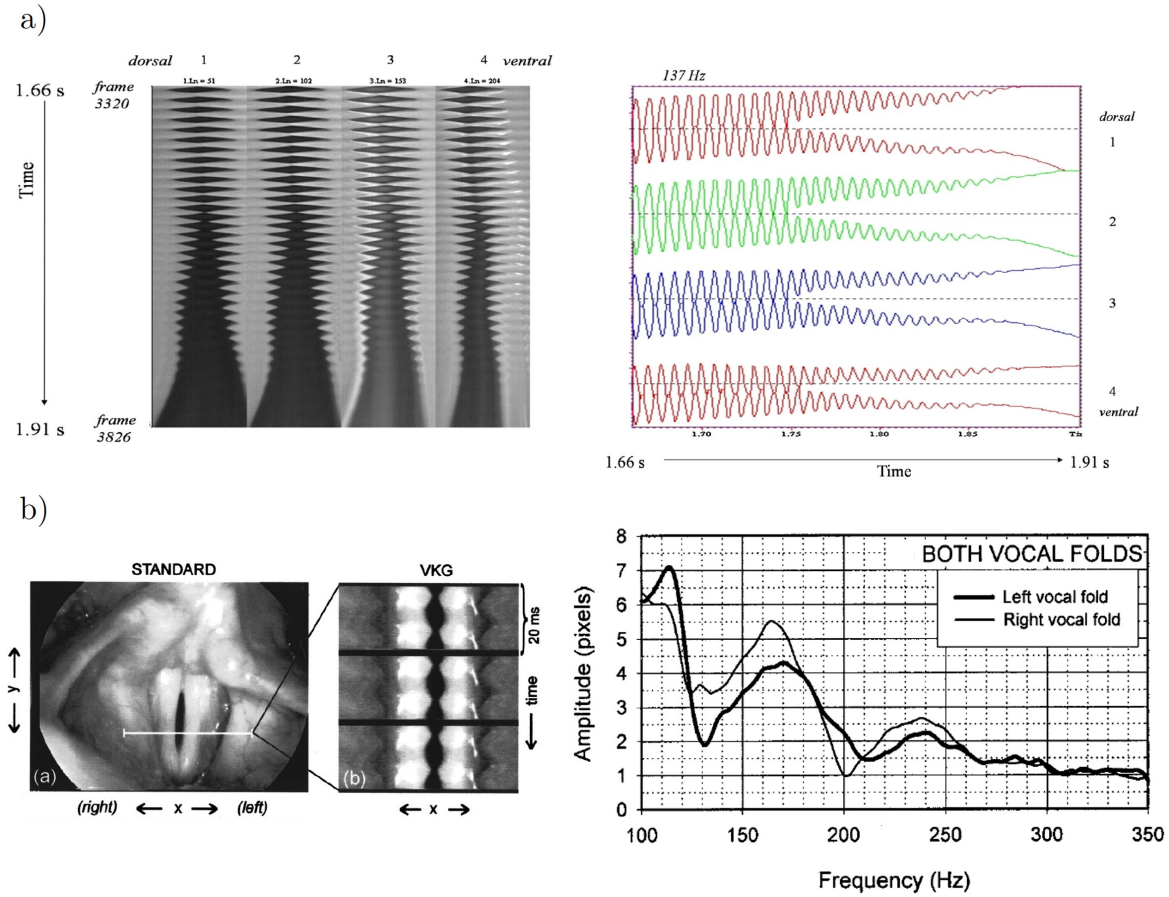

Figure 3.1: Experimental *in vivo* characterization of vocal-fold damping properties: a) videokymographic images of a healthy male subject vibrating glottis obtained from high-speed video recorded at the end of a breathy /a:/ vocal emission (left), corresponding vocal fold edges movements, computed from the videokymograms (right); b) standard laryngostroboscopic image of the vocal folds in neutral phonatory position (prephonatory configuration of the larynx to produce a frequency of about 110 Hz), and high-speed videokymographic image (VKG) at the position marked in the standard recording (left), corresponding frequency response function of the vocal folds (right). Adapted from [65, 237].

[216]; (iii) stress hysteresis with a non-negligible residual strain after cycling [39–41, 44, 45, 54, 143, 146, 254] . Therewith, during the 1980s, the damping ratio of the vocal folds was first assessed on human larynges excised at autopsy ($\zeta \approx 0.23$) or surgery ($\zeta \approx 0.33$), by releasing the vocal folds from a given displaced position and filming the decay of oscillatory amplitude from cycle to cycle [240]. A higher damping obtained in the surgical cases was explained by the formation of tissue edemas due to blood vessels ligation during operations. Over the last twenty years, the viscoelastic properties of excised *lamina propria* samples were mostly studied using either standard shear Dynamic Mechanical Analysis (DMA) or Small-Amplitude Oscillatory Shear (SAOS), *i.e.*, within the linear regime [39, 41, 44, 45, 146, 254], or, more recently, using Large Amplitude Oscillatory Shear (LAOS) [40]. As already detailed in Section 1.3.2, these experiments allowed to provide measurements of storage and loss shear moduli ($G^{'}$ and $G^{''}$) at frequencies up to 250 Hz. In the most recent studies, the damping ratio (or so-called "loss factor") was determined as $\zeta = G^{''}/G^{'}$. It was shown to decrease with the frequency, remaining below 1 past a critical zone around 50 Hz [41], close to 0.73, on average, in the usual phonatory range (100-250 Hz). However, in

prior studies (limited to excitation frequencies of 0.01-15 Hz), this ratio was found much lower, *i.e.*, in the range 0.1-0.5 [44]. Such discrepancies may be ascribed to experimental constraints when examining biological tissues (*e.g.*, inter/intra-individual variability, small number of specimens).

So as to better understand the obtained empirical data and the physical mechanisms underlying the time-dependent and damping behavior of vocal folds, several viscoelastic theories were adopted [45, 48, 130, 275–277]. Three main approaches are commonly reported in previous studies:

- *Low-dimensional lumped-element models*, consisting in different combinations of elastic and viscous elements (*i.e.*, springs and dashpots). Based on the simplest combinations (Maxwell and Kelvin-Voigt models), more sophisticated models (*i.e.*, the Standard Linear Solid Model or Zener model, the generalized Maxwell models and Prony series) are obtained and used to capture the equilibrium state as well as one (or more) rate-dependent networks acting in parallel. These models are motivated by the experimental evidence of the existence of an equilibrium state attained in long-time stress relaxation tests. They also represent a reference for the characterization of elastomers time-dependent behavior [97, 136–138, 221, 222].
- The *quasi-linear viscoelastic theory* (QLV), originally proposed by Fung [87] to model the stress relaxation of soft biological tissues, and applied to oscillatory shear deformation by Chan and Titze [45].
- The *statistical network theory*, largely used for the rheological modeling of polymeric materials [45].

Among the pioneer works proposed to relate the parameters of these viscoelastic models to measurable histological evidence [275–277], the lumped-element approach is often chosen, considering one hyperelastic time-independent equilibrium network in parallel with one (or more, usually two) time-dependent inelastic network(s) (see Section 1.3.2). This is ascribable to the common statement according to which, in soft biological tissues, the equilibrium structural component is commonly driven by the fibrous proteins (collagen and elastin), whereas the viscous contribution is inherited from interstitial proteins and their interactions with the surrounding fibrous components [42, 44, 46, 47, 95, 96, 109, 161, 193, 194, 212]. However, to date, no specific assumption was formulated as to the real physical and mechanical contribution of collagen, elastin or interstitial protein molecules to any of the networks considered in the model. The current understanding of the multiscale phenomena responsible for the macroscopic time-dependent mechanical response of the vocal folds remains therefore unclear.

Thereby, the objective of this chapter is to propose a micro-mechanical model able to reproduce the macroscopic nonlinear and time-dependent mechanical behavior of the vocal fold sublayers. For that purpose, it is proposed to introduce micro-structural time-dependent effects to the hyperelastic network formulation developed in Chapter 2: from a heuristic standpoint, fibril bundles (un)folding and steric interactions are conceived as generalized Zener elements with non-linear solid elasticity and viscoelasticity (see Figure 3.2). Based on the literature biomechanical data obtained from experimental studies using

SAOS and LAOS techniques, as well as quasi-static but multiaxial loadings, the model suitability to predict the time-dependent multiscale mechanics of the vocal fold sublayers is highlighted and discussed.

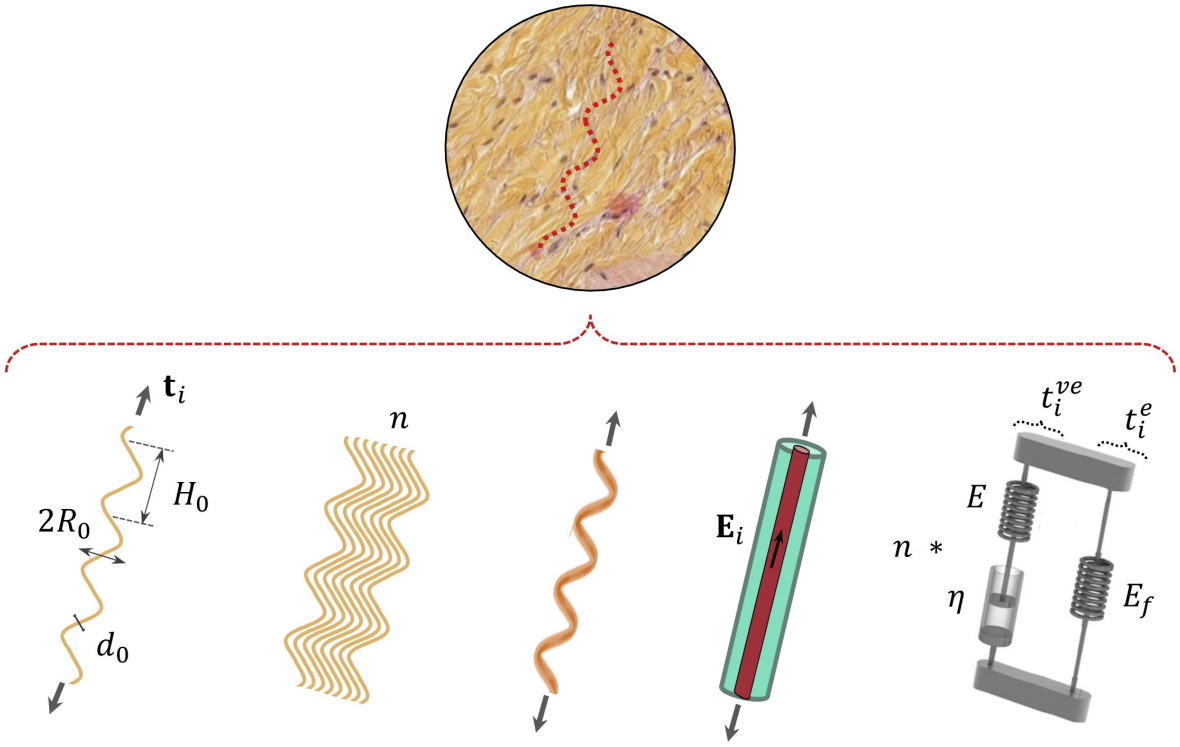

Figure 3.2: Vocal-fold tissue sublayers viscoelastic modeling. Histo-mechanical correspondence fiber-bar for the *lamina propria*, conceived as viscoelastic fiber bundles of n collagen fibrils (in orange).

3.2 Model formulation

Recall of the hyperelastic micro-mechanical model - In Chapter 2 the microstructure of the *lamina propria* (with a collagen fibril content Φ) and the *vocalis* (with collagen fibril and myofibril content of Φ_c and Φ_m, respectively, such that $\Phi = \Phi_c + \Phi_m$) were idealized as organized networks of bars obtained by the periodic repetition of a REV (composed of four bars connected at one node C_0, see Figure 2.2 a for more details). Each bar i of initial (resp. current) orientation $\mathbf{E}_i$ (resp. $\mathbf{e}_i = \mathbf{F}\cdot\mathbf{E}_i/||\mathbf{F}\cdot\mathbf{E}_i||$) and length l_0 (resp. $l_i = l_0||\mathbf{F}\cdot\mathbf{E}_i||$), was the schematic representation of wavy fibril bundles (see Figure 3.2). In the case of the *lamina propria*, each bundle was supposed to be an assembly of n identical and parallel collagen fibrils (of diameter d_0, initial length l_o^f, initial tortuosity $\xi_0 = l_0^f/l_0$) characterized by a waviness of a dozen monomodal sinusoïds (wave amplitude H_0 and spatial periodicity R_0, $l_0 = 10\,R_0$). Similarly, for the *vocalis*, each bundle was constituted by an assembly of parallel myofibrils (of diameter d_{0m}, initial tortuosity ξ_{0m}, with wave amplitude H_{0m} and spatial periodicity R_{0m}, and initial $l_0 = 10R_{0m}$) surrounded by a sheath of collagen fibrils (of diameter d_{0c}, initial tortuosity ξ_{0c}, with wave amplitude H_{0c} and spatial periodicity R_{0c}). Furthermore, fibril bundles are embedded in a ground substance

of HA, elastin fibrils, water and cells. Regardless of the considered tissue, the mechanical behavior of the ground substance, significantly far away from the fibril bundles, was thought as that of an incompressible neo-Hookean medium with a strain energy function $W = 0.5\mu(1-\Phi)(\mathrm{tr}(\mathbf{F}\cdot\mathbf{F}^T)-3)$, where μ is the ground substance shear modulus. In addition, during the deformation of the *lamina propria* (resp. the *vocalis*): (i) the stretching or the compression of each fibril i of a bundle generates a reaction force $\mathbf{t}_i = t_i\mathbf{e}_i$ (resp. $\mathbf{t}_{im} = t_{im}\mathbf{e}_i$ and $\mathbf{t}_{ic} = t_{ic}\mathbf{e}_i$); (ii) the motion of the node C_0 is hindered by steric hindrance with its (unconnected) neighbours C_q. These interactions are characterized by repulsive forces $\mathbf{r}_q = r_q\mathbf{e}_q$ triggered once the distance between C_0 and the neighboring nodes C_q, *i.e.*, δ_q, exceeds a critical distance δ_c (see Figure 2.2 a).

As detailed in Chapter 2, the macroscopic Cauchy stress tensor $\boldsymbol{\sigma}$ resulting from the aforementioned assumptions can be written as:

$$\boldsymbol{\sigma} = -p\boldsymbol{\delta} + \boldsymbol{\sigma}_m + \boldsymbol{\sigma}_f + \boldsymbol{\sigma}_s \tag{3.1}$$

where p is the incompressibility term (pressure), $\boldsymbol{\delta}$ the identity tensor, $\boldsymbol{\sigma}_m = \mathbf{F}\cdot(\partial W/\partial\mathbf{F})^T$ the ground substance (or matrix) stress contribution, and where $\boldsymbol{\sigma}_f$ and $\boldsymbol{\sigma}_s$ are the stress contributions attributable to the (un)folding of fibrils and their steric interactions, respectively. These latter contributions can be expressed as:

$$\boldsymbol{\sigma}_f = \frac{\Phi}{\pi d_0^2\xi_0}\sum_{i=1}^{N} t_i\lambda_i\,\mathbf{e}_i\otimes\mathbf{e}_i \tag{3.2}$$

and

$$\boldsymbol{\sigma}_s = \frac{\Phi}{\pi d_0^2\xi_0}\sum_{q=1}^{M} r_q\delta_q^*\,\mathbf{e}_q\otimes\mathbf{e}_q \tag{3.3}$$

for the *lamina propria*, where $\lambda_i = \frac{\ell_i}{\ell_0}$ and $\delta_q^* = \delta_q/\ell_0$, and:

$$\boldsymbol{\sigma}_f = \frac{\Phi_c}{\pi d_{0c}^2\xi_{0c}}\sum_{i=1}^{N} t_{ic}\lambda_i\,\mathbf{e}_i\otimes\mathbf{e}_i + \frac{\Phi_m}{\pi d_{0m}^2\xi_{0m}}\sum_{i=1}^{N} t_{im}\lambda_i\,\mathbf{e}_i\otimes\mathbf{e}_i \tag{3.4}$$

and

$$\boldsymbol{\sigma}_s = \left(\frac{\Phi_c}{\pi d_{0c}^2\xi_{0c}} + \frac{\Phi_m}{\pi d_{0m}^2\xi_{0m}}\right)\sum_{q=1}^{M} r_q\delta_q^*\,\mathbf{e}_q\otimes\mathbf{e}_q \tag{3.5}$$

for the *vocalis*.

In Chapter 2, it was assumed that the whole algebraic expression of forces involved in the last set of equations, namely t_i, t_{im}, t_{ic} and r_q were nonlinear elastic (hyperelastic) functions of their respective strains $\varepsilon_i = \ln l_i/l_0$, $\varepsilon_{im} = \varepsilon_i$, $\varepsilon_{ic} = \varepsilon_i$ and $\varepsilon_q = \ln(\delta_q/\delta_c)$, *i.e.*, $t_i = t_i^e(\varepsilon_i)$, $t_{im} = t_{im}^e(\varepsilon_{im})$, $t_{ic} = t_{ic}^e(\varepsilon_{ic})$ and $r_q = r_q^e(\varepsilon_q)$. Hence, the two following expressions were

proposed for the collagen fibrils of the *lamina propria*:

$$t_i^e = \frac{\pi d_0^2}{4}\left[E_{eq0}\varepsilon_i + \frac{E_f - E_{eq0}}{2}\left(\varepsilon_i + \sqrt{(\varepsilon_i - \ln\xi_0)^2 + \alpha^2} - \sqrt{\ln^2\xi_0 + \alpha^2}\right)\right] \tag{3.6}$$

when they are stretched and

$$t_i^e = \frac{\pi d_0^2}{4} E_{eq0}\varepsilon_i \tag{3.7}$$

when subjected to compression. In the aforementioned expressions, $E_{eq0} = E_f \langle\cos\beta_0\rangle / [\,\langle\cos^2\beta_0\rangle + 16\langle v^2\rangle / d_0^2\,]$, $\langle\cdot\rangle = \frac{1}{\ell_0}\int_0^{\ell_0}\cdot\, du$, $\langle v^2\rangle = R_0^2/2$ and $\beta_0 = \arctan(2\pi\frac{R_0}{H_0}\cos\frac{2\pi}{H_0}u)$ [211] . They imply the Young's modulus of collagen fibrils E_f and a curvature coefficient α that ensures, during fibril unfolding, the transition between bending- and stretching-dominated regimes. Similar expressions were proposed for the *vocalis*, by replacing: (i) t_{im}^e parameters d_0, E_f, ξ_0, α, R_0 and H_0 by d_{0m}, E_{fm}, ξ_{0m}, α_m, R_{0m} and H_{0m} for myofibrils; (ii) t_{ic}^e parameters E_f, ξ_0, α, R_0 and H_0 by E_{fc}, ξ_{0c}, α_c, R_{0c} and H_{0c} for collagen fibrils. As far as steric interactions are concerned, it was assumed that

$$r_q^e = \beta\, H(\varepsilon_q)\, \varepsilon_q^3 \tag{3.8}$$

where H is the Heaviside function and where β is a phenomenological parameter of interaction.

This hyperelastic formulation already proposed in Chapter 2, adjusted to appropriate biomechanical data and identified using relevant microstructural descriptors from histological evidence, allowed to capture "first order", reversible responses of the *lamina propria* and *vocalis* sublayers for various physiological representative loading modes, *i.e.*, tension along the main fibril preferential orientation, transverse compression and longitudinal shear.

Model limitation - Based on a time-independent physical formulation, the previous micro-mechanical model is not able to encompass time-dependent effects, yet, peculiar to soft tissues [114, 121, 139, 209, 210, 274], exhibiting strain rate sensitivity, stress relaxation and stress hysteresis upon cycling. Time-dependency is often speculated to be induced by the different proteins and/or shorter molecules the fibrils and/or the ground substances are made of, together with their various colloidal interactions. When deformed, these molecular scale systems exhibit finite characteristic relaxation times and dissipation mechanisms [91, 194] that are not taken into account by hyperelastic formulations.

Viscoelastic micro-mechanical model - An appropriate quantification of these complex time-dependent processes would require molecular scale analyses using statistical physics or numerical simulations employing Molecular Dynamics tools [90]. Here, in a first approximation, it was considered a heuristic approach at the fibril and fibril bundle scales to account for these time-dependent effects (see Figure 3.2).

Thereby, the following force decomposition, written along each material director $\mathbf{e}_i$ which is convected with the macroscopic transformation gradient $\mathbf{F}$, was adopted to model the time-dependent effects occurring during the stretching (or the compression) of a fibril

(induced both by the fibril deformation itself and its interactions with the other fibrils or the surrounding ground substance):

$$t_i = t_i^e + t_i^{ve} \tag{3.9}$$

where the hyperelastic contribution t_i^e corresponds to Eq. (3.7) and represents the "neutral" response of the fibrils when the system attains its "relaxed" equilibrium state. Conversely, the viscoelastic tension-compression contribution t_i^{ve} accounts for the aforementioned effects. It was assumed that these phenomena can be reproduced by a nonlinear Maxwell model:

$$\dot{t}_i^{ve} + \frac{E}{\eta} t_i^{ve} = E s_0 \dot{\varepsilon}_i \tag{3.10}$$

where $s_0 = \pi d_0^2/4$ is the collagen fibril cross section, $\dot{\varepsilon}_i = \mathbf{e}_i \cdot \mathbf{L} \cdot \mathbf{e}_i$ is the fibril stretch-compression strain rate, $\mathbf{L}$ the macroscopic velocity gradient tensor, and where E and η are the elastic modulus and the viscosity of the Maxwell model, respectively. An analogous formulation was proposed for the (myo)fibrils of the *vocalis*, by replacing t_i^{ve}, E, η and s_0 by t_{ic}^{ve} and t_{im}^{ve}, E_c and E_m, η_c and η_m, s_{0c} and s_{0m} for the collagen fibrils and the myofibrils, respectively. Therewith, it is worth noticing that the vocal-fold tissues exhibit several relaxation times over a wide range of strain rates, experimentally observed at the macroscale [40, 41, 44, 45]. In particular, SAOS studies [41] report Carreau-like evolutions of the complex viscosity of the *lamina propria* with the shear rate. These findings were taken into consideration assuming that:

$$\eta = \eta_0 \left(1 + \left(\frac{\dot{\varepsilon} - \frac{\dot{t}_i^{ve}}{E s_0}}{\dot{\varepsilon}_0} \right)^2 \right)^{\frac{n-1}{2}} \tag{3.11}$$

where η_0 is the viscosity of the Newtonian regime, $\dot{\varepsilon}_0$ is the strain rate transition between the Newtonian regime and the thinning one, and n is the power-law index driving thinning effects at high strain rates. In the absence of available experimental data at the fibril scale for the *vocalis*, it was assumed, for the sake of simplicity, that: (i) analogous considerations are applicable to muscular collagen fibrils and myofibrils; (ii) $E_{0c} = E_{0m} = E$, $\eta_{0c} = \eta_{0m} = \eta_0$, $\dot{\varepsilon}_{c0} = \dot{\varepsilon}_{m0} = \dot{\varepsilon}_0$, $n_c = n_m = n$.

An equivalent decomposition was applied to the steric reaction forces between fibril bundles, expressed with respect to the relative material reference frame $\mathbf{e}_q$:

$$r_q = r_q^e + r_q^{ve} \tag{3.12}$$

where the hyperelastic term r_q^e is given by Eq. (3.8), and where the viscous contribution can be determined by means of the following Maxwell equation:

$$\dot{r}_q^{ve} + \frac{E'}{\eta'} r_q^{ve} = E'\, s_0 \dot{\varepsilon}_q \tag{3.13}$$

The viscosity η' is similarly assumed to be a Carreau function of the corresponding steric

strain rate:

$$\eta' = \eta'_0 \left(1 + \left(\frac{\dot{\varepsilon}_q - \frac{\dot{r}_q^{ve}}{E' s_0}}{\dot{\varepsilon}'_0} \right)^2 \right)^{\frac{n'-1}{2}} \tag{3.14}$$

where η'_0 is the viscosity of the Newtonian regime, $\dot{\varepsilon}'_0$ is the strain rate transition between the Newtonian and the thinning regime, and n' is the power-law index driving thinning effects at high strain rates. For the sake of simplicity, it was assumed that $n' = n$.

In conclusion, the proposed micro-mechanical model can be simplistically thought as the imbrication of two nonlinear Zener model networks embedded in a hyperelastic matrix, where the first network aims at modeling the visco-hyperelastity of fibril bundles, whereas the second one accounts for the visco-hyperelastic steric interactions. The constitutive parameters of these symbolic operators were mostly fed by histological and histo-mechanical data extrapolated from the literature. In the absence of accessible fibril scale information, the parameters were phenomenologically deduced from macroscopic data. The micro-mechanical parameters of the model are listed hereafter for the *lamina propria* (resp. the *vocalis*) grouped into different categories as it follows:

- *Histological parameters* – The content of collagen fibrils Φ (resp. Φ_c and Φ_m), their initial orientation (θ_0 and φ_0), diameter d_0 (resp. d_{0c} and d_{0m}), initial waviness of spatial periodicity H_0 (resp. H_{0c} and H_{0m}) and wave amplitude R_0 (resp. R_{0c} and R_{0m}) and initial tortuosity ξ_0 (resp. ξ_{0c} and ξ_{0m}), determined from the initial spatial periodicity and wave amplitude.

- *Histo-mechanical parameters* – The fibril elastic modulus E_f (resp. E_{fc} and E_{fm}), the transition parameter α (resp. α_c and α_m) between the bending- and tension-dominated fibrils unfolding regimes, the shear modulus of the ground substance μ.

- *Phenomenological micro-mechanical parameters* – The interaction critical distance δ_c and coefficient β, as well as the viscoelastic parameters E, η_0, $\dot{\varepsilon}_0$, n and E', η'_0, $\dot{\varepsilon}'_0$.

3.3 Model identification

3.3.1 Experimental database

The relevance of the proposed micro-mechanical model was assessed by the comparison of numerical predictions to pertinent biomechanical data recently acquired on various human vocal-fold tissues:

- In order to assess the relevance of the model within the linear visco-elastic regime, the data collected by Chan and Rodriguez [41] were initially considered: human vocal-fold "cover" specimens (*i.e.*, assembly of *epithelium* and superficial sublayer (SL) of the *lamina propria*) were excised from 7 donors (2 females and 5 males), between

53 and 88 years-old (mean age was 67). The *post-mortem* time of the collected tissues varied from 3 to 20 hours prior testing (mean time was 10 hours). Excised tissues were subsequently subjected to Small Amplitude Oscillatory Shear (SAOS) using a simple-shear rheometer at physiological conditions (at 37°C and 100% relative humidity). An oscillatory shear strain $\gamma_{zx} = \gamma_0 \sin(2\pi f t)$ of small amplitude (*i.e.*, $\gamma_0 = 0.01$, linear regime) at a frequency f ranging from 1 to 250 Hz was applied in the longitudinal plane $(\mathbf{e}_z, \mathbf{e}_x)$.

- The model suitability to reproduce time-dependent responses outside of the linear viscoelastic regime, was investigated with respect to the biomechanical data reported by Chan [40]. The author subjected a 60 year old male cover to Large Amplitude Oscillatory Shear (LAOS) by means of a simple-shear rheometer, applying several increasing strain amplitudes $\gamma_0 = [0.05, 0.1, 0.2, 0.5, 1]$ along the longitudinal plane $(\mathbf{e}_z, \mathbf{e}_x)$ at a frequency $f = 75$ Hz. Only stabilized LAOS responses at fixed values of γ_0 were provided, not reporting the whole loading history.

- The relevance of the model to predict vocal fold layers multiaxial cyclic responses upon finite strains was finally assessed comparing numerical predictions to biomechanical data obtained by Cochereau *et al.* [54], previously mentioned in this study (see Chapter 2). In this respect, the same couples of *lamina propria* (LP_1 and LP_2) and *vocalis* (V_1 and V_2) samples were considered. Each sample was sequentially subjected to a series of finite strain and cyclic physiological loadings, *i.e.*, longitudinal tension along $\mathbf{e}_z$, transverse compression along $\mathbf{e}_x$, and longitudinal shear in the longitudinal plane $(\mathbf{e}_z, \mathbf{e}_x)$. Samples were respectively loaded-unloaded (to zero) upon finite (Hencky) ε_{zz}^{max}, ε_{xx}^{min} and shear γ_{zx}^{max} strains, at constant strain rates $|\dot{\varepsilon}_{zz}|$, $|\dot{\varepsilon}_{xx}|$ and $|\dot{\gamma}_{zx}|$ of $\approx \mathcal{O}$ 10^{-3} s^{-1}. Ten of these loading-unloading sequences were carried out.

3.3.2 Optimization protocol

Similarly to Chapter 2, the following optimization protocol was used to determine the optimal sets of constitutive parameters for each of the considered tissues subjected to the aforementioned loading conditions (SAOS, LAOS, and the multiaxial cyclic loading):

(i) **Initial guesses of the histological and elastic parameters** - SAOS and LAOS data initial guesses of histological and elastic parameters were initialized and bounded withing the following physiological corridors reported in the literature: $\Phi \in [0.15\ ;\ 0.55]$, $d_0 \in [10\text{ nm}\ ;\ 500\text{ nm}]$, $H_0 \in [10\ \mu\text{m}\ ;\ 70\ \mu\text{m}]$, $R_0 \in [1\ \mu\text{m}\ ;\ 10\ \mu\text{m}]$, $\theta_0 \in [0°\ ;\ 50°]$, $\varphi_0 \in [20°\ ;\ 90°]$, $E_f \in [1\text{ MPa}\ ;\ 1000\text{ MPa}]$, $\mu \in [1\text{ Pa}\ ;\ 1500\text{ Pa}]$. The strictly positive parameter α was let free. Furthermore, confirming what already emphasized in the previous chapter, steric interactions were not triggered during simple shear: the parameters β and δ_c were thus not determined for the SAOS and LAOS data. Conversely, the already optimized values determined in Chapter 2 were used for multiaxial cyclic data, for both the *lamina propria* and the *vocalis* samples.

(ii) **Initial guesses of visco-elastic parameters** - Regardless of the considered experimental data, the optimization of the strictly positive parameters E, E', η_0, η'_0, $\dot{\varepsilon}_0$ and $\dot{\varepsilon}'_0$ was let free of constraints (please note that E', η'_0 and $\dot{\varepsilon}'_0$ could not be determined for SAOS and LAOS as steric interactions were not activated). Furthermore, the thinning power-law exponent n was fitted on the SAOS data: in the absence of experimental data, the determined value was used throughout the current study.

(iii) **Optimization** - Similarly to what reported in Chapter 2, a least-squared approach based on the nonlinear constraint optimization reported in Chapter 2 was used to minimize the discrepancies between theoretical and experimental stress tensors (or rheological functions, *i.e.*, G', G'', μ', for the SAOS data) for the considered macroscopic loadings. Accounting for the complexity of the optimization problem, the uniqueness of the solution could not be established. The computation of the time-dependent stress tensors predicted by the micro-mechanical model was carried out using the upscaling algorithm reported in Figure 3.3 for $\boldsymbol{\sigma}_f$ (a specular algorithm applies to $\boldsymbol{\sigma}_s$). In particular, the time-integration of the implicit non-linear Maxwell differential equations (3.10) and (3.13) was possible using the *ode15i* solver already implemented in Matlab (Matlab R2020b), a variable-step, variable-order (VSVO) solver based on the backward differentiation formulas (BDFs) of orders 1 to 5 [232].

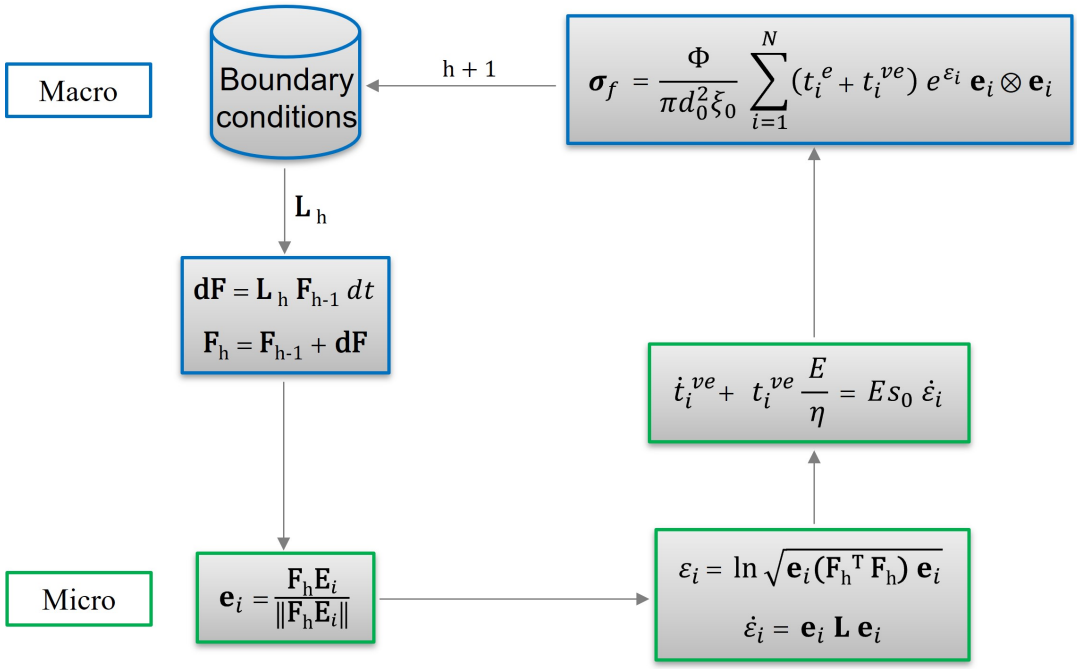

Figure 3.3: Schematic flowchart of the upscaling algorithm employed to compute the time-dependent stress tensor $\boldsymbol{\sigma}_f$.

Due to the presence of viscous terms, differently from Chapter 2, boundary conditions can not be expressed in an analytical closed-form anymore. A coupling algorithm was therefore recursively employed at each $h-$iteration, based on the following classical staggered scheme [75, 183, 187]:

Coupling algorithm staggered scheme

FOR $h = 1 : h_{max}$
WHILE $|\mathbf{F}_h(t) - \mathbf{F}_h(t-1)| < toll$ AND $|\boldsymbol{\sigma}_h(t) - \boldsymbol{\sigma}_h(t-1)| < toll$
$\mathbf{F}_h(t+1) = f(\boldsymbol{\sigma}_h(\mathbf{F}_h(t)) = 0)$
$\boldsymbol{\sigma}_h(t+1) = \boldsymbol{\sigma}_h(\mathbf{F}_h(t+1))$
$t = t + 1$
END
END
The iteration convergence tolerance was set equal to $1e-4$.

3.4 Results and discussion

The optimized values of the model parameters as well as the macro and microscale theoretical predictions are presented hereafter for each considered loading case.

3.4.1 SAOS

Histo-mechanical parameters - To reproduce the mean SAOS data obtained by Chan and Rodriguez [41], the following optimized sets of histological, elastic and viscous parameters, reported in Table 3.1, Table 3.2 and Table 3.3, respectively (the averaged cover target is noted C_{SAOS} hereinafter), were obtained.

Sample C	θ_0 (°)	φ_0 (°)	H_0 (μm)	R_0 (μm)	d_0 (μm)	Φ	ξ_0
C_{SAOS}	10.5	83.7	34.5	7.3	0.21	0.30	1.34
C_{LAOS}	32.6	65.7	45	4.5	0.23	0.30	1.11

Table 3.1: Set of histological parameters identified for cover samples C_{SAOS} and C_{LAOS}. Gray-colored columns refer to quantities computed as a function of the determined histological parameters.

Sample C	E_f (MPa)	μ (Pa)	α	β (N)	δ_c (μm)
C_{SAOS}	720	31	$1.6\,10^{-3}$	-	-
C_{LAOS}	720	30	$4.6\,10^{-3}$	-	-

Table 3.2: Set of mechanical elastic parameters for cover samples C_{SAOS} and C_{LAOS}.

Sample C	E (MPa)	η_0 (MPa s)	$\dot{\varepsilon_0}$ (s^{-1})	E' (MPa)	η'_0 (MPa s)	$\dot{\varepsilon'_0}$ (s^{-1})
C_{SAOS}	3.68	1.56	$2.1\,10^{-3}$	-	-	-
C_{LAOS}	4.19	1.14	$1.9\,10^{-3}$	-	-	-

Table 3.3: Set of mechanical viscous parameters for cover samples C_{SAOS} and C_{LAOS}.

When compared to the set of histological parameters identified on the entire *lamina propria* samples considered in Chapter 2 (see LP_i samples in Table 2.1), three main microstructural

changes can be pointed out at the collagen fibril scale (in addition to inter-individual variability):

1. The collagen content Φ decreased from ≈ 0.47 for the LP_i samples down to ≈ 0.30 for C_{SAOS}. This finding is consistent with prior experimental evidence and shows that the first sublayer beneath the *epithelium* (SL, also called Reinke's space) exhibits a fibril content lower than that found in the intermediate (IL) and the deep (DL) sublayers [15, 105]. The main reason behind such a difference is related to the fact that both the IL and the DL sublayers (forming the so-called "vocal ligament") are considered as the primary load-bearing portion of the vocal fold, and are thus likely to endure the highest collision stresses during phonation [102, 241]. The identifications obtained in Table 2.1 (entire LP_i samples) and Table 3.1 (cover C_{SAOS}) support therefore the assumption accoding to which regions exposed to higher stresses in the vocal tissue exhibit a higher density of collageneous fibrils, produced to strengthen the ECM [96, 142].

2. The optimal collagen fibril diameter d_0 in the cover is close to 200 nm, instead of 400 nm in the entire LP_i samples. Such decrease may be justified by the variation of fibril diameter based on the collagen type (typical values from 10 nm to 500 nm), and by previous data quantifying the distribution of thin, intermediate and thick fibers across the *lamina propria*. In particular, Muñoz-Pinto *et al.* [197] show that the content of thin fibrils decreases steadily and around 10-fold from SL to DL layers. Conversely, the content of thick fibrils was found to increase steadily and around 15-fold from SL to DL layers.

3. For C_{SAOS}, the fibril tortuosity ξ_0 at rest is found 20% higher than that estimated for the LP_i samples. This appears to be consistent with previous observations showing that the IL sublayer of the *lamina propria* is characterized by a dense network of straighter ECM fibrils compared with that of other sublayers [15, 147].

Comparing the elastic parameters reported in Table 2.2 (Chapter 2, entire LP_i samples) with those shown in Table 3.2 (cover C_{SAOS}), a major difference is noticed for the shear modulus μ, reflecting the mechanical contribution of cells, elastin and ground substance and which is nearly 10-fold lower for the cover sample. The identified value stands here in the range of the elastic shear modulus of hyaluronic acid $\mu_{HA} \approx$ 20-50 Pa (estimated at low loading frequencies, up to 10 Hz) [115], *i.e.*, the most abundant polymer of the ground substance in the *lamina propria*. Known to play a key role in shock absorption during vocal-fold collisions, this component is much more present in SL than in DL. The discrepancy found in μ-values in Table 2.2 and Table 3.2 may therefore be ascribed to the notably scarcity of elastin fibrils in the SP layer (and thereby, in the cover) in elderly tissues [218].

Regarding the mechanical viscoelastic parameters (see Table 3.3), the identification procedure led to rather small fibril scale relaxation times, *i.e.*, $\tau = \eta_0/E \approx 0.42$ s at the lowest frequencies. To the author's knowledge, very few experimental data are available at this scale to support and corroborate the relevance of the obtained optimal parameters. Among these (rare) reference data, Shen *et al.* [90, 234] report typical viscosity of solvated collagen

fibrils in the range of 90–1 630 MPa s, and typical relaxation times in the range of 7–102 s (see Figure 1.13 b and Figure 1.13 e). It is interesting to note that Yang [272] measured two distinct processes contributing to the stress relaxation behavior of native collagen fibrils immersed in PBS buffer and subjected to 5-7% strain for 5-10 min: a fast relaxation process with a characteristic time $\tau_1 \approx 1.8 \pm 0.4$ s and a slow relaxation process with $\tau_2 \approx 60 \pm 10$ s. Yang proposed that τ_1 corresponds to the relative sliding of collagen microfibrils, while τ_2 refers to the relative sliding of collagen molecules (due to the high level of cross-links between molecules). The optimization of the present model led to relaxation times close to the time τ_1 measured by Yang [272].

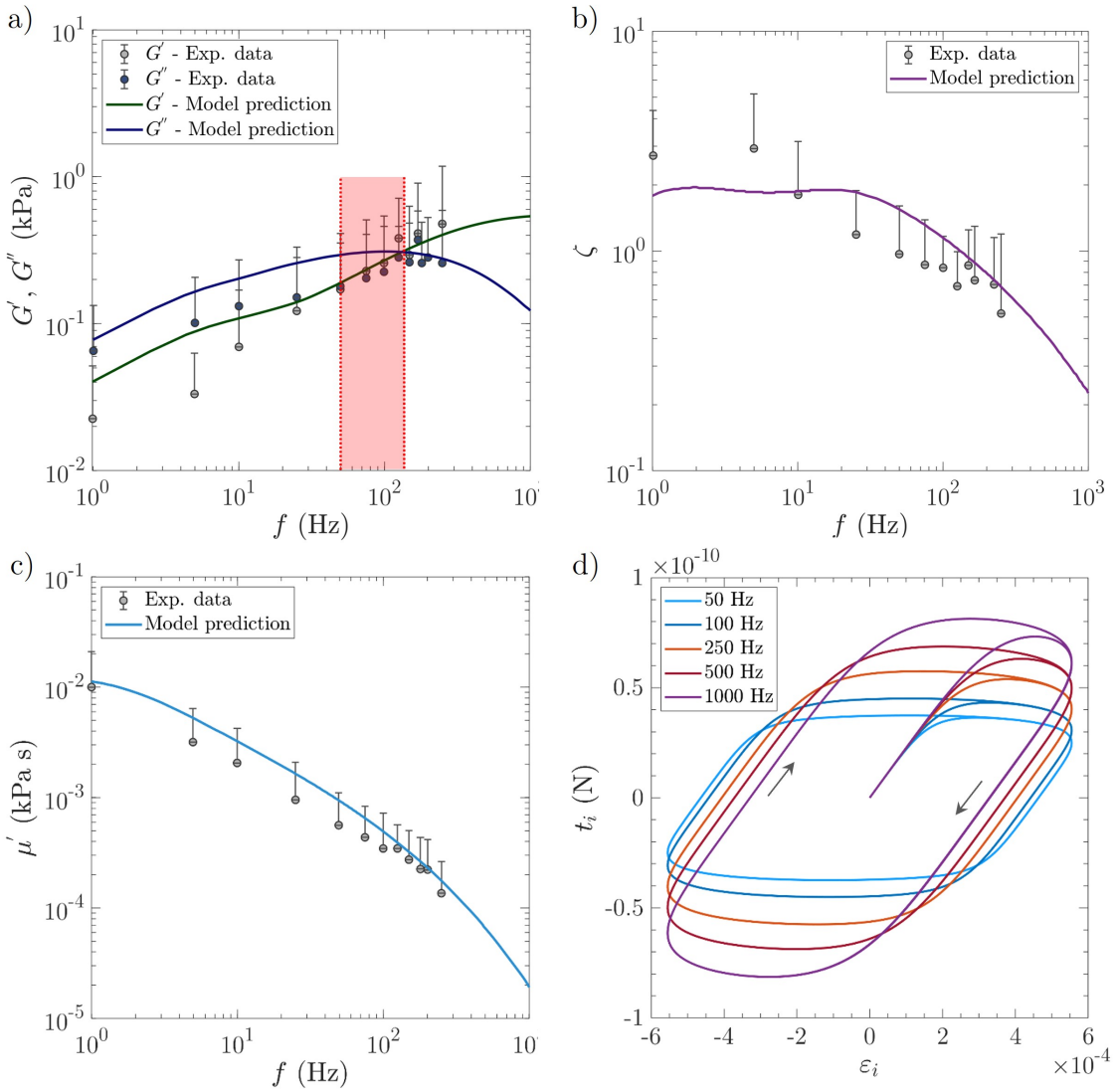

Figure 3.4: SAOS results: evolution of the a) storage G' and loss G'' moduli, b) damping ratio ζ and c) dynamic viscosity μ' (real part of the complex DMA viscosity) as a function of the frequency f. The macroscale model predictions are compared to the experimental data acquired by Chan and Rodriguez [41] on 7 human vocal-fold "cover" specimens (strain amplitude of 1%, the averaged data and standard deviations, upper error bars, of the seven specimens are reported). Red-shaded area in a): frequency range within which a crossover regime is expected to occur. Panel d) finally displays the predicted fibril strain-tension curves at frequencies f ranging from 50 to 1000 Hz.

Multiscale predictions - A comparison between macroscale predictions and corresponding

experimental data is provided by Figure 3.4. Panel a) displays the storage and loss shear moduli $G^{'}$ and $G^{''}$ (mean values over the 7 specimens) as a function of the excitation frequency f, panel b) the damping ratio $\zeta = G^{''}/G^{'}$, and panel c) the dynamic viscosity μ'. Model predictions were extended up to $f = 1$ kHz. The evolution of the fibril tension t_i with respect to the mean fibril strain ε_i upon cycling at different frequencies f is finally shown in panel d). Different trends can be highlighted at both scales:

- A satisfying quantitative agreement is obtained between macroscale model predictions and experimental data for the storage and the loss moduli (see panel a). In particular, the "cross-over" area around 50–100 Hz (red-shaded area in panel a) is well captured by the model. Below (resp. above) this region, $G' < G''$ (resp. $G^{'} > G^{''}$), which indicates predominant fluid-like (resp. solid-like) properties at low (resp. high) frequencies. For polymers or gels, this transition is related to the molecular weight, the spatial distribution and the degree of entanglement of macromolecular chains [16, 76]. Due to the major role of the deformation of the ground substance in longitudinal shear (see Chapter 2), similar mechanisms are expected to occur here. As emphasized in panel d), these mechanisms should be additionally combined with the cyclic stretching-compression of collagen fibrils and their interactions with the molecules of the ground substance.

- The damping ratio $\zeta = G''/G'$ is similarly rather well predicted by the micro-mechanical model, as illustrated in panel b). Below the “cross over” area, both experimental data and predicted results exhibit a practically constant overdamped behavior of the tissues. The situation significantly differs above “cross over” area, *i.e.*, within the standard voice frequency regime, where the tissue shows an underdamped response with a power-law decrease of the damping ratio with the frequency.

- As displayed in panel c), the monotonic decrease of the dynamic viscosity μ' with f is also satisfyingly predicted. This significant decrease, which emphasizes a noticeable shear-thinning of the tissues, is probably ascribed to frequency-evolving deformation and rearrangement mechanisms occurring at the fibril scale, as already noticed for the storage and loss moduli.

- A closer inspection of panel d) shows that the micro-mechanical model predicts an increase of the fibril elastic contribution with f (see Figure 3.4 d). For example, at the lowest frequency $f = 50$ Hz, a marked viscous plateau is reached by the fibril tension magnitude $|t_i|$ after loading, with an important residual strain $|\varepsilon_i^r|$ after unloading. On the contrary, the tension plateau is not observable anymore at the highest frequency $f = 1$ kHz, registering both an increase of $|t_i|$ and a decrease of $|\varepsilon_i^r|$. This trend is mainly ascribed to the viscoelastic term t_i^{ve} of the nonlinear Maxwell fibril model. Indeed, when increasing f from 50 Hz to 1 kHz, the duration of the fibril loading decreases from 6.10^{-1} s, *i.e.*, close to the relaxation time at 50 Hz (≈ 0.42 s), down to 5.10^{-4} s, which is significantly lower than the relaxation time at 1 kHz (≈ 0.01 s). Thus, increasing the frequency leads to a restraint of the viscous contribution. These phenomenological fibril scale trends should be related to the

complex fibrous architectures of the considered tissues and to their time-dependent deformation and rearrangement processes in order to get a further insight with this respect. It is worth noticing that these processes should occur at the molecular scale. Truly: (i) panel d) shows that the mean fibril tension-compression strain, and corresponding (un)folding, is considerably small ($< 6\ 10^{-4}$); (ii) fibrils rotation (not shown here) remains negligible for the considered loading mode.

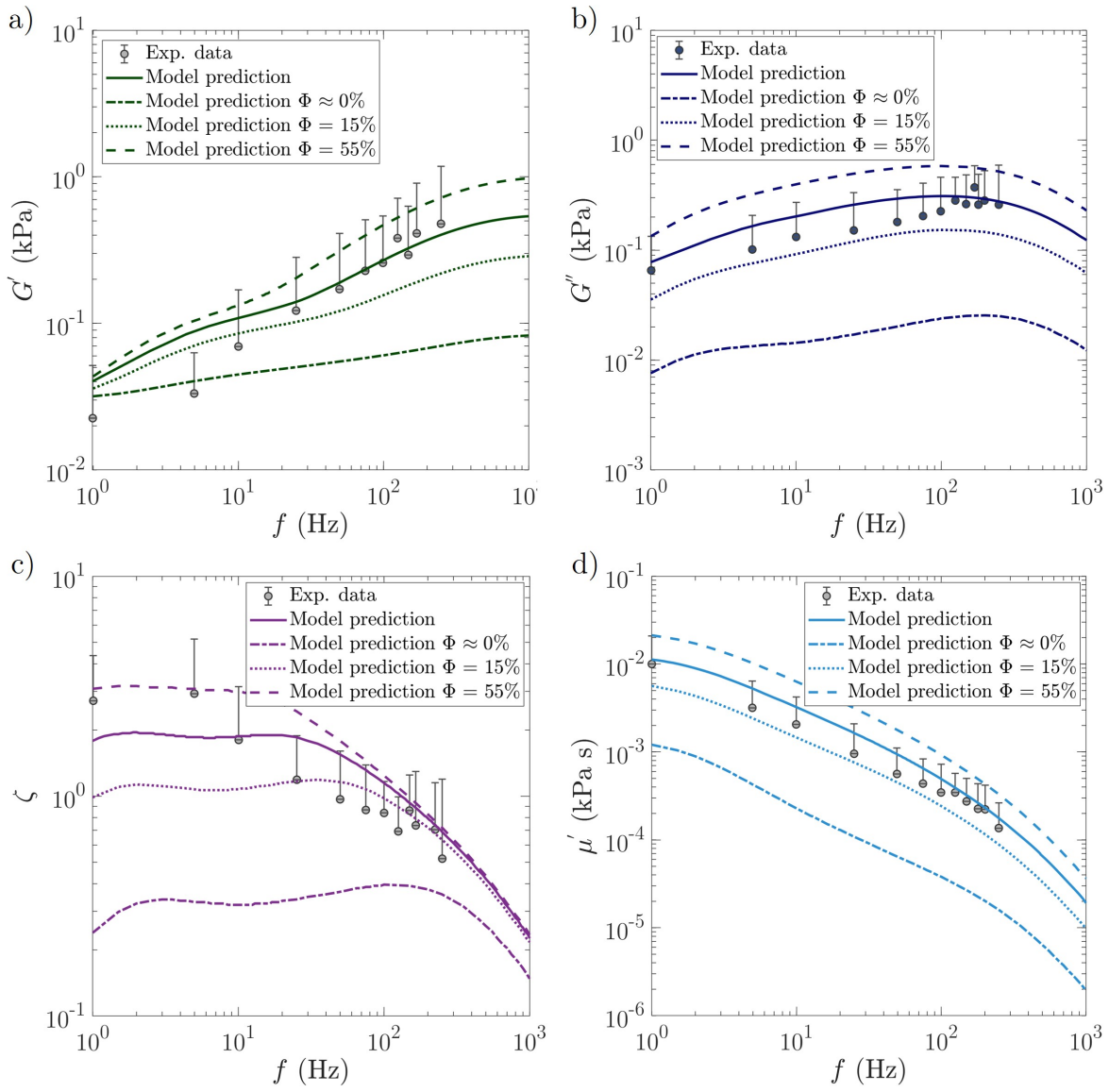

Figure 3.5: SAOS results: parametric evolution of the a) storage G' and b) loss G'' moduli, c) damping ratio ζ, d) dynamic viscosity μ' as a function of the collagen fibrils volume fraction Φ varied within physiological boundaries.

Finally, Figure 3.5 illustrates the impact of the collagen volume fraction Φ on the aforementioned theoretical predictions. Φ was parametrically varied within physiological boundaries to simulate three relevant situations: the assumption of nearly no collagen fibers within the vocal-fold cover ($\Phi \approx 0$), close to a homogeneous isotropic neo-hookean material owning the same mechanical properties as the respective matrix; a volume fraction equal to the minimal (resp. maximal) value of the corridor identified from the literature in the *lamina*

propria, *i.e.*, $\Phi = 0.15$ (resp. $\Phi = 0.55$). These results clearly emphasize the major mechanical role played by the collagen fibrous network, and its interaction with the surrounding ground substance, in the SAOS response of the vocal-fold cover.

3.4.2 LAOS

Histo-mechanical parameters - In order to reproduce the LAOS data obtained by Chan [40] on a single cover (sample noted as C_{LAOS}), the optimization led to three sets of histo-mechanical parameters reported in Table 3.1, Table 3.2, and Table 3.3.

The identified geometrical parameters (*e.g.*, collagen volume fraction Φ, fibril's diameter d_0) are significantly close to the values previously obtained for the cover sample C_{SAOS} subjected to SAOS (see Table 3.1). Yet, some microstructural differences can be noticed with respect to the 3D orientation of the fibrous network as well as the initial fibril tortuosity ξ_0, much closer to that identified in Chapter 2 for the entire *lamina propria* samples (straighter fibrils). These discrepancies are mainly attributable to inter-subject variability.

Mechanical parameters (*e.g.*, collagen fibril Young's modulus E_f, matrix shear modulus μ, microscale relaxation time τ) are nearly identical to those obtained for C_{SAOS} (steric interactions remain untriggered under LAOS).

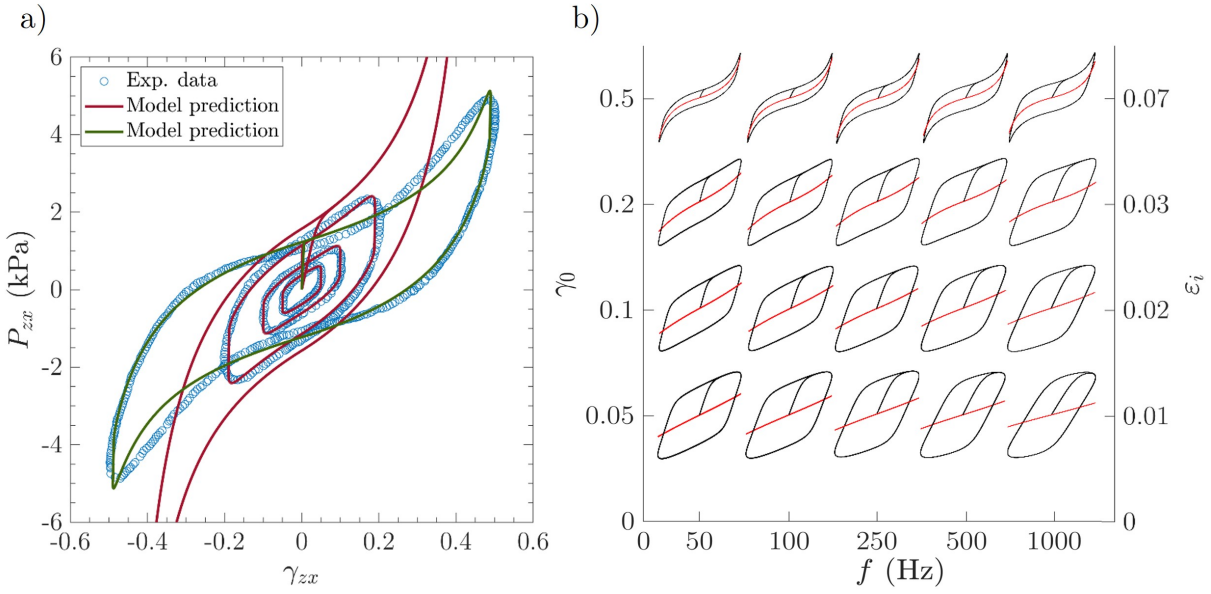

Figure 3.6: LAOS results: a) macroscale stress-strain curves obtained for sample C_{LAOS} tested at $f = 75$ Hz and with γ_0 varied from 0.05 to 0.5, experimental data (adapted from [40]) *vs.* model predictions; b) theoretical rheological fingerprints predicted at the macroscale (resp. microscale) for sample C_{LAOS} in the Pipkin space $\{f, \gamma_0\}$ (resp. $\{f, \varepsilon_i\}$). In this latter graph, black solid lines represent the total stress, while red solid lines the corresponding elastic contribution.

Multiscale predictions - The macroscopic stress-strain predictions of the model are presented in Figure 3.6 a), along with the target LAOS experimental data (at a single $f =$ 75 Hz and increasing strain amplitudes γ_0 from 0.05 to 0.5). Extending the model predictions to multiple frequencies (see also Appendix B. - Figure 1) and strain amplitudes, panel b)

presents a series of theoretical stress-strain contour plots (or "rheological fingerprints") predicted for sample C_{LAOS} at the macroscale (resp. microscale) in the Pipkin space $\{f, \gamma_0\}$ (resp. $\{f, \varepsilon_i\}$) [40, 74]. Within each contour plot, normalized with respect to the strain amplitude γ_0, the black line represents the total viscoelastic stress while the red line represents the hyperelastic stress contribution only. Different trends can be highlighted:

- **Influence of the strain amplitude** γ_0 **–** For $\gamma_0 \leq 0.2$ and a moderate frequency (f = 75 Hz), Figure 3.6 a) shows a satisfying quantitative agreement between the model predictions and the corresponding experimental data at stabilized cycles. In particular, the model is able to capture the strong nonlinear response of the vocal-fold cover which progressively deviates, from a typical linear viscoelastic response at low shear strain amplitudes, *i.e.*, below 0.1, toward cyclic curves with a marked strain-hardening at higher strain magnitudes, where the nonlinear hyperelastic stretching of collagen fibrils is triggered. Regardless of the considered frequency, this trend is equally well emphasized in the macroscale and microscale Pipkin diagrams displayed in Figure 3.6 b) for $\gamma_0 \geq 0.5$. It is worth noticing that the predicted strain-hardening at the highest strain magnitude $\gamma_0 = 0.5$ in panel a) largely overestimates that observed experimentally. Presumably, the tested cover exhibited a Mullins-like effect which is often observed in elastomers, gels and soft living tissues [67, 206], and yields to a softening of their mechanical behavior. There are several possible microscale and irreversible mechanisms responsible of the Mullins effect. To mention a few, the rupture of physical or covalent cross-links, non-reversible rearrangement and/or disentanglement of macromolecules. Such damage or structure evolution mechanisms are not taken into account in the present micro-mechanical formulation. A possible way to account for these phenomena would consist in altering the histo-mechanical properties of the collagen fibrils, such as their modulus E_f (to account for damage) and/or their initial length l_0^f or tortuosity ξ_0 (to account for slippage), with proper kinetic laws. This latter aspect is out of the scope of the present study. However, the green curve plotted in panel a) shows that lowering (resp. increasing) E_f (resp. ξ_0) from 720 MPa to 400 MPa (1.11 to 1.118) would lead to a more appropriate model prediction.

- **Influence of the loading frequency** f **–** As previously observed for C_{LAOS} fibril tension-strain responses (Figure 3.4 d and Supplementary Material : Chapter 3 Figure 1), the Pipkin diagrams show a strong influence of f on the predicted macroscopic stress-strain response. Regardless of the considered strain magnitude γ_0, the higher the f-value, the higher the stress levels and hysteresis. These trends seem to be in qualitative agreement with typical measurements acquired on other vocal-fold cover samples [40].

3.4.3 Finite strain multiaxial cyclic loadings

Histo-mechanical parameters - To reproduce the nonlinear viscoelastic behavior exhibited by the vocal-fold sublayers subjected to cyclic longitudinal tension, transverse compression

and shear [54], the optimization led to a set of microscale viscoelastic parameters per type of sublayer: Table 3.4 reports the values identified for *lamina propria* samples (LP_1 and LP_2), while Table 3.5 those identified for *vocalis* samples (V_1 and V_2). All histological and elastic parameters (except the matrix shear modulus μ), previously optimized in Chapter 2 to reproduce the experimental "neutral" stress-strain curves lying in between the loading and unloading paths, were kept unchanged (see Table 2.1, Table 2.2, Table 2.3, Table 2.4). The μ-coefficient was moderately let free to differ from the previous identifications because the overall mechanical contribution of the matrix is here also related to the viscoelastic parameters of the model (interaction of the fibrils with the surrounding matrix). It was eventually found equal to (200 Pa, 190 Pa) for (LP_1, LP_2), instead of (330 Pa, 290 Pa), and equal to 170 Pa for both V_i samples, instead of (900 Pa, 980 Pa) for (VP_1, VP_2).

The *lamina propria* and *vocalis* optimized viscoelastic parameters (E, η_0, $\dot{\varepsilon}_0$) differ by an order of magnitude in favor of the *lamina propria* (see Table 3.4 and Table 3.5). This discrepancy may be ascribed to the sandwich arrangement of this specific sublayer, as well as to the looser architecture of the Reinke's space (SL). For both vocal-fold sublayers, however, obtained initial relaxation times $\tau = \eta_0/E \approx$ 3-15 s are consistent with previous reported data from MEMS and AFM testing on collagen fibrils [91, 234, 272]. Similar orders of magnitudes were found for relaxation times $\tau' = \eta_0'/E'$ related to steric hindrance between fibril bundles.

Sample LP	E (MPa)	η_0 (MPa s)	$\dot{\varepsilon}_0$ (s^{-1})	E' (MPa)	η_0' (MPa s)	$\dot{\varepsilon}_0'$ (s^{-1})
LP_1	1.47	14.2	$5\ 10^{-4}$	0.99	8.3	$5.5\ 10^{-3}$
LP_2	1.3	19.6	$6\ 10^{-4}$	1.63	16	$4.5\ 10^{-3}$

Table 3.4: Set of mechanical viscous parameters identified for *lamina propria* samples, LP_i.

Sample V	E (MPa)	η_0 (MPa s)	$\dot{\varepsilon}_0$ (s^{-1})	E' (MPa)	η_0' (MPa s)	$\dot{\varepsilon}_0'$ (s^{-1})
V_1	0.11	0.38	$3.6\ 10^{-3}$	0.11	0.53	$4.5\ 10^{-3}$
V_2	0.11	1.06	$3.3\ 10^{-3}$	0.07	0.67	$4.5\ 10^{-3}$

Table 3.5: Set of mechanical viscous parameters identified for *vocalis* samples, V_i.

Multiscale predictions - A comparison between the model macroscale stress-strain predictions and the viscoelastic experimental data [54] is shown in Figure 3.7, for both sublayers (LP_1 and V_1, results obtained for LP_2 and V_2 are reported in Appendix B. - Figure 2) and the three considered cyclic loading modes, *i.e.*, longitudinal tension, transverse compression and longitudinal shear. For each case, the corresponding "neutral" curve predicted in Chapter 2 (see dotted lines, details in Chapter 2) was additionally reported. The strain-induced evolution of multiscale kinematic descriptors is finally displayed in Figure 3.8 for the tension case, and in Figure 3.9 for the compression and shear cases. Focusing on the first load-unload cycle:

- *Longitudinal tension* – Compared with the previous hyperelastic formulation, the model is now able to reproduce stress hysteresis as well as the non-negligible residual strains exhibited by the *lamina propria* and the *vocalis* samples after unloading is completed (see Figure 3.7 a). These tendencies are inherited from the viscoelastic

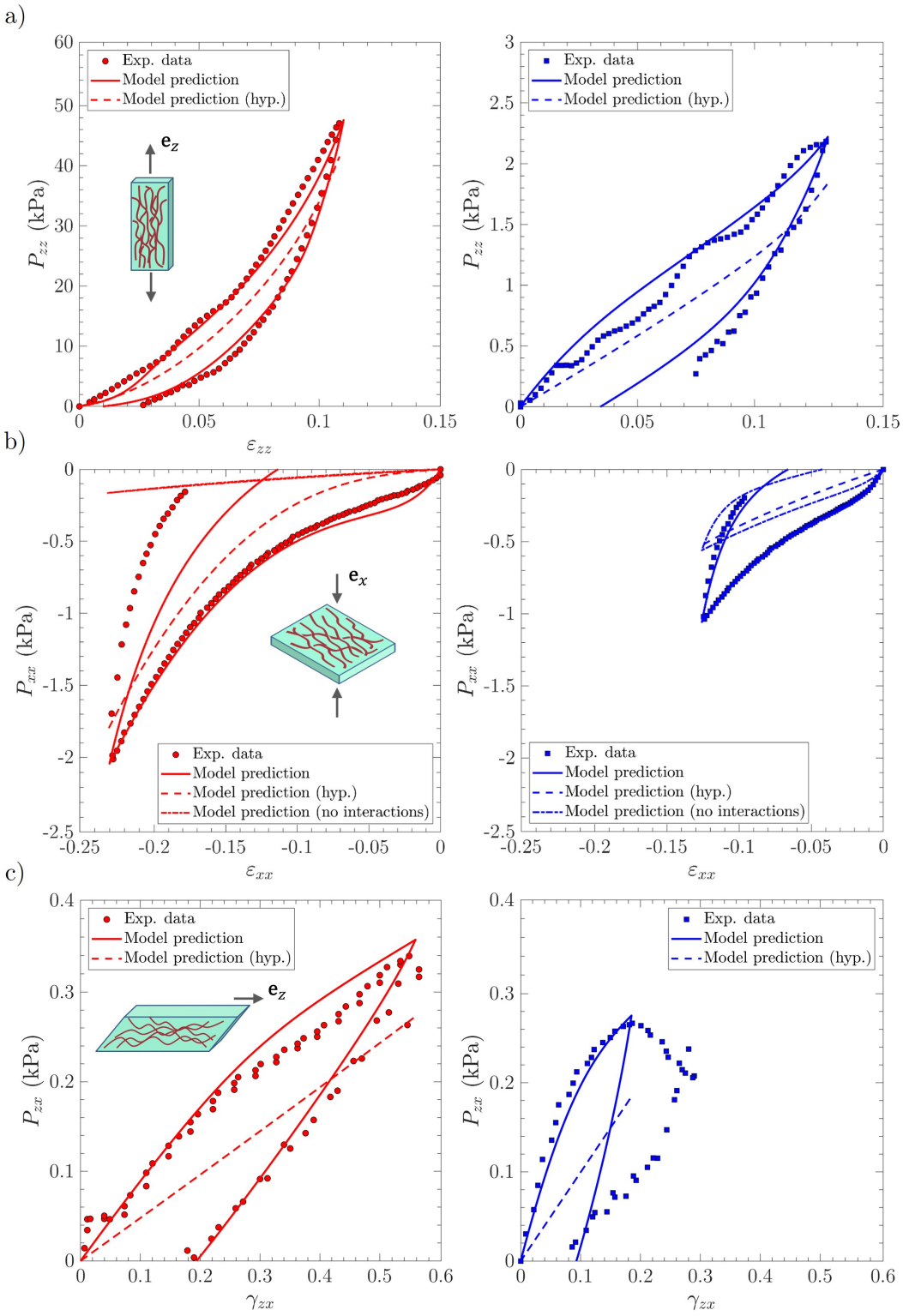

Figure 3.7: Macroscopic viscoelastic stress-strain curves of vocal-fold sublayers under multiaxial cyclic loadings. Experimental data *vs.* model predictions obtained for *lamina propria* sample LP_1 (left, in red) and *vocalis* sample V_1 (right, in blue): a) longitudinal tension; b) transverse compression; c) longitudinal shear.

rearrangement of the tissue microstructure. In particular, irreversible unfolding and rotation of collagen fibrils and myofibrils are predicted during cyclic tension along $\mathbf{e}_z$ for both *lamina propria* and *vocalis* samples, as displayed in Figure 3.8 and Appendix B. - Figure 3. For the *vocalis*, the predicted tension t_i in both collagen fibrils, $t_i c$, and myofibrils, $t_i m$, is plotted in the inset within Figure 3.8 b. It is interesting to notice that mechanical hysteresis and the irreversible lengthening of collagen fibrils as predicted by the model, for both sublayers, were experimentally observed by Yang [272] during cycling stretching at strain levels higher than 6%.

- *Transverse compression* – As already pointed out in Chapter 2, steric interactions are of major importance for *lamina propria* and *vocalis* mechanics under compressive loadings. This peculiar characteristic is preserved with the viscoelastic formulation, as shown in Figure 3.7 b (left graph, dotted lines): the longitudinal stretch-compression of collagen fibrils (and their surrounding matrix) can not account for the *lamina propria* stress hysteresis and residual strain experimentally observed. Conversely, fibril bundle repulsion forces r_q, and in particular, their viscoelastic contribution r_q^{ve}, appear to be of crucial importance to properly reproduce the vocal-fold sublayers behavior (solid lines). No other significant microscale deformation mechanisms (such as rotation and/or unfolding of fibrils) were simulated under transverse compression (see Figure 3.9 a and Figure 2.6 a).

- *Longitudinal shear* – The mechanical contribution of the matrix plays a major role in the overall shear response of the *lamina propria* and the *vocalis*, as already stressed in Chapter 2. On this basis, the fibrils viscoelastic properties and interaction with the surrounding ground substance allowed, *via* the microscopic tension t_i (see Figure 3.9 b), to satisfyingly reproduce the experimental trends observed during the load/unload sequence at the tissue scale (Figure 3.7 c).

The relevance of the micro-mechanical model to simulate the full series of 10 load-unload cycles is here finally assessed. Figure 3.10 compares the obtained theoretical predictions with the experimental data for the three considered loading modes. If the stress hysteresis decrease is qualitatively well reproduced by the model after the first cycle for all loading conditions, predictions fail in simulating the gradual maximal stress decrease and residual strain increase, particularly pronounced in tension and compression. A steady state is instead predicted right after the first cycle, while a stabilized behavior can be experimentally observed only after the 5th cycle (up to the 10th cycle, depending on the sample and the loading mode). As mentioned in the previous subsection for LAOS results, these accommodation behaviors resemble Mullins-like effects, that are not taken into account in the present formulation of the model.

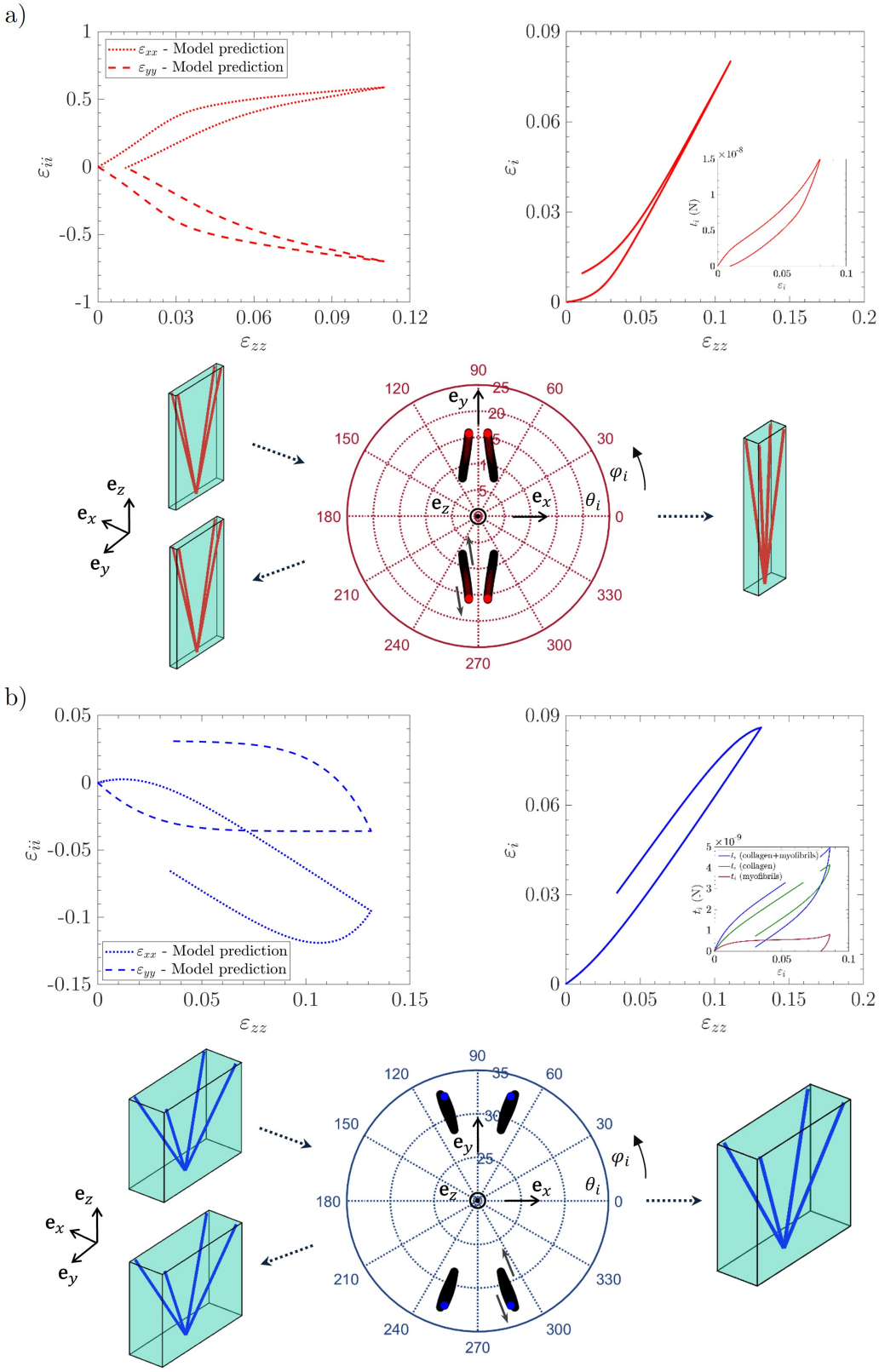

Figure 3.8: Strain-induced time-dependent evolution of multiscale descriptors predicted for a) *lamina propria* LP_1 and b) *vocalis* V_1 during tension along $\mathbf{e}_z$: macroscopic loading paths (top left); stereographic projection of orientation vectors $\mathbf{e}_i$ from initial to final state, $i \in [1..4]$ (bottom); strain variations of the fibril chord ε_i and corresponding tension t_i (top right).

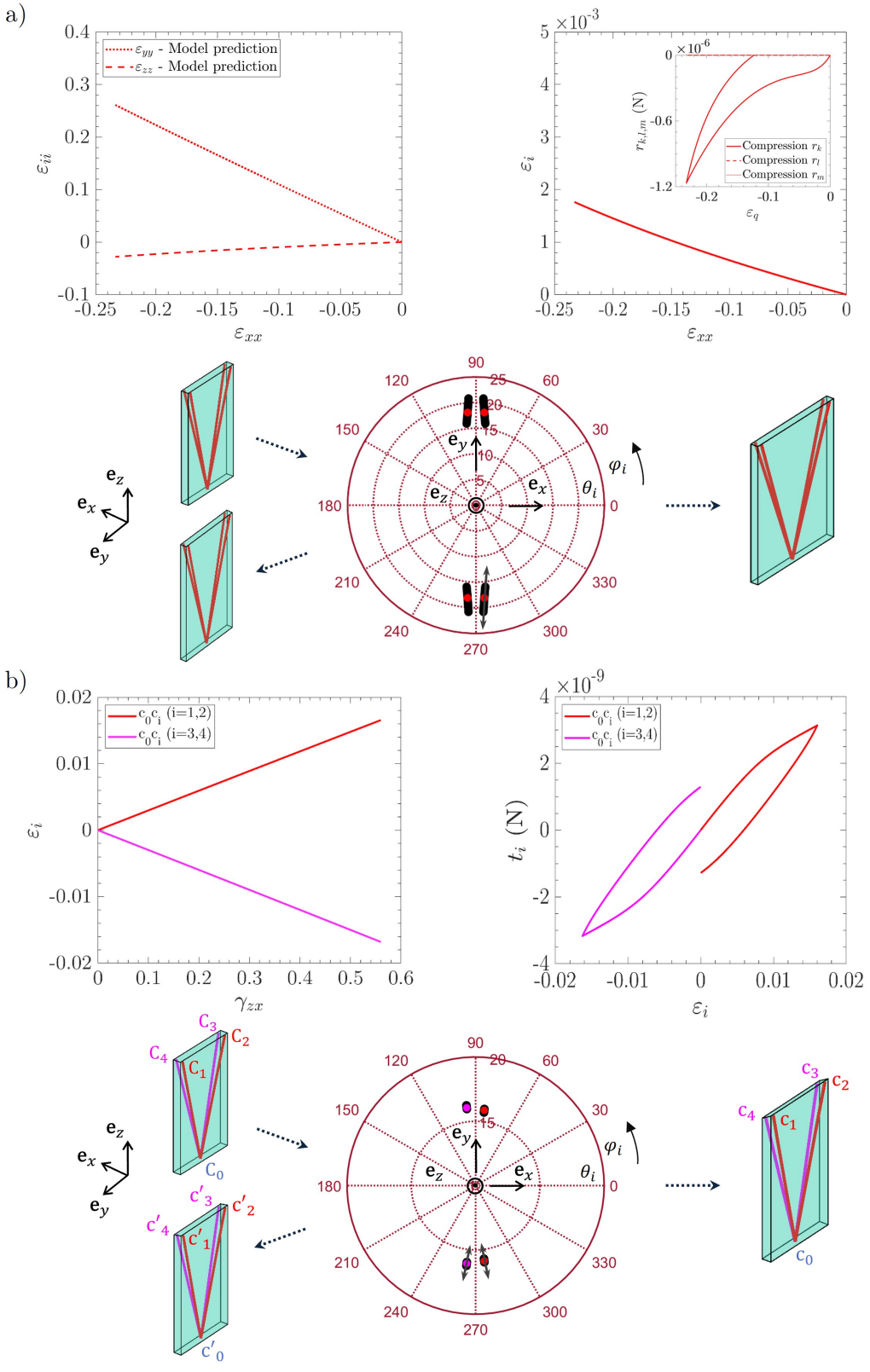

Figure 3.9: Strain-induced time-dependent evolution of multiscale descriptors for *lamina propria* sample LP_1: a) compression along $\mathbf{e}_x$ – macroscopic loading paths (top left), stereographic projection of orientation vectors $\mathbf{e}_i$ from initial to final state, $i \in [1..4]$ (bottom), strain variations of the fibril chord ε_i and corresponding steric interactions $r_{k,l,m}$ (top right); b) shear in the $(\mathbf{e}_z, \mathbf{e}_x)$ plane – strain variations of the fibril chord ε_i (top left) and corresponding tension t_i (top right), stereographic projection of orientation vectors $\mathbf{e}_i$ from initial to final state, $i \in [1..4]$ (bottom).

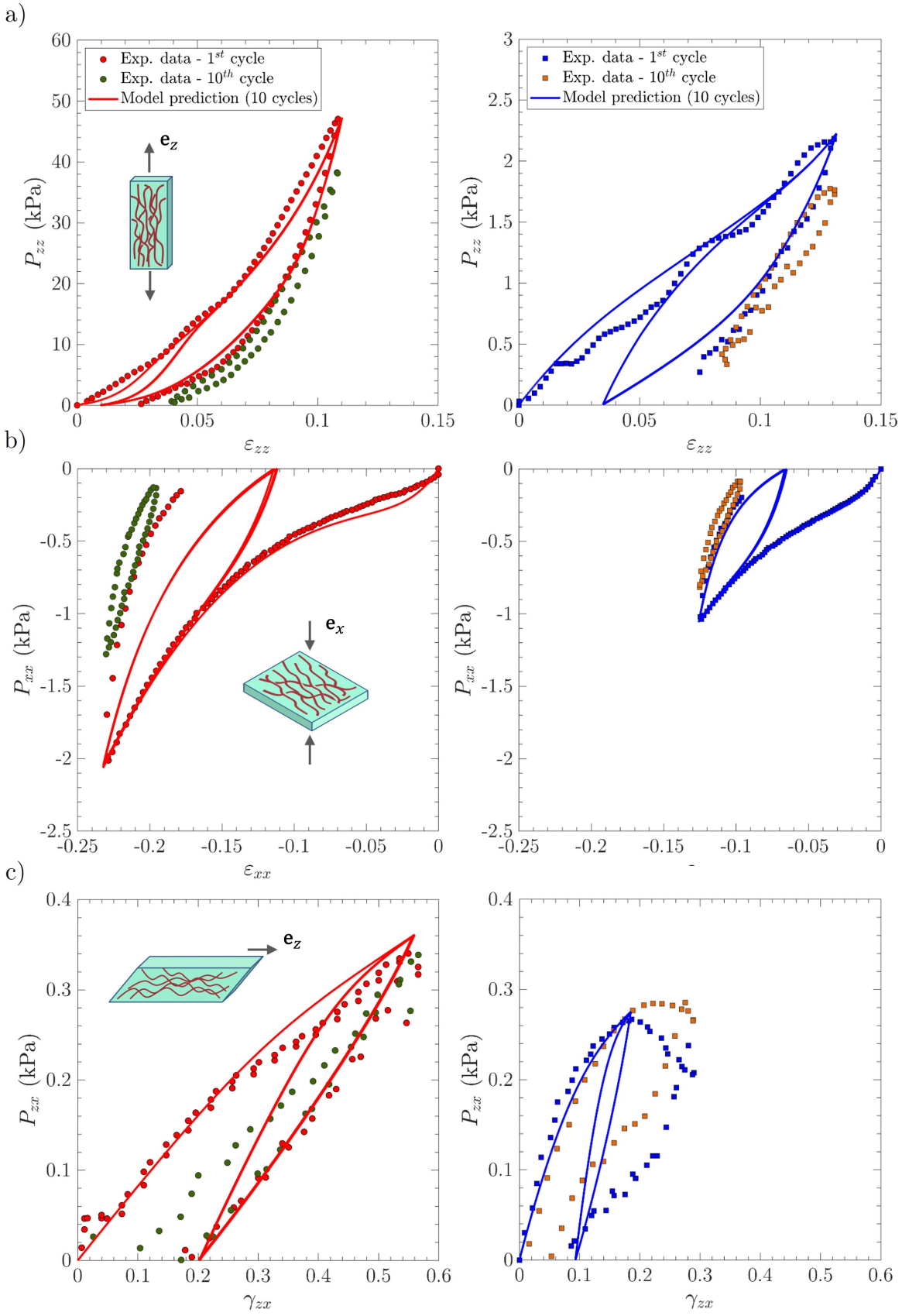

Figure 3.10: Macroscopic stress-strain curves of vocal-fold sublayers under multiaxial loadings: model limitations. Experimental data *vs.* model predictions obtained for *lamina propria* sample LP_1 (left, in red) and *vocalis* sample V_1 (right, in blue) upon hysteresis cycling (10 cycles): a) longitudinal tension; b) transverse compression; c) longitudinal shear.

3.5 Conclusion and future perspectives

A better understanding of human phonation can not prescind from an in-depth insight into vocal-fold viscoelastic properties. For that purpose, this study proposes a micro-mechanical model suitable to reproduce the anisotropic and time-dependent phenomena peculiar of vocal-fold mechanics, such as strain rate-dependency of the stress-strain response under various physiological loadings upon finite strains, stress hysteresis and residual inelastic deformations.

The present model proposes an idealization of the vocal-fold tissues microstructure, accounting for major histological descriptors including the collagen fibril (and myofibril) content, preferential orientation and waviness. Thereby, macroscopic responses are inherited and upscaled from simplified micro-mechanical mechanisms: (i) collagen fibrils (and myofibrils) stretch or compression; (ii) fibril bundle steric interactions, triggered when deforming and/or rotating. It is here proposed to model these micro-mechanisms by the introduction of nonlinear visco-hyperelastic networks (*i.e.*, lumped-element Zener models) in the respective material reference frames. Their nonlinear elasticity derives from histo-mechanical considerations reported in Chapter 2. The nonlinear viscous components were introduced to phenomenologically capture the tissue viscoelasticity, assumed to arise from the interactions between fibrils and the surrounding ground substance. The model parameters were either, mostly, obtained *a priori* from histo-mechanical evidence available in the literature, or estimated *a posteriori* by fitting macroscopic data.

The relevance of the model to reproduce various experimental biomechanical data is additionally assessed: SAOS, *i.e.*, in the linear viscoelasticity domain, LAOS, *i.e.*, in the nonlinear and finite strain viscoelasticity regime, and multiaxial finite strain cyclic loadings. Model predictions are in substantial agreement with macroscopic experimental trends and allow the simulation of significant microstructural descriptors. These promising results indicate the present model as a possible relevant tool to be implemented in FE commercial softwares to simulate vocal fold vibrations. A preliminary study toward this research direction is proposed in Chapter 4.

Nonetheless, there still remain two major drawbacks to be improved in future works. The fibril scale viscoelasticity is here modeled on the basis of phenomenological considerations: fine scale experiments and/or numerical simulations would probably provide more relevant information to strengthen the present formulation. It is additionally shown that the model is not suitable to reproduce Mullins effects experimentally observed: some possible improvements are proposed to account for fibril scale damage and rearrangement mechanisms, which need to be supported by additional experiments and/or fibril scale simulations.

4

Toward the simulation of vocal-fold vibrations

Contents

4.1 Introduction

As detailed in Chapter 1, along with traditional lumped-element models of glottal vibrations, numerous higher-order computational approaches based on the finite element method (FEM) have been proposed since the 2000s [5] to take into account realistic and *a priori* measurable properties of the vocal-fold tissues (*i.e.*, geometrical, biomechanical), and to finely simulate the coupled physical phenomena (*i.e.*, aerodynamical, mechanical, acoustical) involved in the phonation process.

The impact of these material properties on vocal folds vibro-mechanical performances has been investigated only in a few studies so far [106, 278, 279, 281], reporting how even slight vocal tissue stiffness changes can possibly alter both the phonation threshold pressure and onset frequency, but also the vibratory pattern of the vocal fold.
However, predicted trends can greatly differ, quantitatively and even qualitatively, from one study to another. In particular, Zhang [278] showed that a parametric increase in the body or cover stiffness of a two-layer body-cover model yields to a rise in the phonation threshold pressure and onset frequency. Depending on the body-cover stiffness ratio, the body or cover stiffness is reported to be alternatively of major influence on the pitch control. Conversely, Hájek *et al.* [106] recently found an inverse relationship between the stiffness of the *lamina propria* and the fundamental vibration frequency F_0. This latter (unexpected) result was ascribed to the material properties impact on the effective vibratory mass within the whole vocal fold: for *lamina propria* higher Young's modulus values ($\approx$ 5 kPa), the whole vocal fold is vibrating, whereas only the *lamina propria* is found to vibrate for lower values ($\approx$ 1.5 kPa, with a body-cover stiffness ratio around 30). If the body-cover stiffness ratio is thus pointed out as a key parameter in some numerical studies, Zhang [281] encourages the development of reduced-order models of phonation in which the vocal fold is simplified to a single-layer structure. In support of this position, it was reported a minor influence of the vocal-fold stiffness on the closed quotient [*], vertical phase difference and spectral shape of the output acoustics.

In conclusion, the correlation between the structural and mechanical characteristics of the vocal-fold tissues and their vibratory regime remains unclear.
Most of the material mechanical parameters required for continuum modeling of the vocal-fold tissues are not easily accessible due to experimental limitations. Furthermore, chosen values are often poorly correlated to available measurements (*e.g.*, longitudinal Young's modulus of the vocal mucosa or ligament) on account of a significant inter- and intra-subject variability [54, 135].
To reduce the number of required independent material parameters, vocal folds computational models are often based on a set of common simplifying assumptions [24, 57, 63, 129, 223, 256]: homogeneous sublayers, linear stress-strain behavior of the tissues, material (quasi-)incompressibility, planar displacement assumption constraining vocal-fold motion into coronal planes, isotropic (requiring 2 parameters) or transversely isotropic materials (5 independent parameters). Nonetheless, these assumptions mostly appear not be adequate to model vocal folds mechanical properties, characterized by a strong nonlinearity

[*] duration of closing phase divided by the cycle duration

and anisotropy inherited from their fibrous microstructure, as detailed in Chapter 2. To the author's knowledge, currently available computational models do not account for strain-induced mechanisms occurring at the (collageneous, elastinous or muscular) fiber scale.

In this context, the following preliminary study addresses the implementation of the micro-mechanical hyperelastic and anisotropic model presented in Chapter 2 in a finite element code, toward a first microstructure-informed FEM model of the human vocal fold. The chapter is structured as it follows. The numerical implementation of the theoretical model is detailed in Section 4.2. The validation of this implementation is discussed for several quasi-static, finite strain and multiaxial loadings (*i.e.*, tension, compression and shear) in Section 4.3. Section 4.4 finally paves the way for numerical simulations of vocal-fold vibrations, proposing a first 3D simulation of vocal fold transient dynamics driven by relevant histo-mechanical properties of the tissue.

4.2 Implementation of the micro-mechanical model

Toward more realistic simulations of vocal folds vibration under physiological conditions, the hyperelastic micro-mechanical model detailed in Chapter 2 was implemented in the Explicit version of Abaqus finite element (FE) software using linear hexaedral elements C3D8R. Among the available commercial FE softwares, Abaqus/Explicit was chosen based on: (i) the suitability to deal with nonlinear transient dynamic structural boundary value problems in a finite transformations domain, nonlinear constitutive relations as well as with multi-body contacts; (ii) the available facilities to implement user-defined constitutive equations. In the latter respect, Abaqus/Explicit requires the writing of a Fortran 77 subroutine called VUMAT (Vectorized User MATerial).

Thereby, at a given time t, accounting for the (i) fibril content, initial geometrical configuration (*i.e.*, orientation, diameter and waviness) and micro-mechanical parameters (*i.e.*, (un)folding and steric interactions), (ii) shear modulus of the ground substance, (iii) deformation gradient tensor $\mathbf{F}$ at $t + \Delta t$, it is thus possible to compute the Cauchy stress tensor $\boldsymbol{\sigma}$ at $t + \Delta t$ based on the expressions developed in Chapter 2.

Furthermore, Abaqus/Explicit requires the components of the resulting stress tensor to be expressed in a corotational framework. This was taken into account by the introduction of the rotation tensor $\mathbf{R}$ defined by means of the polar decomposition $\mathbf{F} = \mathbf{R} \cdot \mathbf{U}$ ($\mathbf{U}$ being the stretch tensor) and computed at each t.

Finally, it is not possible to assume a fully incompressible formulation in Abaqus/Explicit because the solver has no mechanism for imposing such constraint at each material calculation point [1]. Some slight compressibility was therefore provided by removing and changing the incompressibility pressure term and the ground substance strain energy function, respectively introduced in the micro-mechanical model (see Section 2.2.4), leading

to the following Cauchy stress tensor expression :

$$\boldsymbol{\sigma} = \mu(\det\mathbf{F})^{-5/3}(\mathbf{F}\cdot\mathbf{F}^T - \frac{1}{3}tr(\mathbf{F}\cdot\mathbf{F}^T)\boldsymbol{\delta}) + \kappa(\det\mathbf{F} - 1)\boldsymbol{\delta} \tag{4.1}$$

where μ is the shear modulus of the ground substance and κ its bulk compressibility modulus. Therefrom, the ground substance Poisson's ratio ν is defined as:

$$\nu = \frac{3\,(\kappa/\mu) - 2}{6\,(\kappa/\mu) + 2} \tag{4.2}$$

By default, the Poisson's ratio is set to 0.475, *i.e.*, $\kappa/\mu = 20$ [1]. Lowering this value would conduct to an increase in the medium compressibility, which may result in unrealistic behaviors. Conversely, values close to perfect incompressibility, *i.e.*, $\nu \to 0.5$ or $\kappa/\mu \to \infty$, would conduct to ill-conditioned boundary value problems and to, in the case of an explicit solver, the need for considerably, not affordable, small time steps in order to avoid spurious instabilities.

4.3 Validation of the model implementation

Homogeneous and quasi-static simulations with a single finite element – The correct implementation of the micro-mechanical model was initially studied comparing the results of simulations carried out using a single FE to the mechanical tendencies predicted by the hyperelastic micro-mechanical model for quasi-static multiaxial loading conditions (*i.e.*, longitudinal tension, transverse compression and longitudinal shear) in the case of the *lamina propria*.

For that purpose, the time increment Δt was automatically adjusted by the Explicit solver (can be manually imposed if needed), to fulfil the stability convergence condition required for such explicit time integration schemes. This time step should theoretically not exceed $\Delta t_{max} = 1/\pi F_{max}$, F_{max} being the system highest natural frequency of vibration, related to both the finite element size (mass) and stiffness.
Contrary to what is usually the case for quasi-static simulations using explicit solvers (to speed up the computation time), considering the major interest toward dynamic simulations, mass scaling was not used in this study.
Bulk viscosity coefficients, required in Abaqus/Explicit to improve the modeling of high-speed dynamic events restraining possible instabilities in explicit simulations but not included in the material point stresses because intended as a numerical effect only [1], were set by default to 0.06 and 1.2 .
Furthermore, to minimize the rise of spurious oscillations induced by a sudden discontinuity in the strain rate (from zero, at rest, to the prescribed value), a smoothing process available in Abaqus was used at the very beginning of the quasi-static loading [1].
Lastly, preliminary simulations were carried out to adjust the Poisson's ratio ν to 0.4995, *i.e.*, a value ensuring at the same time the tissue quasi-incompressibility and the stability of the simulations.

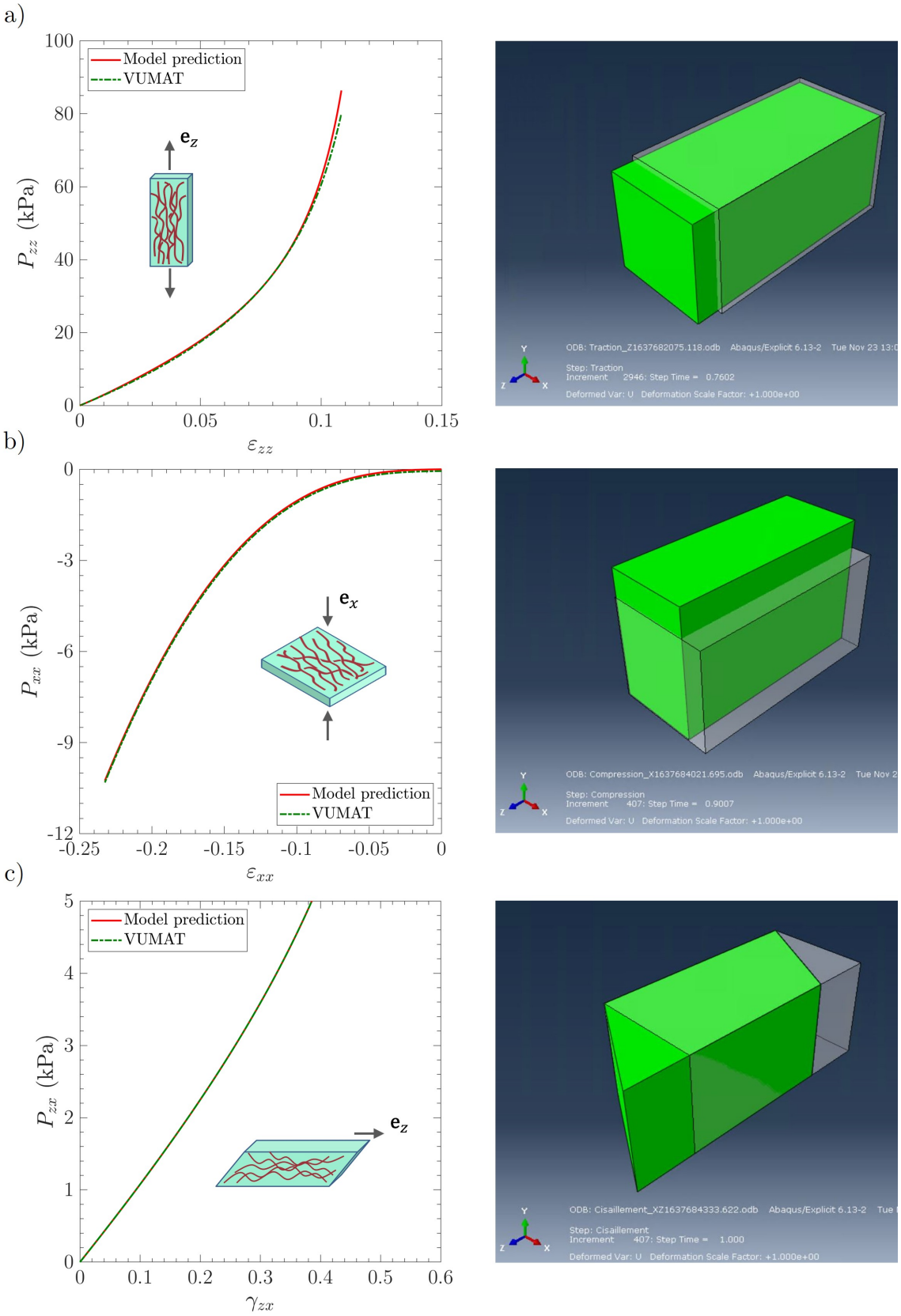

Figure 4.1: Macroscopic stress-strain curves for the equilibrated orthotropic microstructure with moderate fibril orientation (REV_2). One element FE simulations *vs.* Matlab semi-analytical predictions for: a) longitudinal tension; b) transverse compression; c) longitudinal shear. Finite element initial and deformed configurations are reported next to the corresponding curves.

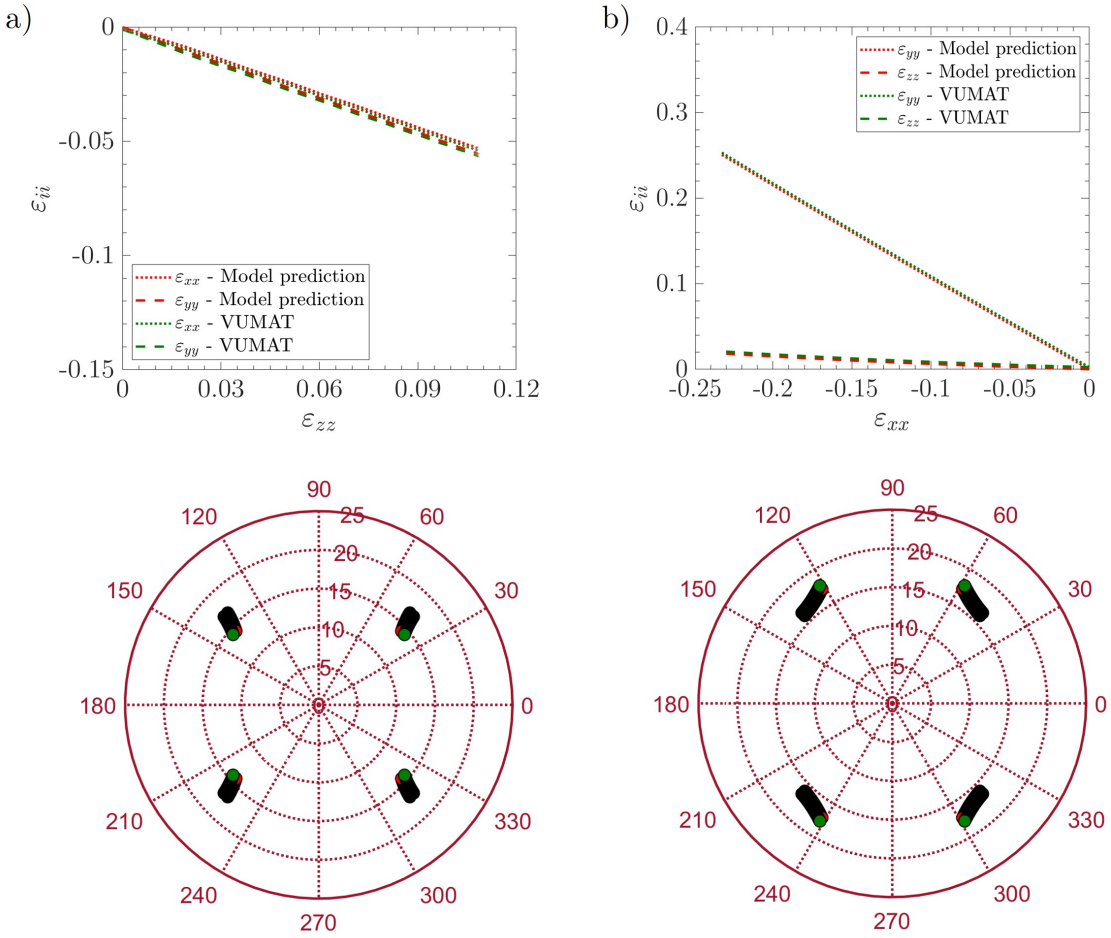

Figure 4.2: Strain-induced evolution of multiscale kinematic descriptors for the equilibrated orthotropic microstructure with moderate fibril orientation (REV_2). One element FE simulations *vs.* Matlab semi-analytical predicted macroscopic loading paths (top) and stereographic projection of orientation vectors $\mathbf{e_i}$ (bottom) for: a) longitudinal tension; b) transverse compression.

Thereby, based on the optimal histo-mechanical identification carried out in Section 2.4 for *lamina propria* sample LP_1, two characteristic microstructural configurations were considered for the validation:

- A first equilibrated (*i.e.*, with in-plane transverse isotropy when projected in the $(\mathbf{e}_x, \mathbf{e}_y)$ plane) configuration with moderate orthotropic fibril orientation (LP_1 optimal set of histo-mechanical parameters but $\varphi_0 = 45°$, see REV_2 in Figure 2.7).
- The optimal highly orientated orthotropic structure identified for LP_1 in Section 2.4 (see REV_1 in Figure 2.7).

In both cases, FE results were compared to the semi-analytical tendencies predicted by Matlab in Section 2.4.2.

Figure 4.1 illustrates the stress-strain responses predicted for the first equilibrated configuration under longitudinal tension along $\mathbf{e}_z$ (see Figure 4.1 a), transverse compression along $\mathbf{e}_x$ (see Figure 4.1 b) and longitudinal shear in the $(\mathbf{e}_z, \mathbf{e}_x)$ plane (see Figure 4.1 c). Finite element initial and deformed configurations are additionally reported next to the

corresponding curves. Figure 4.2 a and Figure 4.2 b respectively provide strain-induced multiscale kinematic descriptors for longitudinal tension and transverse compression. Regardless of the loading mode, FE stress-strain curves satisfyingly reproduce the semi-analytical tendencies predicted by Matlab. Similar conclusions can be extended to multiscale kinematic descriptors. FE macroscopic strain paths are nearly identical to those predicted by the micro-mechanical model (slight discrepancies are probably ascribable to different compressibility formulations): alike contraction along ε_{yy} and ε_{xx} during tension along ε_{zz}, anisotropic expansion with $\varepsilon_{yy} > \varepsilon_{zz}$ during compression along ε_{xx}. Figure 4.2 a and Figure 4.2 b additionally display corresponding fibril orientation vectors $\mathbf{e_i}$ (represented using stereographic projections): FE predictions closely reproduce once more semi-analytical tendencies.

Analogous results are presented in Figure 4.3 and Figure 4.4 for the highly orientated orthotropic microstructure (REV_1). Similarly to what stated for the previous configuration, FE stress-strain curves and strain-induced multiscale kinematic descriptors are in good accordance with the semi-analytical tendencies predicted by the micro-mechanical model. Nonetheless, slightly more significant predictions discrepancies can be observed during longitudinal tension for tensile strains ε_{zz} above 0.05. In particular, FE predictions show higher compressive, $|\varepsilon_{yy}|$, and tensile, ε_{xx} , transverse strains (auxeticity). This may be attributable to the nearly incompressible FE formulation coupled with the marked auxetic effect the microstructure displays during stretch-induced fibrils reorientation. This latter aspect should be further investigated.

Homogeneous and quasi-static simulations with several finite elements – To check whether previous validations were preserved or not when considering higher degrees of freedom, the same homogeneous boundary value problems were carried out once more increasing the number of finite elements (following considerations equally apply for any number > 1). Analogous results were obtained in the case of the equilibrated and moderately orthotropic microstructure (REV_2) regardless of the considered loading mode. Conversely, not plausible oscillatory instabilities were detected in the case of a highly oriented microstructure (LP_1 – REV_1) for longitudinal tension and transverse compression, as shown in Appendix C. - Figure 1. Decreasing the time step and/or the Poisson's ratio, nor increasing the smooth step amplitude at the beginning of the applied loading, didn't allow to overcome this numerical artifact. Note that any mass scaling was tuned for the aforementioned reasons. The incompressibility condition combined with the high directional stiffness and resulting auxeticity could presumably be at the origin of this objectionable behavior. Additional efforts should be addressed to further investigate this aspect. Nonetheless, it is relevant to observe that this numerical effect was sorted out when considering a still highly orientated but equilibrated (*i.e.*, $\varphi = 45°$, without any residual auxetic effects) structure like that of REV_2. Consequently, in the following, only the equilibrated but highly orthotropic microstructure (REV_2) will be considered.

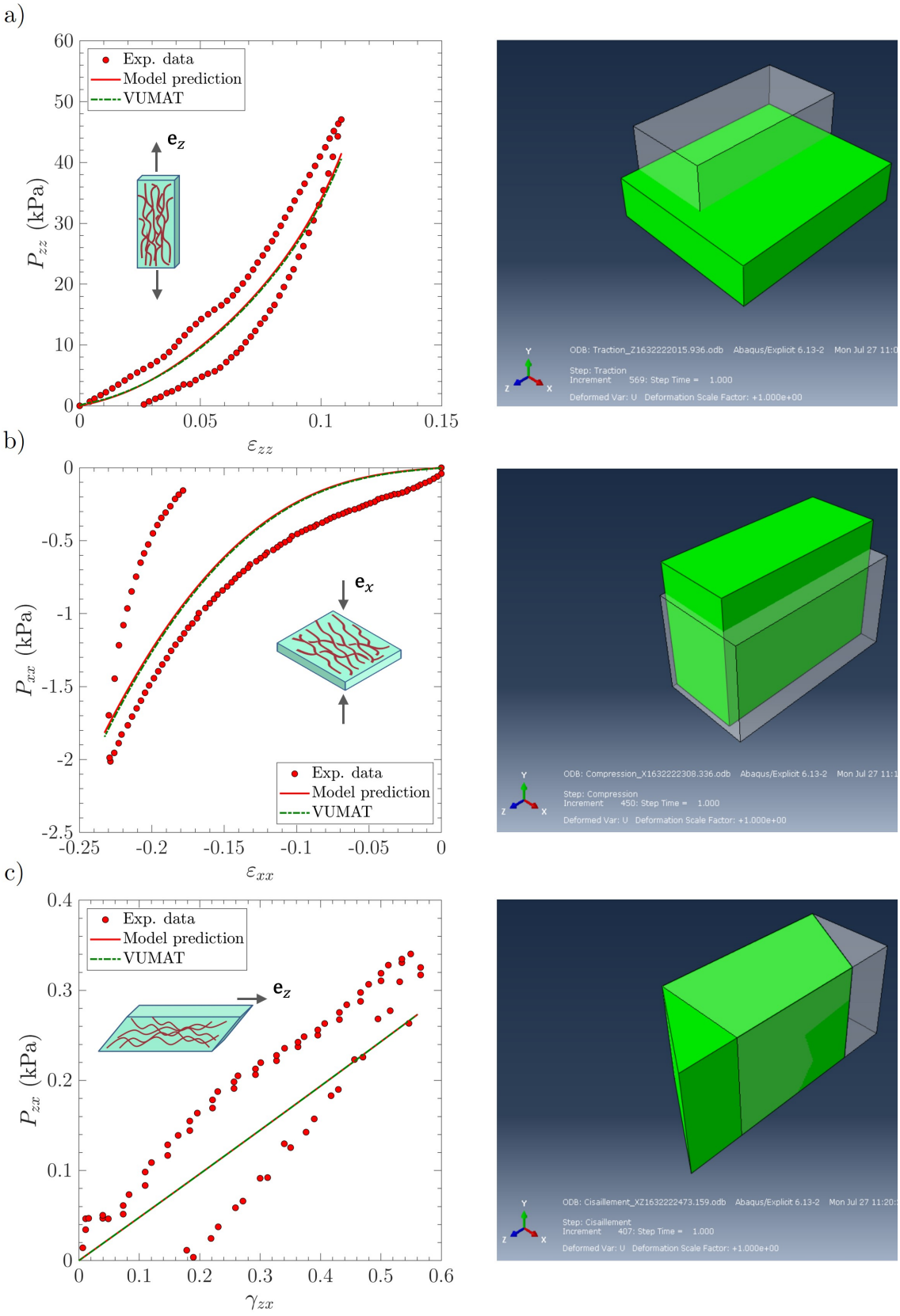

Figure 4.3: Macroscopic stress-strain curves for the non-equilibrated orthotropic microstructure with a marked fibril orientation (REV_1 - LP_1). One element FE simulations *vs.* Matlab semi-analytical predictions for: a) longitudinal tension; b) transverse compression; c) longitudinal shear. Finite element initial and deformed configurations are reported next to the corresponding curves.

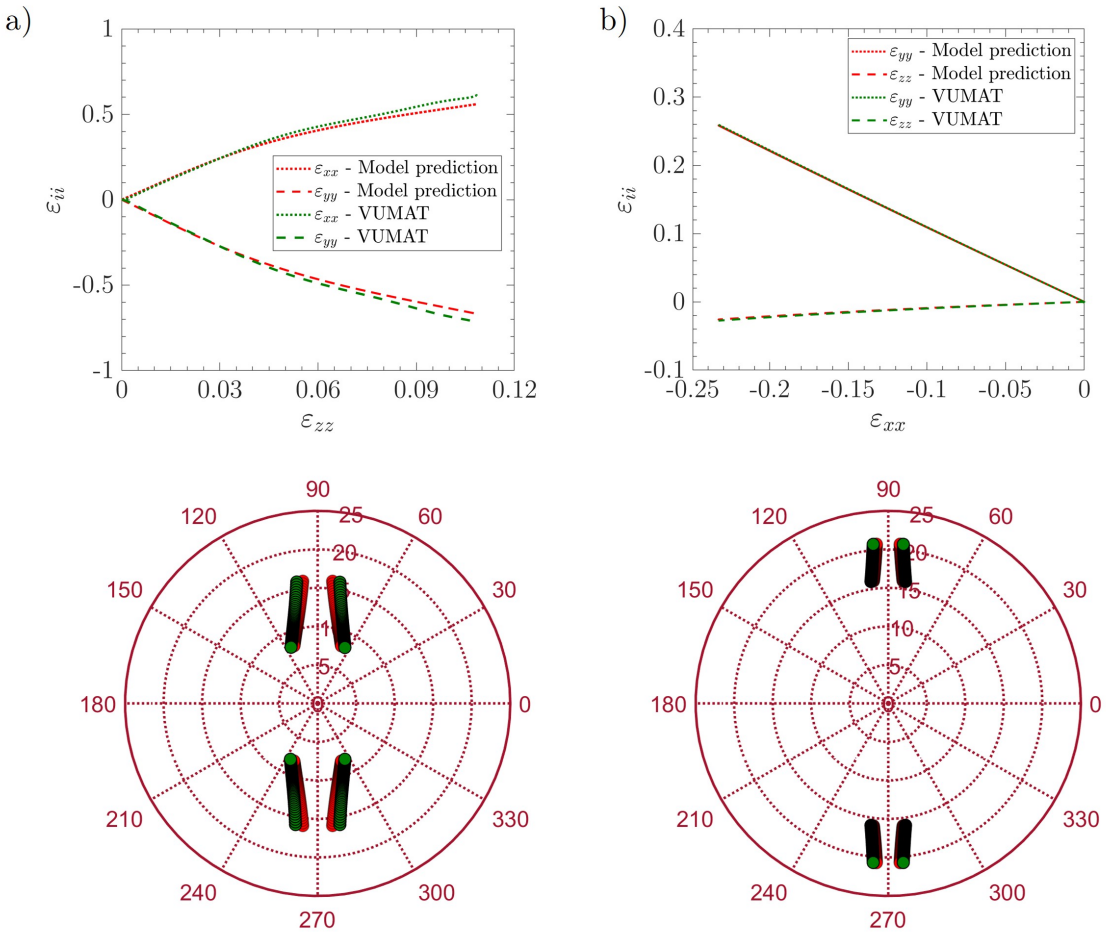

Figure 4.4: Strain-induced evolution of multiscale kinematic descriptors for the non-equilibrated orthotropic microstructure with a marked fibril orientation (REV_1 - LP_1). One element FE simulations *vs.* Matlab semi-analytical predicted macroscopic loading paths (top) and stereographic projection of orientation vectors $\mathbf{e_i}$ (bottom) for: a) longitudinal tension; b) transverse compression.

4.4 A preliminary study of the vibration of a vocal fold

In Section 2.4.3, an analytical pinned-pinned Timoshenko beam model was considered as an oversimplified representation of the *lamina propria* geometry to estimate its vibratory properties using the hyperelastic micro-mechanical model developed in Chapter 2, emulating the study proposed by Kelleher *et al.* [144]. This allowed to emphasize the roles of both the fibrous microstructure and level of pre-stretching on the beam fundamental frequencies of vibration (see Figure 2.8).

Pursuing a specular objective, a preliminary FE simulation of the vibration of a single vocal fold is here proposed to: (i) improve the aforementioned approach; (ii) make a first step toward more realistic analyses of vocal-fold vibrations; (iii) illustrate the practical interest of FE simulations in this study.

Hence, as illustrated in Figure 4.5 a, a 3D CAD model of a vocal fold was initially designed accounting for the following characteristic dimensions reported in the literature [281]: a typical length of $\approx$ 15 mm (along the antero-posterior direction), typical height and

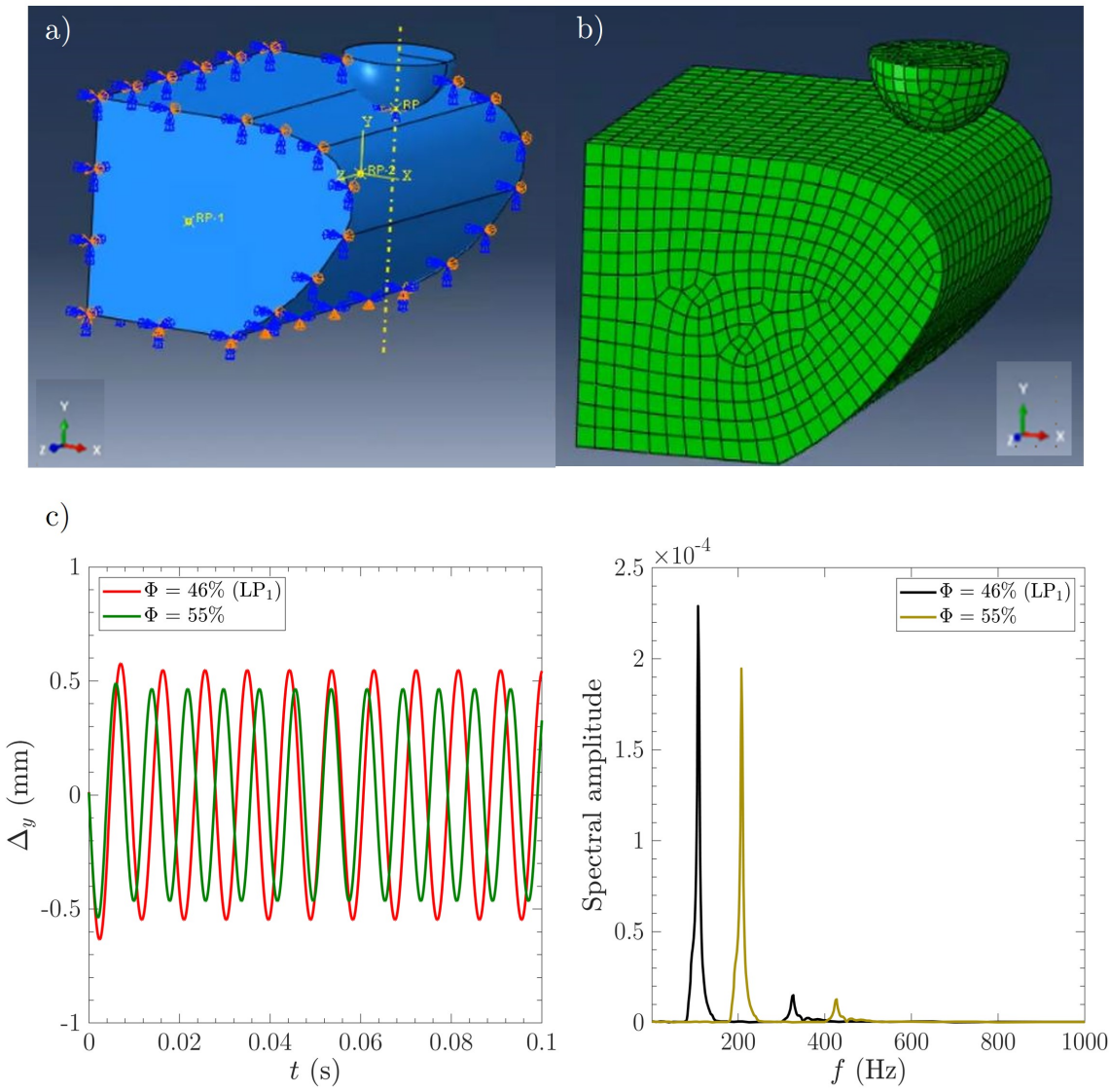

Figure 4.5: Transient structural dynamic analysis of a vocal fold subjected to a shock: a) CAD model of the vocal fold, boundary conditions and hemi-sphere originating the impact; b) mesh of the CAD model; c) time-evolution of the nodal vertical displacement of the vocal fold in the close proximity of the impact point (left) and corresponding frequency domain spectrum computed using a Fast Fourier Transform (right).

width of ≈ 10 mm. The geometry was meshed with C3D8R elements as illustrated in Figure 4.5 b. For the sake of simplicity and as a first illustrative example, the fold was conveniently conceived as a monolayered structure of *lamina propria* complying with the implemented hyperelastic micro-mechanical model. In the latter respect, the previously validated equilibrated and moderately orthotropic microstructure (REV_2) was considered. Yet, two different physiological volume fractions of fibrils $\Phi = 0.46$ (LP_1 and REV_2) and $\Phi = 0.55$ (upper limit reported in the literature for the *lamina propria* depending on the tissue depth $\mathbf{e_x}$ [34, 105, 194, 244]) were taken into consideration. As illustrated in Figure 4.5 a, zero-value displacements were imposed to the external surfaces of the CAD model along the directions of contact with the ligaments and the cartilages of the larynx to mostly excite bending vibrational modes. These Dirichlet boundary conditions represent a more realistic configuration than that considered in Section 2.4.3 using beam theory. They may,

however, be considered as too restraining and could, therefore, possibly be softened up in future simulations.
To analyze the vibratory properties of these biological structures, a 4 mm diameter rigid hemisphere meshed with R3D4 bilinear elements (see Figure 4.5 a and Figure 4.5 b) was projected down to the top of the vocal fold at a velocity of 10^3 mm s^{-1} and rapidly removed upwards without altering the vibration of the impacted vocal fold. Therefrom, the impulse response of the vocal fold was simulated with a proper time step of $\Delta t = 10^{-7}$ s. Similarly to quasi-static simulations, default bulk viscosity coefficients were set to improve the modeling of a high-speed dynamics ensuring the stability of the calculation.

On this basis, Figure 4.5 c shows the nodal vertical (*i.e.*, along $\mathbf{e_y}$) oscillatory displacement of the vocal fold in the close proximity of the impact point for the two examined fibril contents. Figure 4.5 c additionally shows the corresponding frequency domain spectrum computed using a Fast Fourier Transform (FFT). This latter graph highlights the presence of two main modal frequencies (peaks) in both cases: approximately 100 Hz and 350 Hz for $\Phi = 0.46$, shifted to approximately 200 Hz and 450 Hz for $\Phi = 0.55$. Regardless of the considered fibril content, clearly showing the crucial influence of the tissue microstructural configuration on its macroscopic vibratory properties, these preliminary results are qualitatively consistent with those reported in Section 2.4.3 , using an oversimplified beam model, and in the literature [32, 152]. This suggests that the present study, once improved and refined, could represent a possible tool to further analyze the underlying correlation between the vocal-fold tissue microstructure and its peculiar vibratory properties.

4.5 Concluding remarks

In this last chapter, the hyperelastic formulation of the micro-mechanical model developed in Chapter 2 to reproduce the vocal-fold tissues finite strain anisotropic mechanics is implemented in a commercial finite element software providing an explicit solver. The validation of the implementation is corroborated when considering homogeneous simulations with a single finite element. Conversely, if the validation is once more confirmed for simulations of equilibrated orthotropic configurations with more finite elements, additional efforts are required to strengthen the robustness of the simulation for non-equilibrated fibrils orientations which may possibly exhibit auxetic effects.

Nevertheless, a preliminary dynamic study is conducted carrying out a rather elementary impact simulation, to excite the vibration of a homogeneous vocal fold with a equilibrated but highly orientated fibril configuration and to extract relevant first and second modal frequencies, emphasizing at the same time the major role played by a key histological descriptor as the fibril content.

A first improvement of the study would consist in considering different vocal-fold sublayers, *e.g.*, the *lamina propria* and the *vocalis*, to investigate the possible changes induced by a multi-layered architecture owning different microstructures. Considering softer boundary conditions and further investigating simulations for non-equilibrated configurations could

represent an interesting subject of additional research. Finally, before contemplating FE models of increasing complexity to simulate the vibration of two vocal folds, *i.e.*, accounting for vocal fold collision and self-sustained vibrations induced by the sub-glottal airflow, the implementation of the micro-mechanical model full visco-hyperelastic formulation would constitute a considerable improvement of the present study.

Conclusions and perspectives

Vocal folds are soft pliable laryngeal multi-layered tissues exhibiting remarkable vibro-mechanical properties. Structural fibrous networks they are made of, *i.e.*, highly anisotropic and complex architectures of wavy collagen fibrils and myofibrils, play a major role in their vibratory properties. However, due to experimental limitations in the characterization of these tissues, the underlying relationship between their microstructure and macroscopic behavior remains elusive. Furthermore, by contrast with many other soft living tissues, most of the theoretical approaches currently adopted to model the vocal-fold mechanical properties still rely on coarse macroscopic formulations poorly related to the fibril scale. Recent promising microstructure-inspired models have been proposed to get a further insight into this correlation. Nonetheless, the relevance of their predictions for representative physiological multiaxial loadings vocal folds are subjected to during phonation is not assessed. Furthermore, these approaches are commonly based on hyperelastic formulations not allowing to simulate the viscoelastic effects vocal-fold tissues exhibit upon loading. Thereby, an original visco-hyperelastic microstructure-informed model, *i.e.*, based on histological evidence, is here proposed to account for the mechanics of representative vocal-fold tissue sublayers, *i.e.*, the *lamina propria* and the *vocalis*, and whose relevance and limitations are assessed for representative cyclic loadings.

An idealized description of the *lamina propria* and *vocalis* 3D fibrous architectures was initially presented. Representative Elementary Volumes were defined for each sublayer: in spite of the relatively simple topology, several structural descriptors were introduced to account for, in a first approximation, the role of the fibril content, its anisotropic orientation and waviness (more appropriate, realistic and complex representations are possible and do not represent a model limitation). On this basis, a hyperelastic formulation was developed to model wavy fibril bundle micro-mechanics, *i.e.*, (un)folding and steric interactions. Particular attention was drawn to the definition of prevalently histo-mechanical model parameters, limiting the introduction of phenomenological quantities to the minimum extent. The relevance of the model was successfully assessed comparing predictions to biomechanical data of *lamina propria* and *vocalis* specimens subjected to longitudinal tension, transverse compression and longitudinal shear. Regardless of the considered tissue, specimen, and loading path, neutral stress-strain curves could be predicted in accordance with experimental data, and corresponding fibril scale deformation micro-mechanisms and scenarios were discussed. It was also shown how the micro-mechanical model constitutes a first suitable approach to predict and better understand vocal-fold tissues vibratory properties. Nevertheless, the aforementioned purely elastic framework didn't allow to reproduce the non-negligible viscoelastic effects experimentally observed, thus representing a major limitation of the model.

The micro-mechanical model was accordingly extended to a time-dependent formulation. The original frame was preserved, *i.e.*, microstructural idealization and hyperelastic approach to predict neutral stress-strain curves. Nonlinear viscous contributions were added to the fibril mechanics and steric interactions hyperelastic components. Although conceived and implemented at the fibril scale, they rely on phenomenological considerations in

the absence of experimental evidence. The relevance of the model was initially assessed comparing predictions to vocal fold cover samples linear viscoelastic regime, *i.e.*, SAOS, biomechanical data. Most of the experimental trends could be predicted, such as the nonlinear evolution (with the frequency) of the: (i) storage and loss moduli and their cross-over regime; (ii) damping ratio with a transition from a over to under-damped regime; (iii) dynamic viscosity with a transition from a Newtonian to a power-law regime. Model capabilities upon finite strains were additionally investigated by means of LAOS data extrapolated from the literature. Satisfying predictions were obtained except for Mullins-like effects, experimentally observed but not accounted for in the model formulation. Lastly, to assess the relevance of the approach to reproduce finite strain multiaxial loading conditions, the biomechanical data already considered for the hyperelastic formulation were used once more. In this regard, noticeable improvements in model predictions were obtained when using the visco-hyperelastic formulation. In particular, a satisfying modeling of stress hysteresis, regardless of the considered tissue, sample, and loading path. Model limitations in reproducing Mullins-like effects were confirmed.

Finally, toward future numerical simulations of vocal-fold vibrations, the micro-mechanical model proposed in this study was preliminarily implemented in a Finite Element code used for structural applications. A major focus was brought to the hyperelastic formulation as a first step toward the implementation of the full visco-hyperelastic micro-mechanical model. Corresponding constitutive relations were coded in a dedicated VUMAT subroutine for Abaqus Explicit FE code. The explicit formulation was chosen as well-suited to simulate dynamic structural boundary value problems. A first validation was successfully carried out by simulating with a single finite element the previously considered quasi-static multiaxial loadings in the case of the *lamina propria*. When considering multiple finite elements, some numerical instabilities arose for highly orthotropic configurations but were not detected for moderately transversely isotropic ones. In this latter case, as a first structural application, a transient dynamic analysis of a homogeneous vocal fold subjected to a shock was performed, allowing to carry out a corresponding modal analysis.

This work paves the way toward multiple lines of research as possible improvements of the present study. Among them, the following perspectives are here reported:

- The micro-mechanical model still presents some phenomenological constitutive relations, although adopted at the fibril or fiber scale. A first significant improvement would consist in developing more sophisticated formulations of steric interactions and viscoelastic contributions, more closely related to histo-mechanical evidence. This information could be possibly obtained carrying out fibril/fiber scale experiments and/or simulations.
- In its current state, the model formulation does not account for fibril scale damage or plastic (rearrangement) phenomena, yielding to the marked Mullins effects experimentally observed at the tissue scale. Additional research efforts would be required to simulate these major phenomena.

- Only the passive behavior of the *vocalis* was addressed in this study. The modeling of active "myofibrils" would undoubtedly consolidate the micro-mechanical formulation so as to better understand the respective contribution of the *vocalis* and the *lamina propria* in the regulation of phonation. Pertinent developments may rely on the existing literature on the biomechanics of muscles and myofibrils [55, 58, 132].
- Further studies are finally required to pursue the preliminary implementation of the micro-mechanical model in FE codes and carry out more sophisticated dynamic structural and multiphysics analyses toward the simulation of vocal-fold self-sustained vibrations.

Bibliography

[1] *Abaqus documentation*. URL: https://abaqus-docs.mit.edu/2017/English/SIMACAEEXCRefMap/simaexc-c-docproc.htm (cit. on pp. 105, 106).

[2] Adachi, S. and Yu, J. "Two-dimensional model of vocal fold vibration for sound synthesis of voice and soprano singing." In: *The Journal of the Acoustical Society of America* 117.5 (2005), p. 24. DOI: 10.1121/1.1861592 (cit. on pp. 38, 39).

[3] Alberts, B. *et al.* "Molecular biology of the cell." *Garland Science*, 2014. DOI: doi.org/10.1201/9781315735368 (cit. on p. 27).

[4] Alipour, F. *et al.* "A finite-element model of vocal-fold vibration." In: *The Journal of the Acoustical Society of America* 108.6 (2000), p. 12. DOI: 10.1121/1.1324678 (cit. on pp. 40, 41).

[5] Alipour, F. *et al.* "Mathematical Models and Numerical Schemes for the Simulation of Human Phonation." In: *Current Bioinformatics* 6.3 (2011), pp. 323–343. DOI: 10.2174/157489311796904655 (cit. on pp. 37, 39, 42, 104).

[6] Amabili, M. "Nonlinear mechanics of shells and plates in composite, soft and biological materials." *Cambridge University Press*, 2018. DOI: 10.1017/9781316422892 (cit. on p. 76).

[7] Arnold, G. "Vocal rehabilitation of paralytic dysphonia. X. Functional results of intrachordal injection." In: *Archives of Otolaryngology* 78 (1963), pp. 179–186. DOI: 10.1001/archotol.1963.00750020187014 (cit. on p. 22).

[8] Arruda, E. M. and Boyce, M. C. "A three-dimensional constitutive model for the large stretch behavior of rubber elastic materials." In: *Journal of the Mechanics and Physics of Solids* 41.2 (1993), pp. 389–412. DOI: 10.1016/0022-5096(93)90013-6 (cit. on pp. 53, 57).

[9] Asgari, M. *et al.* "In vitro fibrillogenesis of tropocollagen type III in collagen type i affects its relative fibrillar topology and mechanics." In: *Scientific Reports* 7.1 (2017), 1392–undefined. DOI: 10.1038/s41598-017-01476-y (cit. on pp. 33, 34, 60, 61).

[10] Awrejcewicz, J. "Bifurcation portrait of the human vocal cord oscillations." In: *Journal of Sound and Vibration* 136.1 (1990), pp. 151–156. DOI: 10.1016/0022-460X(90)90945-V (cit. on p. 39).

[11] Awrejcewicz, J. "Numerical investigations of the constant and periodic motions of the human vocal cords including stability and bifurcation phenomena." In: *Dynamics and Stability of Systems* 5.1 (1990), pp. 11–28. DOI: 10.1080/02681119008806080 (cit. on p. 39).

[12] Bailly, L. *et al.* "Towards a biomimetism of abdominal healthy and aneurysmal arterial tissues." In: *Journal of the Mechanical Behavior of Biomedical Materials* 10 (2012), pp. 151–165. DOI: 10.1016/j.jmbbm.2012.02.019 (cit. on pp. 52, 57, 59).

[13] Bailly, L. *et al.* "In-plane mechanics of soft architectured fibre-reinforced silicone rubber membranes." In: *Journal of the Mechanical Behavior of Biomedical Materials* 40.12 (2014), pp. 339–353. DOI: 10.1016/J.JMBBM.2014.09.012 (cit. on pp. 52, 57).

[14] Bailly, L. *et al.* "Vocal fold and ventricular fold vibration in period-doubling phonation: physiological description and aerodynamic modeling." In: *The Journal of the Acoustical Society of America* 127.5 (2010), p. 22. DOI: 10.1121/1.3365220 (cit. on p. 39).

[15] Bailly, L. *et al.* "3D multiscale imaging of human vocal folds using synchrotron X-ray microtomography in phase retrieval mode." In: *Scientific Reports* 8.1 (2018). DOI: 10.1038/s41598-018-31849-w (cit. on pp. 24, 26, 35, 51, 53, 60–63, 87).

[16] Barnes, H. *et al.* "An Introduction to Rheology." *Elsevier*, 1989. DOI: 10.1002/jctb.280500316 (cit. on p. 89).

[17] Bartlett, R. S. *et al.* "Biomechanical Screening of Cell Therapies for Vocal Fold Scar." In: *Tissue Engineering - Part A* 21.17-18 (2015), p. 47. DOI: 10.1089/ten.tea.2015.0168 (cit. on p. 23).

[18] Basciano, C. A. and Kleinstreuer, C. "Invariant-based anisotropic constitutive models of the healthy and aneurysmal abdominal aortic wall." In: *Journal of Biomechanical Engineering* 131.2 (2009). DOI: 10.1115/1.3005341 (cit. on p. 52).

[19] Beatty, M. F. "An average-stretch full-network model for rubber elasticity." In: *Journal of Elasticity* 70.1-3 (2003), pp. 65–86. DOI: 10.1023/B:ELAS.0000005553.38563.91 (cit. on p. 53).

[20] Belytschko, T. *et al.* "Nonlinear finite elements for continua and structures." *Wiley*, 2000. DOI: 10.13140/RG.2.1.2800.0089 (cit. on p. 42).

[21] Benninger, M. S. *et al.* "Vocal Fold Scarring: Current Concepts and Management." In: *Otolaryngology–Head and Neck Surgery* 115.5 (1996), pp. 474–482. DOI: 10.1177/019459989611500521 (cit. on p. 19).

[22] Bergström, J. S. and Boyce, M. C. "Constitutive modeling of the large strain time-dependent behavior of elastomers." In: *Journal of the Mechanics and Physics of Solids* 46.5 (1998), pp. 931–954. DOI: 10.1016/S0022-5096(97)00075-6 (cit. on p. 44).

[23] Bergström, J. S. and Boyce, M. C. "Constitutive modeling of the time-dependent and cyclic loading of elastomers and application to soft biological tissues." In: *Mechanics of Materials* 33.9 (2001), pp. 523–530. DOI: 10.1016/S0167-6636(01)00070-9 (cit. on p. 44).

[24] Berry, D. A. and Titze, I. R. "Normal modes in a continuum model of vocal fold tissues." In: *The Journal of the Acoustical Society of America* 100.5 (1996), p. 54. DOI: 10.1121/1.416975 (cit. on p. 104).

[25] Bickley, C. "Acoustic evidence for the development of speech." PhD dissertation, Massachusetts Institute of Technology, Cambridge, 1989 (cit. on p. 69).

[26] *Biology forums*. URL: https://biology-forums.com/ (cit. on p. 29).

[27] Borg, T. K. and Caulfield, J. B. "Morphology of connective tissue in skeletal muscle." In: *Tissue and Cell* 12.1 (1980), pp. 197–207. DOI: 10.1016/0040-8166(80)90061-0 (cit. on pp. 53, 61).

[28] Boyce, M. C. and Arruda, E. M. "Constitutive models of rubber elasticity: A review." In: *Rubber Chemistry and Technology* 73.3 (2000), pp. 504–523. DOI: 10.5254/1.3547602 (cit. on p. 53).

[29] Bozec, L. *et al.* "Collagen fibrils: nanoscale ropes." In: *Biophysical Journal* 92.1 (2007), pp. 70–75. DOI: 10.1529/biophysj.106.085704 (cit. on p. 44).

[30] Brandenburg, J. H. *et al.* "Vocal cord augmentation with autogenous fat." In: *The Laryngoscope* 102.5 (1992), pp. 495–500. DOI: 10.1288/00005537-199205000-00005 (cit. on p. 22).

[31] Branski, R. C. *et al.* "Vocal fold wound healing: a review for clinicians." In: *Journal of Voice* 20.3 (2006), pp. 432–442. DOI: 10.1016/j.jvoice.2005.08.005 (cit. on p. 19).

[32] Brown, W. S. *et al.* "Speaking fundamental frequency characteristics as a function of age and professional singing." In: *Journal of Voice* 5.4 (1991), pp. 310–315. DOI: 10.1016/S0892-1997(05)80061-X (cit. on pp. 71, 113).

[33] Buehler, M. J. "Nanomechanics of collagen fibrils under varying cross-link densities: Atomistic and continuum studies." In: *Journal of the Mechanical Behavior of Biomedical Materials* 1.1 (2008), pp. 59–67. DOI: 10.1016/j.jmbbm.2007.04.001 (cit. on p. 61).

[34] Bühler, R. B. *et al.* "Collagen type I, collagen type III, and versican in vocal fold lamina propria." In: *Archives of Otolaryngology - Head and Neck Surgery* 137.6 (2011), pp. 604–608. DOI: 10.1001/archoto.2011.88 (cit. on pp. 51, 60, 112).

[35] Butler, J. E. *et al.* "Gender-related differences of hyaluronic acid distribution in the human vocal fold." In: *The Laryngoscope* 111.5 (2001), pp. 907–911. DOI: 10.1097/00005537-200105000-00029 (cit. on p. 28).

[36] Caillerie, D. *et al.* "Discrete homogenization in graphene sheet modeling." In: *Journal of Elasticity* 84.1 (2006), pp. 33–68. DOI: 10.1007/S10659-006-9053-5 (cit. on p. 58).

[37] Cavinato, C. *et al.* "Does the knowledge of the local thickness of human ascending thoracic aneurysm walls improve their mechanical analysis?" In: *Frontiers in Bioengineering and Biotechnology* 7.JUL (2019). DOI: 10.3389/fbioe.2019.00169 (cit. on p. 30).

[38] Chagnon, G. *et al.* "Hyperelastic Energy Densities for Soft Biological Tissues: A Review." In: *Journal of Elasticity* 120.2 (2015), pp. 129–160. DOI: 10.1007/s10659-014-9508-z (cit. on p. 43).

[39] Chan, R. W. "Measurements of vocal fold tissue viscoelasticity: Approaching the male phonatory frequency range." In: *The Journal of the Acoustical Society of America* 115.6 (2004), pp. 3161–3170. DOI: 10.1121/1.1736272 (cit. on p. 77).

[40] Chan, R. W. "Nonlinear viscoelastic characterization of human vocal fold tissues under large-amplitude oscillatory shear (LAOS)." In: *Journal of Rheology* 62.3 (2018), pp. 695–712. DOI: 10.1122/1.4996320 (cit. on pp. 31, 32, 51, 77, 82, 84, 91, 92, 150).

[41] Chan, R. W. and Rodriguez, M. L. "A simple-shear rheometer for linear viscoelastic characterization of vocal fold tissues at phonatory frequencies." In: *The Journal of the Acoustical Society of America* 124.2 (2008), pp. 1207–1219. DOI: 10.1121/1.2946715 (cit. on pp. 31, 32, 77, 82, 83, 86, 88).

[42] Chan, R. W. and Titze, I. R. "Viscosities of implantable biomaterials in vocal fold augmentation surgery." In: *The Laryngoscope* 108.5 (1998), pp. 725–731. DOI: 10.1097/00005537-199805000-00019 (cit. on pp. 22, 78).

[43] Chan, R. W. and Titze, I. R. "Hyaluronic acid (with fibronectin) as a bioimplant for the vocal fold mucosa." In: *The Laryngoscope* 109.7 (1999), p. 49. DOI: 10.1097/00005537-199907000-00026 (cit. on p. 22).

[44] Chan, R. W. and Titze, I. R. "Viscoelastic shear properties of human vocal fold mucosa: measurement methodology and empirical results." In: *The Journal of the Acoustical Society of America* 106.4 (1999), pp. 2008–21. DOI: 10.1121/1.427947 (cit. on pp. 31, 32, 43, 77, 78, 82).

[45] Chan, R. W. and Titze, I. R. "Viscoelastic shear properties of human vocal fold mucosa: Theoretical characterization based on constitutive modeling." In: *The Journal of the Acoustical Society of America* 107.1 (2000), pp. 565–580. DOI: 10.1121/1.428354 (cit. on pp. 44, 77, 78, 82).

[46] Chan, R. W. *et al.* "The Importance of Hyaluronic Acid in Vocal Fold Biomechanics." In: *Otolaryngology–Head and Neck Surgery* 124.6 (2001), pp. 607–614. DOI: 10.1177/019459980112400602 (cit. on pp. 28, 51, 61, 78).

[47] Chan, R. W. *et al.* "Relative contributions of collagen and elastin to elasticity of the vocal fold under tension." In: *Annals of Biomedical Engineering* 35.8 (2007), pp. 1471–1483. DOI: 10.1007/s10439-007-9314-x (cit. on pp. 27, 30, 31, 78).

[48] Chan, R. W. *et al.* "Biomechanics of fundamental frequency regulation: Constitutive modeling of the vocal fold lamina propria." In: *Logopedics Phoniatrics Vocology* 34.4 (2009), pp. 181–189. DOI: 10.3109/14015430902913501 (cit. on p. 78).

[49] Chen, H. *et al.* "Non-linear micromechanics of soft tissues." In: *International Journal of Non-Linear Mechanics* 56 (2013), pp. 79–85. DOI: 10.1016/j.ijnonlinmec.2013.03.002 (cit. on pp. 35, 51, 52).

[50] Chen, P. T. *et al.* "Muscle Structure and Function." In: *Orthopaedic Physical Therapy Secrets* (2006), pp. 1–9. DOI: 10.1016/B978-156053708-3.50003-9 (cit. on p. 62).

[51] Chhetri, D. K. *et al.* "Measurement of Young's modulus of vocal folds by indentation." In: *Journal of Voice* 25.1 (2011), pp. 1–7. DOI: 10.1016/j.jvoice.2009.09.005 (cit. on p. 30).

[52] Choi, Y. H. *et al.* "Dual growth factor-immobilized bioactive injection material for enhanced treatment of glottal insufficiency." In: *Acta Biomaterialia* 86 (2019), pp. 269–279. DOI: 10.1016/j.actbio.2018.12.047 (cit. on p. 23).

[53] Cochereau, T. "Structure et Mécanique du pli vocal humain : caractérisation et modélisation multi-échelles." PhD dissertation, 2019 (cit. on p. 30).

[54] Cochereau, T. *et al.* "Mechanics of human vocal folds layers during finite strains in tension, compression and shear." In: *Journal of Biomechanics* 110 (2020). DOI: 10.1016/j.jbiomech.2020.109956 (cit. on pp. 17, 30, 32, 43, 51, 52, 58, 59, 62, 67, 71, 76, 77, 84, 93, 104).

[55] Colomo, F. *et al.* "Active and passive forces of isolated myofibrils from cardiac and fast skeletal muscle of the frog." In: *Journal of Physiology* 500.2 (1997), pp. 535–548. DOI: 10.1113/jphysiol.1997.sp022039 (cit. on pp. 55, 62, 119).

[56] Comninou, M. and Yannas, I. V. "Dependence of stress-strain nonlinearity of connective tissues on the geometry of collagen fibres." In: *Journal of Biomechanics* 9.7 (1976), pp. 427–433. DOI: 10.1016/0021-9290(76)90084-1 (cit. on pp. 52, 55).

[57] Cook, D. D. *et al.* "Reducing the number of vocal fold mechanical tissue properties: evaluation of the incompressibility and planar displacement assumptions." In: *The Journal of the Acoustical Society of America* 124.6 (2008), p. 96. DOI: 10.1121/1.2996300 (cit. on pp. 41, 104).

[58] Cornachione, A. S. *et al.* "The increase in non-cross-bridge forces after stretch of activated striated muscle is related to titin isoforms." In: *American Journal of Physiology-Cell Physiology* 310.1 (2016), p. 26. DOI: 10.1152/AJPCELL.00156.2015 (cit. on p. 119).

[59] Coughlan, C. A. *et al.* "In vivo cross-sectional imaging of the phonating larynx using long-range Doppler optical coherence tomography." In: *Scientific Reports* 6.10 (2016). DOI: 10.1038/SREP22792 (cit. on p. 51).

[60] Cveticanin, L. "Review on mathematical and mechanical models of the vocal cord." In: *Journal of Applied Mathematics* 2012.8 (2012), pp. 1–18. DOI: 10.1155/2012/928591 (cit. on p. 39).

[61] DA, B. and IR, T. "Normal modes in a continuum model of vocal fold tissues." In: *The Journal of the Acoustical Society of America* 100.5 (1996), pp. 3345–54. DOI: 10.1121/1.416975 (cit. on p. 69).

[62] Daamen, W. F. *et al.* "Elastin as a biomaterial for tissue engineering." In: *Biomaterials* 28.30 (2007), p. 98. DOI: 10.1016/j.biomaterials.2007.06.025 (cit. on p. 27).

[63] Decker, G. Z. and Thomson, S. L. "Computational simulations of vocal fold vibration: Bernoulli versus Navier-Stokes." In: *Journal of Voice* 21.3 (2007), pp. 273–284. DOI: 10.1016/j.jvoice.2005.12.002 (cit. on pp. 42, 104).

[64] Deguchi, S. "Mechanism of and threshold biomechanical conditions for falsetto voice onset." In: *PLOS ONE* 6.3 (2011). DOI: 10.1371/JOURNAL.PONE.0017503 (cit. on p. 76).

[65] DeJonckere, P. H. and Lebacq, J. "Damping of vocal fold oscillation at voice offset." In: *Biomedical Signal Processing and Control* 37 (2017), pp. 92–99. DOI: 10.1016/J.BSPC.2016.10.010 (cit. on pp. 76, 77).

[66] Descout, R. *et al.* "Continuous model of the vocal source." In: *Proceedings of the 5th International Conference on Acoustics, Speech and Signal Processing* (1980), pp. 61–64. DOI: 10.1109/icassp.1980.1170922 (cit. on p. 69).

[67] Diani, J. *et al.* "A review on the Mullins effect." In: *European Polymer Journal* 45.3 (2009), pp. 601–612. DOI: 10.1016/J.EURPOLYMJ.2008.11.017 (cit. on p. 92).

[68] Dion, G. *et al.* "Functional assessment of the ex vivo vocal folds through biomechanical testing: A review." In: *Materials science & engineering. C, Materials for biological applications* 64 (2016), pp. 444–453. DOI: 10.1016/J.MSEC.2016.04.018 (cit. on p. 30).

[69] Dollinger, M. *et al.* "Assessment of local vocal fold deformation characteristics in an in vitro static tensile test." In: *The Journal of the Acoustical Society of America* 130.2 (2011), pp. 977–985. DOI: 10.1121/1.3605671 (cit. on p. 30).

[70] Drake, R. *et al.* "Gray's Anatomy for Students." *Elsevier*, 2019 (cit. on pp. 8, 10, 12, 14–16, 18).

[71] Ejnell, H. *et al.* "Laryngeal obstruction after Teflon injection." In: *Acta Oto-Laryngologica* 98.3-4 (1984), pp. 374–379. DOI: 10.3109/00016488409107576 (cit. on p. 22).

[72] Ekman, A. *et al.* "Contact formation in random networks of elongated objects." In: *Physical Review Letters* 113.26 (2014), p. 268001. DOI: 10.1103/PhysRevLett.113.268001 (cit. on pp. 52, 57).

[73] Eppell, S. J. *et al.* "Nano measurements with micro-devices: mechanical properties of hydrated collagen fibrils." In: *Journal of the Royal Society Interface* 3.6 (2006), pp. 117–121. DOI: 10.1098/rsif.2005.0100 (cit. on p. 33).

[74] Ewoldt, R. H. *et al.* "New measures for characterizing nonlinear viscoelasticity in large amplitude oscillatory shear." In: *Journal of Rheology* 52.6 (2008), pp. 1427–1458. DOI: 10.1122/1.2970095 (cit. on p. 92).

[75] Farhat, C. and Lesoinne, M. "Two efficient staggered algorithms for the serial and parallel solution of three-dimensional nonlinear transient aeroelastic problems." In: *Computer Methods in Applied Mechanics and Engineering* 182.3-4 (2000), pp. 499–515. DOI: 10.1016/S0045-7825(99)00206-6 (cit. on p. 85).

[76] Ferry, J. D. "Viscoleastic Properties of Polymers." *Wiley*, 1980. DOI: 10.1002/pi.4980130110 (cit. on p. 89).

[77] Finck, C. "Implantation d'acide hyaluronique estérifié lors de la microchirurgie des lésions cordales bénignes." PhD dissertation, Université de Liège, Liège, 2008 (cit. on pp. 51, 61).

[78] Finck, C. and Lefebvre, P. "Implantation of esterified hyaluronic acid in microdissected Reinke's space after vocal fold microsurgery: First clinical experiences." In: *Laryngoscope* 115.10 I (2005), pp. 1841–1847. DOI: 10.1097/01.mlg.0000173158.22274.8d (cit. on pp. 23, 61).

[79] Finck, C. L. *et al.* "Implantation of esterified hyaluronic acid in microdissected Reinke's space after vocal fold microsurgery: Short- and long-term results." In: *Journal of Voice* 24.5 (2010), pp. 626–635. DOI: 10.1016/j.jvoice.2008.12.015 (cit. on pp. 23, 51, 61).

[80] Fink, B. R. "Human Larynx: a functional study." *Raven Press*, 1975 (cit. on p. 9).

[81] Flanagan, J. L. and Ishizaka, K. "Automatic generation of voiceless excitation in a vocal cord-vocal tract speech synthesizer." In: *IEEE Transactions on Acoustics, Speech, and Signal Processing* 24.2 (1976), pp. 163–170. DOI: 10.1109/TASSP.1976.1162778 (cit. on p. 39).

[82] Flanagan, J. L. and Landgraf, L. L. "Self-oscillating source for vocal-tract synthesizers." In: *IEEE Transactions on Audio and Electroacoustics* 16.1 (1968), pp. 57–64. DOI: 10.1109/TAU.1968.1161949 (cit. on pp. 37–39).

[83] Ford, C. N. *et al.* "Injectable collagen in laryngeal rehabilitation." In: *The Laryngoscope* 94.4 (1984), pp. 513–518. DOI: 10.1288/00005537-198404000-00016 (cit. on p. 22).

[84] Fratzl, P. "Collagen: structure and mechanics, an introduction." In: *Collagen: Structure and Mechanics*. Springer US, 2008, pp. 1–13. DOI: 10.1007/978-0-387-73906-9{_}1 (cit. on pp. 25, 27, 60, 61).

[85] Fratzl, P. *et al.* "Fibrillar structure and mechanical properties of collagen." In: *Journal of Structural Biology* 122.1-2 (1998), pp. 119–122. DOI: 10.1006/jsbi.1998.3966 (cit. on p. 27).

[86] Freed, A. D. and Doehring, T. C. "Elastic model for crimped collagen fibrils." In: *Journal of Biomechanical Engineering* 127.4 (2005), pp. 587–593. DOI: 10.1115/1.1934145 (cit. on p. 52).

[87] Fung, Y. C. "Biorheology of soft tissues." In: *Biorheology* 10.2 (1973), pp. 139–155. DOI: 10.3233/BIR-1973-10208 (cit. on p. 78).

[88] Garcia, J. A. *et al.* "Using attenuation coefficients from optical coherence tomography as markers of vocal fold maturation." In: *The Laryngoscope* 126.6 (2016), E218–E223. DOI: 10.1002/lary.25765 (cit. on pp. 35, 51).

[89] Gasser, T. C. *et al.* "Hyperelastic modelling of arterial layers with distributed collagen fibre orientations." In: *Journal of the Royal Society Interface* 3.6 (2006), pp. 15–35. DOI: 10.1098/rsif.2005.0073 (cit. on pp. 44, 52, 71).

[90] Gautieri, A. *et al.* "Hierarchical structure and nanomechanics of collagen microfibrils from the atomistic scale up." In: *Nano Letters* 11.2 (2011), pp. 757–766. DOI: 10.1021/nl103943u (cit. on pp. 33, 34, 81, 87).

[91] Gautieri, A. *et al.* "Viscoelastic properties of model segments of collagen molecules." In: *Matrix Biology* 31.2 (2012), pp. 141–149. DOI: 10.1016/j.matbio.2011.11.005 (cit. on pp. 34, 55, 60, 61, 81, 93).

[92] Gelse, K. *et al.* "Collagens - Structure, function, and biosynthesis." In: *Advanced Drug Delivery Reviews* 55.12 (2003), pp. 1531–1546. DOI: 10.1016/j.addr.2003.08.002 (cit. on p. 60).

[93] Goodyer, E. *et al.* "In vivo measurement of the shear modulus of the human vocal fold: interim results from eight patients." In: *European Archives of Oto-Rhino-Laryngology* 264.6 (2007), pp. 631–635. DOI: 10.1007/s00405-006-0239-z (cit. on p. 30).

[94] Gray, H. and Vandyke Carter, H. "Gray's anatomy the anatomical basis of clinical practice." Ed. by S. Standring. 41st. *Elsevier*, 2015 (cit. on p. 25).

[95] Gray, S. D. *et al.* "Vocal fold proteoglycans and their influence on biomechanics." In: *Laryngoscope* 109.6 (1999), pp. 845–854. DOI: 10.1097/00005537-199906000-00001 (cit. on pp. 27, 31, 36, 61, 78).

[96] Gray, S. D. *et al.* "Biomechanical and histologic observations of vocal fold fibrous proteins." In: *Annals of Otology, Rhinology and Laryngology* 109.1 (2000), pp. 77–85. DOI: 10.1177/000348940010900115 (cit. on pp. 25, 36, 78, 87).

[97] Green, M. S. and Tobolsky, A. V. "A New Approach to the Theory of Relaxing Polymeric Media." In: *Journal of Chemical Physics* 14.2 (1946), pp. 80–92. DOI: 10.1063/1.1724109 (cit. on p. 78).

[98] Greger, R. and Windhorst, U. "Comprehensive Human Physiology." *Springer*, 1996. DOI: 10.1007/978-3-642-60946-6 (cit. on p. 17).

[99] Gugatschka, M. *et al. Regenerative Medicine of the Larynx. Where are we Today? A Review*. 2012. DOI: 10.1016/j.jvoice.2012.03.009 (cit. on p. 23).

[100] Gundiah, N. *et al.* "The biomechanics of arterial elastin." In: *Journal of the Mechanical Behavior of Biomedical Materials* 2.3 (2009), pp. 288–296. DOI: 10.1016/j.jmbbm.2008.10.007 (cit. on p. 27).

[101] Gunter, H. E. "A mechanical model of vocal-fold collision with high spatial and temporal resolution." In: *The Journal of the Acoustical Society of America* 113.2 (2003), pp. 994–1000. DOI: 10.1121/1.1534100 (cit. on pp. 39, 41, 52).

[102] Gunter, H. E. "Modeling mechanical stresses as a factor in the etiology of benign vocal fold lesions." In: *Journal of Biomechanics* 37.7 (2004), pp. 1119–1124. DOI: 10.1016/j.jbiomech.2003.11.007 (cit. on pp. 19, 87).

[103] Guthold, M. *et al.* "A comparison of the mechanical and structural properties of fibrin fibers with other protein fibers." In: *Cell Biochemistry and Biophysics* 49.3 (2007), pp. 165–181. DOI: 10.1007/S12013-007-9001-4 (cit. on p. 33).

[104] Hahn, M. S. *et al.* "Quantitative and comparative studies of the vocal fold extracellular matrix I: elastic fibers and hyaluronic acid." In: *Annals of Otology, Rhinology and Laryngology* 115.2 (2006), pp. 156–164. DOI: 10.1177/000348940611500213 (cit. on pp. 27, 44, 53, 61).

[105] Hahn, M. S. *et al.* "Quantitative and comparative studies of the vocal fold extracellular matrix II: collagen." In: *Annals of Otology, Rhinology and Laryngology* 115.3 (2006), pp. 225–232. DOI: 10.1177/000348940611500311 (cit. on pp. 25, 44, 53, 60, 87, 112).

[106] Hájek, P. *et al.* "Numerical simulation of the effect of stiffness of lamina propria on the self-sustained oscillation of the vocal folds." In: *Engineering Mechanics*. 2016 (cit. on p. 104).

[107] Hammond, T. H. *et al.* "Age- and gender-related elastin distribution changes in human vocal folds." In: *Otolaryngology - Head and Neck Surgery* 119.4 (1998), pp. 314–322. DOI: 10.1016/S0194-5998(98)70071-3 (cit. on p. 45).

[108] Hammond, T. H. *et al.* "Age- and gender-related collagen distribution in human vocal folds." In: *Annals of Otology, Rhinology and Laryngology* 109.10 (2000), pp. 913–920. DOI: 10.1177/000348940010901004 (cit. on p. 45).

[109] Hammond, T. H. *et al.* "The intermediate layer: a morphologic study of the elastin and hyaluronic acid constituents of normal human vocal folds." In: *Journal of Voice* 11.1 (1997), pp. 59–66. DOI: 10.1016/S0892-1997(97)80024-0 (cit. on pp. 27, 28, 53, 61, 78).

[110] Hansen, J. K. and Thibeault, S. L. "Current understanding and review of the literature: vocal fold scarring." In: *Journal of Voice* 20.1 (2006), pp. 110–120. DOI: 10.1016/j.jvoice.2004.12.005 (cit. on p. 22).

[111] Hantzakos, A. *et al.* "Exudative lesions of Reinke's space: A terminology proposal." In: *European Archives of Oto-Rhino-Laryngology* 266.6 (2009), pp. 869–878. DOI: 10.1007/s00405-008-0863-x (cit. on pp. 20, 51).

[112] Hartnick, C. J. *et al.* "Development and maturation of the pediatric human vocal fold lamina propria." In: *Laryngoscope* 115.1 (2005), pp. 4–15. DOI: 10.1097/01.mlg.0000150685.54893.e9 (cit. on p. 24).

[113] Hascall, V. C. and Laurent, T. C. *Hyaluronan: structure and physical properties*. 1997. URL: https://www.glycoforum.gr.jp/article/01A2.html (cit. on p. 28).

[114] Hayes, W. C. and Mockros, L. F. "Viscoelastic properties of human articular cartilage." In: *Journal of applied physiology* 31.4 (1971), pp. 562–568. DOI: 10.1152/jappl.1971.31.4.562 (cit. on pp. 76, 81).

[115] Heris, H. K. *et al.* "Characterization of a Hierarchical Network of Hyaluronic Acid/Gelatin Composite for use as a Smart Injectable Biomaterial." In: *Macromolecular Bioscience* 12.2 (2012), pp. 202–210. DOI: 10.1002/mabi.201100335 (cit. on pp. 33, 35, 61, 87).

[116] Herrera, V. L. *et al.* "Tesla magnetic resonance microimaging of laryngeal tissue architecture." In: *Laryngoscope* 119.11 (2009), pp. 2187–2194. DOI: 10.1002/lary.20643 (cit. on pp. 35, 51).

[117] Hirano, M. "Morphological structure of the vocal cord as a vibrator and its variations." In: *Folia Phoniatrica et Logopaedica* 26.2 (1974), pp. 89–94. DOI: 10.1159/000263771 (cit. on pp. 24, 51).

[118] Hodge, A. J. "The fine structure of striated muscle: a comparison of insect flight muscle with vertebrate and invertebrate skeletal muscle." In: *The Journal of biophysical and biochemical cytology* 2.4 (1956), pp. 131–142. DOI: 10.1083/jcb.2.4.131 (cit. on p. 28).

[119] Hoh, J. F. "Laryngeal muscle fibre types." In: *Acta Physiologica Scandinavica* 183.2 (2005), pp. 133–149. DOI: 10.1111/j.1365-201X.2004.01402.x (cit. on p. 28).

[120] Hollingsworth, N. T. and Wagner, D. R. "Modeling shear behavior of the annulus fibrosus." In: *Journal of the Mechanical Behavior of Biomedical Materials* 4.7 (2011), pp. 1103–1114. DOI: 10.1016/j.jmbbm.2011.03.019 (cit. on p. 52).

[121] Holzapfel, G. A. *et al.* "Single lamellar mechanics of the human lumbar anulus fibrosus." In: *Biomechanics and Modeling in Mechanobiology* 3.3 (2005), pp. 125–140. DOI: 10.1007/s10237-004-0053-8 (cit. on pp. 76, 81).

[122] Holzapfel, G. A. and Ogden, R. W. "Mechanics of Biological Tissue." *Springer*, 2006. DOI: 10.1007/3-540-31184-X (cit. on p. 43).

[123] Holzapfel, G. A. *et al.* "A new constitutive framework for arterial wall mechanics and a comparative study of material models." In: *Journal of Elasticity* 61.1-3 (2000), pp. 1–48. DOI: 10.1023/A:1010835316564 (cit. on p. 52).

[124] Horáček, J. *et al.* "Estimation of impact stress using an aeroelastic model of voice production." In: *Logopedics Phoniatrics Vocology* 32.4 (2007), pp. 185–192. DOI: 10.1080/14015430600628039 (cit. on p. 42).

[125] Horáček, J. *et al.* "Numerical simulation of self-oscillations of human vocal folds with Hertz model of impact forces." In: *Journal of Fluids and Structures* 20.6 spec. iss. (2005), pp. 853–869. DOI: 10.1016/j.jfluidstructs.2005.05.003 (cit. on p. 42).

[126] Hornebeck, W. and Wallach, J. "Formation et dégradation des fibres élastiques." In: *Medecine et Longevite* 1.2 (2009), pp. 76–82. DOI: 10.1016/j.mlong.2009.10.003 (cit. on p. 27).

[127] Hu, R. *et al.* "Characterization of extracellular matrix proteins during wound healing in the lamina propria of vocal fold in a canine model: A long-term and consecutive study." In: *Acta Histochemica* 116.5 (2014), pp. 730–735. DOI: 10.1016/j.acthis.2013.12.014 (cit. on p. 22).

[128] Humphrey, H. D. "Cardiovascular Solid Mechanics." *Springer*, 2002. DOI: 10.1007/978-0-387-21576-1 (cit. on p. 43).

[129] Hunter, E. J. *et al.* "A three-dimensional model of vocal fold abduction/adduction." In: *The Journal of the Acoustical Society of America* 115.4 (2004), pp. 1747–1759. DOI: 10.1121/1.1652033 (cit. on p. 104).

[130] Hunter, E. J. *et al.* "Comparison of two laryngeal tissue fiber constitutive models." In: *Mechanics of Time-Dependent Materials* 18.1 (2014), pp. 179–196. DOI: 10.1007/s11043-013-9221-5 (cit. on p. 78).

[131] Husson, R. "Physiologie de la phonation." *Elsevier Masson*, 1962 (cit. on p. 17).

[132] Iorga, B. *et al.* "Micromechanical function of myofibrils isolated from skeletal and cardiac muscles of the zebrafish." In: *The Journal of General Physiology* 137.3 (2011), pp. 255–270. DOI: 10.1085/JGP.201010568 (cit. on p. 119).

[133] Ishizaka, K. and Flanagan, J. L. "Synthesis of voiced sounds from a two-mass model of the vocal cords." In: *Bell System Technical Journal* 51.6 (1972), p. 68. DOI: 10.1002/j.1538-7305.1972.tb02651.x (cit. on p. 39).

[134] Ishizaka, K. and Isshiki, N. "Computer simulation of pathological vocal-cord vibration." In: *Journal of the Acoustical Society of America* 60.5 (1976), p. 8. DOI: 10.1121/1.381221 (cit. on p. 39).

[135] Jiang, W. *et al.* "Computational modeling of fluid–structure–acoustics interaction during voice production." In: *Frontiers in Bioengineering and Biotechnology* 5.2 (2017). DOI: 10.3389/FBIOE.2017.00007 (cit. on p. 104).

[136] Johnson, A. R. and Quigley, C. J. "A Viscohyperelastic Maxwell Model for Rubber Viscoelasticity." In: *Rubber Chemistry and Technology* 65.1 (1992), pp. 137–153. DOI: 10.5254/1.3538596 (cit. on p. 78).

[137] Johnson, A. R. *et al.* "A viscohyperelastic finite element model for rubber." In: *Computer Methods in Applied Mechanics and Engineering* 127.1-4 (1995), pp. 163–180. DOI: 10.1016/0045-7825(95)00833-4 (cit. on p. 78).

[138] Johnson, A. R. and Stager, R. G. "Rubber Viscoelasticity Using the Physically Constrained System's Stretches as Internal Variables." In: *Rubber Chemistry and Technology* 66.4 (1993), pp. 567–577. DOI: 10.5254/1.3538329 (cit. on p. 78).

[139] Johnson, G. A. *et al.* "A single integral finite strain viscoelastic model of ligaments and tendons." In: *Journal of Biomechanical Engineering* 118.2 (1996), pp. 221–226. DOI: 10.1115/1.2795963 (cit. on pp. 76, 81).

[140] Kastelic, J. *et al.* "A structural mechanical model for tendon crimping." In: *Journal of Biomechanics* 13.10 (1980), pp. 887–893. DOI: 10.1016/0021-9290(80)90177-3 (cit. on p. 52).

[141] Kazarine, A. *et al.* "Multimodal virtual histology of rabbit vocal folds by nonlinear microscopy and nano computed tomography." In: *Biomedical Optics Express* 10.3 (2019), p. 64. DOI: 10.1364/boe.10.001151 (cit. on pp. 35, 51).

[142] Kelleher, J. E. *et al.* "Spatially varying properties of the vocal ligament contribute to its eigenfrequency response." In: *Journal of the Mechanical Behavior of Biomedical Materials* 3.8 (2010), pp. 600–609. DOI: 10.1016/J.JMBBM.2010.07.009 (cit. on p. 87).

[143] Kelleher, J. E. *et al.* "Empirical measurements of biomechanical anisotropy of the human vocal fold lamina propria." In: *Biomechanics and Modeling in Mechanobiology* 12.3 (2013), pp. 555–567. DOI: 10.1007/s10237-012-0425-4 (cit. on pp. 30, 43, 44, 51, 52, 77).

[144] Kelleher, J. E. *et al.* "The anisotropic hyperelastic biomechanical response of the vocal ligament and implications for frequency regulation: a case study." In: *The Journal of the Acoustical Society of America* 133.3 (2013), pp. 1625–1636. DOI: 10.1121/1.4776204 (cit. on pp. 53, 69, 71, 111).

[145] Kimura, M. *et al.* "Viscoelastic properties of phonosurgical biomaterials at phonatory frequencies." In: *The Laryngoscope* 120.4 (2010), pp. 764–768. DOI: 10.1002/lary.20816 (cit. on p. 22).

[146] Klemuk, S. A. and Titze, I. R. "Viscoelastic properties of three vocal-fold injectable biomaterials at low audio frequencies." In: *Laryngoscope* 114.9 I (2004), pp. 1597–1603. DOI: 10.1097/00005537-200409000-00018 (cit. on p. 77).

[147] Klepacek, I. *et al.* "The Human Vocal Fold Layers. Their Delineation Inside Vocal Fold as a Background to Create 3D Digital and Synthetic Glottal Model." In: *Journal of Voice* 30.5 (2016), pp. 529–537. DOI: 10.1016/j.jvoice.2015.08.004 (cit. on pp. 26, 35, 51, 87).

[148] Kniesburges, S. *et al.* "In vitro experimental investigation of voice production." In: *Current bioinformatics* 6.3 (2011), pp. 305–322. DOI: 10.2174/157489311796904637 (cit. on p. 30).

[149] Kobler, J. B. *et al.* "Dynamic imaging of vocal fold oscillation with four-dimensional optical coherence tomography." In: *The Laryngoscope* 120.7 (2010), p. 62. DOI: 10.1002/lary.20938 (cit. on pp. 35, 51).

[150] Koizumi, T. *et al.* "Two-mass models of the vocal cords for natural sounding voice synthesis." In: *Journal of the Acoustical Society of America* 82.4 (1987), p. 92. DOI: 10.1121/1.395254 (cit. on p. 37).

[151] Koufman, J. "Laryngoplasty for vocal cord medialization: an alternative to Teflon." In: *The Laryngoscope* 96.7 (1986), pp. 726–731. DOI: 10.1288/00005537-198607000-00004 (cit. on p. 22).

[152] Krook, M. I. P. "Speaking Fundamental Frequency Characteristics of Normal Swedish Subjects Obtained by Glottal Frequency Analysis." In: *Folia Phoniatrica et Logopaedica* 40.2 (1988), pp. 82–90. DOI: 10.1159/000265888 (cit. on pp. 71, 113).

[153] Kutty, J. K. and Webb, K. "Tissue Engineering Therapies for the Vocal Fold Lamina Propria." In: *Tissue Engineering - Part B: Reviews* 15.3 (2009), pp. 249–262. DOI: 10.1089/ten.teb.2008.0588 (cit. on p. 22).

[154] Lanir, Y. "Structure-strength relations in mammalian tendon." In: *Biophysical Journal* 24.2 (1978), pp. 541–554. DOI: 10.1016/S0006-3495(78)85400-9 (cit. on p. 52).

[155] Lanir, Y. "A structural theory for the homogeneous biaxial stress-strain relationships in flat collagenous tissues." In: *Journal of Biomechanics* 12.6 (1979), pp. 423–436. DOI: 10.1016/0021-9290(79)90027-7 (cit. on p. 55).

[156] Lanir, Y. "Constitutive equations for fibrous connective tissues." In: *Journal of Biomechanics* 16.1 (1983), pp. 1–12. DOI: 10.1016/0021-9290(83)90041-6 (cit. on p. 52).

[157] Lapčík, L. *et al.* "Hyaluronan: preparation, structure, properties, and applications." In: *Chemical Reviews* 98.8 (1998), pp. 2663–84. DOI: 10.1021/cr941199z (cit. on p. 28).

[158] *Larynx and nearby structures - Wikipedia*. URL: https://en.wikipedia.org/wiki/File:Larynx_and_nearby_structures.jpg (cit. on p. 8).

[159] Laurent, T. C. "The chemistry, biology and medical applications of hyaluronan and Its derivatives." *Portland Press*, 1998 (cit. on p. 28).

[160] Le Huche, F. and Allali, A. "La Voix : T1. Anatomie et physiologie des organes de la voix et de la parole." *Elsevier Masson*, 2010. DOI: 10.1016/c2011-0-09522-4 (cit. on p. 17).

[161] Lebl, M. D. A. *et al.* "Concentration and distribution of hyaluronic acid in human vocal folds." In: *Laryngoscope* 117.4 (2007), pp. 595–599. DOI: 10.1097/MLG.0b013e31802ffe17 (cit. on p. 78).

[162] Li, L. *et al.* "Tissue engineering-based therapeutic strategies for vocal fold repair and regeneration." In: *Biomaterials* 108 (2016), pp. 91–110. DOI: 10.1016/j.biomaterials.2016.08.054 (cit. on p. 23).

[163] Lieber, R. L. "Skeletal muscle adaptability. I: review of basic properties." In: *Developmental Medicine & Child Neurology* 28.3 (1986), pp. 390–397. DOI: 10.1111/j.1469-8749.1986.tb03890.x (cit. on pp. 28, 62).

[164] Limbert, G. and Middleton, J. "A constitutive model of the posterior cruciate ligament." In: *Medical Engineering and Physics* 28.2 (2006), pp. 99–113. DOI: 10.1016/j.medengphy.2005.03.003 (cit. on p. 52).

[165] Lin, D. H. and Yin, F. C. "A multiaxial constitutive law for mammalian left ventricular myocardium in steady-state barium contracture or tetanus." In: *Journal of Biomechanical Engineering* 120.4 (1998), pp. 504–517. DOI: 10.1115/1.2798021 (cit. on p. 52).

[166] Ling, C. *et al.* "Bioengineered vocal fold mucosa for voice restoration." In: *Science Translational Medicine* 7.314 (2015), 314ra187. DOI: 10.1126/scitranslmed.aab4014 (cit. on p. 23).

[167] Long, J. L. and Chhetri, D. K. "Restoring voice: Engineered vocal cords could soon replace damage damaged tissue." In: *Science* 350.6263 (2015), pp. 908–909. DOI: 10.1126/science.aad7695 (cit. on p. 23).

[168] Lorenzo, A. C. and Caffarena, E. R. "Elastic properties, Young's modulus determination and structural stability of the tropocollagen molecule: A computational study by steered molecular dynamics." In: *Journal of Biomechanics* 38.7 (2005), pp. 1527–1533. DOI: 10.1016/j.jbiomech.2004.07.011 (cit. on p. 61).

[169] Lous, N. J. C. *et al.* "A symmetrical two-mass vocal-fold model coupled to vocal tract and trachea, with application to prosthesis design." In: *Acta Acustica united with Acustica* 84.6 (1998), pp. 1135–1150 (cit. on p. 39).

[170] Lucero, J. C. and Koenig, L. L. "Simulations of temporal patterns of oral airflow in men and women using a two-mass model of the vocal folds under dynamic control." In: *The Journal of the Acoustical Society of America* 117.3 (2005), p. 72. DOI: 10.1121/1.1853235 (cit. on pp. 38, 39).

[171] Luo, H. *et al.* "An immersed-boundary method for flow-structure interaction in biological systems with application to phonation." In: *Journal of Computational Physics* 227.22 (2008), p. 32. DOI: 10.1016/j.jcp.2008.05.001 (cit. on pp. 40, 42).

[172] Macé, B. *et al.* "Histologie, bases fondamentales." *Omniscience*, 2008 (cit. on pp. 25, 27, 28).

[173] Maceri, F. *et al.* "From cross-linked collagen molecules to arterial tissue: a nano-micro-macroscale elastic model." In: *Acta Mechanica Solida Sinica* 23.S1 (2010), pp. 98–108 (cit. on p. 52).

[174] Maceri, F. *et al.* "A unified multiscale mechanical model for soft collagenous tissues with regular fiber arrangement." In: *Journal of Biomechanics* 43.2 (2010), pp. 355–363. DOI: 10.1016/j.jbiomech.2009.07.040 (cit. on p. 52).

[175] Maceri, F. *et al.* "Age-Dependent Arterial Mechanics via a Multiscale Elastic Approach." In: *International Journal of Computational Methods in Engineering Science and Mechanics* 14.2 (2013), pp. 141–151. DOI: 10.1080/15502287.2012.744114 (cit. on p. 52).

[176] Madruga De Melo, E. C. *et al.* "Distribution of collagen in the lamina propria of the human vocal fold." In: *The Laryngoscope* 113.12 (2003), p. 91. DOI: 10.1097/00005537-200312000-00027 (cit. on pp. 24, 25, 53).

[177] Magid, A. and Law, D. J. "Myofibrils bear most of the resting tension in frog skeletal muscle." In: *Science* 230.4731 (1985), pp. 1280–1282. DOI: 10.1126/science.4071053 (cit. on p. 63).

[178] Marino, M. and Vairo, G. "Computational modeling of soft tissues and ligaments." In: *Computational Modelling of Biomechanics and Biotribology in the Musculoskeletal System: Biomaterials and Tissues* 81.5 (2014), pp. 141–172. DOI: 10.1533/9780857096739.2.141 (cit. on p. 52).

[179] Marino, M. and Vairo, G. "Equivalent stiffness and compliance of curvilinear elastic fibers." In: *Lecture Notes in Applied and Computational Mechanics* 61 (2012), pp. 309–332. DOI: 10.1007/978-3-642-24638-82-1 (cit. on p. 52).

[180] Marino, M. and Vairo, G. "Multiscale elastic models of collagen bio-structures: from cross-linked molecules to soft tissues." In: *Studies in Mechanobiology, Tissue Engineering and Biomaterials* 14 (2013), pp. 73–102. DOI: 10.1007/8415-2012-154 (cit. on p. 52).

[181] Marino, M. and Vairo, G. "Stress and strain localization in stretched collagenous tissues via a multiscale modelling approach." In: *Computer Methods in Biomechanics and Biomedical Engineering* 17.1 (2014), pp. 11–30. DOI: 10.1080/10255842.2012.658043 (cit. on p. 52).

[182] Marino, M. and Wriggers, P. "Finite strain response of crimped fibers under uniaxial traction: An analytical approach applied to collagen." In: *Journal of the Mechanics and Physics of Solids* 98 (2017), pp. 429–453. DOI: 10.1016/j.jmps.2016.05.010 (cit. on p. 52).

[183] Martins, J. M. *et al.* "A new staggered algorithm for thermomechanical coupled problems." In: *International Journal of Solids and Structures* 122-123.9 (2017), pp. 42–58. DOI: 10.1016/J.IJSOLSTR.2017.06.002 (cit. on p. 85).

[184] Mattei, A. *et al. Cell therapy and vocal fold scarring*. 2017. DOI: 10.1016/j.anorl.2017.06.006 (cit. on p. 23).

[185] Maturo, S. *et al.* "Quantitative distinction of unique vocal fold subepithelial architectures using optical coherence tomography." In: *Annals of Otology, Rhinology and Laryngology* 121.11 (2012), pp. 754–760. DOI: 10.1177/000348941212101109 (cit. on pp. 35, 51).

[186] May-Newman, K. *et al.* "A hyperelastic constitutive law for aortic valve tissue." In: *Journal of Biomechanical Engineering* 131.8 (2009). DOI: 10.1115/1.3127261 (cit. on p. 52).

[187] Meftah, F. *et al.* "A three-dimensional staggered finite element approach for random parametric modeling of thermo-hygral coupled phenomena in porous media." In: *International Journal for Numerical and Analytical Methods in Geomechanics* 36.5 (2012), pp. 574–596. DOI: 10.1002/NAG.1017 (cit. on p. 85).

[188] Mermelstein, P. "An extension of Flanagan's model of vocal-cord oscillations." In: *The Journal of the Acoustical Society of America* 50.4B (1971), p. 10. DOI: 10.1121/1.1912756 (cit. on p. 39).

[189] Mescher, A. L. "Junqueira's Basic Histology: Text and Atlas." *McGraw-Hill Medical*, 2018. DOI: 10.26641/1997-9665.2019.3.101-104 (cit. on pp. 9, 29).

[190] Min, Y. B. *et al.* "Stress-strain response of the human vocal ligament." In: *Annals of Otology, Rhinology & Laryngology* 104.7 (1995), pp. 563–569. DOI: 10.1177/000348949510400711 (cit. on p. 30).

[191] Miri, A. K. "Mechanical characterization of vocal fold tissue: a review study." In: *Journal of Voice* 28.6 (2014), pp. 657–667. DOI: 10.1016/j.jvoice.2014.03.001 (cit. on pp. 17, 43, 51).

[192] Miri, A. K. *et al.* "Nonlinear laser scanning microscopy of human vocal folds." In: *The Laryngoscope* 122.2 (2012), pp. 356–363. DOI: 10.1002/lary.22460 (cit. on pp. 26, 35, 44).

[193] Miri, A. K. *et al.* "Quantitative assessment of the anisotropy of vocal fold tissue using shear rheometry and traction testing." In: *Journal of Biomechanics* 45.16 (2012), pp. 2943–46. DOI: 10.1016/j.jbiomech.2012.08.030 (cit. on pp. 43, 51, 53, 78).

[194] Miri, A. K. *et al.* "Microstructural characterization of vocal folds toward a strain-energy model of collagen remodeling." In: *Acta Biomaterialia* 9.8 (2013), pp. 7957–7967. DOI: 10.1016/j.actbio.2013.04.044 (cit. on pp. 43, 44, 52, 53, 55, 60, 78, 81, 112).

[195] Mithieux, S. M. and Weiss, A. S. "Elastin." In: *Advances in Protein Chemistry* 70 (2005), pp. 437–461. DOI: 10.1016/S0065-3233(05)70013-9 (cit. on p. 27).

[196] Mukund, K. and Subramaniam, S. "Skeletal muscle: A review of molecular structure and function, in health and disease." In: *Wiley Interdisciplinary Reviews: Systems Biology and Medicine* 12.1 (2020). DOI: 10.1002/wsbm.1462 (cit. on p. 62).

[197] Muñoz-Pinto, D. *et al.* "Lamina propria cellularity and collagen composition: an integrated assessment of structure in humans." In: *The Annals of Otology, Rhinology and Laryngology* 118.4 (2009), pp. 299–306. DOI: 10.1177/000348940911800411 (cit. on p. 87).

[198] Nakayama, M. *et al.* "Teflon vocal fold augmentation: failures and management in 28 cases." In: *Otolaryngology-Head and Neck Surgery* 109.3 (1993), pp. 493–498. DOI: 10.1177/019459989310900318 (cit. on p. 22).

[199] Natali, A. N. *et al.* "Biomechanical behaviour of oesophageal tissues: Material and structural configuration, experimental data and constitutive analysis." In: *Medical Engineering and Physics* 31.9 (2009), pp. 1056–1062. DOI: 10.1016/j.medengphy.2009.07.003 (cit. on p. 52).

[200] Neukirch, S. and Van der Heijden, G. H. M. "Geometry and mechanics of uniform n-plies: from engineering ropes to biological filaments." In: *Journal of Elasticity* 69.1-3 (2002), pp. 41–72. DOI: 10.1023/A:1027390700610 (cit. on p. 44).

[201] Nierenberger, M. *et al.* "A new multiscale model for the mechanical behavior of vein walls." In: *Journal of the Mechanical Behavior of Biomedical Materials* 23 (2013), pp. 32–43. DOI: 10.1016/j.jmbbm.2013.04.001 (cit. on p. 52).

[202] Ogden, R. W. "Large deformation isotropic elasticity: on the correlation of theory and experiment for compressible rubberlike solids." In: *Proceedings of the Royal Society of London, Series A, Mathematical and Physical Sciences* 328.1575 (1972), pp. 567–583. DOI: 10.1098/rspa.1972.0096 (cit. on p. 44).

[203] Ogden, R. W. and Saccomandi, G. "Introducing mesoscopic information into constitutive equations for arterial walls." In: *Biomechanics and Modeling in Mechanobiology* 6.5 (2007), pp. 333–344. DOI: 10.1007/s10237-006-0064-8 (cit. on p. 52).

[204] Orgéas, L. *et al.* "Déformation superélastique non homogène d'une éprouvette de traction NiTi. Expérience et modélisation numérique." In: *Revue Européenne des Eléments Finis* 7.8 (1998), pp. 111–136 (cit. on p. 55).

[205] Pelorson, X. *et al.* "Theoretical and experimental study of quasisteady-flow separation within the glottis during phonation. Application to a modified two-mass model." In: *The Journal of the Acoustical Society of America* 96.6 (1994), p. 3416. DOI: 10.1121/1.411449 (cit. on p. 39).

[206] Peña, E. *et al.* "On the Mullins effect and hysteresis of fibered biological materials: A comparison between continuous and discontinuous damage models." In: *International Journal of Solids and Structures* 46.7-8 (2009), pp. 1727–1735. DOI: 10.1016/j.ijsolstr.2008.12.015 (cit. on p. 92).

[207] Peng, X. Q. *et al.* "An anisotropic hyperelastic constitutive model with fiber-matrix shear interaction for the human annulus fibrosus." In: *Journal of Applied Mechanics, Transactions ASME* 73.5 (2006), pp. 815–824. DOI: 10.1115/1.2069987 (cit. on p. 52).

[208] Pinsky, P. M. *et al.* "Computational modeling of mechanical anisotropy in the cornea and sclera." In: *Journal of Cataract and Refractive Surgery* 31.1 (2005), pp. 136–145. DOI: 10.1016/j.jcrs.2004.10.048 (cit. on p. 52).

[209] Pioletti, D. P. *et al.* "Viscoelastic constitutive law in large deformations: application to human knee ligaments and tendons." In: *Journal of Biomechanics* 31.8 (1998), pp. 753–757. DOI: 10.1016/S0021-9290(98)00077-3 (cit. on pp. 76, 81).

[210] Pioletti, D. P. and Rakotomanana, L. R. "Non-linear viscoelastic laws for soft biological tissues." In: *European Journal of Mechanics, A/Solids* 19.5 (2000), pp. 749–759. DOI: 10.1016/S0997-7538(00)00202-3 (cit. on pp. 76, 81).

[211] Potier-Ferry, M. and Siad, L. "Homogénéisation géométrique d'une poutre ondulée. (Geometrical homogenization of a corrugated beam)." In: *Comptes rendus de l'Académie des sciences* t314.Série II, Mécanique, physique, chimie, sciences de l'univers, sciences de la terre (1992), pp. 425–430 (cit. on pp. 56, 81).

[212] Prades, J. M. *et al.* "Lamina propria of the human vocal fold: Histomorphometric study of collagen fibers." In: *Surgical and Radiologic Anatomy* 32.4 (2010), pp. 377–382. DOI: 10.1007/s00276-009-0577-9 (cit. on p. 78).

[213] R, C. *et al.* "Skeletal muscle extracellular matrix - What do we know about its composition, regulation, and physiological roles? A narrative review." In: *Frontiers in Physiology* 11.3 (2020), p. 253. DOI: 10.3389/FPHYS.2020.00253 (cit. on p. 53).

[214] Ramirez, F. and Pereira, L. "The fibrillins." In: *International Journal of Biochemistry and Cell Biology* 31.2 (1999), pp. 255–259. DOI: 10.1016/S1357-2725(98)00109-5 (cit. on p. 27).

[215] Remacle, M. *et al.* "Endoscopic cordectomy. A proposal for a classification by the working committee, European Laryngological Society." In: *European Archives of Oto-Rhino-Laryngology* 257.4 (2000), pp. 227–231. DOI: 10.1007/s004050050228 (cit. on p. 21).

[216] Riede, T. *et al.* "Elasticity and stress relaxation of a very small vocal fold." In: *Journal of Biomechanics* 44.10 (2011), p. 40. DOI: 10.1016/J.JBIOMECH.2011.04.024 (cit. on p. 77).

[217] Rihkanen, H. "Vocal fold augmentation by injection of autologous fascia." In: *The Laryngoscope* 108.1 (1998), pp. 51–54. DOI: 10.1097/00005537-199801000-00010 (cit. on p. 22).

[218] Roberts, T. *et al.* "Microstructure of the vocal fold in elderly humans." In: *Clinical Anatomy* 24.5 (2011), pp. 544–551. DOI: 10.1002/ca.21114 (cit. on pp. 51, 87).

[219] Rodney, D. *et al.* "Reversible dilatancy in entangled single-wire materials." In: *Nature Materials* 15.1 (2016), pp. 72–77. DOI: 10.1038/nmat4429 (cit. on p. 53).

[220] Rohlfs, A. K. *et al.* "The anisotropic nature of the human vocal fold: An ex vivo study." In: *European Archives of Oto-Rhino-Laryngology* 270.6 (2013), pp. 1885–1895. DOI: 10.1007/s00405-013-2428-x (cit. on p. 51).

[221] Roland, C. M. "Network Recovery from Uniaxial Extension. I. Elastic Equilibrium." In: *Rubber Chemistry and Technology* 62.5 (1989), pp. 863–879. DOI: 10.5254/1.3536280 (cit. on p. 78).

[222] Roland, C. M. and Warzel, M. L. "Orientation Effects in Rubber Double Networks." In: *Rubber Chemistry and Technology* 63.2 (1990), pp. 285–297. DOI: 10.5254/1.3538259 (cit. on p. 78).

[223] Rosa, M. D. O. *et al.* "A contribution to simulating a three-dimensional larynx model using the finite element method." In: *The Journal of the Acoustical Society of America* 114.5 (2003), p. 905. DOI: 10.1121/1.1619981 (cit. on pp. 42, 104).

[224] Rosen, C. A. "Phonosurgical vocal fold injection: procedures and materials." In: *Otolaryngologic Clinics of North America* 33.5 (2000), pp. 1087–1096. DOI: 10.1016/S0030-6665(05)70267-X (cit. on p. 22).

[225] Rosen, C. A. "Vocal fold scar: evaluation and treatment." In: *Otolaryngologic Clinics of North America* 33.5 (2000), pp. 1081–1086. DOI: 10.1016/S0030-6665(05)70266-8 (cit. on p. 19).

[226] Ruty, N. *et al.* "An in vitro setup to test the relevance and the accuracy of low-order vocal folds models." In: *The Journal of the Acoustical Society of America* 121.1 (2007), pp. 479–490. DOI: 10.1121/1.2384846 (cit. on p. 39).

[227] S, W. *et al.* "Pipette aspiration applied to the characterization of nonhomogeneous, transversely isotropic materials used for vocal fold modeling." In: *Journal of the Mechanical Behavior of Biomedical Materials* 17.1 (2013), pp. 137–151. DOI: 10.1016/J.JMBBM.2012.08.005 (cit. on p. 69).

[228] Sasaki, N. and Odajima, S. "Elongation mechanism of collagen fibrils and force-strain relations of tendon at each level of structural hierarchy." In: *Journal of Biomechanics* 29.9 (1996), p. 36. DOI: 10.1016/0021-9290(96)00024-3 (cit. on p. 33).

[229] Sato, K. *et al.* "Age-related changes of collagenous fibers in the human vocal fold mucosa." In: *Annals of Otology, Rhinology and Laryngology* 111.1 (2002), pp. 15–20. DOI: 10.1177/000348940211100103 (cit. on p. 51).

[230] Sato, T. and Tauchi, H. "Age changes in human vocal muscle." In: *Mechanisms of Ageing and Development* 18.1 (1982), pp. 67–74. DOI: 10.1016/0047-6374(82)90031-8 (cit. on pp. 28, 51, 62).

[231] Schultz, P. "Vocal fold cancer." In: *European Annals of Otorhinolaryngology, Head and Neck Diseases* 128.6 (2011), pp. 301–308. DOI: 10.1016/j.anorl.2011.04.004 (cit. on p. 19).

[232] Shampine, L. F. "Solving F(t,y(t),y(t)) = 0 in Matlab." In: *Journal of Numerical Mathematics* 10.4 (2002), pp. 291–310. DOI: 10.1515/JNMA.2002.291 (cit. on p. 85).

[233] Shen, Z. L. *et al.* "Stress-strain experiments on individual collagen fibrils." In: *Biophysical Journal* 95.8 (2008), p. 63. DOI: 10.1529/biophysj.107.124602 (cit. on pp. 33, 34, 61).

[234] Shen, Z. L. *et al.* "Viscoelastic Properties of Isolated Collagen Fibrils." In: *Biophysical Journal* 100.12 (2011), pp. 3008–3015. DOI: 10.1016/j.bpj.2011.04.052 (cit. on pp. 33, 87, 93).

[235] Steinecke, I. and Herzel, H. "Bifurcations in an asymmetric vocal-fold model." In: *Journal of the Acoustical Society of America* 97.3 (1995), p. 84. DOI: 10.1121/1.412061 (cit. on p. 39).

[236] Story, B. H. and Titze, I. R. "Voice simulation with a body-cover model of the vocal folds." In: *Journal of the Acoustical Society of America* 97.2 (1995), pp. 1249–1260. DOI: 10.1121/1.412234 (cit. on p. 24).

[237] Švec, J. G. *et al.* "Resonance properties of the vocal folds: in vivo laryngoscopic investigation of the externally excited laryngeal vibrations." In: *The Journal of the Acoustical Society of America* 108.4 (2000), p. 1397. DOI: 10.1121/1.1289205 (cit. on pp. 76, 77).

[238] Svensson, R. B. *et al.* "Tensile properties of human collagen fibrils and fascicles are insensitive to environmental salts." In: *Biophysical Journal* 99.12 (2010), p. 27. DOI: 10.1016/j.bpj.2010.11.018 (cit. on pp. 33, 34).

[239] Svensson, R. B. *et al.* "Viscoelastic behavior of discrete human collagen fibrils." In: *Journal of the Mechanical Behavior of Biomedical Materials* 3.1 (2010), pp. 112–115. DOI: 10.1016/j.jmbbm.2009.01.005 (cit. on pp. 33, 34).

[240] Tanabe, M. *et al.* "Damping ratio of the vocal cord." In: *Folia Phoniatrica et Logopaedica* 31.1 (1979), pp. 27–34. DOI: 10.1159/000264147 (cit. on p. 77).

[241] Tao, C. and Jiang, J. J. "Anterior-posterior biphonation in a finite element model of vocal fold vibration." In: *The Journal of the Acoustical Society of America* 120.3 (2006), pp. 1570–1577. DOI: 10.1121/1.2221546 (cit. on p. 87).

[242] Tao, C. and Jiang, J. J. "Mechanical stress during phonation in a self-oscillating finite-element vocal fold model." In: *Journal of Biomechanics* 40.10 (2007), pp. 2191–2198. DOI: 10.1016/j.jbiomech.2006.10.030 (cit. on p. 52).

[243] Tao, C. *et al.* "Simulation of vocal fold impact pressures with a self-oscillating finite-element model." In: *The Journal of the Acoustical Society of America* 119.6 (2006), p. 94. DOI: 10.1121/1.2197798 (cit. on p. 42).

[244] Tateya, T. *et al.* "Collagen subtypes in human vocal folds." In: *Annals of Otology, Rhinology and Laryngology* 115.6 (2006), pp. 469–476. DOI: 10.1177/000348940611500612 (cit. on pp. 25, 53, 60, 112).

[245] Thomson, S. *et al.* "Physical and numerical flow-excited vocal fold models." In: *Proceedings of models and analysis of vocal emissions for biomedical applications* (2003), pp. 147–50 (cit. on p. 40).

[246] Thomson, S. L. *et al.* "Aerodynamic transfer of energy to the vocal folds." In: *The Journal of the Acoustical Society of America* 118.3 Pt 1 (2005), pp. 1689–1700. DOI: 10.1121/1.2000787 (cit. on p. 76).

[247] Titze, I. R. "The human vocal cords: A mathematical model. I." In: *Phonetica* 28.3 (1973), pp. 129–170. DOI: 10.1159/000259453 (cit. on p. 39).

[248] Titze, I. R. and Alipour, F. "The Myoelastic-Aerodynamic Theory of Phonation." *National Center for VoiceSpeech*, 2006 (cit. on pp. 13, 31).

[249] Titze, I. R. "The human vocal cords: a mathematical model. II." In: *Phonetica* 29.1 (1974), pp. 1–21. DOI: 10.1159/000259461 (cit. on p. 39).

[250] Titze, I. R. "Principles of Voice Production." *Prentice-Hall*, 1994 (cit. on pp. 13, 24).

[251] Titze, I. R. and Hunter, E. J. "Normal vibration frequencies of the vocal ligament." In: *The Journal of the Acoustical Society of America* 115.5 (2004), pp. 2264–2269. DOI: 10.1121/1.1698832 (cit. on p. 69).

[252] Titze, I. R. *et al.* "Preliminaries to the body-cover theory of pitch control." In: *Journal of Voice* 1.4 (1988), pp. 314–319. DOI: 10.1016/S0892-1997(88)80004-3 (cit. on pp. 24, 76).

[253] Titze, I. R. *et al.* "Role of the thyroarytenoid muscle in regulation of fundamental frequency." In: *Journal of Voice* 3.3 (1989), pp. 213–224. DOI: 10.1016/S0892-1997(89)80003-7 (cit. on p. 13).

[254] Titze, I. R. *et al.* "Methodology for rheological testing of engineered biomaterials at low audio frequencies." In: *The Journal of the Acoustical Society of America* 115.1 (2004), pp. 392–401. DOI: 10.1121/1.1631941 (cit. on pp. 30, 77).

[255] Treloar, L. R. G. "The elasticity of a network of long-chain molecules." In: *Transactions of the Faraday Society* 39.1 (1943), pp. 241–246. DOI: 10.1039/TF9433900241 (cit. on p. 55).

[256] Vampola, T. *et al.* "Computer simulation of mucosal waves on vibrating human vocal folds." In: *Biocybernetics and Biomedical Engineering* 36.3 (2016), pp. 451–465. DOI: 10.1016/j.bbe.2016.03.004 (cit. on pp. 41, 42, 52, 104).

[257] Van den Berg, J. "Myoelastic-aerodynamic theory of voice production." In: *Journal of speech and hearing research* 1.3 (1958). DOI: 10.1044/jshr.0103.227 (cit. on p. 16).

[258] Van den Berg, J. *et al.* "On the air resistance and the Bernoulli effect of the human larynx." In: *The Journal of the Acoustical Society of America* 29.5 (1957), pp. 626–631. DOI: 10.1121/1.1908987 (cit. on p. 17).

[259] Van Der Rijt, J. A. *et al.* "Micromechanical testing of individual collagen fibrils." In: *Macromolecular Bioscience* 6.9 (2006), pp. 697–702. DOI: 10.1002/mabi.200600063 (cit. on p. 33).

[260] Verdolini, K. and Ramig, L. O. "Review: Occupational risks for voice problems." In: *Logopedics Phoniatrics Vocology* 26.1 (2001), pp. 37–46. DOI: 10.1080/14015430130010912 5 (cit. on p. 19).

[261] Vindin, H. *et al.* "Elastin architecture." In: *Matrix Biology* 84 (2019), pp. 4–16. DOI: 10.1016/j.matbio.2019.07.005 (cit. on p. 27).

[262] *Vocal cord nodules, polyps and cysts: treatment and prevention*. URL: https://my.clevelandclinic.org/health/diseases (cit. on p. 20).

[263] *Voice health 101*. URL: http://www.voicehealth101.com (cit. on p. 20).

[264] Von Leden, H. and Moore, P. "The mechanics of the cricoarytenoid joint." In: *Archives of Otorhinolaryngology-Head and Neck Surgery* 73.5 (1961), pp. 541–550. DOI: 10.1001/archotol.1961.00740020553008 (cit. on p. 10).

[265] Vries, M. P. de *et al.* "Glottal flow through a two-mass model: comparison of Navier–Stokes solutions with simplified models." In: *The Journal of the Acoustical Society of America* 111.4 (2002), p. 53. DOI: 10.1121/1.1323716 (cit. on p. 40).

[266] Ward, S. R. *et al.* "Non-linear Scaling of Passive Mechanical Properties in Fibers, Bundles, Fascicles and Whole Rabbit Muscles." In: *Frontiers in Physiology* 11 (2020). DOI: 10.3389/fphys.2020.00211 (cit. on pp. 33, 36, 53, 62, 63, 67).

[267] Weissmann, B. and Meyer, K. "The structure of hyalobiuronic acid and of hyaluronic acid from umbilical cord." In: *Journal of the American Chemical Society* 76.7 (1954), p. 57. DOI: 10.1021/ja01636a010 (cit. on p. 28).

[268] Woo, P. *et al.* "Diagnosis and treatment of persistent dysphonia after laryngeal surgery: a retrospective analysis of 62 patients." In: *The Laryngoscope* 104.9 (1994), pp. 1084–91. DOI: 10.1288/00005537-199409000-00007 (cit. on p. 22).

[269] Wurzbacher, T. *et al.* "Model-based classification of nonstationary vocal fold vibrations." In: *The Journal of the Acoustical Society of America* 120.2 (2006), p. 27. DOI: 10.1121/1.2211550 (cit. on pp. 38, 39).

[270] Wurzbacher, T. *et al.* "Spatiotemporal classification of vocal fold dynamics by a multimass model comprising time-dependent parameters." In: *The Journal of the Acoustical Society of America* 123.4 (2008), p. 34. DOI: 10.1121/1.2835435 (cit. on p. 40).

[271] Yang, A. *et al.* "Biomechanical modeling of the three-dimensional aspects of human vocal fold dynamics." In: *The Journal of the Acoustical Society of America* 127.2 (2010), p. 31. DOI: 10.1121/1.3277165 (cit. on pp. 38, 40).

[272] Yang, L. "Mechanical properties of collagen fibrils and elastic fibers explored by AFM." PhD dissertation, University of Twente, Enschede, 2008 (cit. on pp. 61, 88, 93, 95).

[273] Yang, L. *et al.* "Mechanical properties of native and cross-linked type I collagen fibrils." In: *Biophysical Journal* 94.6 (2008), pp. 2204–2211. DOI: 10.1529/biophysj.107.111013 (cit. on pp. 33, 60, 61).

[274] Yousefi, A. A. K. *et al.* "A visco-hyperelastic constitutive model and its application in bovine tongue tissue." In: *Journal of Biomechanics* 71 (2018), pp. 190–198. DOI: 10.1016/j.jbiomech.2018.02.008 (cit. on pp. 76, 81).

[275] Zhang, K. *et al.* "A constitutive model of the human vocal fold cover for fundamental frequency regulation." In: *The Journal of the Acoustical Society of America* 119.2 (2006), p. 1050. DOI: 10.1121/1.2159433 (cit. on pp. 30, 43, 44, 78).

[276] Zhang, K. *et al.* "A two-layer composite model of the vocal fold lamina propria for fundamental frequency regulation." In: *The Journal of the Acoustical Society of America* 122.2 (2007), pp. 1090–1101. DOI: 10.1121/1.2749460 (cit. on pp. 69, 78).

[277] Zhang, K. *et al.* "Predictions of fundamental frequency changes during phonation based on a biomechanical model of the vocal fold lamina propria." In: *Journal of Voice : official journal of the Voice Foundation* 23.3 (2009), p. 282. DOI: 10.1016/J.JVOICE.2007.09.010 (cit. on pp. 44, 69, 78).

[278] Zhang, Z. "Characteristics of phonation onset in a two-layer vocal fold model." In: *The Journal of the Acoustical Society of America* 125.2 (2009), p. 1102. DOI: 10.1121/1.3050285 (cit. on p. 104).

[279] Zhang, Z. "The influence of material anisotropy on vibration at onset in a three-dimensional vocal fold model." In: *The Journal of the Acoustical Society of America* 135.3 (2014), p. 90. DOI: 10.1121/1.4863266 (cit. on p. 104).

[280] Zhang, Z. "Mechanics of human voice production and control." In: *The Journal of the Acoustical Society of America* 140.4 (2016), pp. 2614–2635. DOI: 10.1121/1.4964509 (cit. on p. 76).

[281] Zhang, Z. "Effect of vocal fold stiffness on voice production in a three-dimensional body-cover phonation model." In: *The Journal of the Acoustical Society of America* 142.4 (2017), p. 21. DOI: 10.1121/1.5008497 (cit. on pp. 104, 111).

Appendices

A. Supplemental Material Chapter 2

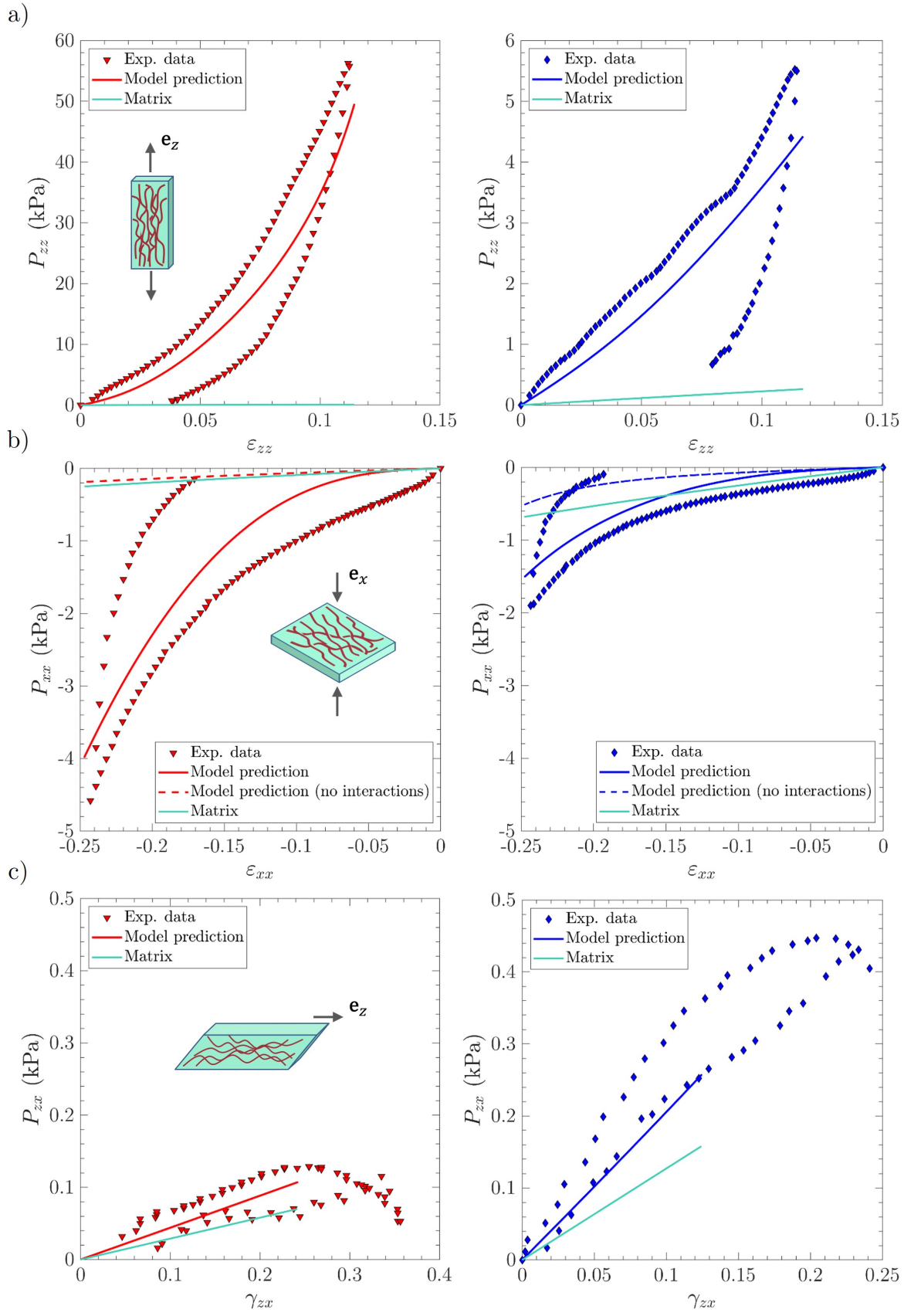

Figure 1: Macroscopic stress-strain curves of vocal-fold sublayers under multiaxial loadings. Experimental data *vs.* model predictions obtained for *lamina propria* sample LP_2 (left, in red) and *vocalis* sample V_2 (right, in blue): a) longitudinal tension; b) transverse compression; c) longitudinal shear.

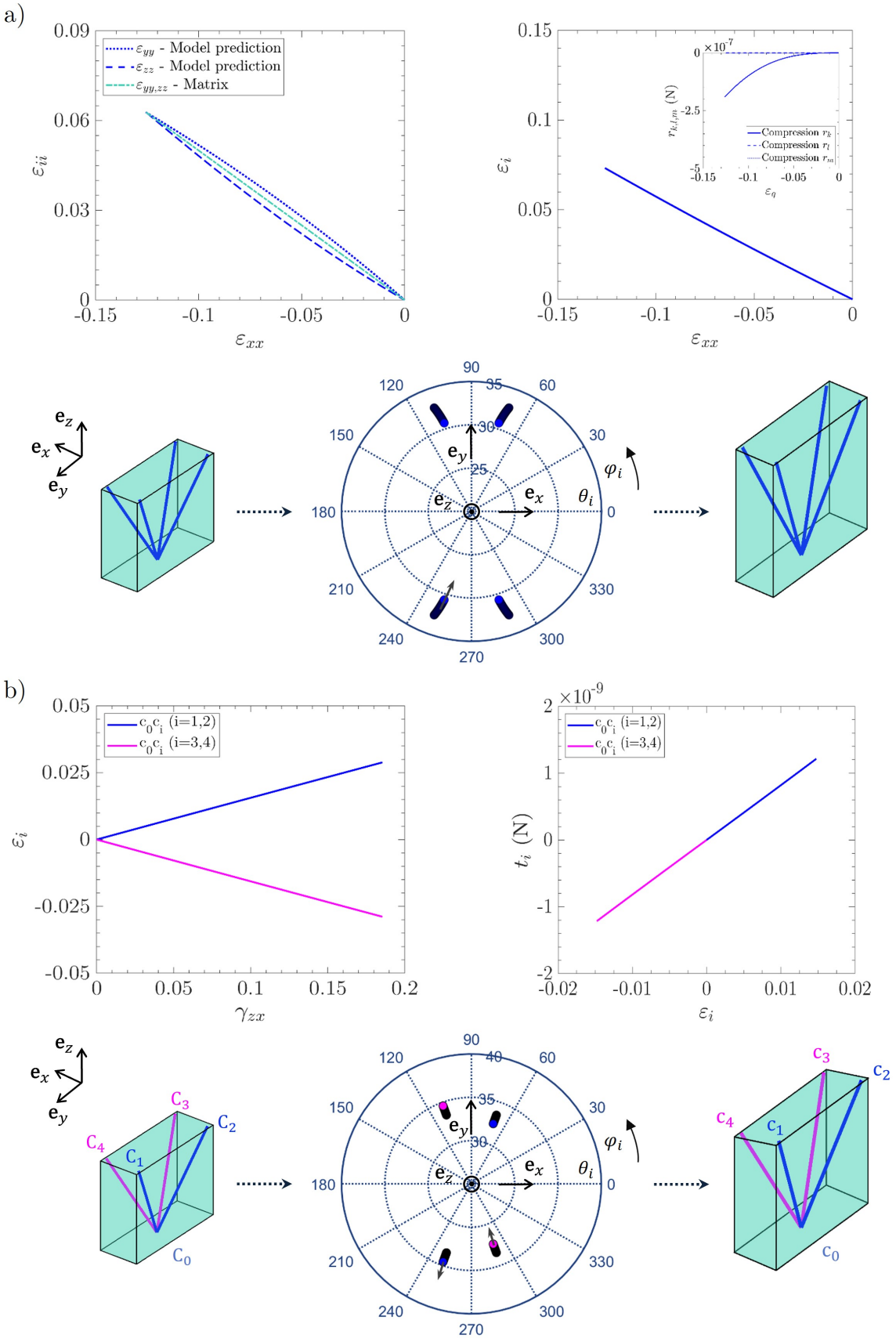

Figure 2: Strain-induced evolution of multiscale descriptors for *vocalis* sample V_1: a) compression along $\mathbf{e}_x$ – macroscopic loading paths (top left), stereographic projection of orientation vectors $\mathbf{e}_i$ from initial to final state, $i \in [1..4]$ (bottom), strain variations of the fibril chord ε_i and corresponding steric interactions $r_{k,l,m}$ (top right); b) shear in the ($\mathbf{e}_z$, $\mathbf{e}_x$) plane – strain variations of the fibril chord ε_i (top left) and tension t_i (top right), stereographic projection of orientation vectors $\mathbf{e}_i$ from initial to final state, $i \in [1..4]$ (bottom).

B. Supplemental Material Chapter 3

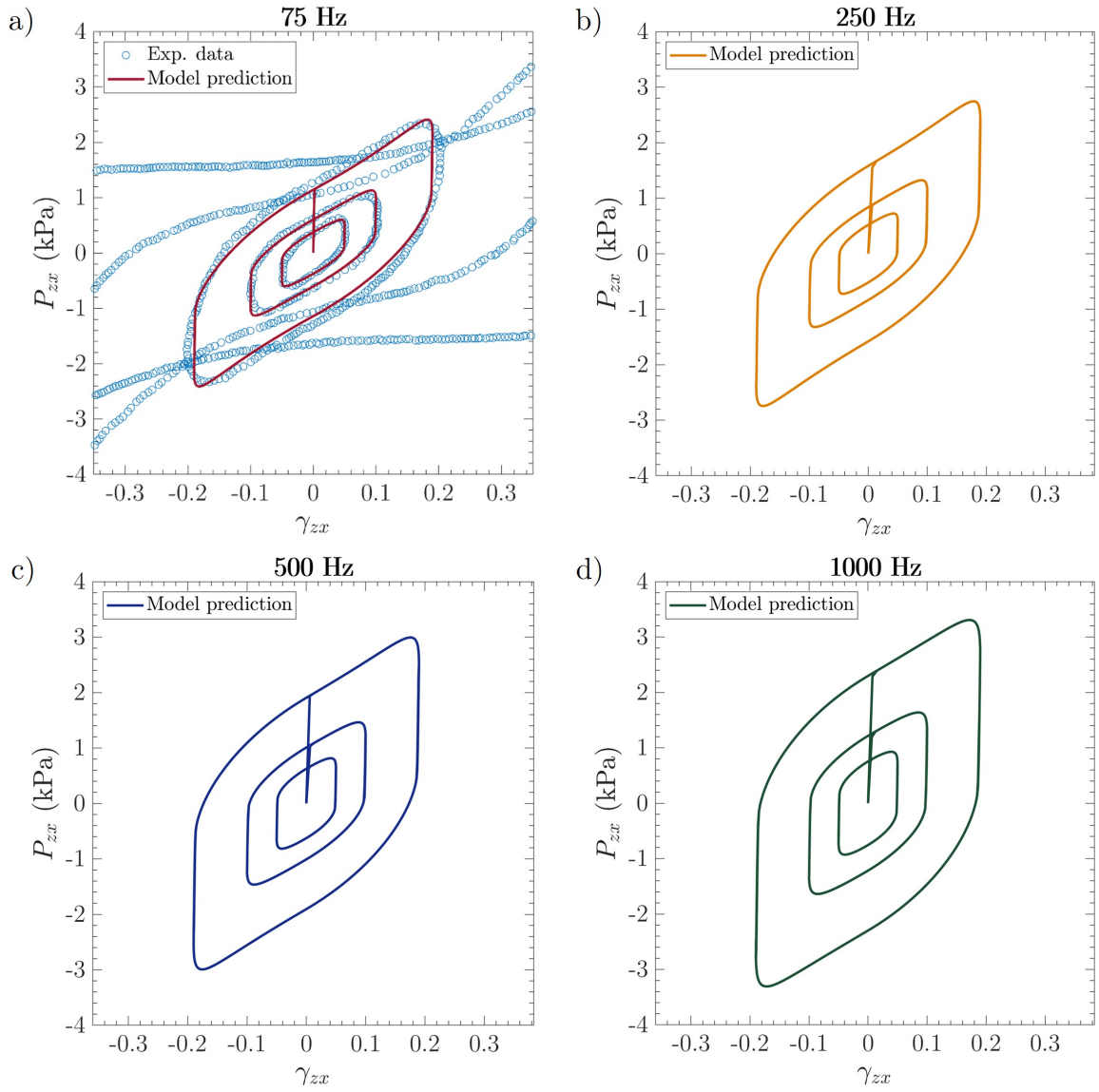

Figure 1: LAOS results: macroscale stress-strain model predictions obtained for sample C_{LAOS} at f = a) 75 Hz, b) 250 Hz, c) 500 Hz and d) 1000 Hz with γ_0 varied from 0.05 to 0.2. Adapted from [40].

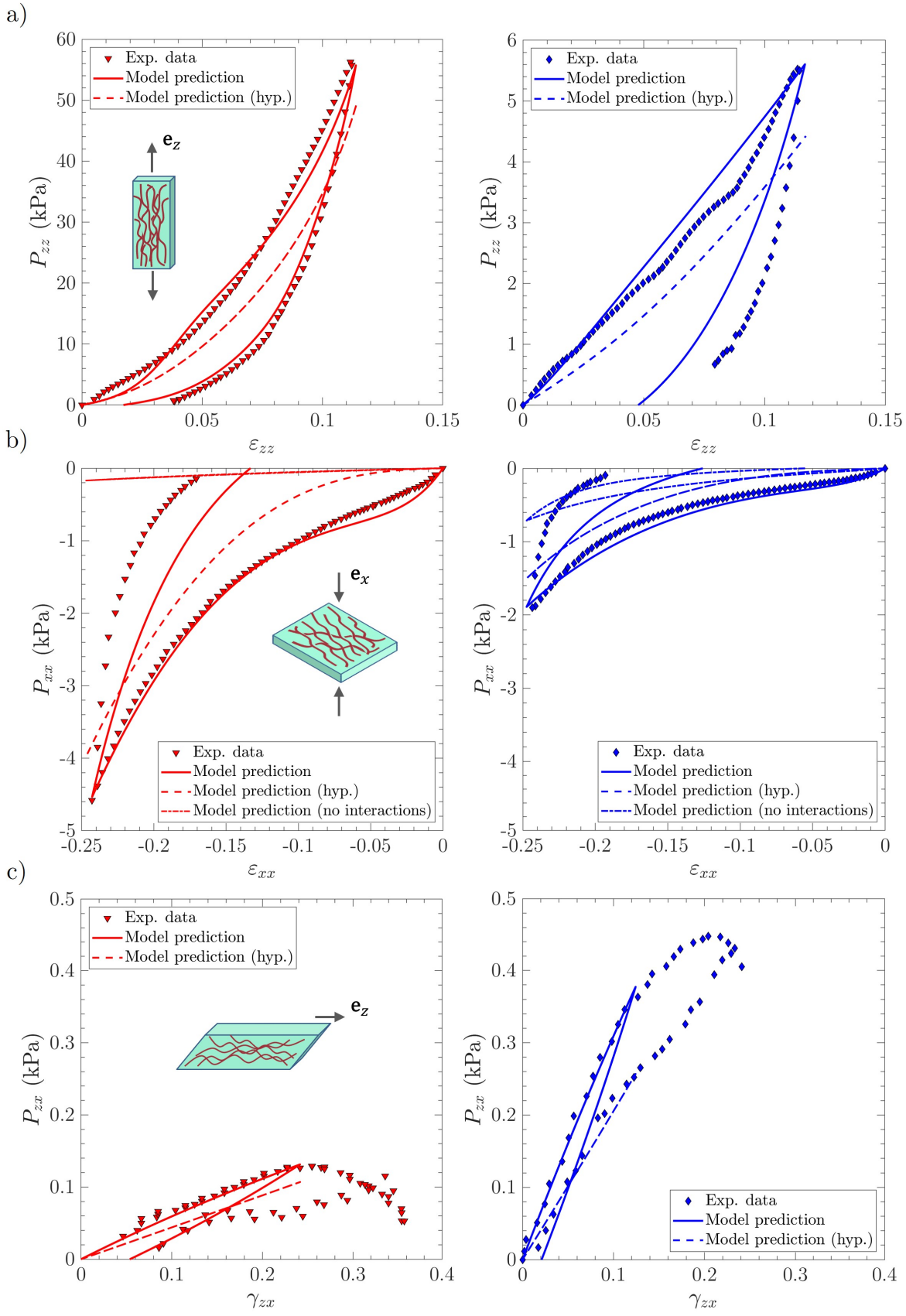

Figure 2: Macroscopic viscoelastic stress-strain curves of vocal-fold sublayers under multiaxial cyclic loadings. Experimental data *vs.* model predictions obtained for *lamina propria* sample LP_2 (left, in red) and *vocalis* sample V_2 (right, in blue): a) longitudinal tension; b) transverse compression; c) longitudinal shear.

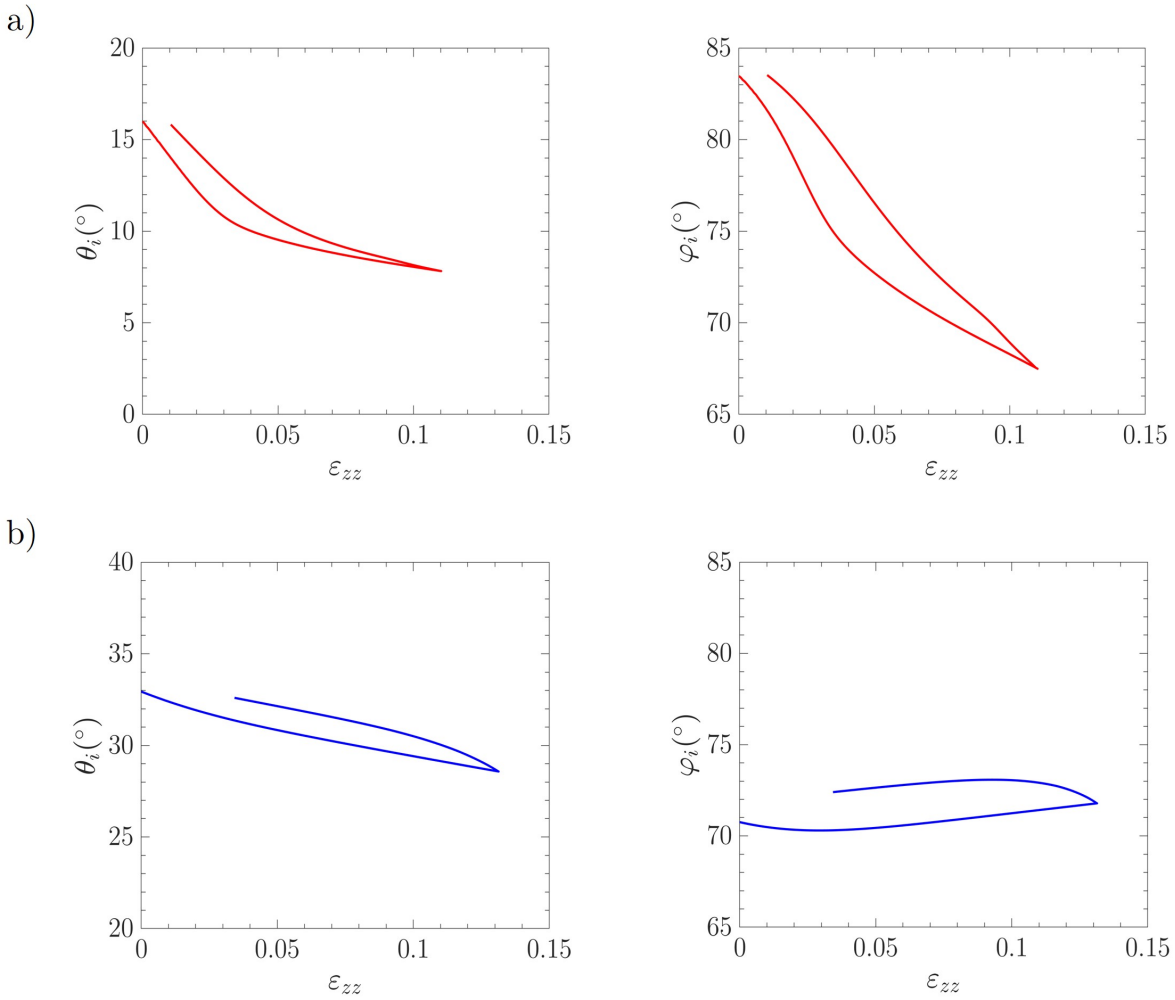

Figure 3: Viscoelastic strain-induced evolution of the orientation vectors $\mathbf{e}_i$ from initial to final state, $i \in [1..4]$ during tension along $\mathbf{e}_z$: a) *lamina propria*; b) *vocalis*.

C. Supplemental Material Chapter 4

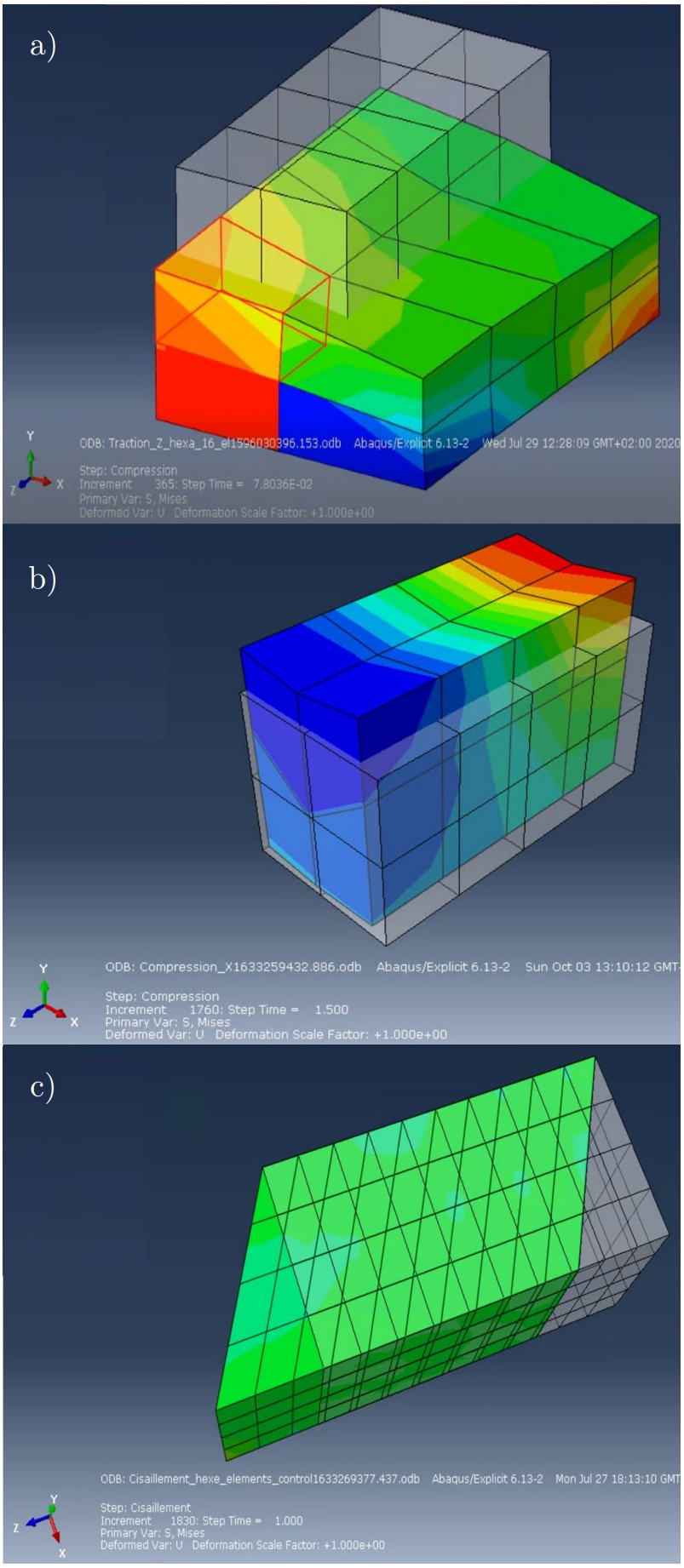

Figure 1: Simulations with several finite elements in the case of a highly oriented microstructure (LP_1 – REV_1). Deformed configurations and stress fields predicted by Abaqus/Explicit for: a) longitudinal tension (16 elements); b) transverse compression (16 elements); c) longitudinal shear (160 elements).

Résumé

Composés de réseaux de fibres de collagène, d'élastine et de fibres musculaires, les plis vocaux humains sont deux structures déformables du larynx, organisées en différentes couches, et aux propriétés vibratoires remarquables. Cependant, les connaisses acquises aujourd'hui ne sont pas encore suffisantes pour comprendre la relation entre les spécificités histologiques du tissu vocal et ses propriétés vibro-mécaniques singulières aux échelles supérieures. Ainsi, ce travail propose un modèle micro-mécanique capable de décrire l'architecture fibreuse 3D des différentes couches du pli vocal, leurs matrices environnantes, et de prédire leur comportement mécanique multi-échelles en réponse à des chargements variés, quasi-statiques et vibratoires. Pour chaque couche, les paramètres du modèle ont été identifiés à l'aide des données histo-mécaniques disponibles dans la littérature, et notamment de leur réponse mécanique sous chargements physiologiques (tension, compression et cisaillement). Dans chaque cas, l'évolution de descripteurs microscopiques tels que la cinématique des fibres, leur comportement mécanique et possibles interactions a été simulée. Quel que soit le chemin de chargement, ce travail a montré comment les propriétés fortement non-linéaires, viscoélastiques et anisotropes des tissus à la macro-échelle découlent des réarrangements et mécanismes de déformation mis en œuvre à l'échelle des fibres. Plusieurs micro-mécanismes du tissu ont ainsi pu être proposés, pour des conditions de chargement quasi-statiques et vibratoires : (i) chargements cycliques et multiaxiaux à basse fréquence en déformations finies; (ii) cisaillement à haute fréquence en petites (SAOS) et grandes (LAOS) déformations. En particulier, ce travail a montré le rôle majeur de l'orientation des fibres 3D en traction, de l'encombrement stérique en compression et de la contribution de la matrice en cisaillement. Enfin, le modèle micro-mécanique a été implémenté dans un code de calcul éléments finis (EF) afin de mener des premières simulations 3D de la dynamique transitoire des plis vocaux, en tenant compte de leurs propriétés histo-mécaniques majeures. Ce travail ouvre la voie à des futures simulations multi-échelles de vibrations glottiques, pour mieux comprendre l'impact de la microstructure fibreuse spécifique du tissu vocal, dans les cas sain et pathologique.

Mots-clés : Plis vocaux, Architecture fibreuse 3D, Modélisation mécanique multi-échelles, Anisotropie, Chargements multiaxiaux, Propriétés vibratoires

Abstract

Composed of collagen, elastin and muscular fibrous networks, human vocal folds are soft larygeal multi-layered tissues owning remarkable vibro-mechanical performances. However, the impact of these tissues' histological peculiarities on their overall mechanical properties remains elusive. Therefore, this work proposes a micro-mechanical model able to describe the 3D fibrous architecture and the surrounding matrices of the vocal-fold sublayers, and to predict their multiscale behavior accordingly. For each layer, the model parameters were identified using available histo-mechanical data, including their quasi-static response to physiological loading conditions (*i.e.*, tension, compression and shear). The evolution of microscopic descriptors such as fiber kinematics, deformation and interactions was simulated. Regardless of the loading mode, it was shown how macroscale nonlinear, viscoelastic and anisotropic tissue responses are inherited from fiber scale phenomena. Original scenarios of micro-mechanisms were also predicted for a large variety of loading conditions at various rates: (i) low-frequency cyclic and multiaxial loadings upon finite strains; (ii) high-frequency small (SAOS) and large (LAOS) deformation oscillatory shear. In particular, the major role of 3D fiber orientation in tension, steric hindrance in compression, and the matrix contribution in shear was highlighted. Finally, the micro-mechanical model was implemented in a finite element (FE) code, yielding to a prior 3D simulation of vocal fold transient dynamics with relevant histo-mechanical properties. This work paves the way toward future multiscale simulations of vocal fold vibrations, accounting for various 3D fibrous healthy and pathological architectures.

Keywords: Vocal folds, 3D fibrous architecture, Multiscale mechanical modeling, Anisotropy, Multiaxial loadings, Vibratory properties